STANDARDS DEVELOPMENT BRANCH OMOE
3693600004797

NATIONAL WATER RESEARCH INSTITUTE

INSTITUT NATIONAL de RECHERCHE sur les EAUX

MEASURING GROUNDWATER VELOCITY AND HYDRODYNAMIC DISPERSION IN A SINCLE FRACTURE IN FRACTURED SHALE

FINAL REPORT
MINISTRY OF THE ENVIRONMENT, ONTARIO
GRANT NO. 393G

TC
171
.C44
M43
1993
MOE

TC
171
.C44
M43
1993

Measuring groundwater velocity and hydrodynamic dispersion in a single fracture in fractured shale / Lapcevic, P. A.

77018

Copyright Provisions and Restrictions on Copying:

This Ontario Ministry of the Environment work is protected by Crown copyright (unless otherwise indicated), which is held by the Queen's Printer for Ontario. It may be reproduced for non-commercial purposes if credit is given and Crown copyright is acknowledged.

It may not be reproduced, in all or in part, part, for any commercial purpose except under a licence from the Queen's Printer for Ontario.

For information on reproducing Government of Ontario works, please contact Service Ontario Publications at copyright@ontario.ca

Measuring Groundwater Velocity and Hydrodynamic Dispersion in a Single Fracture in Fractured Shale

Final Report
Ministry of the Environment, Ontario
Grant No. 393G

Principal Investigator:

J. Cherry[1]

Co-Investigators:

E.A. Sudicky[1]
C.W. Mase[1]
K.S. Novakowski[2]

report authored by:
P.A. Lapcevic[2] and K.S. Novakowski

[1]Waterloo Centre for Groundwater Research
University of Waterloo

and

[2]National Water Research Institute
Environment Canada

April 1993

TC
171
.C44
M43
1993

ABSTRACT

Fractures play an important role in the migration of contaminants through otherwise impermeable media. In the heavily industrialized regions of Southern Ontario, large areas of the underlying bedrock are composed of flat lying shale formations in which extensive horizontal fractures dominate the flow system. In this study, field, laboratory and modelling studies were conducted to characterize a single fracture zone. The objective was to develop new hydraulic and tracer testing techniques for more accurately determining the parameters necessary for predicting groundwater velocity within the medium. A total of twenty-five boreholes were drilled in a 30 x 30 m area. Hydraulic tests were conducted to determine the aperture distribution of two horizontal fracture zones intersecting the boreholes. One of the two zones was isolated in each borehole for periods of up to a year using pneumatic packers. Hydraulic head was monitored using either electronic pressure transducers or a standpipe arrangement. Multiple well tracer experiments were conducted using both radially convergent and radially divergent flow formats. Laboratory tracer experiments were conducted in an artificial fracture constructed using two glass plates as a means of simulating a fracture plane. Modelling studies were conducted to improve the interpretation of hydraulic tests conducted in low-storativity media. A computer program (TYPCURV) which incorporates the effects of well bore storage and skin zones for the analysis of pumping and pulse tests was developed.

The results of this study show that flow in shale discretely fractured in the horizontal orientation is strongly influenced by skewed aperture distributions and greater than 20% closure of the fracture planes. Measurements of hydraulic head show substantial variation on a daily basis due to barometric effects and longer-term variation due to seasonal effects. Measuring hydraulic gradients in low gradient fractured rock systems remains an unresolved problem.

Uncertainty in the meaning of aperture measurements determined from radially convergent tracer experiments leads to uncertainty in the prediction of groundwater velocity in fractured rock. The interpretation of radially divergent tracer tests suggests that diffusion of solute into the rock matrix is a significant process which may substantially diminish the concentration of contaminant at the solute front. To further resolve the issues related to solute transport, experiments conducted under conditions of natural gradients, must be undertaken. To do so, technical development of an appropriate experimental method must be conducted. This is a non-trivial problem that may require significant resources and many years of research.

CONTENTS

Abstract ii

INTRODUCTION 1

METHODS 4

Field Studies 4
Location and Geology 4
Drilling Program 4
Hydraulic Testing Program 6
Borehole Instrumentation 7
Tracer Experiments 10
Laboratory Studies 16
Modelling Studies 17

RESULTS AND DISCUSSION 19

Field Studies 19
Hydraulic Tests 19
Measurement of Hydraulic Head 20
Tracer Experiments 26
Laboratory Studies 32
Modelling Studies 33

SUMMARY 34

REFERENCES 36

APPENDIX A 39

APPENDIX B 60

APPENDIX C 80

APPENDIX D 120

APPENDIX E 138

APPENDIX F 184

APPENDIX G 200

INTRODUCTION

Fractures in rocks with a matrix of low permeability can provide pathways for contaminants from waste and industrial sites to underlying aquifers. Discrete horizontal fractures extensive over large areas, in conjunction with short vertical fractures, can lead to the widespread migration of contaminants through otherwise impermeable units. Much of the heavily industrialized regions of south-central Ontario are underlain by relatively impermeable shale units which are fractured in this manner. The accurate determination of groundwater velocity and hydrodynamic dispersion within single fracture planes is necessary for the prediction of the rate of contaminant migration within these shale units. The development of realistic conceptual models to describe the hydrogeology and behaviour of groundwater flow systems in this environment is based on detailed experimental studies which are validated using mathematical descriptions of the flow and transport processes.

Groundwater flow and mass transport through fractures is interpreted using a conceptual model in which the fracture walls are approximated by two smooth parallel plates separated by a uniform opening (aperture). Previous studies have shown that this simple conceptual model may not be appropriate and can lead to large errors in the estimation of groundwater velocity (Raven and Gale, 1985; Tsang and Tsang, 1987; Brown, 1987 ; Novakowski, 1988; Raven et al., 1988). Factors which lead to the failure of the parallel plate model include fracture surface roughness, tortuosity of the flow paths and fracture contact area.

Predictions of contaminant migration in the subsurface is generally conducted using models which incorporate constant coefficients for the advective and dispersive components of the transport process. The determination of these constants is influenced both by the choice of

field techniques and the methods by which they are interpreted. A large component of the uncertainty and error associated with the model predictions is due to differences between the scale at which the parameters are obtained and the scale at which prediction is required. Since adequate scaling laws have yet to be developed for fractured rock it is found that field scale measurements will yield the most appropriate measurements for local to regional scale model predictions.

The hydraulic properties of fractured sedimentary rock formations, such as hydraulic conductivity, storativity and fracture aperture, can be determined at the field scale using a variety of hydraulic testing techniques. These techniques include constant-head injection, slug, pulse and interference tests. The results of single-well tests such as constant-head injection and slug tests are representative of the properties of the region adjacent to the wellbore. Multiple-well interference and pulse tests are representative of larger volumes of the rock mass. Determining the properties of the formation from hydraulic tests can be influenced by the presence of skin zones, wellbore storage, methods of analyses , test interval length and field methodology (Doe and Remer, 1980; Doe et al., 1987; Novakowski, 1990).

Tracer experiments conducted either under induced gradient or natural flow conditions, can be used to determine the dispersive and diffusive properties of the fracture and bulk rock matrix. Induced gradient tests can be conducted as two well injection-withdrawal tests, radially convergent flow tests, or radially divergent experiments (eg. Raven et al. (1988), Novakowski (1988)). One of the factors recently found to influence these experiments is mixing of the tracer in the wellbore (Palmer, 1988). The dispersive properties of the fracture may be overestimated due to incomplete mixing of tracer in the injection and observation wells. Tracer experiments conducted under natural flow conditions similar to ones carried out in heterogeneous

sand aquifers (eg. Mackay et al, 1986 and LeBlanc et al., 1991) are difficult to conduct in fractured rock due to the complications of small fracture porosity in comparison to the volumes of water contained in the intersecting wellbores.

In flat-lying fractures, differences in hydraulic head between boreholes several metres apart may be in the order of only a few centimetres. Because such small differences are difficult to measure, calculations of hydraulic gradients necessary for prediction of contaminant transport rates and direction are uncertain. Hydraulic head can be determined either by measuring water levels manually using standpipes open to atmosphere or monitoring pressure changes electronically with pressure transducers isolated from atmospheric influences. Changes in hydraulic head may be influenced by seasonal variations, barometric changes, or tidal effects.

The objective of this study is to characterize a single fracture zone transecting relatively unfractured rock with a view to developing new experimental techniques for more accurately determining the parameters necessary for predicting groundwater velocity and estimates of hydrodynamic dispersion. Hydraulic techniques for determining the in-situ aperture of fractures including constant-head injection, interference and pumping test methods are examined. Methods for tracer experiments conducted using different flow field geometries and unique borehole instrumentation are also developed. This study is an extension of a previous study (Ministry of the Environment, Ontario Grant No. 214)

METHODS

Field Studies

Location and Geology:

The field site used in this study is located in the village of Clarkson, west of Toronto, approximately 1.5 km north of the Lake Ontario shoreline. The site is covered by approximately 3 m of clayey-sand overburden which overlies the Upper Ordovician Meaford-Dundas Formation. The upper 20 m of the bedrock consists of a weathered fissile grey to reddish-grey shale with numerous soft mud seams and interbeds of pink fossiliferous dolostone up to 0.2 m in thickness. The unit is relatively flat-lying with a slight dip to the south. Individual open fractures, as logged in drill core, are often associated with the contacts between the shale and dolostone interbeds. Some evidence of vertical fracturing is noted within the dolostone. Fractures generally occur as bedding plane partings which have developed in horizontal orientations due to stress heterogeneity arising from erosional unloading or isostatic rebound.

Drilling Program:

Seven boreholes were installed at the site as part of a previous study (Blackport et al., 1986; Novakowski and Cherry, 1988). Between May 1988 and February 1990 an additional 18 boreholes were drilled in three sets of six boreholes each (May 1988, May 1989 and February

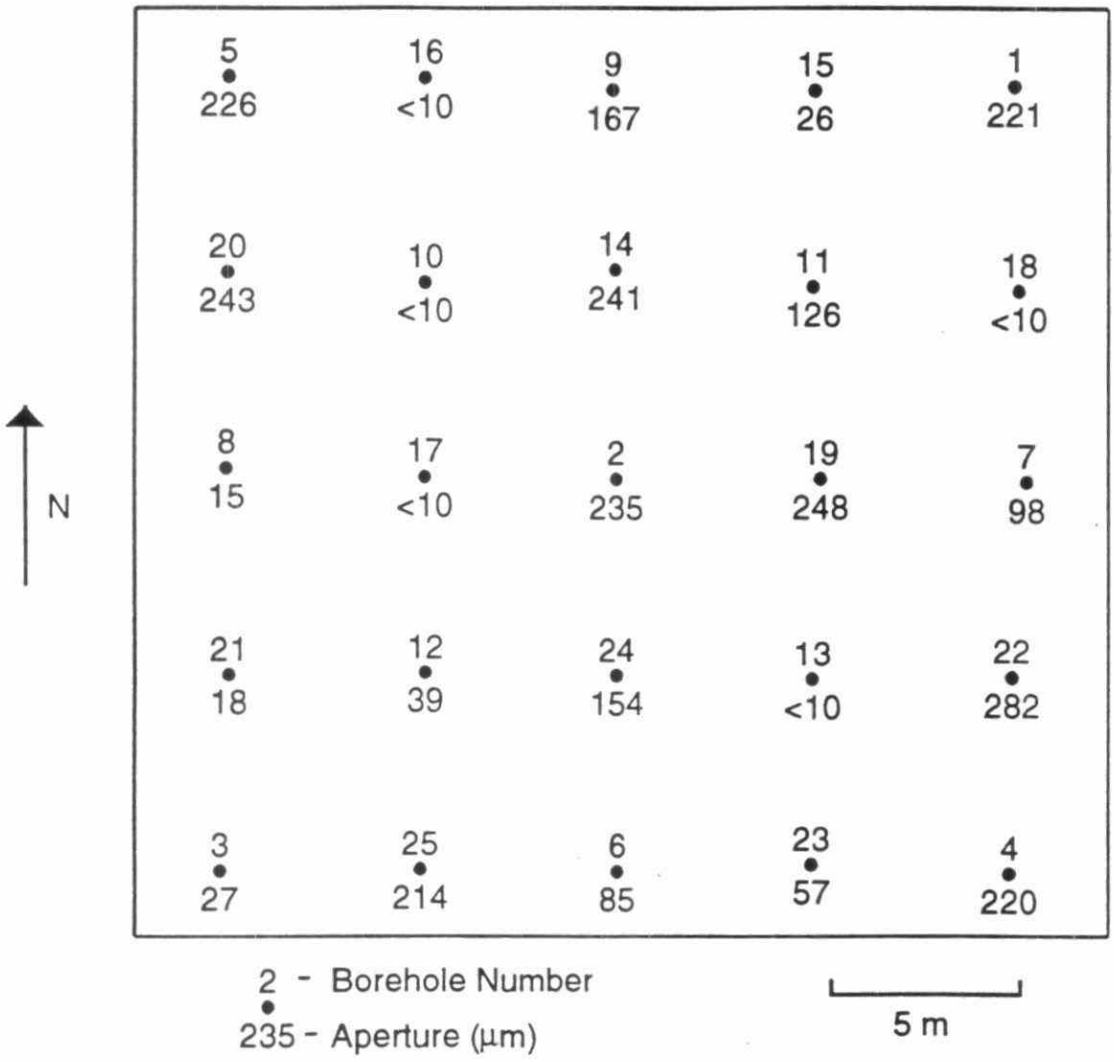

Figure 1: Site map showing the location of all boreholes numbered in order of completion. Also shown is the hydraulic aperture as determined from constant-head tests.

1990). The 25 boreholes (numbered in order of completion) are 17-18.5 m in depth, 76 mm in diameter and are located within a 30 m x 30 m area in a regular grid pattern (Figure 1). All boreholes were drilled using triple tube methods of core recovery. Steel casing was installed through the overburden into the bedrock. Core recovery was greater than 98% in most cases. Core samples from boreholes UW8-UW25 were photographed and logged for both lithology and the presence of fractures immediately following removal from the core barrel. A compilation of lithology and fracture logs for each of the boreholes is included in Appendix C. This grid of boreholes is believed to be the most detailed field site of this type yet to be studied in North America.

Hydraulic Testing Program:

During previous work at the site (Blackport et al. 1986; Novakowski and Cherry, 1988) two fracture zones intersecting the original seven boreholes were identified. An upper fracture zone located at about 9.8 m below ground surface and a lower zone, located at about 10.5 m below ground surface, were characterized. Other permeable fracture zones are present in the boreholes although while suitable for further studies they are not discussed further in this report.

Over 300 constant-head injection tests were conducted in the 25-borehole array. A constant-head injection test is conducted by injecting water into an isolated portion of the borehole at a steady pressure, ΔH. The flow rate of water, Q, is allowed to achieve steady conditions. Fracture aperture, 2b, (μm), is then determined by using the cubic law (Witherspoon et al., 1980):

$$2b = \left(\frac{Q}{\Delta H} \cdot \frac{6\mu}{\pi \rho g}\right)^{\frac{1}{3}} \cdot 1x10^{-6} \qquad (1)$$

where Q is the steady-state flow rate (m^3/s), ΔH is the difference in hydraulic head between static initial conditions and a steady flow condition (m), ρ is the fluid density (kg/m^3), g is gravitational acceleration (m/s^2) and μ is the kinematic viscosity (m^2/s).

Two inflatable packers with a variable separation length were used to isolate specific zones in each borehole. Constant-head tests were conducted along the entire length of each borehole using a 1.5 -2.0 m test interval. Further testing of the more permeable zones was conducted using test intervals of 0.5 m and 0.1 m. The shorter test zones were used to differentiate between discrete closely spaced fractures. It is assumed that the results of the constant-head tests represent an average value of the aperture immediately adjacent to the borehole. The lower detection limit for the particular testing system used is estimated to be approximately 10 micrometres. Detailed aperture logs are shown in Appendix C. The methodology for constant-head injection tests is described in more detail in Novakowski (1988). Pulse interference tests and constant-rate pumping tests were also conducted to verify inter-well connections, determine apertures and establish that no vertical connection between the upper and lower fractures exists (Appendix A).

Borehole Instrumentation:

Considerable effort was undertaken over the course of this study to improve the borehole instrumentation necessary to isolate the fracture plane studied. To isolate the fracture zone two inflatable packers were used (Figure 2a) for periods up to a year. The design of the packers

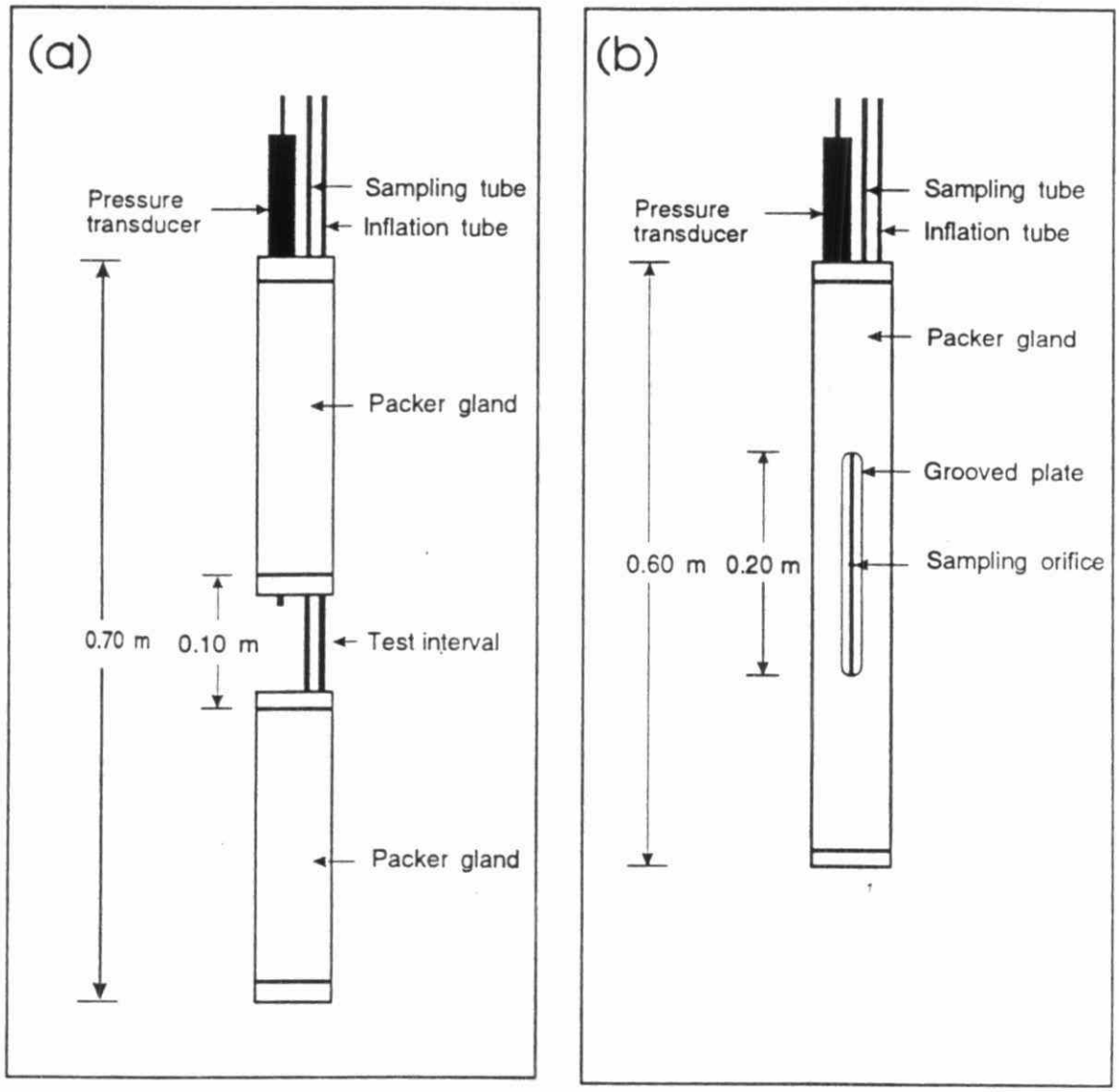

Figure 2: Illustration of borehole instrumentation: (a) double-packer system, (b) zero-volume sampling packer.

evolved from a system of straddle packers separated by steel rod to a single packer with a solid PVC mandrel. Factors such as the ease of maintenance, durability and cost were considered in design of the packer systems. Packer separations ranging from 0.1 m to 0.7 m were used to ensure that only the fracture being studied was isolated. All packers were maintained at pressures of 414-427 kPa (60-62 psi). Packer inflation was maintained on a weekly basis. Deflation of the packers due to leaks in fittings or clamps, or line breakage has at times been a significant problem influencing the ability to measure hydraulic head in a completely isolated system.

Prior to June 1990, measurements of water level within the isolated fracture were obtained using a 0.013 m (1/2") standpipe of nylon tubing connected to the test zone and exposed at the ground surface. This arrangement provides measurements accurate within ± 0.005 m. Measurements were obtained on a weekly basis.

In June 1990, pressure transducers of vibrating wire type (Geokon® model 4500HS) were installed in each of the 25 boreholes to continuously monitor the hydraulic head in the lower fracture. The transducers were installed directly above the top packer and connected through the packer to the test section. Signals from the transducers were measured using a Campbell Scientific CR10® data logger on an hourly basis.

Between June 1990 and January 1991, hydraulic head measurements were obtained by both manual measurements using the standpipe tubing and by continuous monitoring using the pressure transducers. Water level measurements were obtained once a week while the transducers recorded pressures at intervals of 20-60 minutes. Barometric pressure was monitored continuously using a Setra 270® pressure transducer. In January 1991, the manometers were removed from the borehole instrumentation. Continuous readings were taken

between January and June 1991 at 60 minute intervals using only the pressure transducers. In June 1991 the transducers were removed and reinstalled after verifying all measurements.

In September 1991 a new single packer system was developed to minimize the wellbore volume during tracer tests (Figure 2b). Hydraulic head measurements are also obtained using this system. The packer is described in detail in Appendix G. All boreholes were instrumented with this packer design in January 1992.

Tracer Experiments:

A total of thirteen induced gradient tracer experiments were conducted in the lower fracture during the fall of 1991 and spring of 1992. Ten tracer experiments were conducted using a radially convergent flow format. In this format tracer is instantaneously injected into one well (source well) while a second well (observation well) is pumped continuously (Figure 3a). Complete mixing of the tracer in both wellbores is ensured by circulating water in the test section using a submersible pump below the bottom packer and static mixers located in the test interval between the two packers. Withdrawal flow rates in the observation well ranged between 100 and 920 mL/min.

An additional three tracer experiments were conducted using a radially divergent flow format. In this case water is injected continuously in the source well and sampled in one or more observation wells (Figure 3b). One, two and six observation wells were monitored in each of the three experiments, respectively. In the third experiment the observation wellbore volumes were minimized by using the sampling packer. Test conditions for all tracer experiments are shown in Tables 1-3. More complete descriptions of the methodology for convergent and

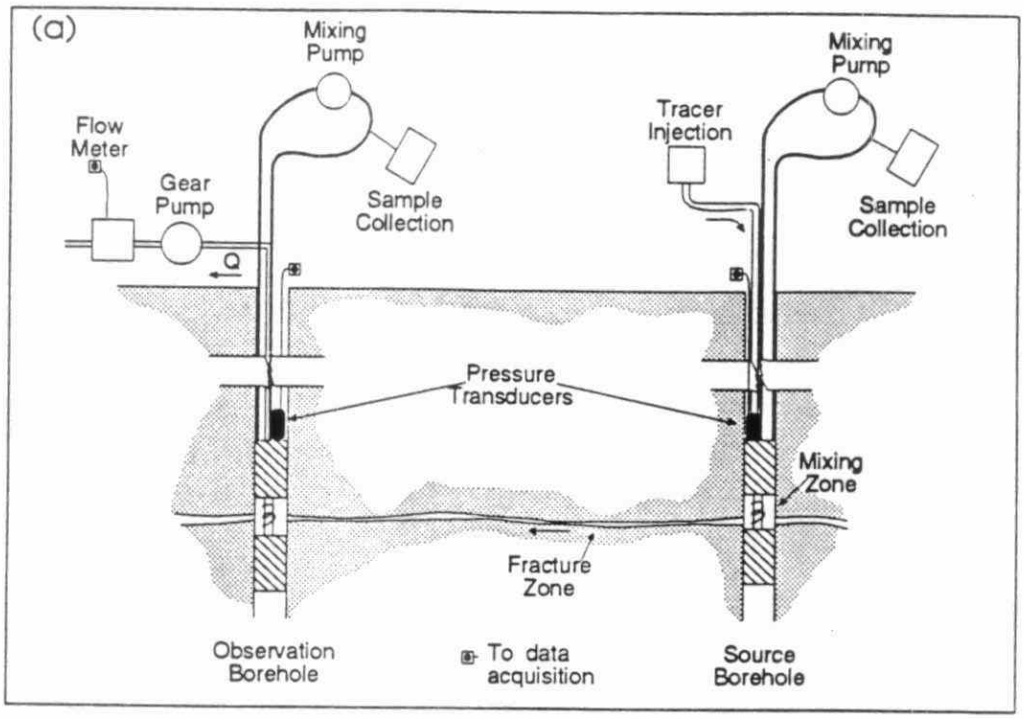

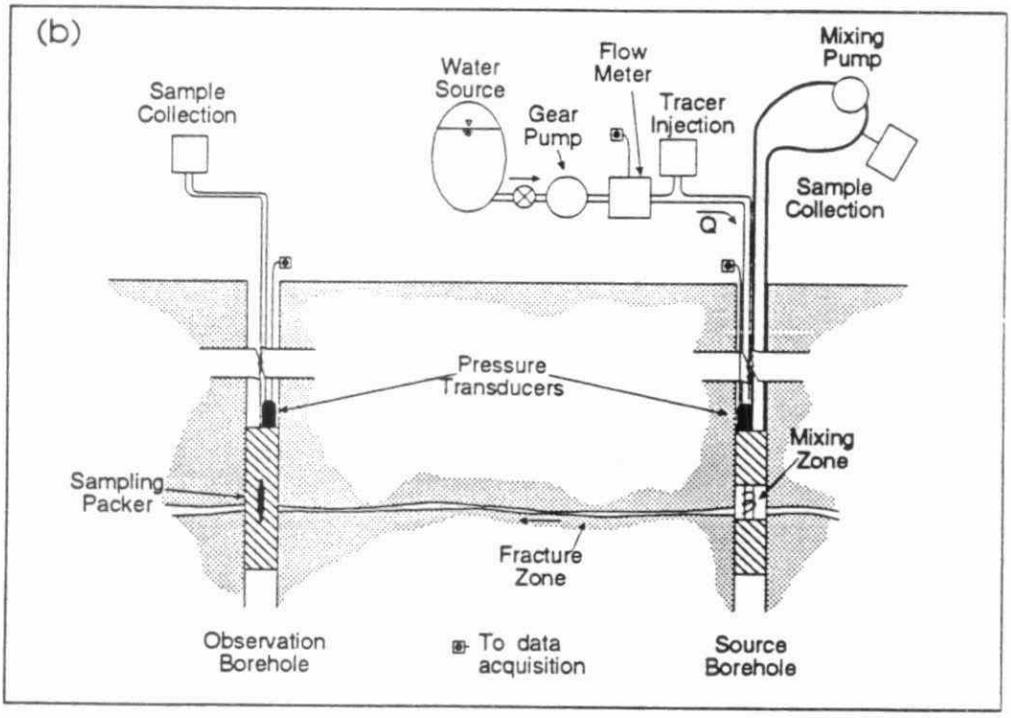

Figure 3: Schematic diagram of apparatus used to conduct tracer experiments: (a) radial convergent flow format , (b) radially divergent flow format.

Table 1: Summary of test conditions for tracer experiments conducted in 1991 using a radially convergent flow format.

Test I.D.	TT1-91	TT3-91	TT5-91	TT6-91	TT7-91	TT8-91	TT9-91
Date	15-Aug-91	11-Sep-91	19-Sep-91	5-Nov-91	6-Nov-91	7-Nov-91	8-Nov-91
Injection Well	UW19	UW14	UW1	UW19	UW19	UW19	UW19
Observation Well	UW2	UW2	UW2	UW2	UW2	UW2	UW2
Well Radius (r_w) (m)	0.038	0.038	0.038	0.038	0.038	0.038	0.038
Radial Distance (r_i) (m)	5.55	5.42	15.03	5.55	5.55	5.55	5.55
Head Difference (ΔH) (m)	0.33	0.03	1.30	0.14	0.39	0.78	1.22
Flow rate (Q)[a] (ml/min)	308	400	n/a	109	276	594	910
Std. Deviation (ml/min)	19	37	n/a	2	3	15	20
Flow rate (Q) [b] (ml/min)	260-300	360	923	n/a	n/a	n/a	n/a
C_o (ppm)	5.0	3.1	3.0	2.4	2.0	2.6	2.9
Decay Half Life (min)	46	29	30	32	8	5	4
Peak C/C_o	1.70e-03	5.30e-03	5.90e-04	6.90e-03	8.40e-03	6.10e-03	6.50e-03
Tracer Breakthrough (min)	70	30	200	150	50	25	15
Time to peak (min)	180	70	400	360	105	60	37
Tracer mass recovery (%)	90	48	70	78	65.25	68.83	85.55
Tracer C (ppm)	60	1000	1000	1000	1000	1000	1000
Tracer Volume (ml)	10	0.6	0.8	0.6	0.6	0.6	0.6
Observation Well Volume (ml)	308	308	308	308	308	308	308
Injection Well Volume (ml)	431	431	431	431	431	431	431

[a] Flow rate determined from measurements obtained using a rotary-gear flowmeter.
[b] Flow rate determined by manual measurements of outflow.

Table 2: Summary of test conditions for tracer experiments conducted in 1992 using a radially convergent flow format.

Test I.D.	TT2-92	TT3-92	TT4-92
Date	25-May-92	28-May-92	3-Jun-92
Injection Well	UW1	UW1	UW5
Observation Well	UW2	UW2	UW4
Well Radius (r_w) (m)	0.038	0.038	0.038
Radial Distance (r_i) (m)	15.03	15.03	30.07
Head Difference (ΔH) (m)	1.10	0.77	1.35
Flow rate (Q)[a] (ml/min)	976	1125	n/a
Std. Deviation (ml/min)	15	86	
Flow rate (Q) [b] (ml/min)	761	565	785
C_o (ppm)	2.9	3.1	5.5
Decay Half Life (min)			
Peak C/C_o	3.27e-04	3.32e-04	8.16e-05
Tracer Breakthrough (min)	270	390	1170
Time to peak (min)	450	870	3229
Tracer mass recovery (%)			
Tracer C (ppm)	1000	1000	1000
Tracer Volume (ml)	0.8	0.8	2.5
Observation Well Volume (ml)	310	310	310
Injection Well Volume (ml)	286	286	286

[a] Flow rate determined from measurements obtained using a rotary-gear flowmeter.
[b] Flow rate determined by manual measurements of outflow.

Table 3: Summary of test conditions for tracer experiments conduced in 1991 using a radially divergent flow format.

Test I.D.	RD1	RD2		RD3					
Test Date	8-Oct-91	17-Oct-91		11-Dec-91					
Injection Well	UW2	UW2		UW2					
Observation Well	UW19	UW19	UW4	UW24	UW14	UW19	UW11	UW22	UW5
Well Radius (r_w) (m)	0.038	0.038	0.038	0.038	0.038	0.038	0.038	0.038	0.038
Radial Distance (r_i) (m)	5.55	5.55	14.95	5.3	5.42	5.55	7.41	11.75	15.13
Head Difference (ΔH) (m)	n/a	n/a	n/a	0.6	0.3	0.55	0..5	0.65	0.3
Flowrate (Q) (ml/min)	363	441		269					
Std. Deviation (ml/min)	13	10		n/a					
Circulation Flowrate (ml/min)	459	362		425					
Std. Deviation (ml/min)	13	12		n/a					
C_o (ppm)	37	26		52					
Peak C/ C_o	2.9e-02	4.8e-02	3.7e-03	2.6e-02	3.9e-02	2.0e-02	6.3e-03	6.8e-03	5.4e-04
Tracer breakthrough (min)	70	50	240	54	54	60	282	126	630
Time to peak (min)	180	90	630	102	72	126	324	330	726
Tracer C (ppm)	1000	1000		1000					
Tracer Volume (ml)	90	45		45					
Observation Well Volume (ml)	666	0	431	0	0	0	0	0	0
Injection Well Volume (ml)	3335	3335		3335					

divergent tracer experiments can be found in Novakowski (1988) and Appendix G respectively.

A computer program containing various solutions for the different flow field geometries was used to interpret both the convergent and divergent tracer experiments. The mathematical development and parameter definitions are discussed in detail in Appendix G. A type curve matching procedure was used to estimate aperture, dispersivity, and matrix porosity based on the breakthrough of tracer at observation wells. For the radially convergent tests, Equation 37, in Appendix G was used to simulate field data of C/C_p vs time, where C_p is the peak concentration . Two parameters, a dimensionless correction factor accounting for flow captured by the open well, ξ, and dispersivity, α_r, influence the analysis of these tests. Using dimensionless time, t_D, as determined from the type curve and a value of t (s) from the field data, apertures based on hydraulic head and flow rate ($2b_{\Delta H}$ and $2b_Q$) are calculated using respectively:

$$2b_{\Delta H}=\left\{\frac{12\mu t_D \ln(r/r_w)\alpha_r^2}{t\Delta H\rho g}\right\}^{1/2}\cdot 1x10^{-6} \qquad (2)$$

$$2b_Q=\frac{tQ}{2\pi t_D\alpha_r^2}\cdot 1x10^{-6} \qquad (3)$$

where α_r is radial dispersivity (m), r is radial distance between the observation and source wells (m), and r_w is the radius of the well (m). The radial divergent experiments are interpreted in a similar manner using Equation 24 of Appendix G for the case where the observation well volume is minimized and Equation 31 of Appendix G for the case where there is mixing in the

wellbore. Data from each observation well was analyzed in four different ways. The fits were obtained by using 1) C/C_p vs time with $\theta_m = 0$ and $\tau = 1$, 2) C/C_o vs time with $\theta_m > 0$ and $\tau = 1$, 3) C/C_o vs time with $\theta_m > 0$ and $\tau > 1$, and 4) C/C_p vs time with $\theta_m > 0$ and $\tau > 1$. During the first two experiments, the observation wells (UW19 and UW4 respectively) were instrumented with a double packer system and a re-circulating pump to ensure complete mixing of the test section. In the remainder of the experiments, zero-volume sample packers were used.

Laboratory Studies

The effect of tracer mixing in the wellbore was investigated in a laboratory study conducted in an artificial fracture (Appendix B; Novakowski, 1989). A single fracture was simulated using two glass or plexiglass plates laid horizontally and separated by metal shims, 0.75 mm thick, distributed throughout the area of the fracture. Two sides are sealed while the other two sides are attached to constant head boxes. Two artificial fractures were manufactured in this manner. The first apparatus had dimensions of 1 m square with a 1.5 m long acrylic tube (7.6 cm I.D) intersecting the fracture plane to simulate a well. Two electrode ports used for monitoring tracer concentration were located in the fracture plane. A second fracture 2 m long and 0.4 m in width was constructed in a similar manner using glass plates 0.02 m thick. Tracer experiments were conducted in the artificial fractures by establishing a steady-flow field between the constant-head boxes and then introducing tracer in the higher-head box in a step-function fashion. The anion Br^- was employed as tracer in all cases. The tracer is continuously mixed in the constant-head box using a mechanical stirrer. A red dye was also added to the tracer

solution during several of the experiments so that the flow process could be visualized. Measurements of concentration were made using specific ion electrodes.

Fourteen tracer experiments were conducted using the artificial fractures. In twelve of the experiments, packers spaced 0.10 m apart were used in the well, giving an interval volume of 0.36 L. In the other two experiments the interval volume was reduced to 0.025 L by placing blocks in the test section. Several of the initial experiments were conducted without active recirculation or sampling so as to obtain undisturbed measurements of concentration from the electrode ports in the fracture plane.

The results of the lab experiments were interpreted using the method by Palmer (1988) in the case where wellbore samples were analyzed and using the Ogata-Banks solution where the results from electrode measurement ports only were interpreted (Appendix B).

The artificial fractures were also used to qualitatively examine the performance of field instrumentation prior to use in the field scale experiments.

Modelling studies

An analytical model for interpreting the results of pulse interference tests influenced by well bore storage in the observation well was derived. The solution was used to develop a simple graphical method of analysis (Novakowski, 1989). The solution was developed from the equation describing transient groundwater flow around a well in a geological formation, subject to a slug test boundary condition and the effects of wellbore storage in the observation well. The graphical method of analysis was developed using the magnitude and elapsed time lag of the peak of the response in an observation well at a given radial distance away from the

source well. Transmissivity and storativity are calculated from two separate graphs. The graphs can also be used to design pulse interference tests using rough estimates of storativity. The method was used to interpret pulse interference tests where the tests were conducted with and without the effect of well bore storage.

To assist in the analysis of aquifer tests conducted in fractured rock, a simulation package was developed and given the name TYPCURV. TYPCURV is a type curve generating program written in FORTRAN 77. The code consists of an interactive input section, type curve generating loop and a numerical inverter. The program consists of several analytical solutions in Laplace space which incorporate the effects of skin and wellbore storage in both observation and source wells. The solutions are numerically inverted from Laplace space using a Fourier series approximation of the inversion integral. The type curves are matched to field data from which transmissivity and storativity are calculated based on a match point. The computer program can be used to analyze pumping and pulse interference tests conducted in two or more wells. The development and use of TYPCURV is described in Novakowski (1990).

The use of fractal methods as a means of generating stochastic fields to describe the aperture distributions of single fracture surfaces was investigated through a literature review of existing studies (Unger, 1989). Further numerical studies were undertaken to investigate the hydromechanical behaviour of fractures at the field site (Unger, 1991).

RESULTS AND DISCUSSION

Field Studies

Hydraulic Tests:

The results of the constant-head tests conducted in both the upper and lower fractures in all 25 boreholes are shown in Table 4 and Appendix C. The lower fracture ranges in aperture between 282 micrometres to below the detection limit while the upper fracture apertures ranges between 138 micrometres to below the detection limit. The large number of non-detectable apertures results in multi-modal distributions (Lapcevic et al., 1990) and therefore the apertures are not normally or log-normally distributed as is commonly postulated at this scale (eg. Gale et al., 1985). In 25% of the boreholes the aperture of the lower fracture was below the detection limit and in 32% of the boreholes the aperture of the upper fracture was below the detection limit. This suggests that large areas of the fracture planes may be in contact. Due to the presence of closure, the transport of solute will follow tortuous pathways.

Numerical studies using artificially generated aperture distributions showed that by increasing the contact area from 0-20% flow pathways through the plane become more tortuous and exhibit a greater degree of channelling (Unger, 1991). However flux through the fracture agrees well with the parallel plate model.

Table 4: Summary of fracture aperture widths (in micrometres) as determined from the results of constant-head injection tests.

Borehole #[a]	Upper Fracture 2b(μm)	Lower Fracture 2b(μm)	Borehole #	Upper Fracture 2b(μm)	Lower Fracture 2b(μm)
1	90	221	14	106	241
2	66	235	15	94	26
3	138	27	16	<10	<10
4	67	220	17	104	<10
5	<10[b]	226	18	18	<10
6	80	85	19	<10	248
7	115	98	20	39	243
8	62	15	21	<10	18
9	<10	167	22	58	282
10	<10	<10	23	120	57
11	107	126	24	54	154
12	<10	94	25	120	214
13	<10	<10			

[a] 'UW' removed from borehole I.D. ie. 1 is the same as UW1
[b] aperture is below measurement limit of testing apparatus

Measurement of Hydraulic Head:

Measurements of hydraulic head in the lower fracture over the course of this study are given in Appendix D. Obtaining reliable measurements of hydraulic head for periods of time a few weeks or longer was found to be difficult due to a number of factors. For example, several of the air inflated packers were prone to leaks at different times which disrupted the entire flow system when one failed completely. Other problems included the lack of sensitivity of the transducers, and electronic measurement errors. Transducers rated for 0-5 psi (0-35 kPa) and 0-50 psi (0-345 kPa) were both used during this study. A comparison of the two pressure ranges was undertaken by installing both in the same well for a period of two weeks. The results are shown in Figure 4. A difference in measured hydraulic head between the two

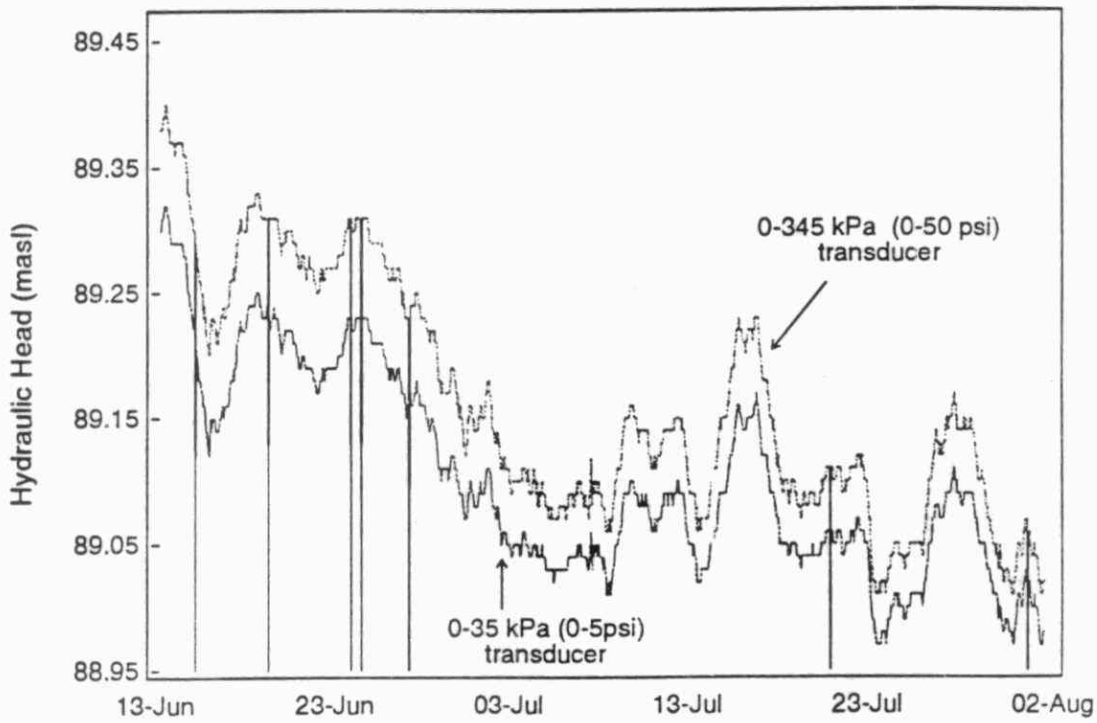

Figure 4: Comparison of hydraulic head measurements determined with 0-35 kPa (0-5 psi) and 0-345 kPa (0-50 psi) pressure transducers.

transducers ranges from 0.04-0.08 m over the course of the two week period. The difference between the two measurements decreases with time suggesting that the rate of stabilization of the two transducers differs. Because the differences in hydraulic head across the site are only a few centimetres, the difference between the two pressure ranges of transducers is significant.

A compilation of the measurements of hydraulic head in the lower fracture plane from a representative borehole is shown in Figure 5. Measurements in 1989 were obtained weekly (Figure 5a). The 1990-1991 compilation (Figure 5b) is not corrected for barometric influences. Seasonal trends show a general decrease in hydraulic head in the summer months and an increase in the winter and spring months. Increased recharge due to spring run-off is evident in both graphs . The influence of barometric pressure on hydraulic head is shown in Figure 6. The measurements of hydraulic head uncorrected for barometric pressure mimic the trends in barometric pressure. When barometric pressure is eliminated from the measurements, the results show evidence of recharge due to precipitation (precipitation records at the nearby Toronto International Airport, show thunderstorms on April 13th, with 7.2 mm and 12.5 mm of precipitation on April 14 and 15th respectively (AES, 1991)). From preliminary analysis of the effects of tides and barometric pressure in the frequency domain, it was concluded that the hydraulic head is most sensitive to barometric changes (Appendix E). It was further concluded that to interpret the tidal effects on hydraulic head for the determination of fracture aperture, long term ($>$ 1024 hrs) continuous data would be required.

Spatially contoured measurements of hydraulic head within the lower fracture plane indicate the direction of groundwater flow to be generally south to southeast (Figure 7). Only boreholes with hydraulic apertures greater than 50 μm were contoured. A contour of the October 1990 measurements (Figure 7a) shows maximum differences in hydraulic head of

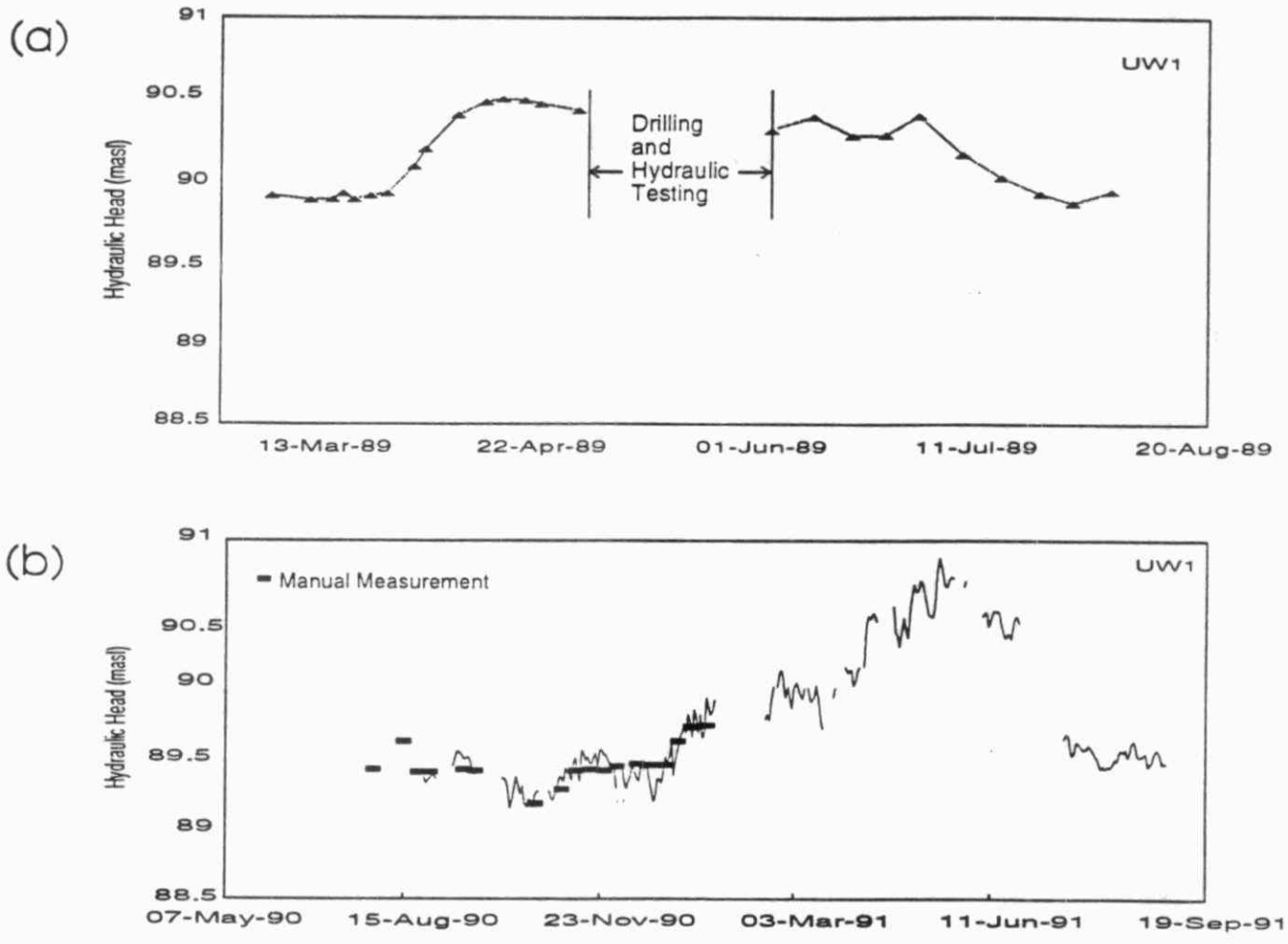

Figure 5: Measurements of hydraulic head in the lower fracture plane (a) manual measurements taken on a weekly basis, (b) manual measurements taken on a weekly basis and transducer signals recorded every 20- 60 minutes

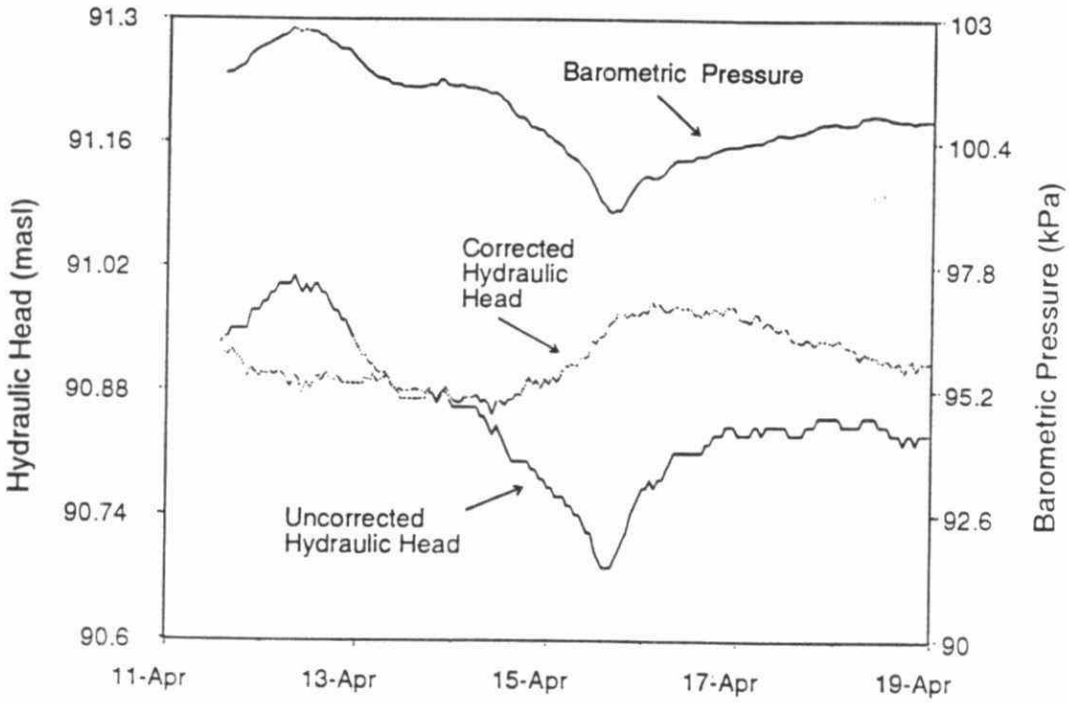

Figure 6: Comparison of measurements of hydraulic head corrected for the influence of barometric pressure versus uncorrected measurements of hydraulic head.

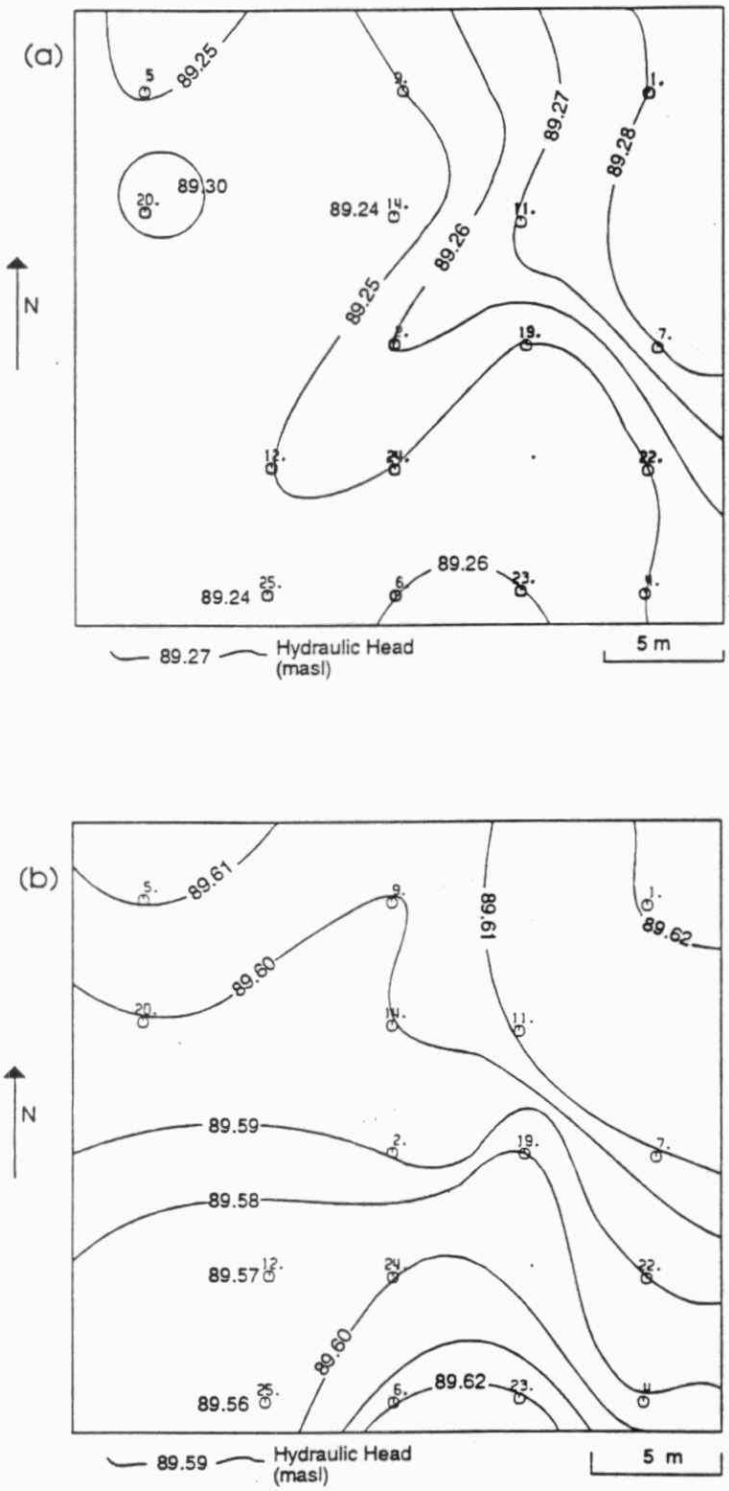

Figure 7: Spatially contoured measurements of hydraulic head within the lower fracture plane: (a) October 10,1990, (b) December 6, 1990.

0.04 m across the site. A contour of the December 1990 measurements (Figure 7b) shows a maximum difference of 0.06 m. Hydraulic gradients calculated using these measurements are between 0.001 and 0.004. A detailed analysis of the variations in hydraulic head in the fracture and the concomitant implications for contaminant transport will require specially designed field experiments and further model development.

Tracer Experiments:

A summary of the interpretation of the ten tracer experiments conducted in a radially convergent format are shown in Table 5. An example breakthrough curve and model fit is shown in Figure 8 and the remaining fits are compiled in Appendix F. Model fits were obtained using C/C_p breakthrough curves and adjusting the parameters α_r and ξ. At a radial distance of 5.5 m, ξ ranges from 6-9, at 15 m, ξ ranges from 2 to 4 and at 30 m, ξ is 1 . This decline in ξ with increasing distance suggests that an additional effect causing apparent dispersion is unaccounted for in the interpretation. An additional complication in the interpretation of the convergent experiments was found when fits were attempted to real field concentrations. With no exceptions, fits to field concentration were only achieved when completely unrealistic values of the mixing coefficients for both the source and pumping wells were used. Values 2-3 orders of magnitude greater than values calculated using appropriate measurements of the mixing geometry were necessary. This appears to be characteristic of convergent tracer experiments conducted in this fashion and has been observed elsewhere (Silliman, pers. comm.). Therefore, in all further interpretation of these experiments, only the fits obtained with normalized concentration will be discussed.

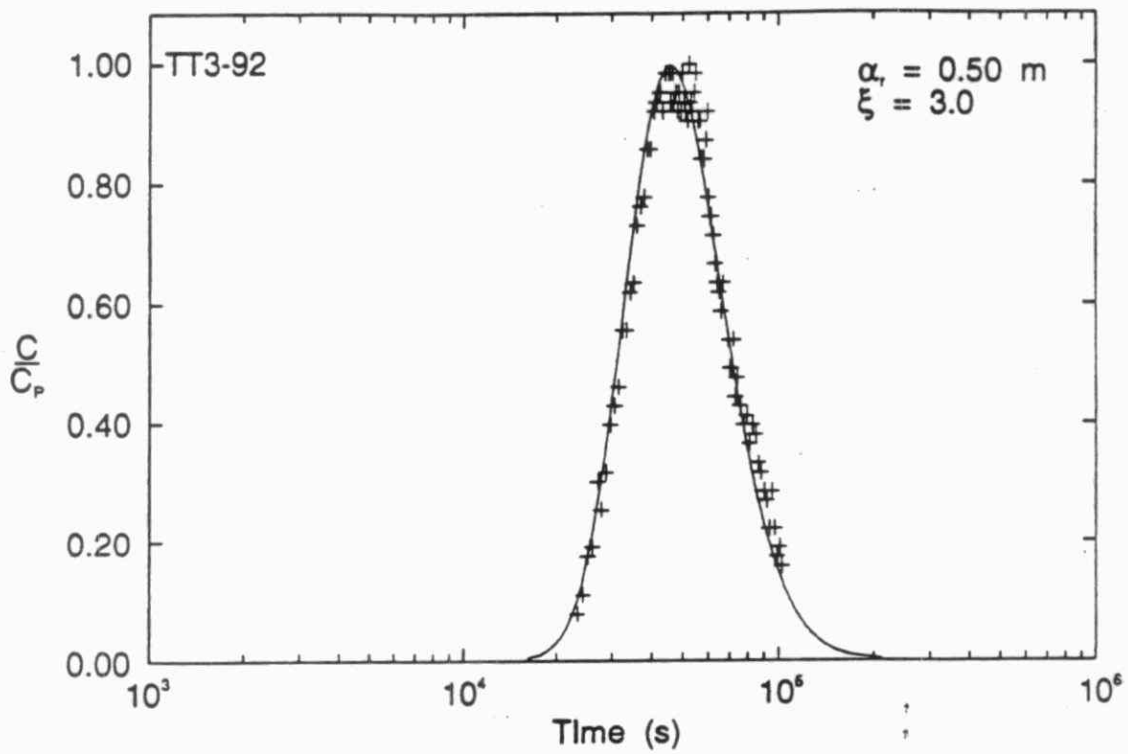

Figure 8: Type curve match to field breakthrough curve for a tracer experiment conducted using a radially convergent flow format.

Table 5: Summary of results from type-curve analyses of tracer experiments conducted in 1991 and 1992 in a radially convergent flow format.

Test I.D.	Obser-vation Well	Source Well	r_i (m)	Q (ml/ min)	ΔH (m)	ξ	θ_m	α_r (m)	$2b_Q$ (μm)	$2b_{\Delta H}$ (μm)
TT3-91	UW2	UW14	5.42	360	0.03	6	0	0.08	213	1123
TT6-91	UW2	UW19	5.55	109	0.14	7	0	0.08	301	241
TT7-91	UW2	UW19	5.55	276	0.39	9	0	0.08	257	249
TT1-91	UW2	UW19	5.55	280	0.33	7	0	0.09	393	220
TT8-91	UW2	UW19	5.55	594	0.78	9	0	0.08	287	244
TT9-91	UW2	UW19	5.55	910	1.22	7.5	0	0.06	283	243
TT3-92	UW2	UW1	15.03	565	0.77	3	0	0.50	546	190
TT2-92	UW2	UW1	15.03	761	1.10	2	0	0.20	421	211
TT5-91	UW2	UW1	15.03	923	1.30	4	0	0.10	422	213
TT4-92	UW4	UW5	30.07	785	1.35	1	0	0.85	576	174
TT4-92	UW4	UW5	30.07	785	1.35	1	0.05	0.40	266	257

Several tests were conducted between identical borehole pairs at varying withdrawal rates to examine the role of velocity in the determination of dispersivity and aperture. Experiments conducted between boreholes 5.55 m apart at flow rates ranging from 100-900 mL/min show dispersivities ranging from 0.09-0.06 m with increasing velocity. Apertures based on flow ($2b_Q$) show a range between 257-301μm while apertures based on hydraulic head ($2b_{\Delta H}$) show a range between 220-249 μm. The apertures based on hydraulic head are insensitive to flow rate and agree with the hydraulic aperture calculated at the source well (248 μm). The experiments conducted at a spacing of 15 m show a decrease in dispersivity from 0.5 m to 0.1 m with increasing velocity from 565 mL/min to 923 mL/min. Apertures based on flow decrease with increasing flow rate (546-421 μm) whereas the converse is true for apertures based on hydraulic head (190-213 μm). The apertures based on flow are about 100%

larger than the hydraulic apertures while the apertures based on hydraulic head agree with the source well hydraulic aperture (221 μm). These results suggest that the effect of increasing average velocity on the determination of aperture and dispersivity is counter-intuitive (ie. dispersivity decreasing with velocity rather than increasing). Considering the possible effects of matrix diffusion, however, this trend can be explained. Where velocity is highest, average travel time is shortest and less time is available for the reduction of concentration due to matrix diffusion. Where velocity is slower, matrix diffusion influences the shape of the concentration curve such that larger apparent dispersion is observed. Independent verification of matrix diffusion is required to confirm this.

The results of the tracer experiments conducted using a radially divergent flow format are shown in Table 6. A type curve matching procedure similar to that described for the radial convergent tests was used (Figure 9). Fits obtained using normalized concentration where $\theta_m = 0$ shows dispersivity (α_r) increasing with radial distance from 0.09 to 0.70 m. Generally apertures based on flow are greater than hydraulic apertures while apertures based on hydraulic head agree more closely with hydraulic apertures. Using field concentrations, the type curves considering only α_r, overestimate the field data, suggesting that other dispersive processes must be incorporated. Fits using C/C_o where $\theta_m > 0$ were obtained by adjusting both α_r and θ_m. In general, the value of α_r influences the rising limb of the curve and θ_m affects the tail. Increasing θ_m at a given α_r lowers the peak concentration and delays the arrival of concentration at later time. The estimates of α_r range from 0.02-0.08 m and θ_m ranges between 0.039 and 0.12. An independent laboratory measurement of porosity in a core sample from this site yielded a porosity of 0.07 (Johnson, pers. comm.). Apertures based on flow are less than hydraulic apertures while apertures based on hydraulic head are greater than hydraulic

Table 6: Summary of results from type-curve analyses of tracer experiments conducted in 1991 in a radially divergent flow format (UW2 is the source well in all tests).

	Test I.D.	Obser-vation Well	r_i (m)	α_r (m)	θ_m	τ	$2b_Q$ (μm)	$2b_{\Delta H}$ (μm)	$2b_{CH}$ (μm)
Fit #1: C/C_p, $\theta_m=0$	RD1[a]	UW19	5.55	0.02	0	1	960	n/a	248
	RD2	UW19	5.55	0.1	0	1	351	n/a	248
	RD2[b]	UW4	14.95	0.35	0	1	273	n/a	220
	RD3	UW24	5.30	0.30	0	1	277	190	154
	RD3	UW14	5.42	0.20	0	1	127	396	241
	RD3	UW19	5.55	0.20	0	1	357	175	248
	RD3	UW11	7.41	0.09	0	1	550	152	126
	RD3	UW22	11.75	0.35	0	1	218	221	282
	RD3	UW05	15.13	0.70	0	1	469	227	226
Fit #2: C/C_o, $\theta_m>0$	RD2	UW19	5.55	0.04	0.093	1	244	n/a	248
	RD2[c]	UW4	14.95	0.08	0.039	1	183	n/a	220
	RD3	UW24	5.30	0.02	0.119	1	139	267	154
	RD3	UW14	5.42	0.02	0.094	1	123	403	241
	RD3	UW19	5.55	0.02	0.125	1	167	256	248
	RD3	UW11	7.41	0.02	0.127	1	184	263	126
	RD3	UW22	11.75	0.04	0.048	1	116	303	282
	RD3	UW05	15.13	0.04	0.077	1	117	455	226
Fit #3: C/C_o, $\theta_m>0$, $\tau>1$	RD2	UW19	5.55	0.15	0.025	1.53	149	n/a	248
	RD3	UW24	5.30	0.05	0.064	1.32	104	319	154
	RD3	UW14	5.42	0.02	0.055	1.29	92	477	241
	RD3	UW19	5.55	0.18	0.018	2.16	67	436	248
	RD3	UW11	7.41	0.05	0.026	2.16	65	474	126
	RD3	UW22	11.75	0.05	0.025	1.36	75	387	282
	RD3	UW05	15.13	0.07	0.028	1.65	70	610	226
Fit #4: C/C_p, $\theta_m>0$	RD2	UW19	5.55	0.08	0.05	1	292	n/a	248
	RD3	UW24	5.30	0.25	0.020	1	259	196	154
	RD3	UW14	5.42	0.08	0.025	1	186	328	241
	RD3	UW19	5.55	0.15	0.018	1	317	186	248
	RD3	UW11	7.41	0.08	0.025	1	464	166	126
	RD3	UW22	11.75	0.25	0.010	1	163	256	282
	RD3	UW05	15.13	0.25	0.025	1	285	291	226

[a]$\xi=7$, [b]$\xi=2.5$, [c]$\xi=4$
n/a-not available

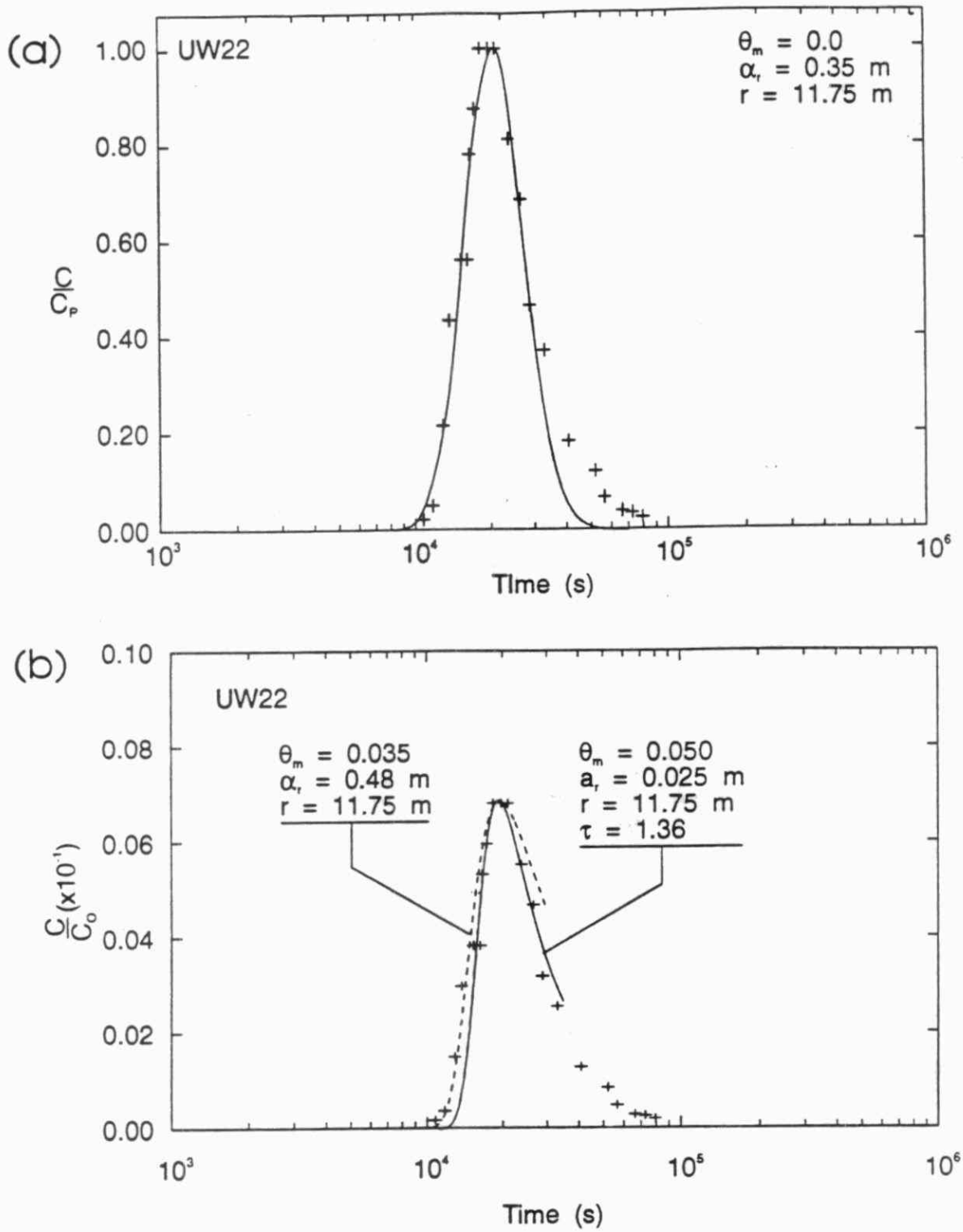

Figure 9: Type curve match to field breakthrough curve for a tracer experiment conducted using a radially divergent flow format: (a) C/C_p vs time, $\theta_m=0$ (Fit #1), (b) C/Co vs time, $\theta_m>0$ (Fit #2) and $\theta_m>0$, $\tau>1$ (Fit #3).

apertures. Fits were also obtained where tortuosity, τ, was simulated by increasing the radial distance between the wells. Tortuosity ,τ, is the ratio of flow path length to distance along the macroscopic gradient. For this fit α_r, θ_m and τ are used as fitting parameters. These results show porosity ranging from 0.018-0.064 and dispersivity ranging from 0.02-0.18 m. Tortuosity ranges from 1.32-2.16. Apertures based on flow are less than hydraulic apertures while apertures based on hydraulic head are greater than hydraulic apertures. With reference to the latter fits, the radially divergent tracer experiments show that diffusion into the matrix and tortuosity may act as significant processes of dispersion even at short radial distances and in tests of short duration. The scale effects observed in the dispersion coefficient are eliminated when diffusion into the matrix and tortuosity are considered.

Laboratory Studies

The results of the tracer experiments carried out in the artificial fracture are presented in Appendix B. Based on the visualization of the flow using red dye, it was observed that most of the mass was transported along a channel about 0.30 m wide and 1.4 m long, transversely oriented in the fracture plane. Interpretations of the experimental data using the channel dimensions were compared to interpretations using the full dimensions of the fracture plane. Estimates of both velocity and dispersivity are lower when the dimensions of the fracture plane are used as compared to using only the channel dimensions. Apertures calculated from the cubic law showed that when the channel dimensions were used, the calculated aperture matched the physical value (the thickness of the shims, 0.75 mm) but when the full dimensions of the plane was used the average 2b was only 2/3 of the expected value. An order of

magnitude difference between the calculated dispersivities was also observed. This suggests that the geometry of flow through the fracture plane can strongly influence the dispersive properties of the media. A comparison of tests conducted using small and large test interval volumes showed larger dispersivities are observed using the smaller test volumes. This result is opposite to what was expected. Visualization of the flow during the smaller volume tests showed a substantial increase in the divergence of the streamlines near the wellbore relative to larger interval volume tests. This may have resulted in flow separation and stagnation near the wellbore-fracture interface causing an increase in dispersive flux into the wellbore. This finding suggests that the one-dimensional mass transport equation will not suffice when used to simulate the two-dimensional dispersive effects around a wellbore.

Modelling Studies

The modelling studies undertaken in this study improve the interpretation of well tests carried out in fractured rock of low storativity. This was accomplished by examining the inner boundary conditions which can significantly influence the results of aquifer tests in this media. A theoretical analysis of the effects of radial distance and well bore storage in the interpretation of pulse interference tests showed that the radius of observable response to pulse interference tests can be large in low-storativity formations (Novakowski, 1989). The effects of well bore storage can be substantial and persistent even at large distances from the source well. Error of 35% for transmissivity and 140% for storativity was determined when a model not accounting for well bore storage was used to analyze the results of interference tests which were influenced by well bore storage.

SUMMARY

The conclusions from the field, laboratory and modelling investigations completed during this study are as follows:

1. The flow systems in discretely fractured shale at shallow depths are characterized by skewed aperture distributions and greater than 20% closure of the fracture planes. These large areas of closure significantly influence flow and solute transport through the fracture plane.

2. The development of new field methods such as the short-interval packer technique are necessary for the detailed field characterization of single fractures. The development of the sampling packer device eliminates the standing water volume in observation wells. This significantly improves the accuracy of the estimate of true concentration in discrete fractures.

3. Long-term monitoring of hydraulic head in a single fracture shows substantial variations due to seasonal and barometric effects. Hydraulic gradients across the site range from 0.001-0.004. Difficulties in measuring hydraulic head in low gradient fractured rock systems are a result of the lack of transducer sensitivity and difficulties related to maintaining a sealed system. Measuring accurate hydraulic gradients in this type of groundwater flow system remains an unresolved problem.

4. Experiments in an artificial fracture have shown that divergence of flow resulting in flow separation and stagnation near the wellbore-fracture interface may cause increased dispersive flux into the wellbore and will have implications on future experimental design in both laboratory and field settings.

5. The development of analytical solutions to interpret well tests allows for the incorporation of factors such as well bore storage, and skin zones in order that more realistic values for formation parameters such as fracture aperture and storativity can be determined.

6. Apertures based on hydraulic head which were determined from radially convergent tracer tests agree closely with hydraulic apertures while apertures based on flow overestimate the permeability of the fracture. Because of uncertainty in the meaning of these measurements, the prediction of groundwater velocity in fractured rock is equally uncertain.

7. The methods for tracer experiments developed in this study which includes the reduction of the volume in the test interval and the development of new analytical solutions incorporating wellbore mixing, diffusion and dispersion, will lead to more accurate determinations of the field scale parameters necessary to the prediction of rates of contaminant transport in fractured rock aquifers.

8. To resolve the issues related to solute transport, tracer experiments conducted under conditions of natural flow must be conducted. This will require considerable development of new experimental methods.

ACKNOWLEDGEMENTS

The assistance of the following individuals in various aspects of this study is gratefully acknowledged: L. Benner, G. Bickerton, K. Bouck, S. Brown, Z. Lyall, O. Resler, D. Sullivan, C. Talbot, A. Unger, J. Voralek, and E. Walker.

REFERENCES

Blackport R., E. A. Sudicky and J. A. Cherry, 1986. Evaluation of contaminant velocity in low-permeability fractured shale. In. Proc. Technology Transfer Conference, Ontario Ministry of Environment, Dec., Toronto, Ontario, Canada, pp. 338-348.

Doe, T., J. Osnes, M. Kenrick, J. Geier and S. Warner. Design of well testing programs for waste disposal in crystalline rock.In Proceedings of 6th Congress of the International Society for Rock Mechanics, Montreal, Canada, 1987 .

Doe, T. and Remer J. Analysis of Constant-Head Well Tests in Nonporous Fractured Rock. Third Invitational well-testing symposium-"well testing in Low Permeability Environments", Berkeley California, pp. 84-89, 1980.

Gale, J.E., A. Rouleau and L.C. Atkinson, Hydraulic properties of fractures, In: Hydrogeology of rocks of low permeability, Memoirs, Intern. Assoc. Hydrogeologists, Vol. XVII, Parts 1 and 2, Tuscon, Arizona, pp. 1-16, 1985.

Johnson, H. Personal Communication. Ontario Hydro , Toronto,Ontario.

+ Lapcevic P. A. , K. S. Novakowski and J. A. Cherry, 1990. The characterization of two discrete horizontal fractures in shale, In: Proc. Technology Transfer Conference, Ontario Ministry of Environment, Nov., Toronto, Ontario, Canada.

LeBlanc, D.R., S. P. Garabedian, K.M. Hess, L.W. Gelhar, R.D. Quadri, K.G. Stollenwerk and W.W. Wood, 1991. Large-Scale Natural Gradient Tracer Test in Sand and Gravel, Cape Cod, Massachusetts 1. Experimental Design and Observed Tracer Movement, Water Resources Research, Vol. 27, No. 5, pp 895 - 910.

Mackay, D. M. , D. L. Freyburg, P. V. Roberts, and J.A. Cherry, 1986. A natural gradient experiment on solute transport in a sand aquifer, 1, Approach and overview of plume movement, Water Resources Research, Vol. 22, No. 13, pp 2017-2029.

Novakowski K.S., 1988. Comparison of fracture aperture widths determined from hydraulic measurements and tracer experiments, In Proc: 4th Canadian/American Conference on Hydrogeology, Ed: B. Hitchon and S. Bachu, Nat. Water Well Assoc., Dublin, Ohio, pp.68-80, 1988.

+ Novakowski K.S, 1989. Analysis of pulse interference tests, Water Resour. Res., Vol. 25, No. 11, pp. 2377-2387.

+ Novakowski, K.S. 1990. Analysis of aquifer tests conducted in fractured rock: A review of the physical background and the design of a computer program for generating type curves, Groundwater, **28**: 99-107.

+ Novakowski K.S., and J. A. Cherry, 1988. Evaluating groundwater velocity in a low-permeability fractured shale, In: Proc. Technology Transfer Conference, Ontario Ministry of Environment, Dec., Toronto, Ontario, Canada.

+ Novakowski K.S., and J. A. Cherry, 1989. The effect of wellbore dilution on the results of tracer experiments conducted in fractured rock, In: Proc. Technology Transfer Conference, Ontario Ministry of Environment, Dec., Toronto, Ontario, Canada.

Raven, K.G. and J.E. Gale, Water flow in a natural rock fracture as a function of stress and sample size, Int. J. Rock Mech. Min. Sci. & Geomech. Abstr., Vol. 22, No. 4, pp. 251-261, 1985.

Raven, K.G., Hydraulic characterization of a small ground-water flow system in fractured monzonitic gneiss, Nat. Hyd. Res. Inst. scientific series No. 149, paper no. 30, 133 p., 1986.

Raven, K.G., K.S. Novakowski, and P.A. Lapcevic, Interpretation of field tracer tests of a single fracture using a transient solute storage model, Water Resources Research, Vol. 24, No. 12, pp. 2019-2032, 1988.

Tsang, Y.W., The effect of tortuosity of fluid flow through a single fracture, Water Resources Research, Vol. 20, No. 9, pp.1209-1215, 1984.

Tsang, Y.W. and C.F. Tsang, Channel model of flow through fractured media, Water Resources Research, Vol. 23, No.3, pp.467-479, 1987.

+ Unger J. A. 1991 Hydromechanical Behaviour of Fractures at the Clarkson field site In: Proc. Technology Transfer Conference, Ontario Ministry of Environment, Nov., Toronto, Ontario, Canada.

+ Unger J.A. 1990. Fractal geometry of rock fracture surfaces, B.Sc. thesis, University of Waterloo, Waterloo, Ont.

Witherspoon, P.A., J.S.Y. Wang, K. Iwai and J.E. Gale, Validity of the cubic law for fluid flow in a deformable rock fracture, Water Resources Research, Vol. 16, No. 6, pp.1016-1024, 1980.

Yeh, T.-C., A review of the scale problem and applications of stochastic methods to determine groundwater travel time and path, Technical Report No. HWR 89-010, University of Arizona, 252 pp., 1989

+ Publications supported by this research project

APPENDIX A

Progress Report : December 1988

MEASURING GROUNDWATER VELOCITY AND HYDRODYNAMIC DISPERSION IN A SINGLE FRACTURE

Progress Report, December 1988

Environment Ontario Grant No. 393G

Principal Investigator: John A. Cherry

Co-Investigators: C.W. Mase

E.A. Sudicky

K.S. Novakowski

Waterloo Centre for Groundwater Research

University of Waterloo

Waterloo, Ontario

INTRODUCTION

Predictions of groundwater velocity and hydrodynamic dispersion in discrete fractures in fractured rock are currently based on simple conceptual models which describe flow and mass transport by fluid circulation between two parallel and uniform plates. Recent tracer experiments conducted in the field setting (Abelin et al., 1982; Novakowski et al., 1985; Raven et al., 1988; Novakowski, 1988a) have shown that these conceptual models are probably inappropriate due to the heterogeneous character of the surface of natural fractures. Therefore, use of these models may lead to erroneous prediction of groundwater velocity and contaminant dilution (Novakowski, 1988a). The objectives of this study are to investigate the validity of these conceptual models, evaluate the field methods that are employed in conjunction with the conceptual models and to develop new techniques and models with which to more accurately predict groundwater velocity and contaminant dispersion. These objectives are addressed using a combination of detailed field and numerical modelling studies. More background to this study can be found in Novakowski (1988a) and the reports from Environment Ontario Grant No. 214RR. Selection and development of the field site and site characterization were conducted between 1986 and 1988 as part of Grant No. 214RR.

The field site is located in the village of Clarkson about 1.5 km north of the Lake Ontario shoreline. Two discrete horizontal fractures were identified during preliminary drilling at about 9.8 m

and 10.5 m depth in the Meaford-Dundas shale. These fractures were selected as host for the various field comparisons to be conducted. A total of seven N-sized boreholes were drilled to intersect the study fractures. The fractures are laterally interconnected amongst all boreholes but exhibit no interconnection vertically between them.

The following information details the field and laboratory work conducted under OME Grant No. 393G since April 1988. See Novakowski and Cherry (1988) for a summary of the field work conducted up to April 1988 as part of Grant No. 214RR.

SITE CHARACTERIZATION

During May of 1988, six new boreholes were drilled at the field study site in Clarkson, Ontario. The purpose of the new boreholes was to fill in gaps in the existing borehole array. The boreholes were drilled using NQ-3 coring techniques in the vertical direction to depths of 50 to 55 ft. Casing of N-size was emplaced into the upper 0.5 m of bedrock without a grout seal. Figure 1 shows the location of all boreholes within the borehole array. The new boreholes are labelled 8 to 13. The core obtained during drilling was field logged, photographed and packaged for indoor storage. The new boreholes were surveyed in to the existing survey grid.

Following completion of drilling, the exact locations of the fracture intersections were determined in each borehole using constant-head test methods. The constant-head tests were conducted

using a packer spacing of about 0.5 m with a 0.40 m overlap for each test. A profile of fracture flux ($Q/\Delta H$) with a 0.10 m resolution was obtained in this way. For more detail on the constant head test methodology see Novakowski (1988a). Table 1 shows the aperture widths of both the upper and lower fractures determined from the fracture flux obtained from those tests where a fracture intersected the test interval. Values of <10 μm are below the measurement limit of the test apparatus. Results for all the boreholes are shown. Figure 1 also shows contours of the aperture widths for the lower fracture.

Table 1. Summary of fracture aperture widths (in micrometers) as determined from the results of the constant head tests.

Bore Hole	Upper Fracture 2b (μm)	Lower Fracture 2b (μm)
UW1	69	229
UW2	34	236
UW3	135	<10
UW4	52	186
UW5	26	164
UW6	75	76
UW7	120	57
UW8	52	<10
UW9	12	152
UW10	10	<10
UW11	80	145
UW12	<10	65
UW13	<10	<10
Arithmetic mean	53	104

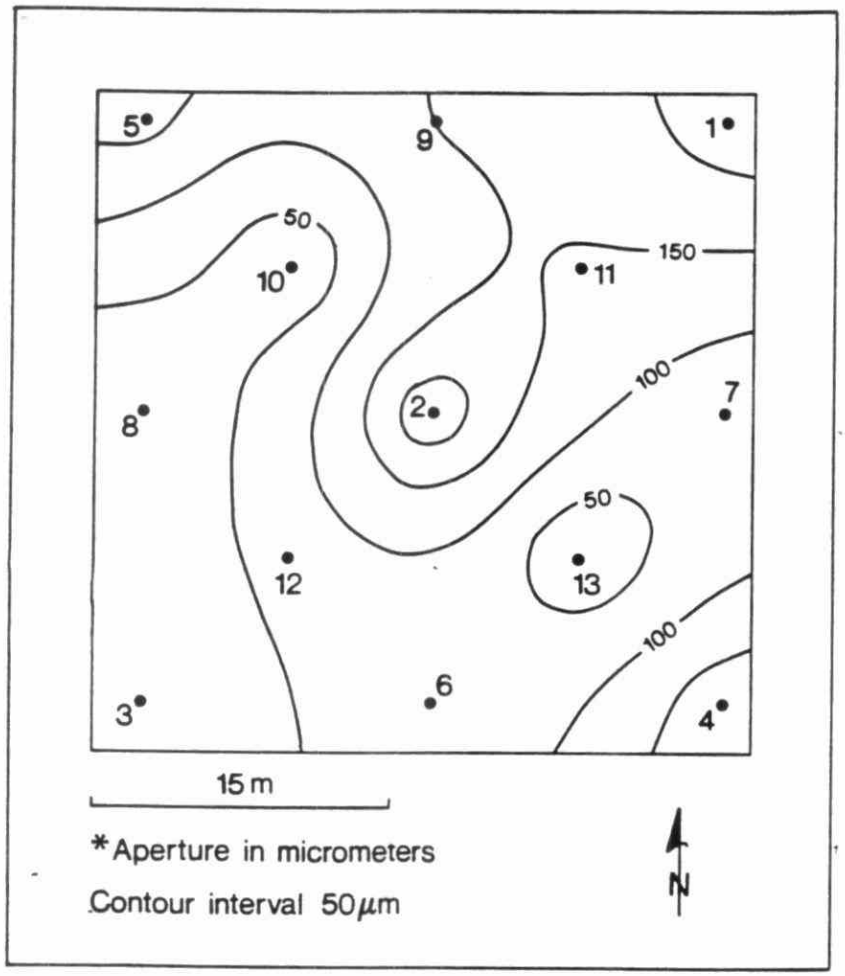

Figure 1. Location of the site boreholes in plan view and contours of the fracture apertures as determined from the constant-head tests.

During September and October, pumping tests were conducted in both the upper and the lower fractures. Both fractures were isolated during the tests using triple-packer apparatus designed and built for these boreholes. Standpipes of ½" ID were used to access the isolated intervals for water level measurement. Pumping was conducted from boreholes UW2 in the lower fracture and UW3 in the upper fracture using a low-capacity gear pump. Flowrate was monitored using a turbine flowmeter and by manual measurement. In six of the boreholes the standpipes were replaced by pressure transducers to provide a continuous and accurate record of drawdown measurement. The transducer measurements were recorded digitally on computer. Drawdown was measured by electric water level tape in all other intervals. Flowrates ranged from 300 to 450 mL/min. On the basis of the measured responses, no discernible vertical connection is evident between the two fractures.

The pumping tests were analysed using standard Theis analysis to obtain transmissivity (T) and storativity (S). Fracture aperture was determined from T following the method given in Novakowski (1988a). Table 2 shows the results of the pumping tests for both the upper and lower fractures expressed as fracture aperture width in micrometers. In general, the apertures determined from the pumping tests are much larger than those determined from the constant head tests. This suggests that the reduced fracture apertures identified using the constant-head methods are likely very small in area and thus flow patterns in the fracture plane may be very tortuous.

Table 2. Results of the pumping tests conducted in boreholes UW2 and UW3.

Borehole	Upper Fracture[+] 2b (μm)	Lower Fracture[x] 2b (μm)
UW1	174	217
UW2	153	-
UW3	-	127
UW4	151	-
UW5	-	213
UW6	140	231
UW7	188	202
UW8	127	224
UW9	-	213
UW10	160	144
UW11	181	243
UW12	-	-
UW13	-	-
Arithmetic mean	159	202

[+] Pumping borehole - UW3
[x] Pumping borehole - UW2

Pulse interference tests were also conducted to determine inter-borehole apertures in the lower fracture. These tests were conducted by monitoring the response in an observation well to a slug test (Cooper et al., 1967) carried out in a source borehole. Wells UW1, UW2, UW4 and UW5 were used as source boreholes with observation in boreholes UW1, UW2, UW4, UW5, UW9, and UW11. Initial head rise in the source borehole averaged about 6.2 m and the decline in hydraulic head in the source well and response in the observation boreholes were continuously monitored using pressure transducers and recorded digitally on computer.

The results of the pulse interference tests conducted in the lower fracture were analysed using a type-curve method (Novakowski, 1988b) and are shown in Table 3 as fracture aperture widths expressed in micrometers. Similar results are found in comparison to the results of the pumping tests shown in Table 2. It is interesting to note that in cases where the source and observation wells are exchanged for repeat tests, virtually the same result is obtained independent of direction. The reason for this is somewhat unclear, however, the suggestion is that the fracture plane is of relatively uniform character and the variation in fracture aperture as observed using the constant-head methods are relatively small in area (this is in agreement with the pumping test result). Therefore, the results of constant-head tests when used alone, may lead to very erroneous predictions of groundwater velocity and direction.

Table 3. Summary of the fracture apertures obtained from the pulse interference tests conducted in the lower fracture+.

		Source Boreholes			
		UW1	UW2	UW4	UW5
Observation Boreholes	UW1	-	225	195	225
	UW2	225	-	220	235
	UW4	223	225	-	-
	UW5	225	112	187	-
	UW9	220	225	-	228
	UW11	263	238	249	277

+in micrometers

Upon completion of the hydraulic tests, the triple-packer apparatus were left in place so that an accurate measure of the natural distribution of hydraulic head could be obtained. Water level measurements were collected at least bi-weekly over a period of six weeks. The results show that pressures induced in some low-permeability intervals by the shut-in procedure require a considerable length of time to decay away. Figure 2 shows the hydraulic head distribution (masl) in the lower fracture using water levels obtained from boreholes UW1, UW2, UW4, UW5, and UW7. The water levels from these boreholes were selected because the apertures as determined from the constant-head tests are the largest in the borehole array and are most likely to reflect the macroscopic gradient. According to these measurements, the macroscopic gradient is oriented towards the northwest at an approximate magnitude of $3x10^{-3}$. Considering that the regional hydraulic gradient is probably oriented southwards toward Lake Ontario, this suggests that this fracture is poorly connected to the regional flow system. In fact, the macroscopic gradient in the upper fracture is oriented in a much different direction and shows no evidence of connection to the lower fracture. The hydraulic head in the upper fracture is about 2 m higher than that in the lower fracture. This has significant ramification in terms of predicting contaminant migration at waste sites. For example, suppose open piezometers were completed in boreholes UW3 and UW5 so that both fractures intersected the completed interval. The hydraulic head in UW3 would tend to equilibrate towards the head in the upper fracture

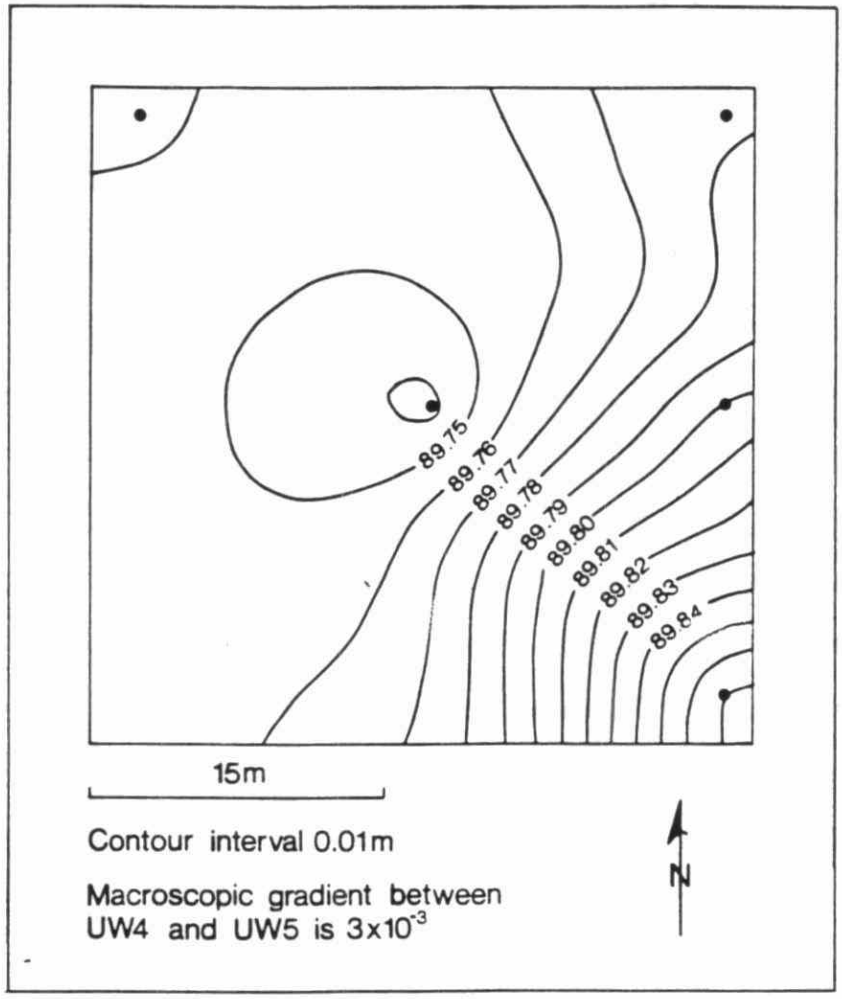

Figure 2. The hydraulic head distribution in metres above sea level for the lower fracture. The symbols indicate the boreholes from which the water level data was obtained.

while the head in UW5 would equilibrate towards that in the lower fracture, erroneously suggesting groundwater flow in a northerly direction under a very large hydraulic gradient. Measurement of hydraulic head in both fractures will continue with the intent to verify these initial findings.

DEVELOPMENT OF FIELD METHODS

The triple-packer apparatus employed for the hydraulic tests and the gradient measurements will also be used for a preliminary tracer experiment to be conducted January 1989. The design of the packers is such that a minimum volume between packer seals can be achieved. The packers are manufactured of polyvinylchloride with two ½" ID plastic feedthroughs. A solid mandril is employed to prevent gland pinch. Inflation is by nitrogen pressure through ¼" nylon tubing from a surface pressure source. With a minimum packer spacing of about 0.10 m, a test interval volume of 0.30 L can be achieved. Plate 1 shows an example of this in straddle-packer configuration. Variable packer spacings are obtained by using nylon tubing to interconnect each packer element. Currently, obtaining a patent for the packer design is being considered.

In preparation for the natural gradient tracer experiment, tracer injection and tracer sampling methodologies were designed. Figure 3 shows both methodologies schematically. Tracer injection will be achieved by pumping a small volume of tracer into the fracture

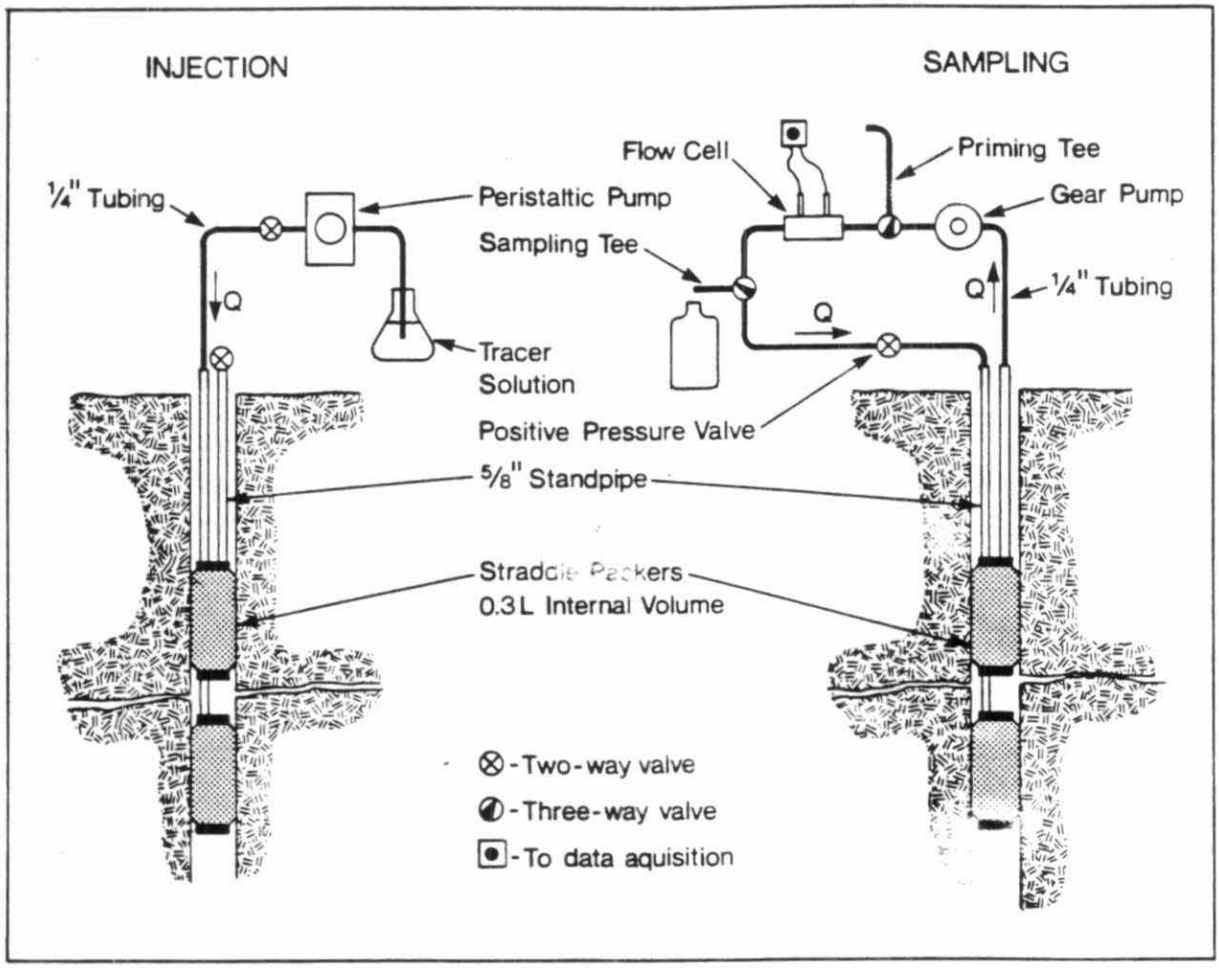

Figure 3. The tracer injection and sampling methodology to be employed during the natural gradient experiment.

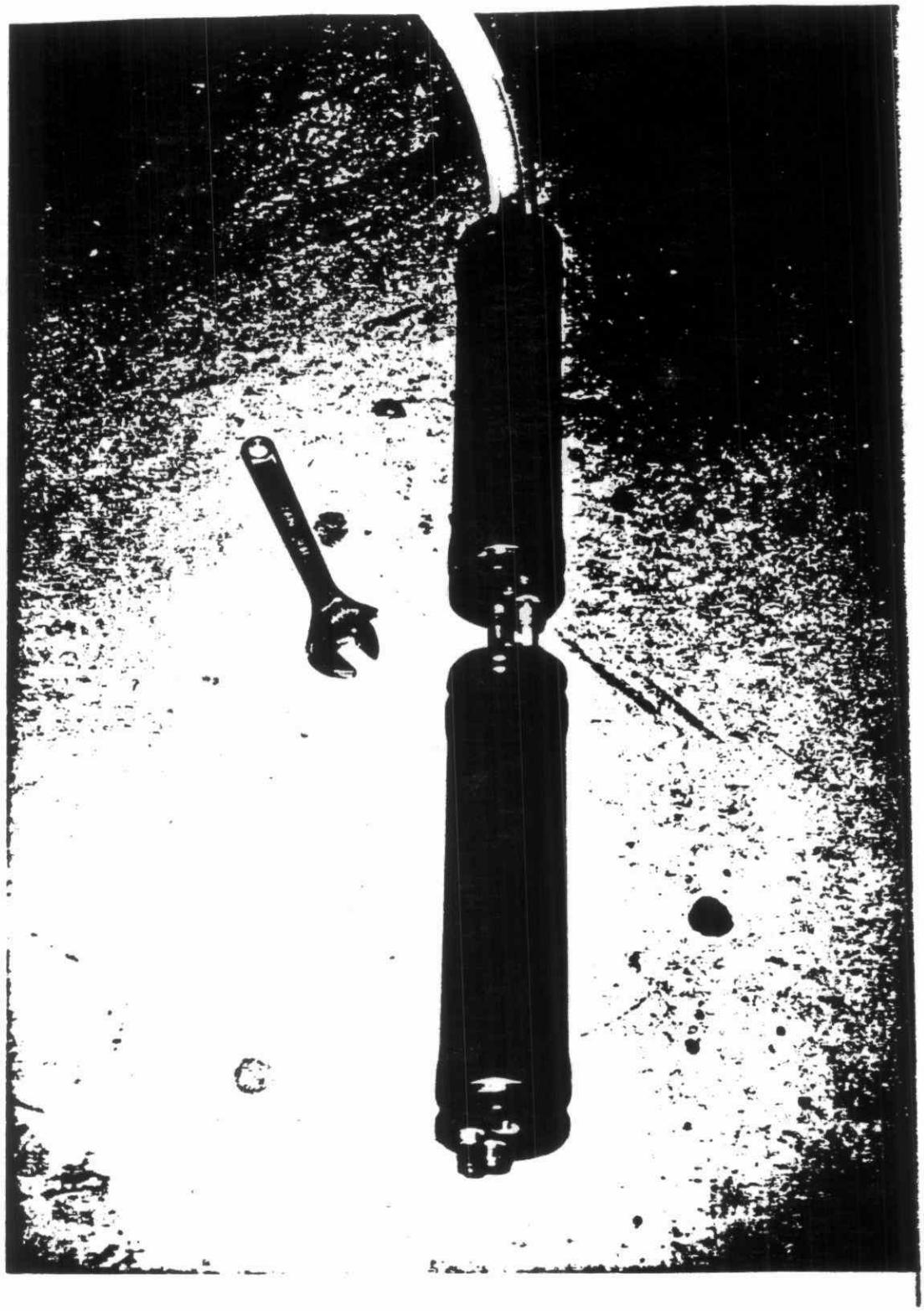

Plate 1. The packer elements in straddle-packer configuration with minimum interval volume.

plane followed by enough chaser fluid to displace any remaining tracer from the test interval into the fracture plane. Sampling for the arrival of tracer at observation wells will be conducted using a recirculation technique. Referring to Figure 3, groundwater will be initially drawn up through a gear pump head using a peristaltic pump and then a continuous flow system will be established by re-injecting the withdrawn water. The flow system will be driven by the gear pump. Continuous measure of the tracer concentration will be achieved using a flow cell. Discrete samples will be obtained from a sampling tee. In both the injection and sampling methodology, ¼" nylon tubing is employed to carry the groundwater.

The injection and sampling methodology as depicted in Figure 3 will be tested in an artificial fracture apparatus. Plate 2 shows a view of the artificial fracture which was designed and manufactured during September and October, 1988. The apparatus consists of two plexiglass plates about 1 m square and 3/8" thick lying together on an aluminum table. The plates are separated by 0.01 m square shims of 0.75 mm thickness interspersed about the plate surfaces to form the open fracture. Two of the sides are sealed and the other two sides are connected to constant-head boxes about 0.10 m high and 0.05 m deep. A uniform flow field can be established between the boxes by regulating the hydraulic head in each box. An artificial borehole and two measurement ports for measuring concentration are placed across the fracture plane mid-way between the boxes. Several configurations of tracer injection and withdrawal can be tested with this apparatus.

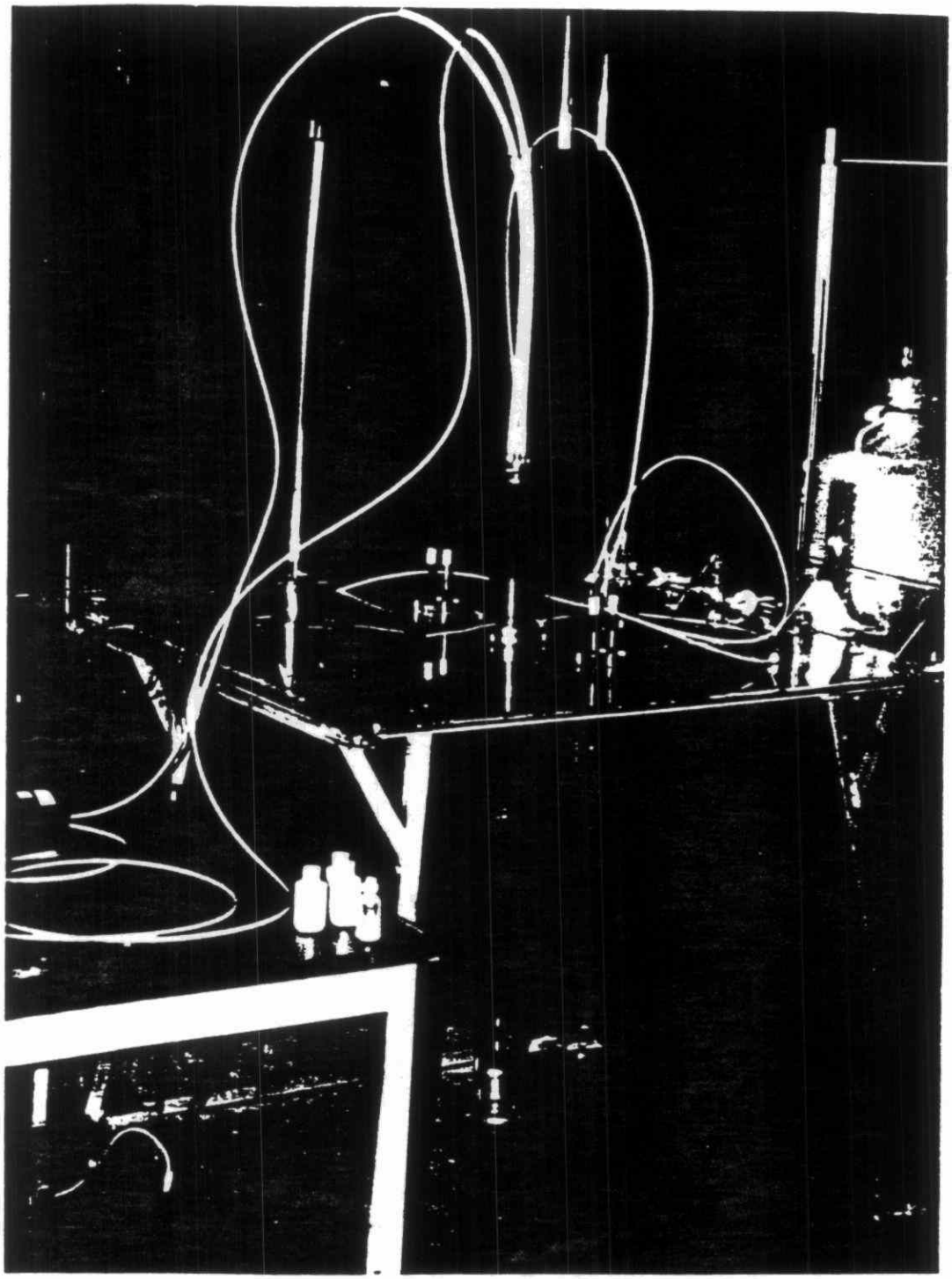

Plate 2. The artificial fracture apparatus.

DEVELOPMENT OF ANALYTICAL METHODS

During the review period considerable effort was also placed on developing new analytical methods in support of the field testing program. A computer program which numerically inverts analytical solutions from the Laplace domain was developed and tested. This program can be employed to analyse the results of pumping tests and pulse interference tests affected by wellbore storage in the source or pumped well, wellbore storage in both the source and observation wells, infinitesimally thin skin and finite-thickness skin. The program is designed to be user friendly and is easily modified to accommodate additional solutions. A review of the theory and a description of the program is given in Novakowski (1988b).

In addition, a composite analytical model was developed for analysing the results of pumping tests affected by wellbore storage and finite-thickness skin. The governing equations were solved using the Laplace transform method for dimensionless drawdown in the pumped well, observation well and the formation. A sensitivity analysis was conducted to determine the effect of finite-skin thickness, the magnitude of the influence of the wellbore storage coefficient and the effect of radial distance on the results of pumping tests. This model was included in the aforementioned computer program and is described in detail, including the solution method, in Novakowski (1988c).

An analytical model accounting for wellbore storage in the observation well was also developed for analysing the results of pulse interference tests. As with the pumping test problem, the solution is found in the Laplace domain for dimensionless hydraulic head in the source well, observation well and formation. The effect of observation well storage and radial distance were determined by generating type curves using various wellbore storage coefficients at different radial distance. A field example was also analysed to illustrate the use of the analytical model and to provide a comparison between the field case where observation well storage is present to that where it is not. The analytical model is described in Novakowski (1988d).

FUTURE WORK

To begin January 1, 1989:

1. Natural Gradient Tracer Experiment

   A natural gradient tracer experiment will be conducted when hydraulic head has equilibrated in the lower fracture. A KBr ionic tracer and a fluorescent dye will be injected into the lower fracture from the central borehole UW2. Tracer arrival at the observation wells will be monitored on a continuing basis until stable background concentrations indicate complete passage of the tracer plume.

2. Experiments with the Artificial Fracture

A detailed assessment of the injection and sampling method will be initiated in early January. Several experiments will be conducted using the artificial fracture in which the volume of the straddle-packer interval is varied. The injection method will be studied by injecting tracer into the artificial borehole and monitoring tracer arrival in the downstream constant-head box. These experiments will be modelled using a new analytical model developed by Allen Moench (Water Resour. Res., in press).

3. Numerical Modelling

The numerical modelling of uniform and radial flow in a fracture of random aperture width will be initiated. The intent of the modelling is primarily to support the field testing results by simulating these results with realistic properties of the test fracture. In addition, the modelling will be used to develop new conceptual models which help explain the contradictory field results often observed in detailed studies of fluid flow in natural fractures. The fracture surfaces will be represented using both fractal and stochastic methods. Numerical simulation of flow and transport will be conducted at the microscopic scale using the program FRACTRAN developed by E. Sudicky.

REFERENCES

Abelin, H., J. Gidlund and I. Neretnieks, Migration experiments in a single fracture in the Stripa Granite: Preliminary results, In: Proc. Workshop on the Geol. Disp. Rad. Waste, Nuclear Energy Agency of the Organization for Economic Cooperation and Development, Paris, pp. 154-163, 1983.

Cooper, H.H., Jr., J.D. Bredehoeft and I.S. Papadopolus, Response of a finite diameter well to an instantaneous charge of water, Water Resour. Res., 3(1), 263-269, 1967.

Novakowski, K.S., Comparison of fracture aperture widths determined from hydraulic measurements and tracer experiments, In: Proc. 4th Canadian/American Conf. Hydrogeol., Banff, Alta, June, 1988a.

Novakowski, K.S., A computer program to generate type curves for well testing problems in fractured rock, Groundwater, in submittal, 1988b.

Novakowski, K.S., A composite analytical model for analysis of pumping tests affected by wellbore storage and finite thickness skin, Water Resour. Res., in submittal, 1988c.

Novakowski, K.S., An analytical model for pulse interference tests affected by wellbore storage in the observation well, Water Resour. Res., in submittal, 1988d.

Novakowski, K.S., G.V. Evans, D.A. Lever and K.G. Raven, A field example of measuring hydrodynamic dispersion in a single fracture, Water Resour. Res., 21(8), 1165-1174, 1985.

Novakowski, K.S. and J.A. Cherry, Evaluating groundwater velocity in a low-permeability fractured shale, In: Proc. 8th Tech. Transfer Conf., Environment Ontario, Session C, pp. 273-282, Nov., 1988.

Raven, K.G., K.S. Novakowski and P.A. Lapcevic, Interpretation of field tracer tests of a single fracture using a transient solute storage model, Water Resour. Res., 24(12), 1988.

APPENDIX B

Progress Report : June 1989

RRB-89-37

Progress Report, June 1989

Environment Ontario Grant No. 393

Principle Investigator: J.A. Cherry

Co-Investigators: C.W. Mase
E.A. Sudicky
K.S. Novakowski

Report Authored by: K.S. Novakowski

Waterloo Centre for Groundwater Research
University of Waterloo
Waterloo, Ontario

MEASURING GROUNDWATER VELOCITY AND HYDRODYNAMIC DISPERSION IN A SINGLE FRACTURE

May 1989

INTRODUCTION

The purpose of this study is to investigate uncertainty in the accuracy of predictions of the velocity of groundwater flowing in a single fracture. Specifically, the relation between field measurements of fracture aperture width obtained using different measurement techniques are studied. In addition, the relation between the aperture density distribution and hydrodynamic dispersion is investigated in both the field setting and using stochastic simulation methods. The study is conducted at a field site in which a single fracture, oriented horizontally, is characterized using different field methods. Predictions of groundwater velocity based on commonly employed conceptual models are then compared to the results of a natural gradient tracer experiment which should yield the most accurate result.

The purpose of this progress report is to detail the advances made in the last six months with regard to the equipment development required for the natural gradient tracer experiment and to describe recent study site characterization. In addition, the direction of future field, laboratory and modeling work is outlined.

FIELD SITE CHARACTERIZATION

New Boreholes

During May 1989, six additional boreholes were added to the existing borehole grid at the field study site. This brings the total number in the grid area to 19. The new boreholes were located to provide more detail in an area of the study fracture which is believed to be of larger aperture. Also, based on measurements of hydraulic head obtained from the existing holes, it is anticipated that the natural groundwater flow directions may be towards this area of the borehole grid. The locations of the new boreholes are shown on Figure 1. Drilling methods were identical to those employed for the previous drilling programs (see December 1988 progress report). Total depth of the boreholes range from 50 to 55 feet.

Following completion of the drilling, constant-head hydraulic tests were conducted along the length of each borehole using a 2-m packer spacing. A detailed characterization was also conducted in each borehole to determine the exact location of the fracture intersection. These tests were conducted using a packer spacing of 0.10 m. Table 1 shows a summary of the fracture aperture widths for both the upper and lower fractures as determined from the detailed tests conducted in the new boreholes. Upon completion of the hydraulic tests, the new boreholes were instrumented with a double-packer arrangement (see December 1988 progress report) to provide

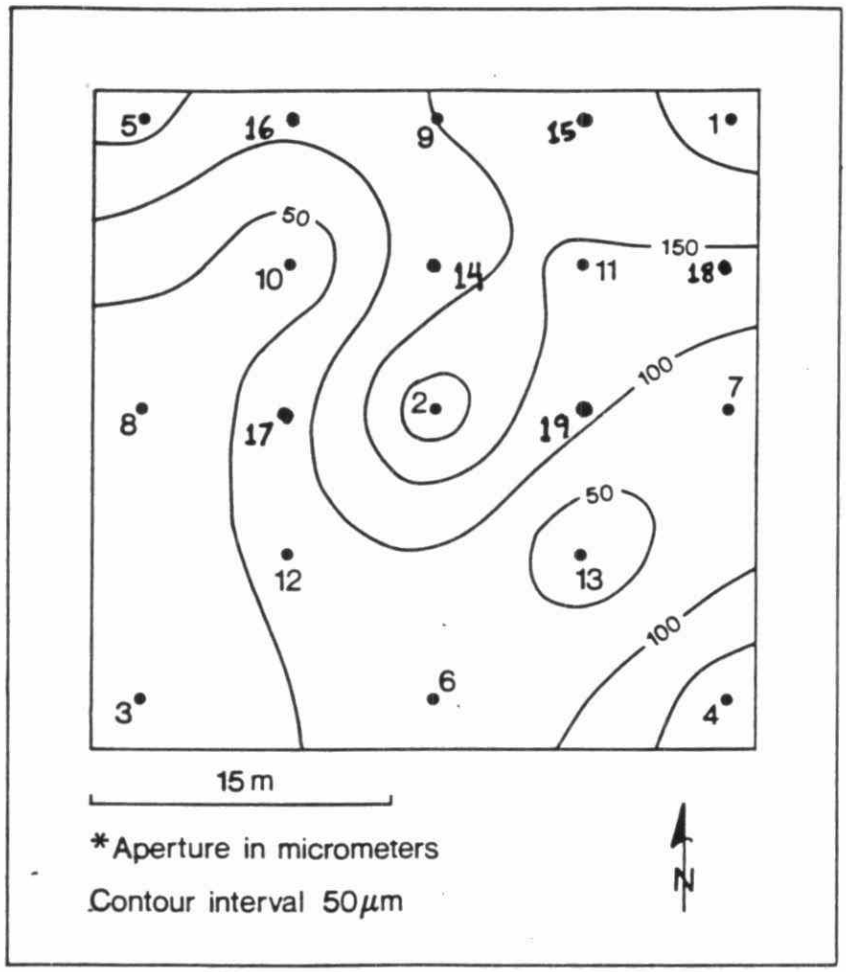

Figure 1. Location of the site boreholes in plan view. The contour values of fracture aperture do not include UW14-UW19.

access for the measurement of accurate water levels during the ensuing summer months.

Table 1. Summary of the fracture aperture widths as determined using constant-head tests conducted in the new boreholes.

Borehole	Upper Fracture 26 (μm)	Lower Fracture 26 (μm)
UW14	105	183
UW15	63	38
UW16	<10	<10
UW17	81	<10
UW18	32+	32+
UW19	<10	209

+Test section interval 9.61-11.38 mbgs

Hydraulic Head Measurements

During the period February-April 1989, water level measurements were obtained from the instrumented boreholes (the boreholes were first instrumented September-October, 1988) on a bi-weekly basis. Figure 2 shows contours of the hydraulic head measurements obtained on March 9, 1989. Borehole UW8 was excluded from the contouring process, due to the presence of anomolously high hydraulic heads suggesting that the water levels in this borehole have not yet reached equilibrium. The hydraulic head measurements shown in Figure 2 suggest that boreholes UW7 and UW10 have also not reached equilibrium although the fracture plane had been isolated for over four months by this time. Because both of these boreholes possess anomolously high hydraulic heads, apparent interwell gradients seem substantial. However, in

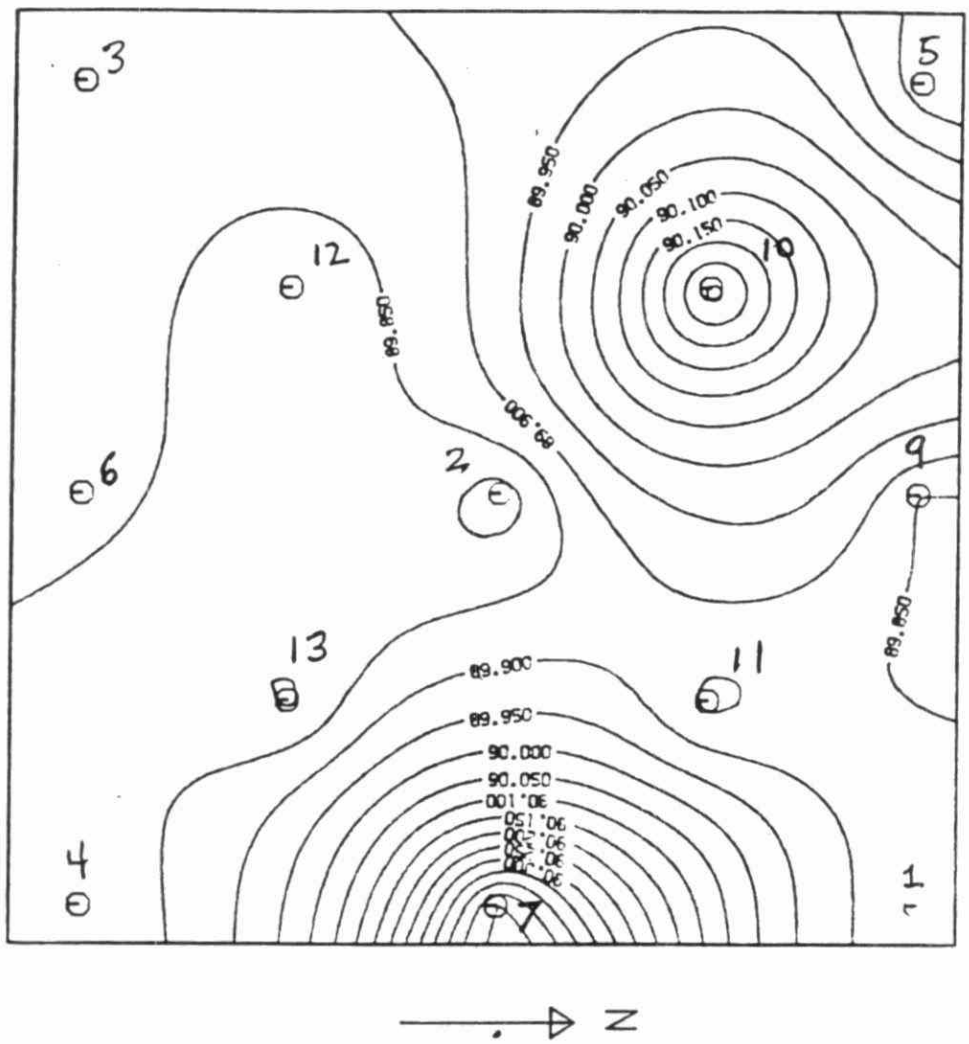

Figure 2. Contours of the hydraulic head measurements obtained on March 9, 1989.

consideration of the diminutive size of the apertures, very little groundwater is flowing from these boreholes towards the zones of lower hydraulic head. Thus, the influence of these hydraulic gradients on the patterns of groundwater flow, is probably minimal. The presence of the high hydraulic heads in boreholes UW7 and UW10 suggests that there may be some leakage past the packers or from the exterior of the packer to the test section.

Spring thaw occurred during the monitoring period, thus providing an opportunity to assess the connection of the fracture plane to the surfacial groundwater environment. Figures 3, 4 and 5 show the response in hydraulic head for all boreholes except UW8. As is evident, the response to spring thaw is rapid and direct suggesting that the fracture plane is well connected to the surface. However, pumping test results show that this vertical connection is not likely to be present within the confines of the study site.

LABORATORY STUDY

Analytical Methods

A literature review was conducted to assess the current state of knowledge regarding wellbore mixing effects incurred during sampling procedures. This is important in determining the technique to be employed for sampling during the natural gradient tracer experiment. The results of the literature review show that minimal research has

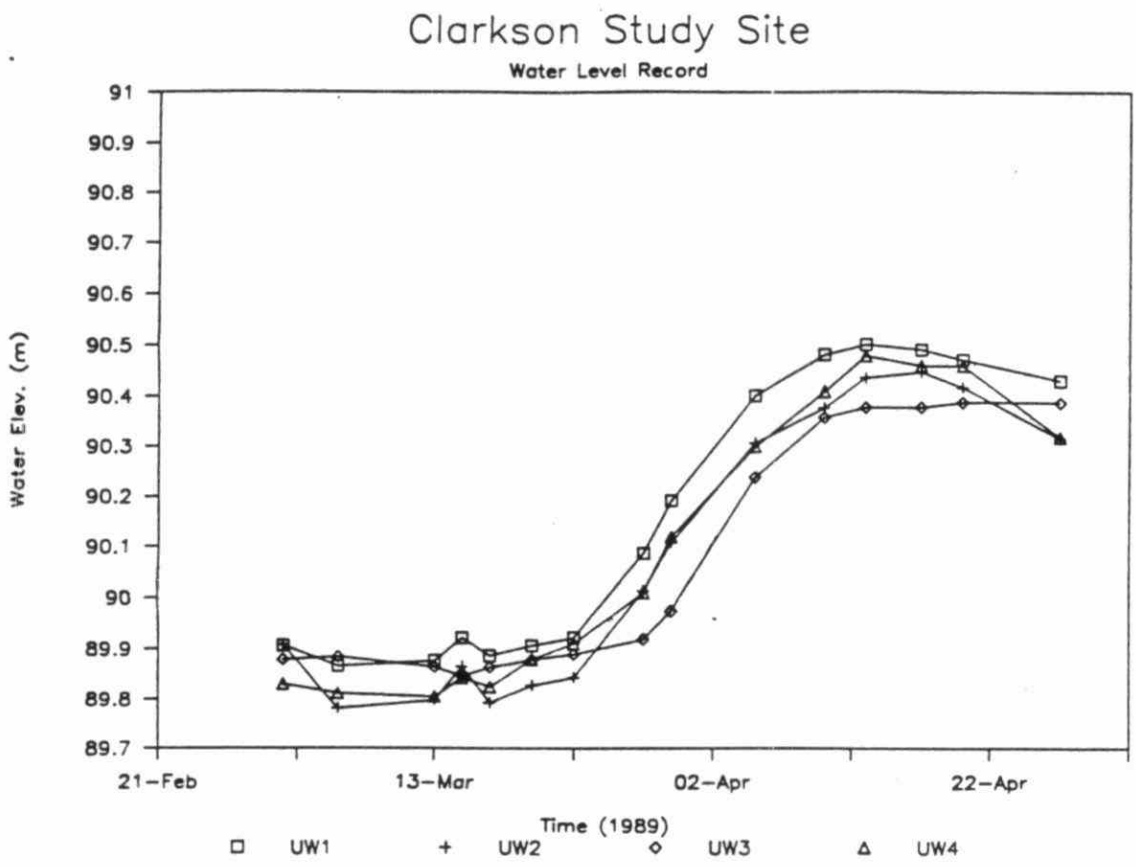

Figure 3. Water levels for UW1-UW4.

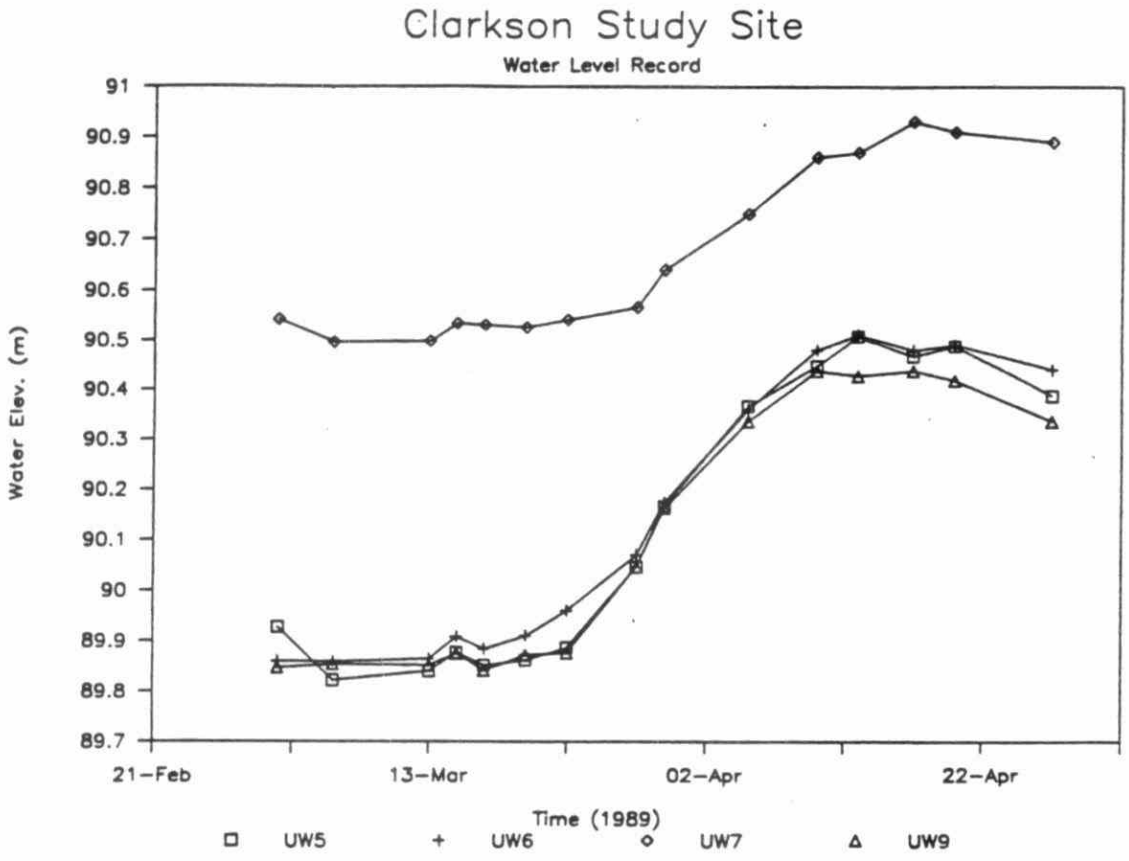

Figure 4. Water levels for UW5-UW9.

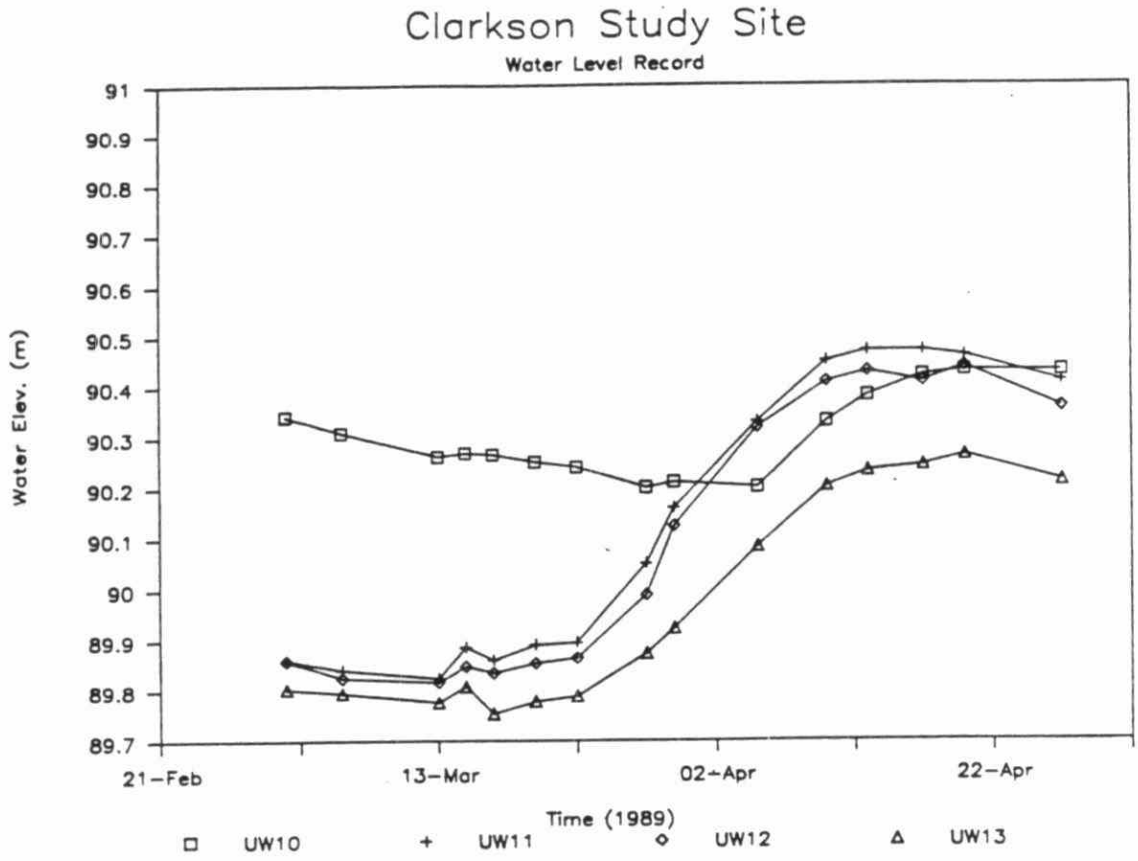

Figure 5. Water levels for UW10-UW13.

been conducted on the effects of mixing in wellbores. Therefore, to analyse the results of the experiments conducted in both the laboratory fracture (see December 1988 progress report) and the field setting, new solutions to the boundary value problem are required. As a means of evaluating sampling techniques to be used in the field experiment, laboratory experiments were initiated. Therefore, the first attempts at detailing boundary conditions for wellbore mixing problems are conducted with the laboratory apparatus in mind.

The laboratory apparatus was designed to provide uniform flow between two boxes in which a constant head could be maintained. A wellbore was placed in the centre of the fracture plane and sampling ports were placed such that concentrations can be determined from both the fracture plane and the wellbore (Figure 6). The boundary value problem (BVP) for these boundary conditions is based on mass transport by steady, uniform flow in a composite medium:

$$\frac{\partial c_1}{\partial t} + \bar{v}_1 \frac{\partial c_1}{\partial x} - D_{L1} \frac{\partial^2 c_1}{\partial x^2} = 0 \qquad 0 \leq X \leq L \tag{1}$$

$$\frac{\partial c_2}{\partial t} + \bar{v}_2 \frac{\partial c_2}{\partial x} - D_{L2} \frac{\partial^2 c_2}{\partial x^2} = 0 \qquad L \leq X \leq \infty \tag{2}$$

where subscripts 1 and 2 denote the upstream and downstream characteristics of the medium, respectively, the wellbore to be sampled lies at $x = L$, $\bar{v}$ is velocity and D_L is hydrodynamic dispersion. Because the concentration, c, is unknown in the wellbore at $x = L$, the BVP

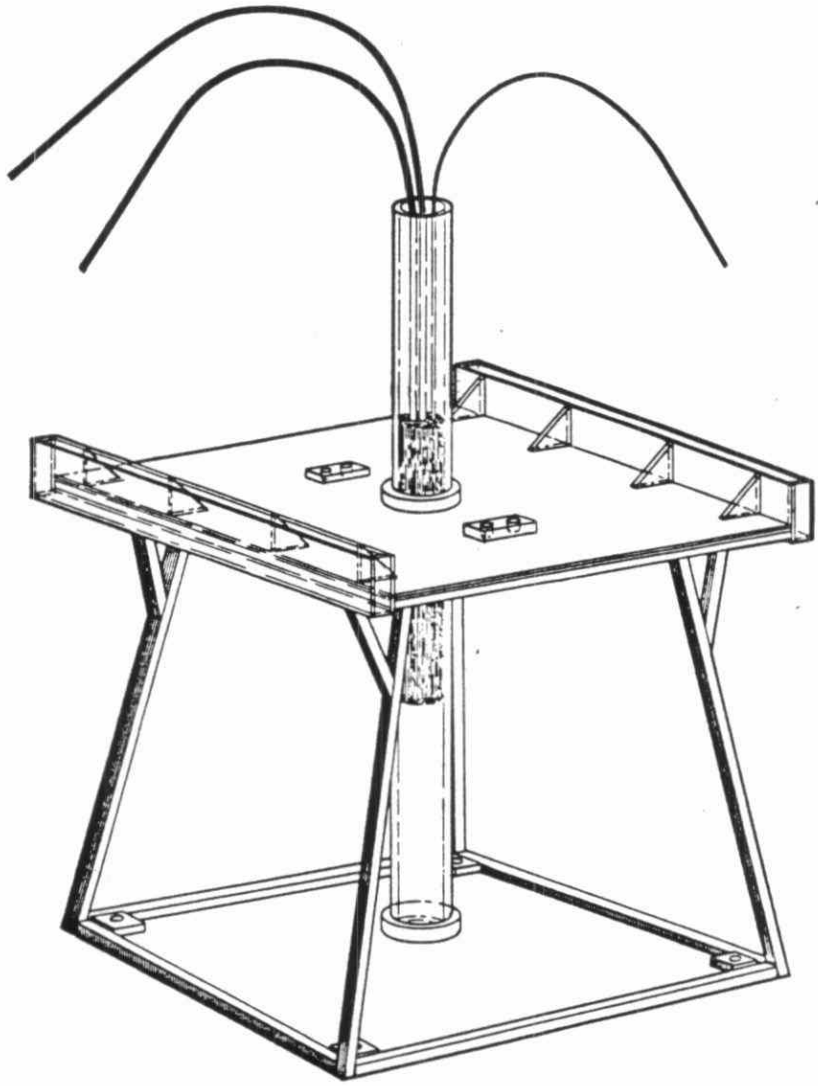

Figure 6. Schematic of the fracture apparatus used for the laboratory tracer experiments.

takes on a form similar to classical Stefan problems (see Crank, 1984). The input boundary condition for (1) is third type and is given as:

$$\bar{v}\, C_0 = \bar{v}\, c_2(0,t) - D_L \frac{\partial c_1}{\partial x}\,(0,t) \qquad (3)$$

where C_0 is the fully mixed concentration in the source box. Equations (1) and (2) are linked by the wellbore in which the concentration is monitored. Assuming complete mixing, the concentration in the wellbore, c_w, located at $x = L$ is given as:

$$\pi\, r_w^2\, h_w \frac{dc_w(t)}{dt} = m_{in} - m_{out} \qquad (4)$$

where $\pi\, r^2_w\, h_w$ is the volume of the interval in which the mixing takes place and m is mass flux. The mass flux, m_{in} and m_{out}, depend on components of advection and hydrodynamic dispersion. The mass flux in and out are given by:

$$m_{in} = \xi \left[\bar{v}\, c_1\,(L,t) - D_{L1} \frac{\partial c_1(L,t)}{\partial x}\right] \qquad (5)$$

$$m_{out} = \xi \left[\bar{v}\, c_2\,(L,t) - D_{L2} \frac{\partial c_2(L,t)}{\partial x}\right] \qquad (6)$$

where ξ is equal to f $2r_w$ 2b and 2b is fracture aperture. The correction factor, f, accounts for the distortion in the flow field resulting from the presence of the borehole. Combining (4)-(6) and re-arranging gives:

$$\frac{1}{\beta}\frac{dc_w(t)}{dt} = \bar{v}c_1(L,t) - \frac{D_{L1}\,\partial c_1\,(L,t)}{\partial x} - \bar{v}c_2(L,t) + D_{L2}\frac{\partial c_2(L,t)}{\partial x} \qquad (7)$$

where β is the mixing coefficient and is given as $\xi/\pi r^2_w h_w$. Continuity is also required across the boundary to provide a closed BVP:

$$c_w(t) = c_1(L,t) = c_2(L,t) \qquad (8)$$

The solution of (1) and (2) with respect to boundary conditions (3)-(8) can be found in a straightforward manner, although a solution has not yet been attempted.

Laboratory Experiments

To date, 14 tracer experiments have been conducted using the laboratory apparatus. The anion Br^- was employed as tracer in all cases. Two different monitoring configurations have, so far, been evaluated. Most of the early experiments were conducted using a 0.10 m packer spacing with an open isolated section. Several of these

experiments were conducted without sampling from the borehole so as to determine the dispersivity of the fracture plane in the absence of recirculation. Experiment 7 was conducted with recirculation in the borehole, but not sampling and the results obtained from the electrode monitoring ports only are interpreted. Experiments 13 and 14 were conducted with the packer spacing reduced and interval volume filled such that the total mixing volume was approximately 5% of that for the preceding experiments.

The experiments were conducted by establishing a steady-flow field between the constant-head boxes and then introducing tracer in the higher-head box in a step-function fashion. The tracer is continuously mixed using a mechanical stirrer, so as to satisfy boundary condition (3). A red dye was added to the water during several of the experiments so that the flow process could be visualized. Measurements of concentration were made using specific ion electrodes in all cases.

The results of the experiments were analysed using the method developed by Palmer (1988) in the case where wellbore samples were analysed and using the Ogata-Banks solution where the results from electrode measurement ports only were interpreted. Based on visualization of the flow, it was observed that most of the mass was transported along a channel about 0.30 m wide and 1.4 m long, transversely oriented in the fracture plane. The simulations were carried using these dimensions as well as the dimensions of the entire plane. Tables 2 and 3 show the results of the simulations (electrode port

data only) using the channel dimensions and the dimensions of the plane, respectively. Substantial difference in the Peclet number and dispersivity between the tables is observed. Although the Peclet numbers are highest using the full dimensions of the plane (and are similar to what would be expected based on existing conceptual models), it is likely that the results obtained using the dimensions of the channel are more correct. The smaller Peclet numbers are probably a result of mixing effects in the electrode measurement ports.

Table 2. Results of the simulations of the tracer experiments where the channel dimensions are employed.

flow length (m)	flow width (m)	Exp.	delta h (m)	Q (m^3/s)	2b (m)	$\bar{v}$ (m/s)	Peclet Number	Dispersivity (m)
1.400	0.300	4	0.0495	3.233E-06	0.000721	0.01494	68.1	0.02057
1.400	0.300	5	0.0330	2.183E-06	0.000724	0.01004	100.4	0.01395
1.400	0.300	7	0.0105	1.303E-06	0.000893	0.00486	136.4	0.01027
1.400	0.300	8	0.0296	1.027E-06	0.000584	0.00585	266.1	0.00530
1.400	0.300	9	0.0310	1.200E-06	0.000605	0.00659	220.6	0.00643
1.400	0.300	10	0.0373	1.800E-06	0.000652	0.00918	137.8	0.01040
1.400	0.300	12	0.0142	1.467E-06	0.000841	0.00581	129.3	0.01089
1.400	0.300	13	0.0100	1.667E-06	0.000989	0.00562	96.8	0.01456
1.400	0.300	14	0.0096	1.453E-06	0.000956	0.00507	114.3	0.01226

Table 3. Results of the simulations of the tracer experiments where the dimensions of the fracture plane are employed.

flow length (m)	flow width (m)	Exp.	delta h (m)	Q (m^3/s)	2b (m)	$\bar{v}$ (m/s)	Peclet Number	Dispersivity (m)
1.200	1.200	4	0.0495	3.233E-06	0.000431	0.00624	389.9	0.00308
1.200	1.200	5	0.0330	2.183E-06	0.000433	0.00420	575.0	0.00209
1.200	1.200	7	0.0105	1.303E-06	0.000534	0.00203	781.3	0.00154
1.200	1.200	8	0.0296	1.027E-06	0.000349	0.00245	1524.7	0.00079
1.200	1.200	9	0.0310	1.200E-06	0.000362	0.00275	1263.7	0.00096
1.200	1.200	10	0.0373	1.800E-06	0.000390	0.00384	789.5	0.00156
1.200	1.200	12	0.0142	1.467E-06	0.000503	0.00243	740.7	0.00163
1.200	1.200	13	0.0100	1.667E-06	0.000591	0.00235	554.6	0.00218
1.200	1.200	14	0.0096	1.453E-06	0.000572	0.00212	655.2	0.00183

Table 4. Results of the simulations of experiments 8, 10, 13 and 14. Data obtained from the samples only are used. Aperture width assumed equal to 0.75 mm.

Expt. num.	Coeff. of Disp. (m^2/s)	Velocity (m/s)	Dispersivity (m)	Peclet Number
8	5.00E-05	3.00E-03	1.67E-02	36.0
10	1.00E-04	4.00E-03	2.04E-02	29.4
13	6.00E-05	6.00E-04	1.00E-01	6.0
14	2.00E-05	4.00E-04	4.65E-02	12.9

For comparative purposes, Table 4 shows the results of the simulation of the concentrations determined from the samples obtained from experiments 8, 10, 13 and 14. Recalling that experiments 8 and 10 were conducted using the large volume test interval and 13 and 14 were conducted using the small volume intervals, the difference in Peclet number is notable; the opposite trend to that observed was anticipated. The possible explanation for the substantial decrease in Peclet number using the smaller test interval volume depends on the flow distortion around the borehole. Visualization of the flow during experiments 13 and 14 showed a substantial increase in the divergence of the streamline near the wellbore relative to previous experiments. This may have resulted in flow separation and stagnation near the wellbore-fracture interface causing increased dispersive flux into the wellbore. Irrespective of the cause, this finding is important because future modifications of the test interval size will need to be conducted in consideration of flow divergence. Numerical/analytical modelling may be employed to help determine the optimum interval size.

A complete report on the laboratory experiments is in preparation, and will be included in the next progress report. The laboratory method and method of analysis will be described in full.

FUTURE WORK

Field

1. Continued monitoring of the hydraulic head distribution.
2. Conduct a detailed series of pulse interference tests using different source boreholes.

Laboratory

1. Construct new artificial fracture with dimensions 2.0 m x 0.4 m.
2. Develop fiberoptic/fluorometric measurement techniques for laboratory tracer experiments.
3. Conduct tracer experiments.

Modelling

1. Complete development of the Fractal surface generation code. Compare results to Turning Bands method.

2. Begin supercomputer runs using E. Sudicky's LTG transport code with a variable aperture generated from the Fractal method.

REFERENCES

Crank, J. Free and Moving Boundary Problems, Oxford University Press, New York, 425 p., 1984.

Palmer, C.D. The effect of monitoring well storage on the shape of breakthrough curves - A theoretical study, J. Hydrol., 97, 45-57, 1988.

APPENDIX C

Progress Report : August 1990

Progress Report, August 1990

Environment Ontario Grant No. 393

Principal Investigator: J. A. Cherry[1]

Co-Investigators: C. W. Mase[1]
E. A. Sudicky[1]
K. S. Novakowski[2]

Report Authored by: P. A. Lapcevic[2] and K. S. Novakowski

[1]Waterloo Centre for Groundwater Research
University of Waterloo
Waterloo, Ontario

and

[2]National Water Research Institute
Environment Canada
Burlington, Ontario

MEASURING GROUNDWATER VELOCITY AND HYDRODYNAMIC DISPERSION IN A SINGLE FRACTURE

INTRODUCTION

The estimation of groundwater velocity in fractured rock is essential in determining the potential for contaminant transport from many waste and industrial sites throughout Southern Ontario. Simple conceptual models of fracture geometry developed with an incomplete understanding of the flow system may lead to erroneous predictions of velocity. Fracture aperture, the width of the fracture required to determine an estimation of velocity, is characterized by surface roughness, tortuosity, and areas of closure. The purpose of this study is to investigate the relation between various field methods in determining fracture aperture.

This progress report describes the work carried out in this study during the last six months. The study is focussed on the field characterization of the two fractures at the Clarkson field research site using detailed hydraulic tests, in preparation for future natural gradient tracer tests. The direction of future work is also presented.

FIELD SITE CHARACTERIZATION

New Boreholes

During February 1990, six additional boreholes were drilled at the Clarkson field site. The boreholes were located to complete a 30-m by 30-m grid (Figure 1). A total of 25 boreholes have now been

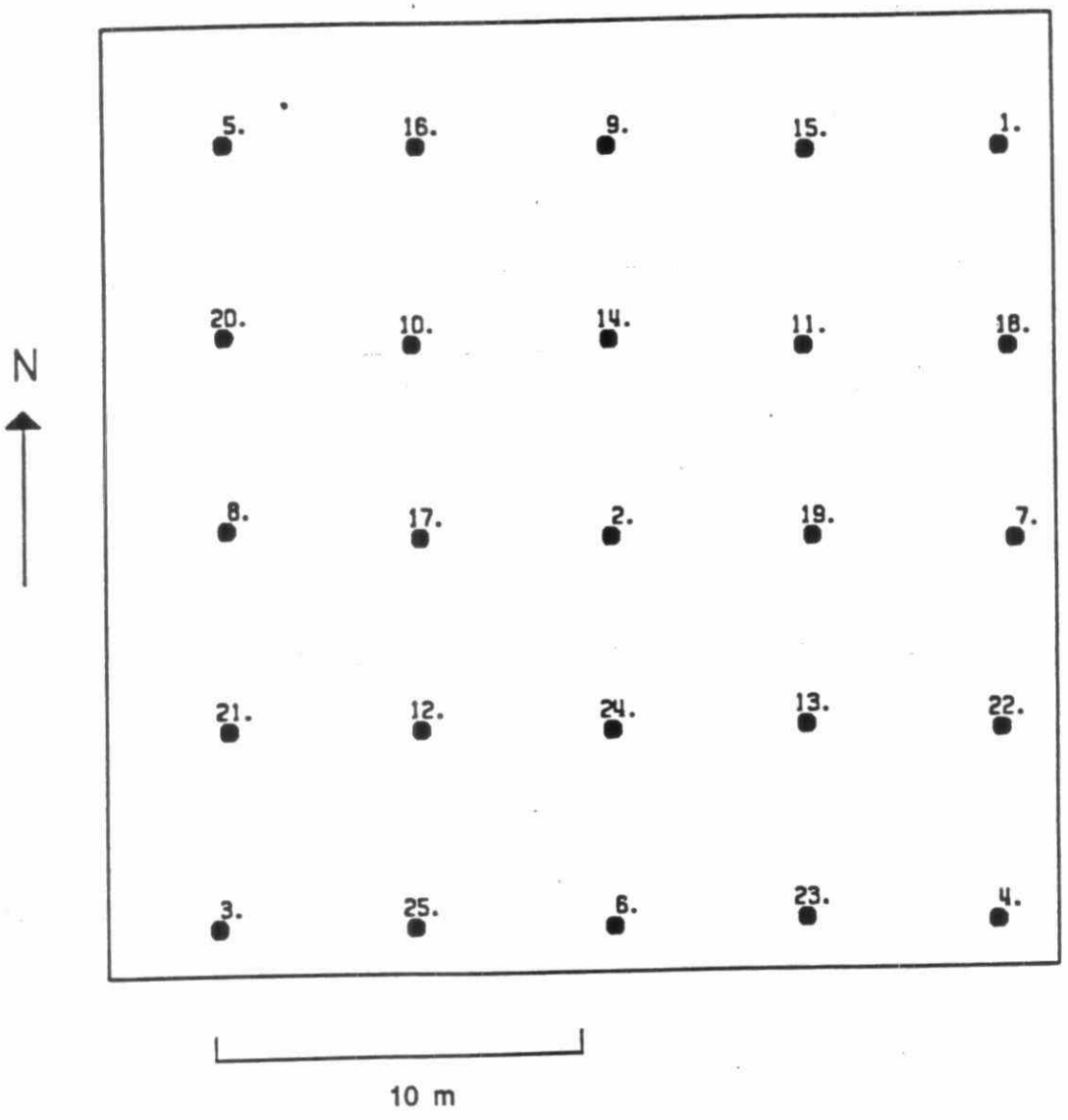

Figure 1: Clarkson site map showing location of all boreholes.

drilled and the boreholes are numbered in the order in which they were completed. Drilling methods were identical to those employed in previous drilling programs (see December 1988 progress report). After completion of the drilling program the boreholes were developed by pumping using a 6 HP centrifugal pump. The location of all 25 boreholes were surveyed by an Ontario Land Surveyor for both elevation relative to sea level and position in the grid. The top of the surface casing was used as the reference point for each borehole.

Hydraulic Testing

Constant head injection tests using a 1.6 m packer spacing were carried out over the entire length of the six new boreholes. A 0.5 m packer spacing was then used over the zone of interest. Finally, a 0.1 m packer separation length was used to characterize in detail the two fractures being studied at the site (referred to in this report as lower and upper fracture respectively). The methodology used is described in Novakowski (1988). Tests were also carried out in the 19 other boreholes to characterize in detail the two fractures. In previous years, overlapping test intervals were used to pinpoint the location and aperture of the fractures. It was found that this method can be ambiguous at times and since the fractures of interest are less than a metre apart vertically, short packer spacings (ie. less than a metre) are essential to ensure distinction between the two fractures.

Lithology and Fracture Log Compilation

Lithology and fracture logs for the portion of the boreholes containing the two fractures were constructed for 22 of the boreholes. Data was not available for UW4, UW6 and UW7. The logs were compiled from core logging completed at the time of drilling and examination of core pictures. Due to the fissile nature of the shale, the core deteriorates with time and could not be re-examined.

Borehole Instrumentation

During the winter 19 boreholes were instrumented with a double packer arrangement isolating the lower fracture. Equipment modifications have been made on an ongoing basis over the last two years to ensure that the packers remain sealed over a period of several months. Packer separation lengths range from 0.10 to 0.50 m and are based on the results of the hydraulic testing program (see December 1988 progress report for details on packer construction). Additional packer systems were constructed for the new holes and all 25 boreholes were shut-in in June 1990. Vibrating wire transducers (Geokon model 4500HS) were installed in all 25 boreholes to obtain continuous records of hydraulic head within the lower fracture over the next few months. The transducer in each hole is attached to the top of the upper packer and is in direct connection with the test interval via a sealed line through the packer body. Pressure measurements from the transducers are collected by a data logger 3 times per hour. A rain gauge and barometric pressure transducer have also been installed on site. The borehole instrumentation in each

borehole is designed to be flexible and easily modified. For example, to monitor the hydraulic head in the upper fracture the packers could be simply deflated and moved. Other hydraulic tests such as pumping and pulse tests could also be carried out without modifying the present configuration.

RESULTS AND DISCUSSION

Over 250 constant head tests were completed this spring in order to determine the location and aperture of both fractures in all of the boreholes. A summary of the fracture aperture widths is shown in Table 1. Aperture logs for each hole are included with lithology and fracture logs in Appendix A. Only results from the tests conducted using the 0.1 m packer spacing tests are shown in these figures.

The apertures in the lower fracture range from 282 micrometers to below detection limit. The apertures in the upper fracture range from 138 micrometers to below detection limit. The detection limit for this particular testing system is estimated to be approximately 10 micrometers. The distribution of aperture widths (Figures 2 and 3) show that in a significant number of boreholes the fractures are not detected. In over 20% of the boreholes the aperture of the lower fracture was below the detection limit and in 36% of the boreholes the aperture of the upper fracture was below the detection limit. The apertures are contoured in Figures 4 and 5.

The purpose of the geological compilation was to examine in greater detail the possibility of geological controls on the location of the

Table 1. Summary of fracture aperture widths (in micrometers) as determinined from the results constant head tests.

Borehole	Upper Fracture 2b (μm)	Lower fracture 2b (μm)
UW1	90	221
UW2	66	235
UW3	138	27
UW4	67	220
UW5	<10[a]	226
UW6	80	85
UW7	115	98
UW8	62	15
UW9	<10	167
UW10	<10	<10
UW11	107	126
UW12	<10	94
UW13	<10	<10
UW14	106	241
UW15	94	26
UW16	<10	<10
UW17	104	<10
UW18	18	<10
UW19	<10	248
UW20	39	243
UW21	<10	18
UW22	58	282
UW23	120	57
UW24	54	154
UW25	120	214

[a] fracture aperture is below measurement limit and can be considered not detectable.

two fractures. The lithology of the rock in the zone adjacent to the fractures is a reddish green shale with fossiliferous dolostone and soft mudstone interbeds. The dolostone interbeds are important, because fractures associated with them appear to provide the bulk of the permeability in the zone. The lower fracture is associated with a dolostone bed identified in all the boreholes. This bed ranges in thickness from 0.10 m to 0.18 m. The upper fracture also appears to be associated with a smaller dolostone bed. This bed was identified in 16 of the boreholes. Vertical fracturing is evident in 11 of the

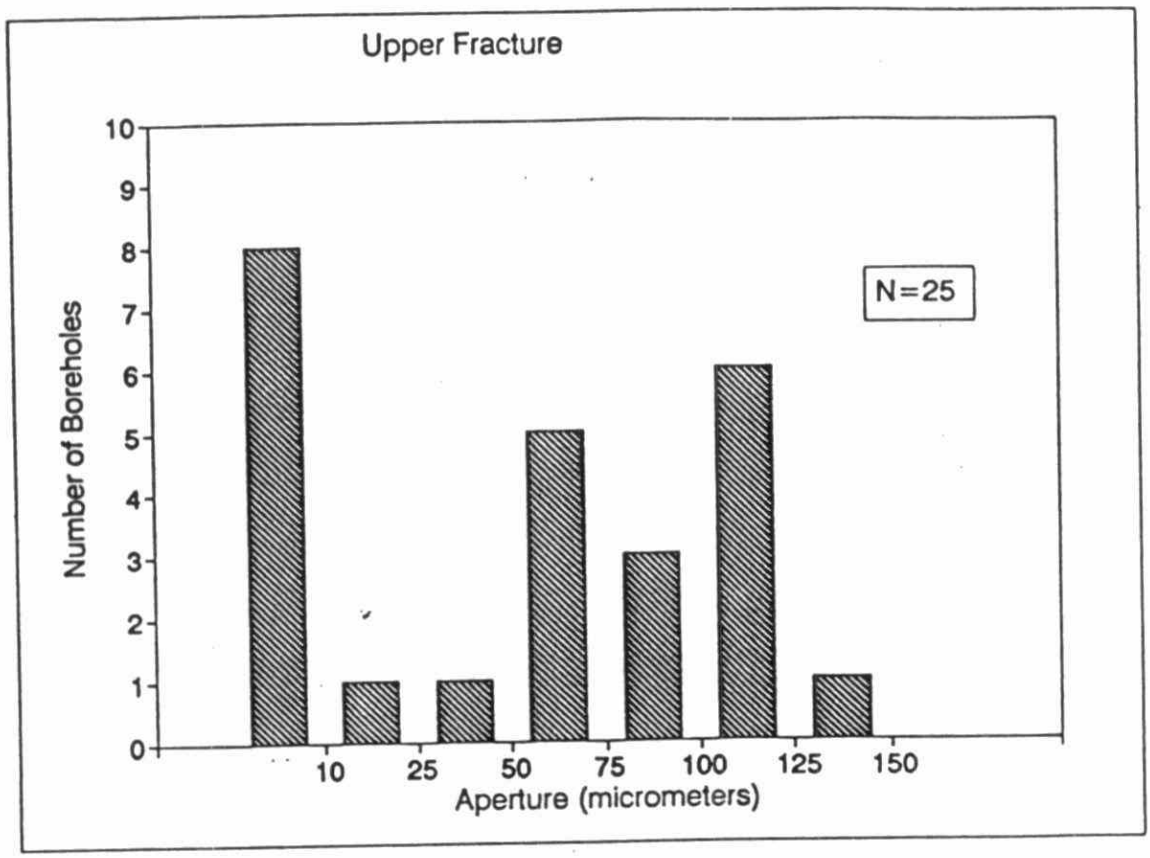

Figure 2: Aperture distribution of upper fracture.

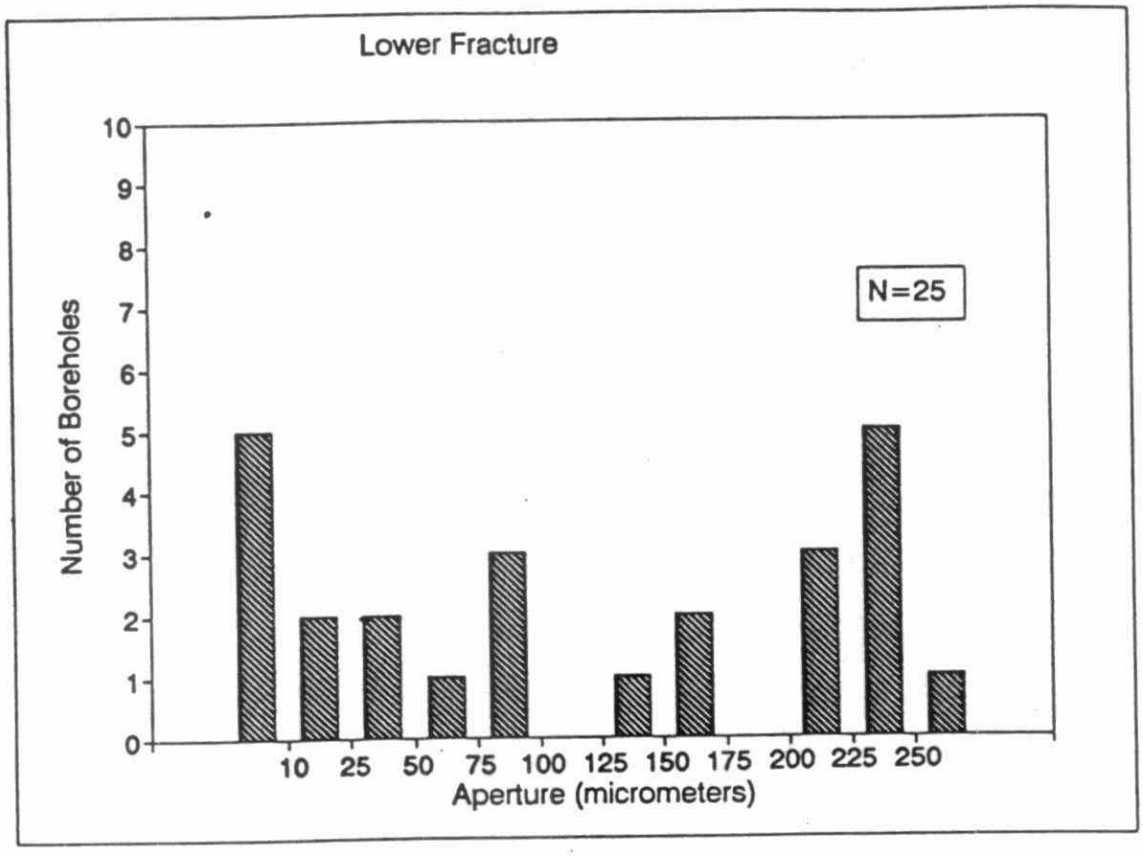

Figure 3: Aperture distribution for lower fracture.

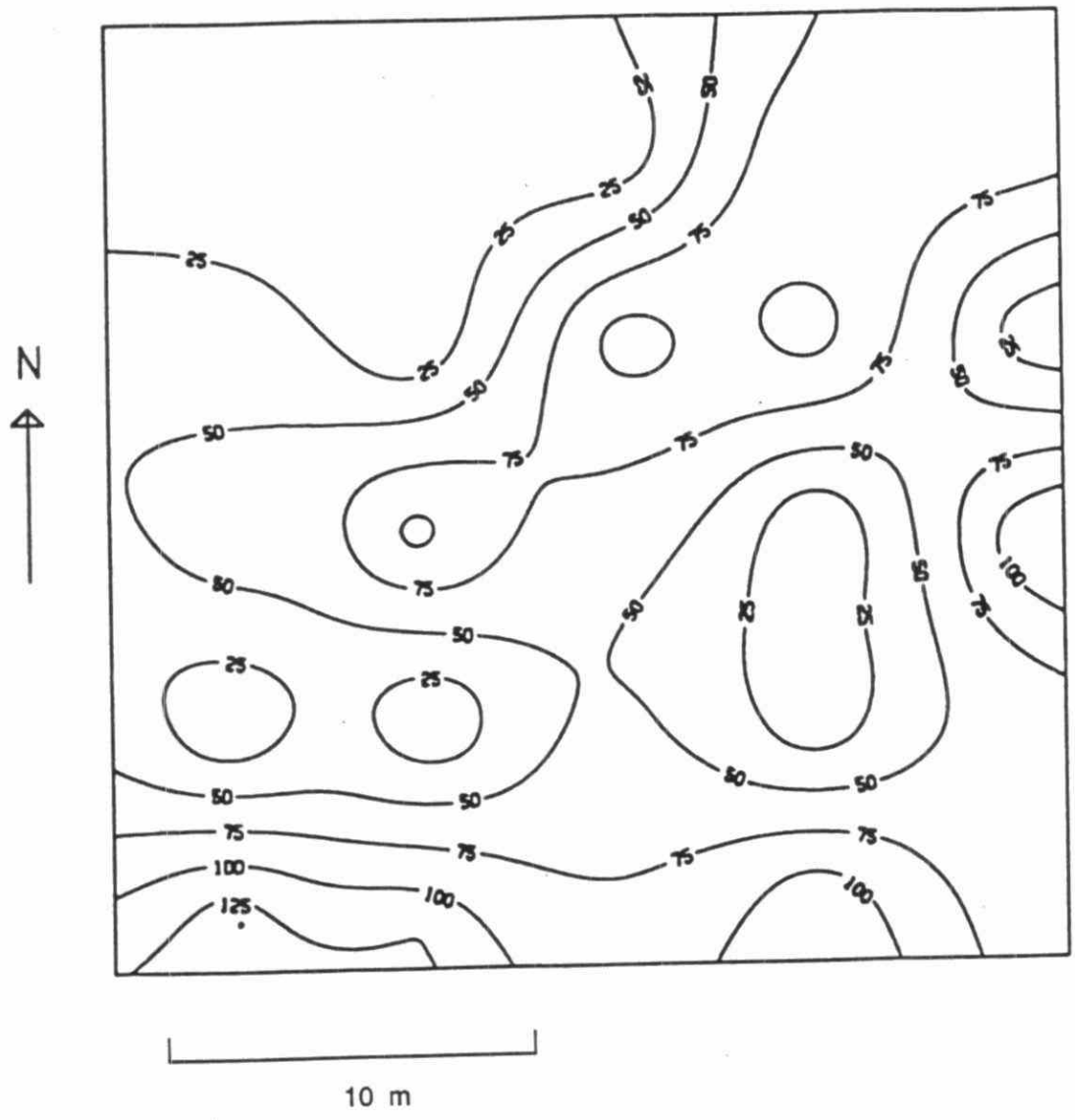

Figure 4: Contour map of upper fracture apertures (contour interval is 25 μm).

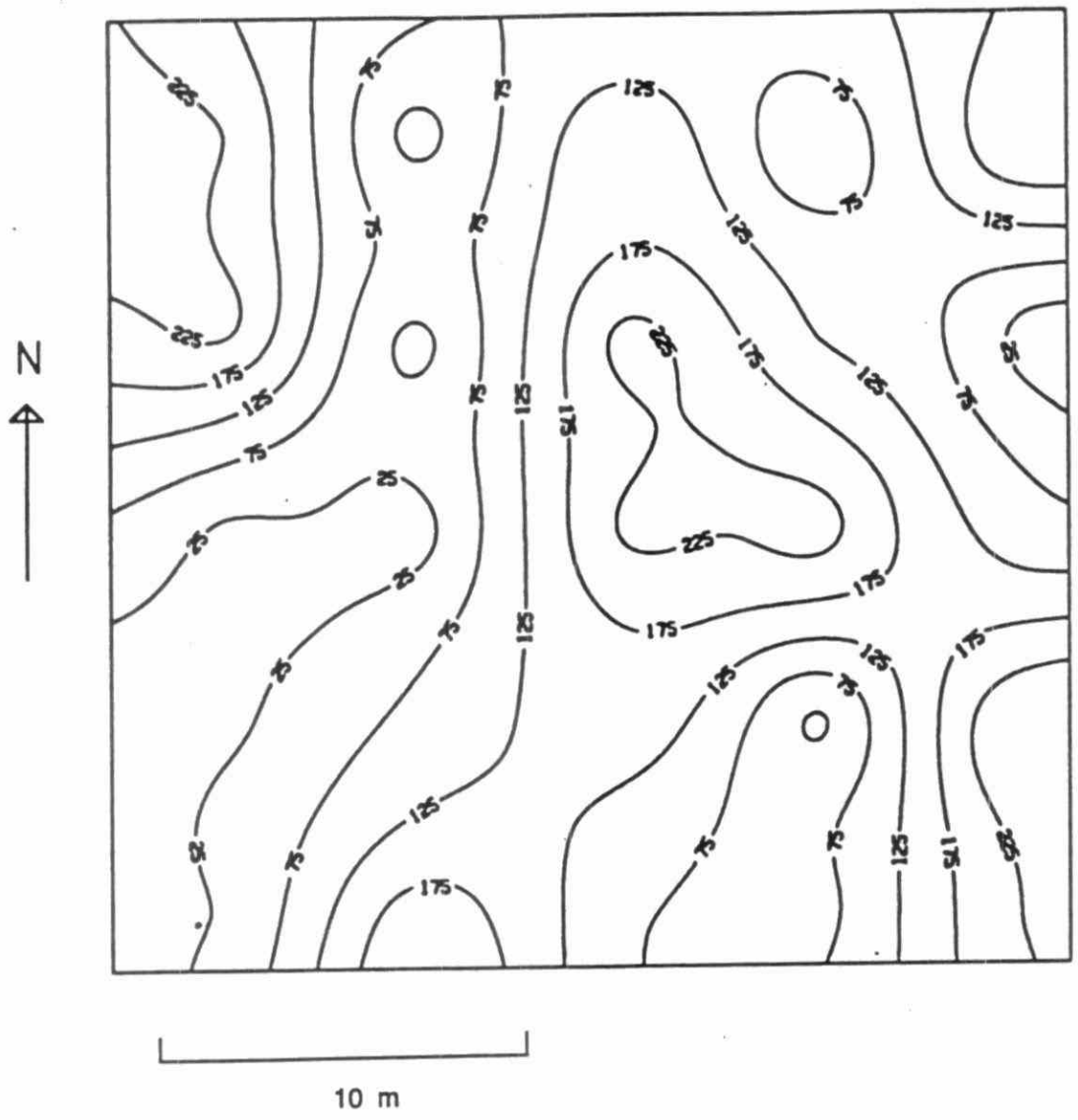

Figure 5: Contour map of lower fracture apertures (contour interval is 50 μm).

boreholes (over 40%). In UW25, a vertical fracture goes through the thickness of the lower dolostone bed. In UW20 a smaller vertical fracture goes through the lower portion of the dolostone bed associated with the lower fracture.

MODELLING STUDIES

The following is an excerpt from the introduction of a thesis completed in conjunction with this study (Unger, 1990).

Stochastic models of geological systems have received widespread attention as a method of recognizing spatial variations affecting hydrogeological and mechanical models. Fractal geometry is a specific method of modelling and generating stochastic fields and its use in describing the random and deterministic components of many natural phenomena has been pursued extensively and popularized by Mandelbrot (1982).

The objective of this work is to determine if fractal geometry can be used to provide a model exhibiting the same statistical and time-series properties as profiles obtained from rock fracture surfaces providing a conclusive understanding of the irregularities observed by Brown (1985). Measurement of fractal dimension using time series, statistical and other forms of analysis, such as Richardson's walk, is clearly explained by Voss (1985a) and Feder (1988). Surfaces are to be modelled using one-dimensional profiles while fractal geometry is used to provide an equivalent two-dimensional surface which corresponds statistcally to the surface in

question. The purpose of this literature review is to provide an understanding of the mathematical theory and algorithms required to analyze and generate fractals. Measurement of fractal dimension using time series, statistical and other forms of analysis is provided along with a review of past efforts with these methods.

FUTURE WORK

Field

1. Continued monitoring of the hydraulic head distribution in the lower fracture.
2. Conduct several forced gradient tracer tests between selected boreholes.
3. Conduct a 24-48 hour pumping test using all boreholes as monitoring wells.
4. Monitor hydraulic head in the upper fracture.
5. Conduct natural gradient tracer tests in both fractures.

REFERENCES

Novakowski, K.S., Comparison of fracture aperture widths determined from hydraulic measurements and tracer experiments, In: Proc. 4th. Canadian/American Conf. Hydrogeol., Banff, Alta., June, 1988.

Unger, J.A., Fractal Geometry of rock fracture surfaces, B.Sc. thesis, University of Waterloo, Waterloo, Ont., 1990.

Appendix A

Lithology, fracture and aperture logs

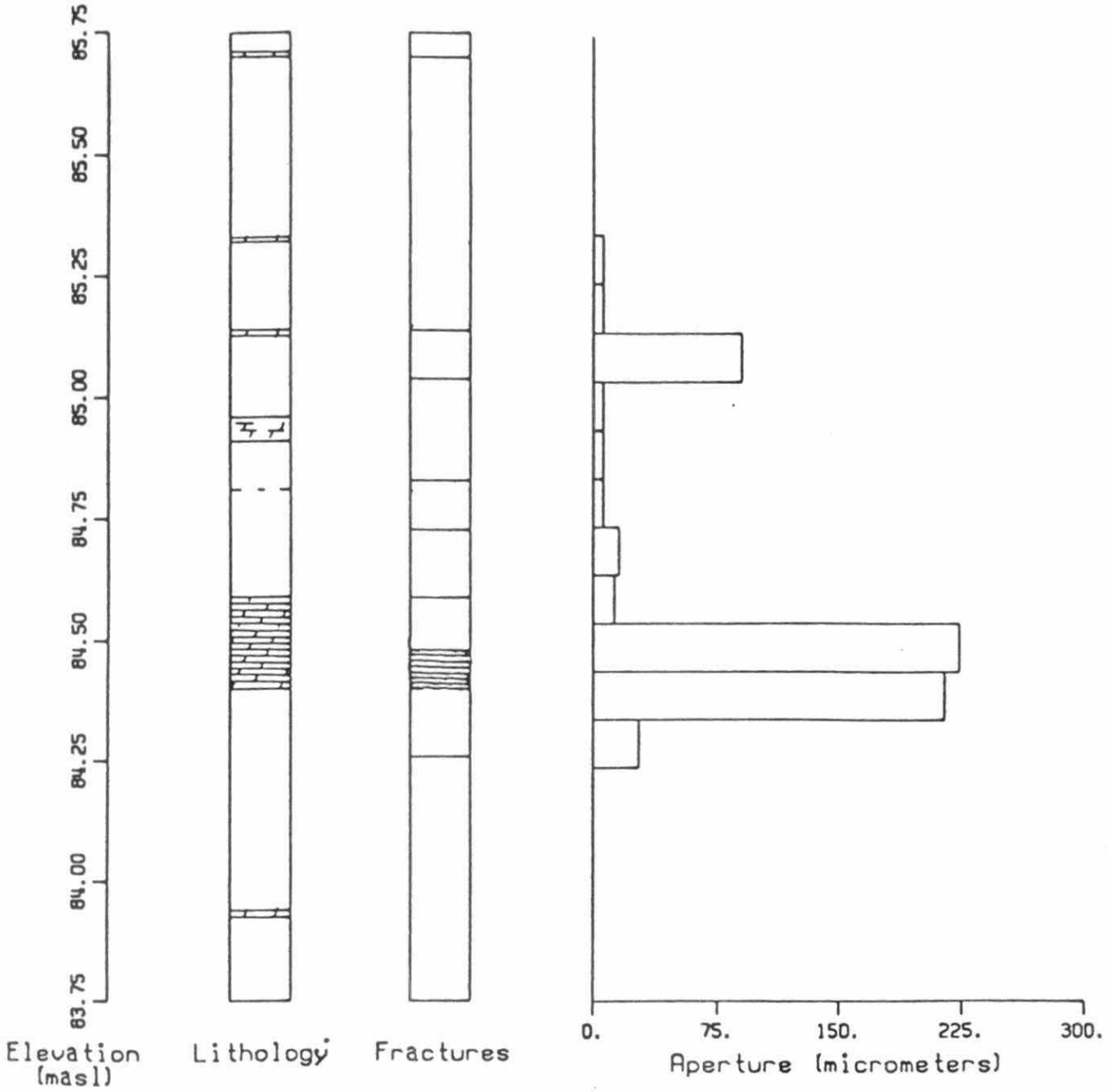

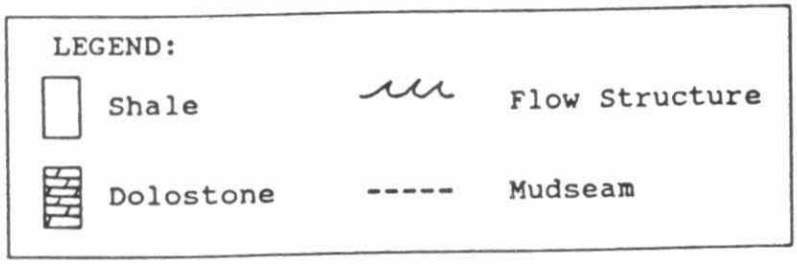

Figure A1: Lithology, fracture and aperture logs for UW1.

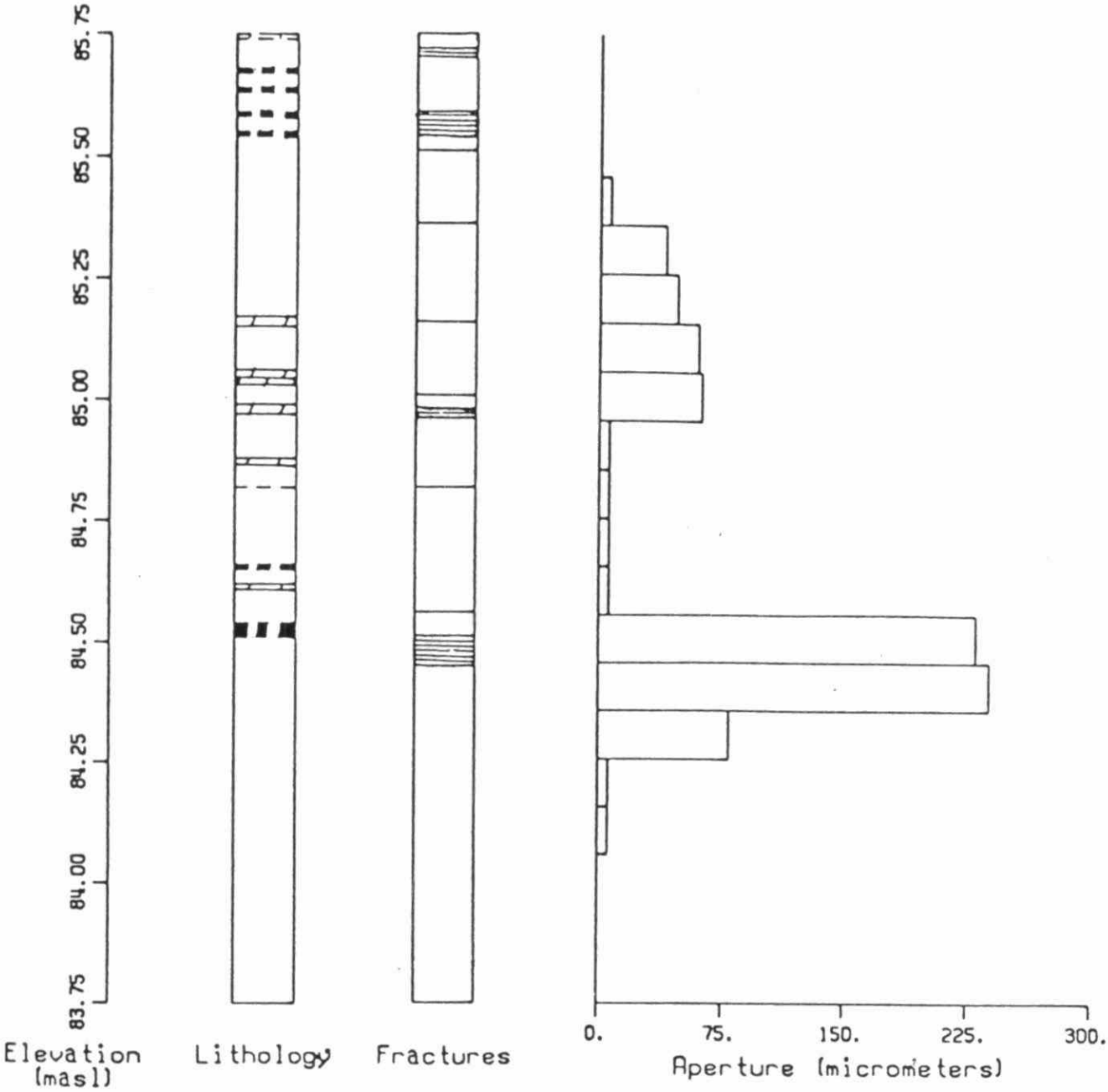

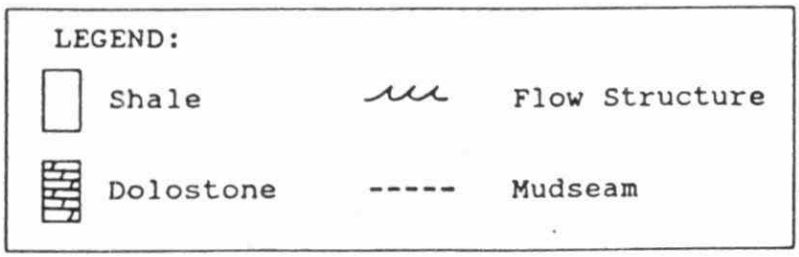

Figure A2: Lithology, fracture and aperture logs for UW2. Lithology and fracture logs between 83.75 m and 84.45 m are unavailable.

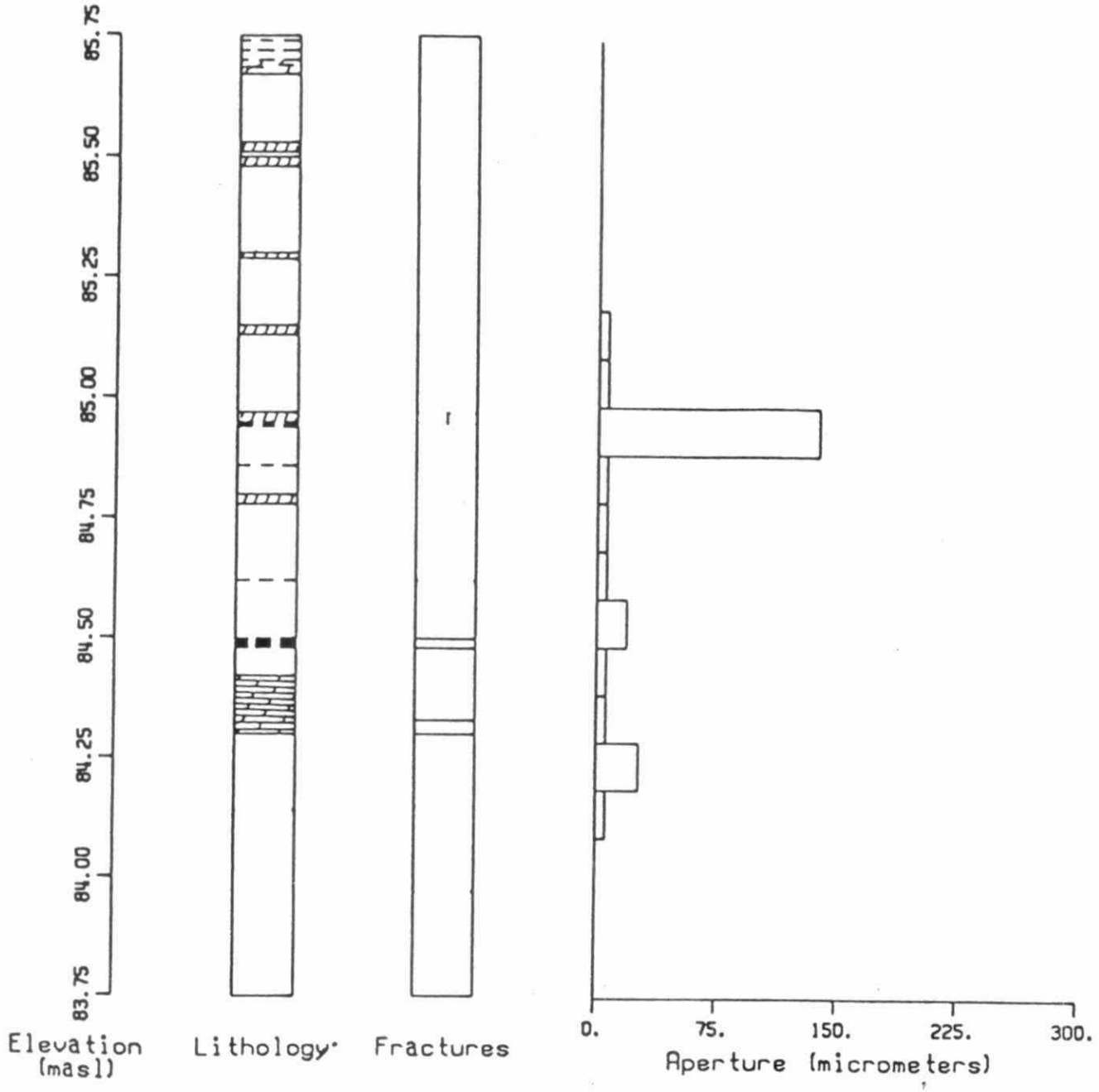

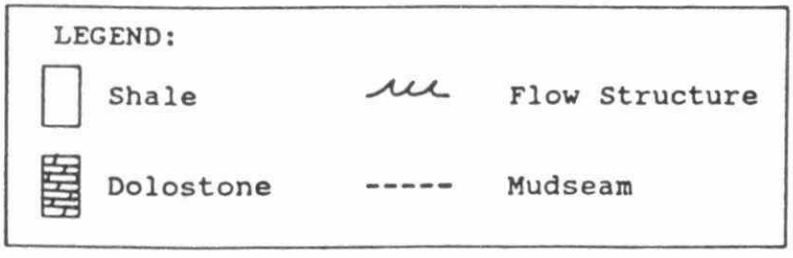

Figure A3: Lithology, fracture and aperture logs for UW3.

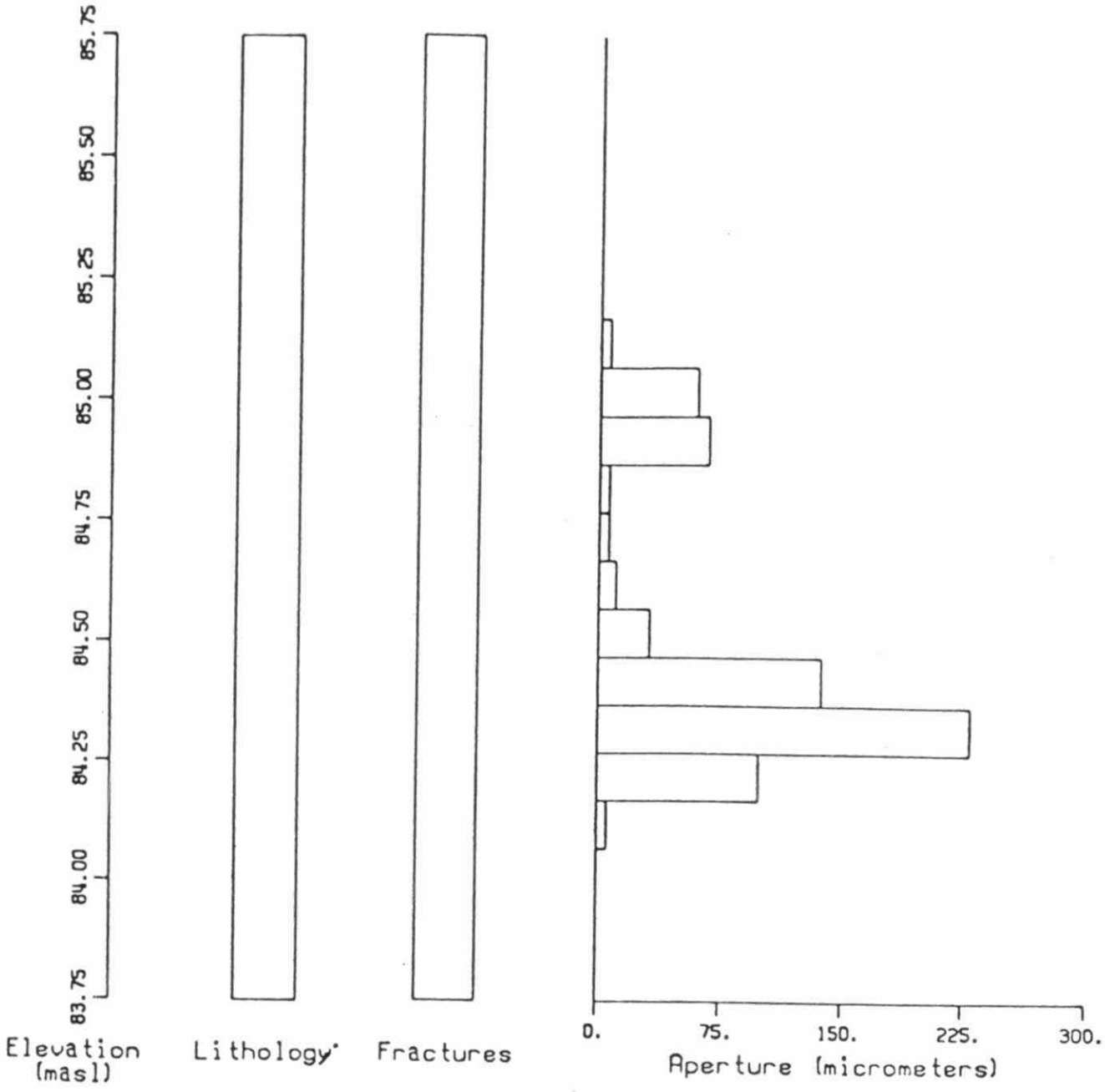

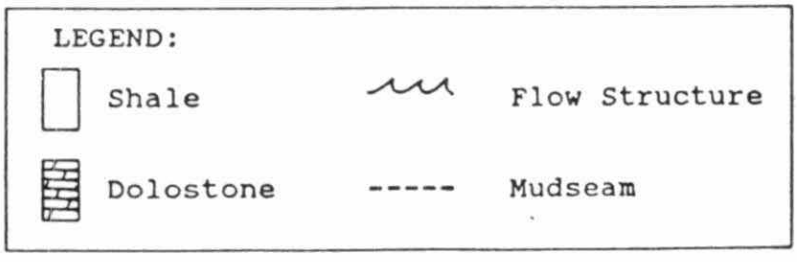

Figure A4: Aperture log for UW4. Lithology and fracture logs unavailable.

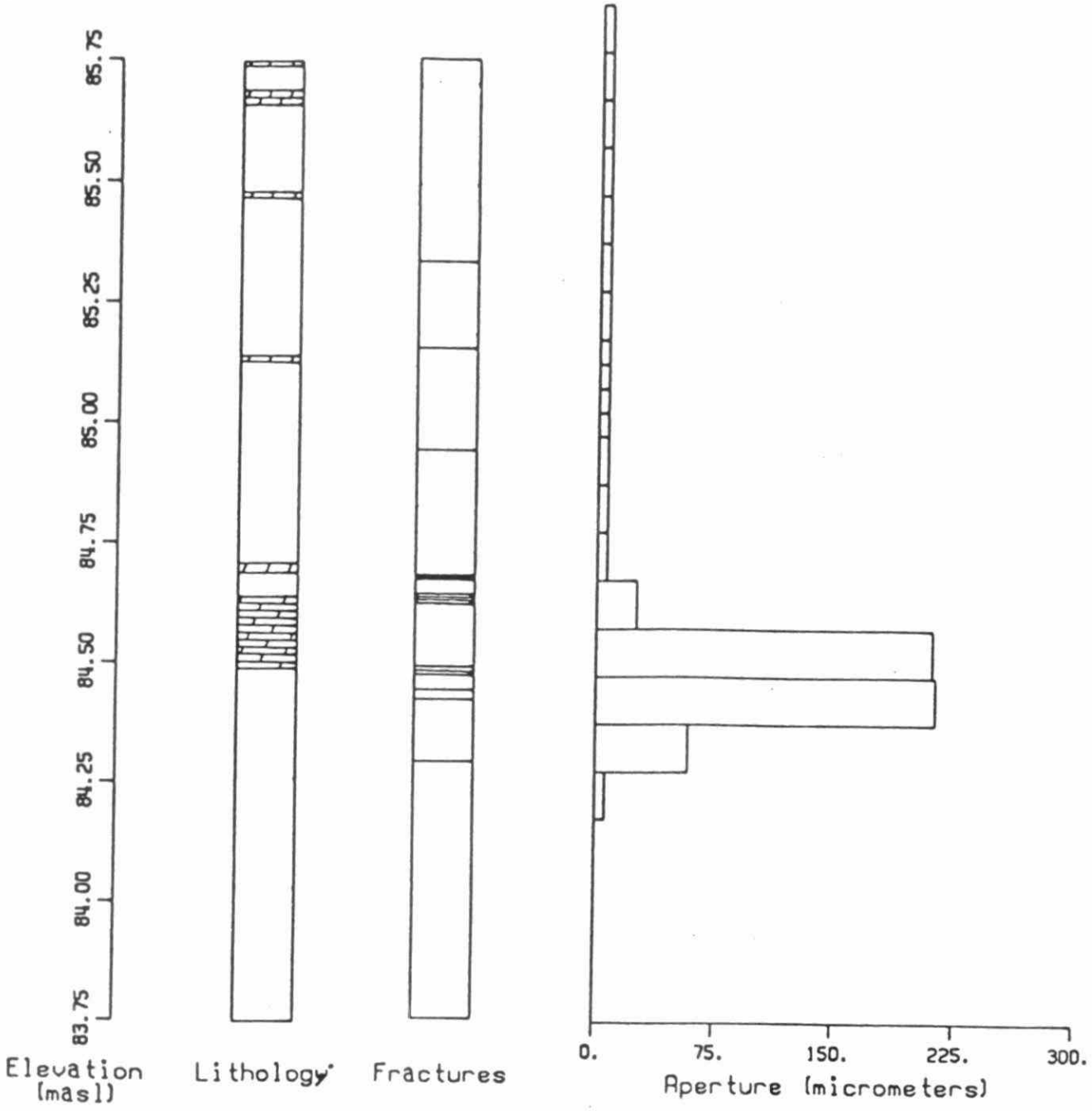

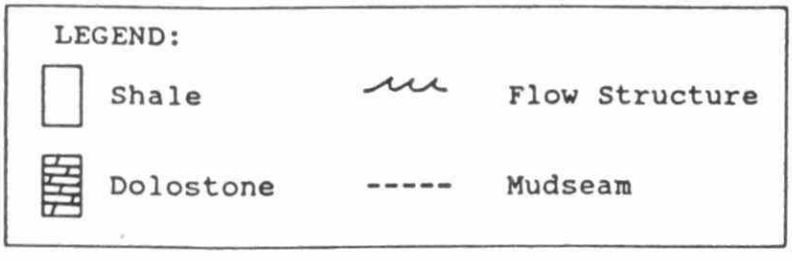

Figure A5: Lithology, fracture and aperture logs for UW5.

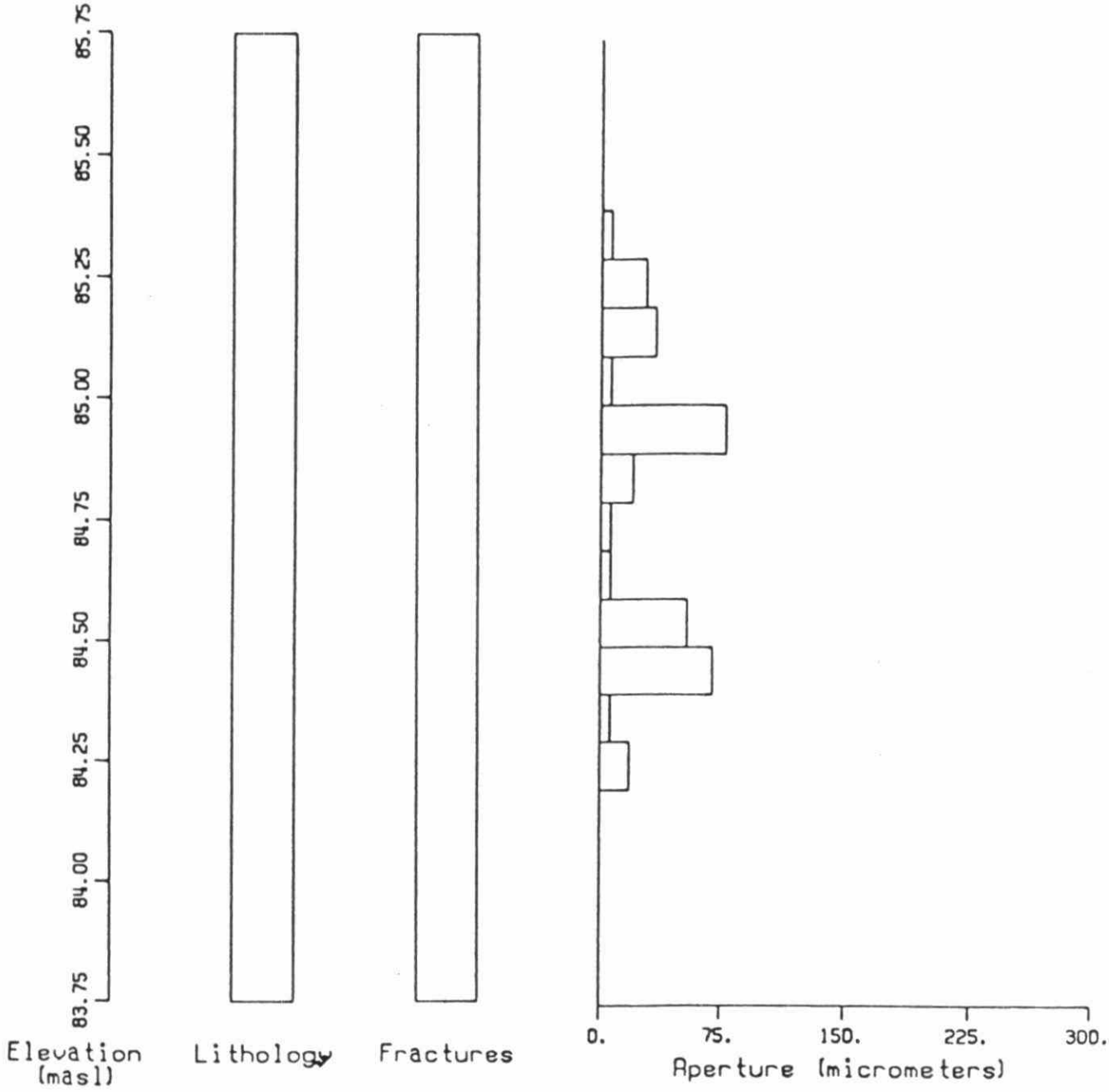

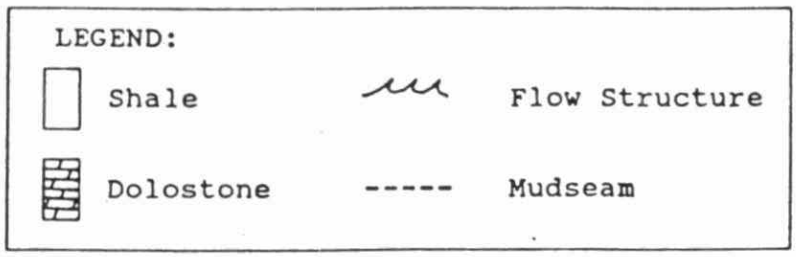

Figure A6: Aperture log for UW6. Lithology and fracture logs unavailable.

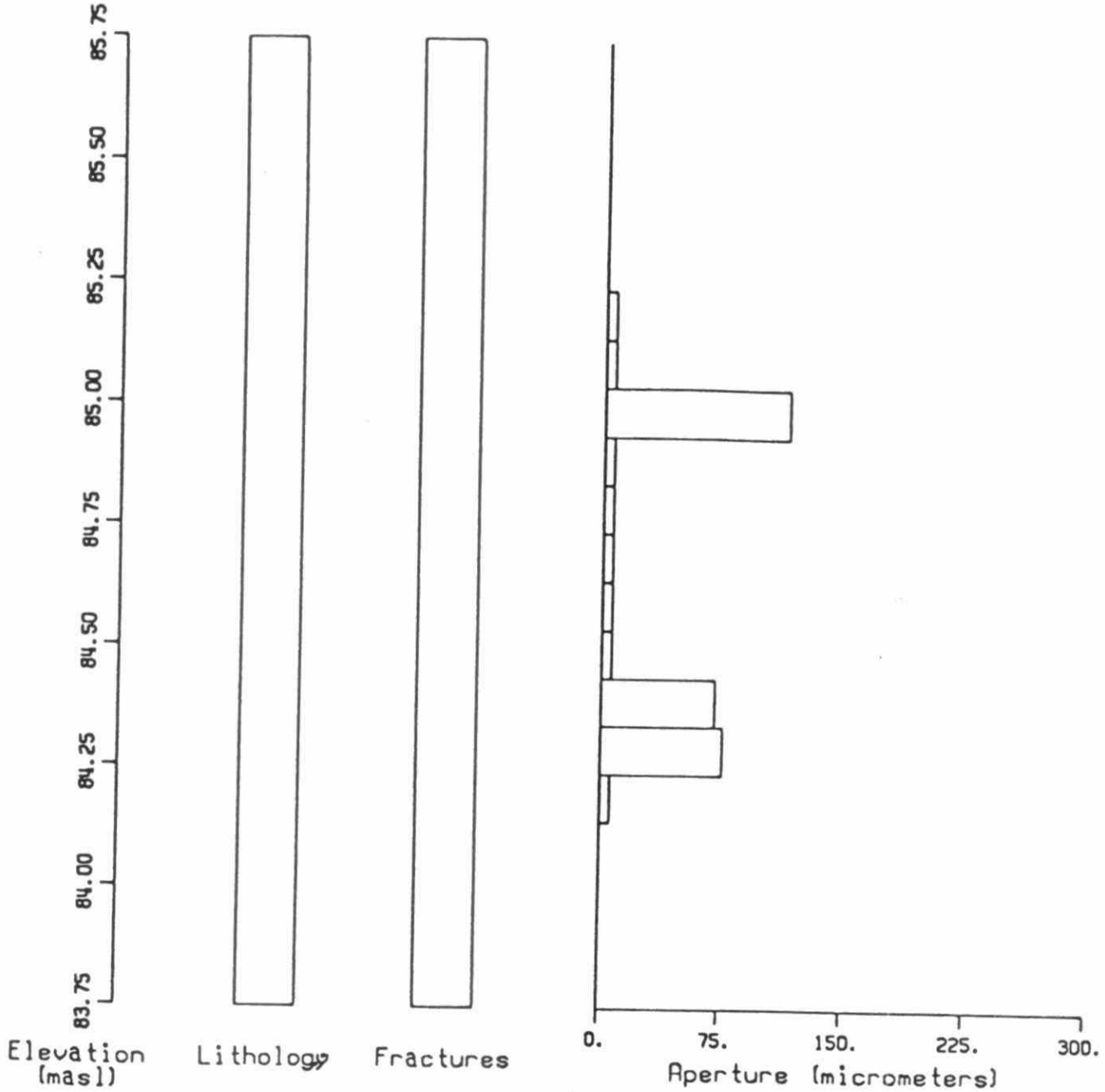

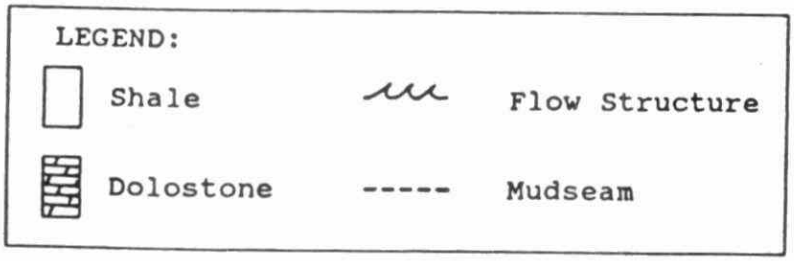

Figure A7: Aperture log for UW7. Lithology and fracture logs unavailable.

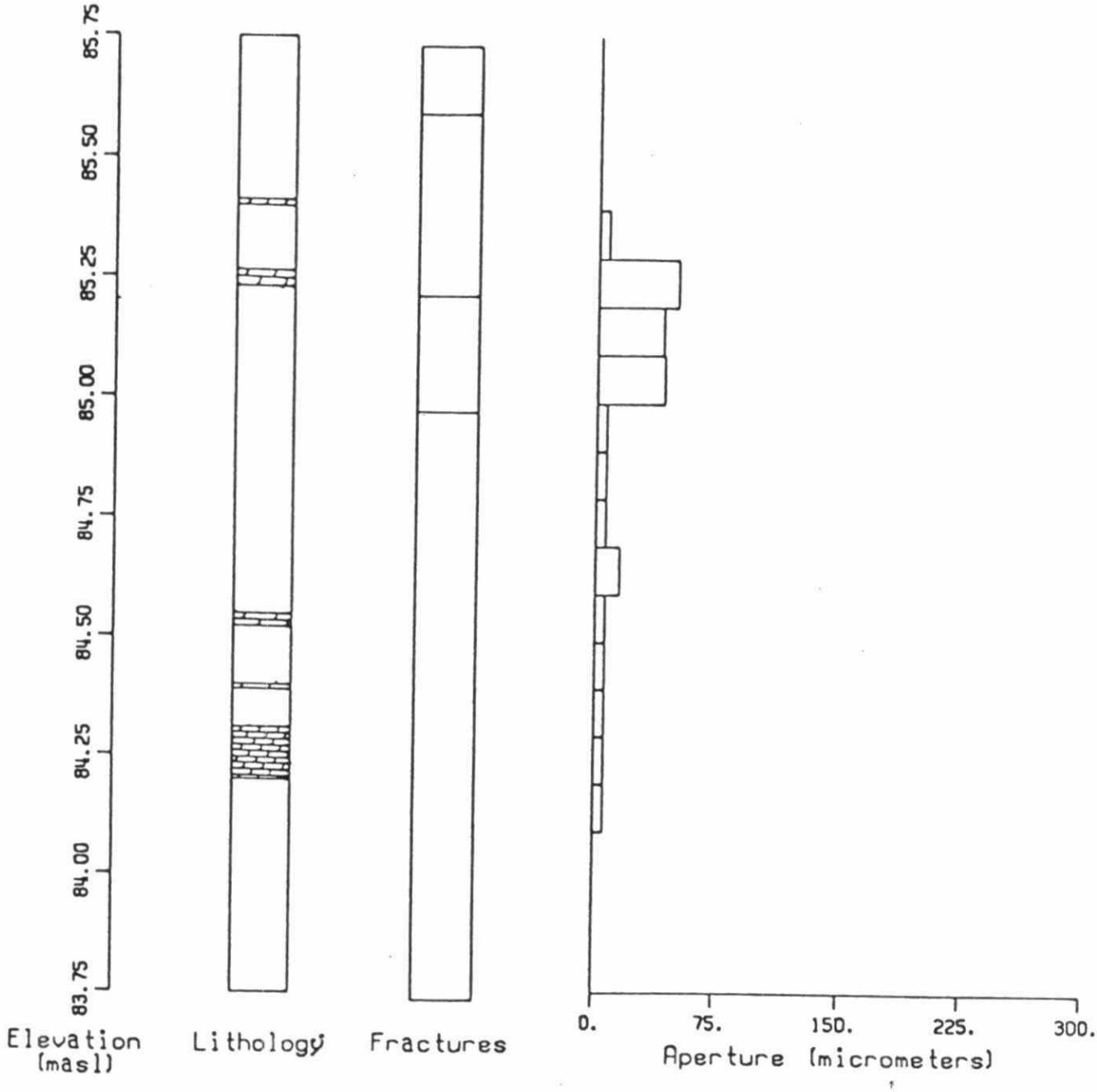

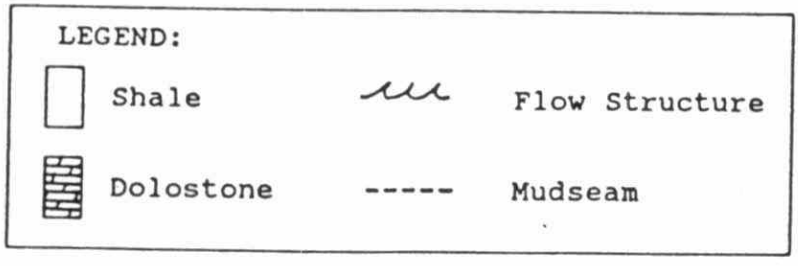

Figure A8: Lithology, fracture and aperture logs for UW8.

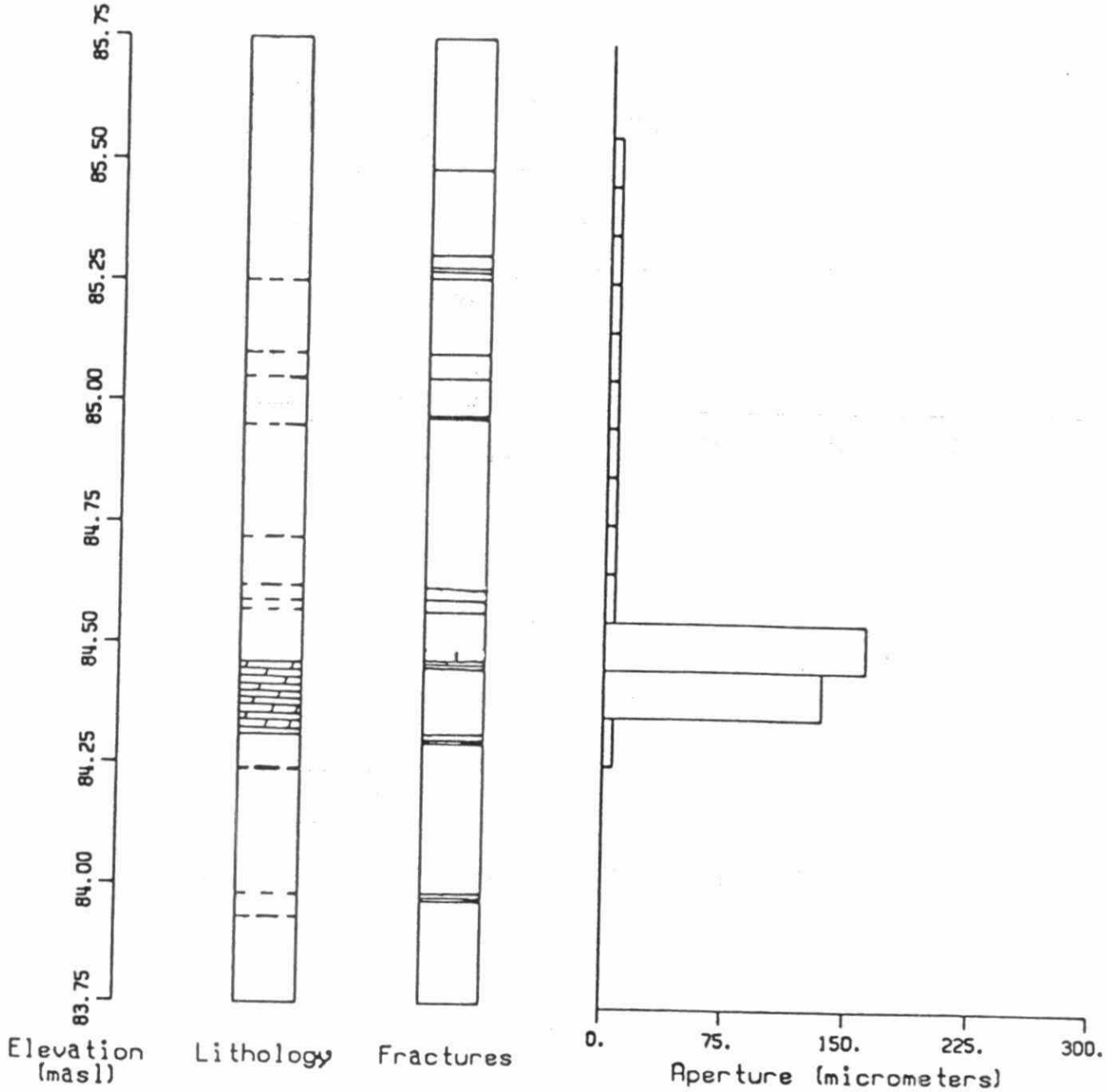

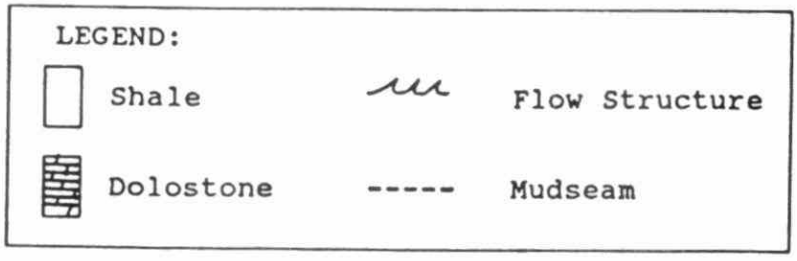

Figure A9: Lithology, fracture and aperture logs for UW9.

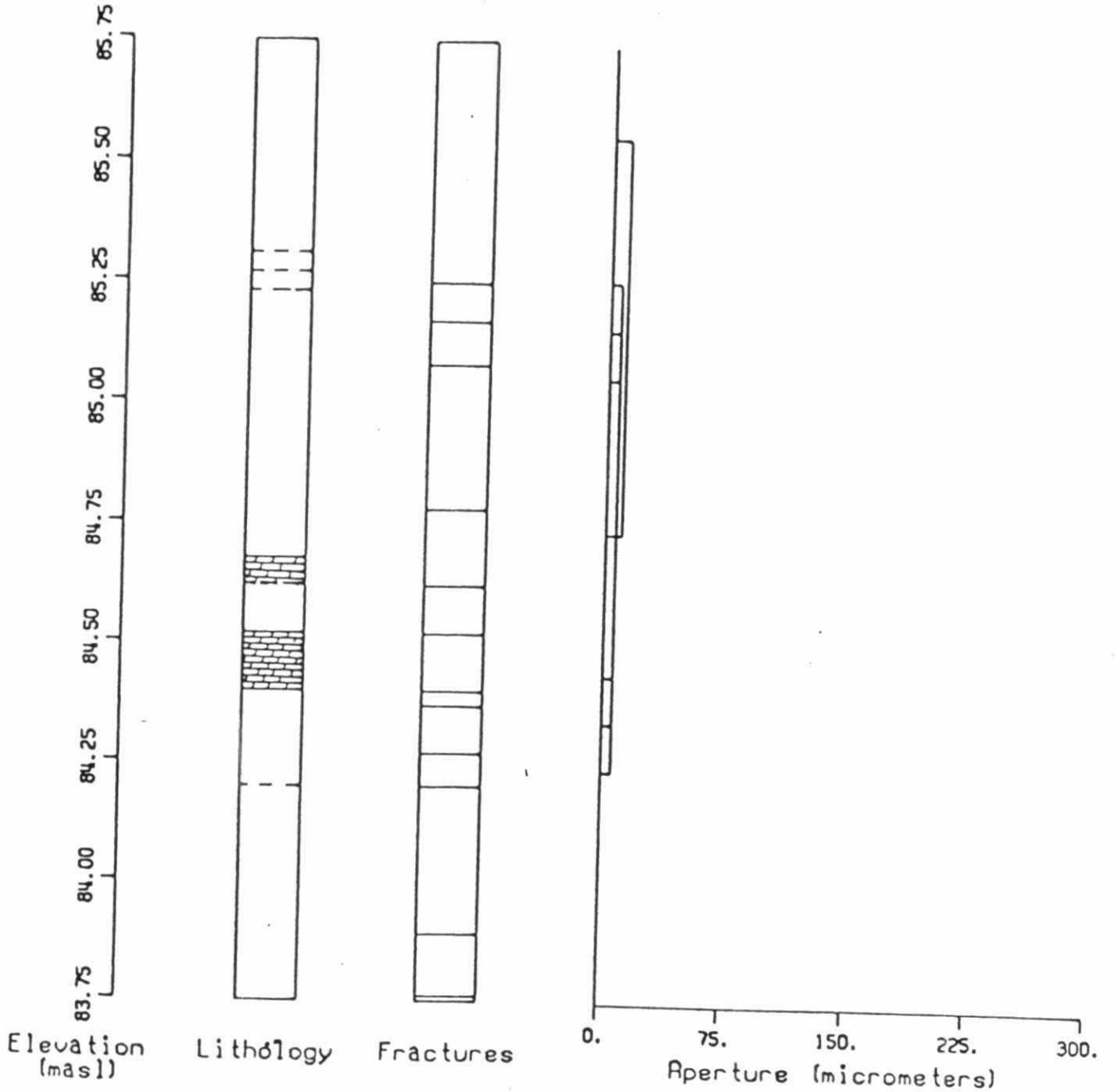

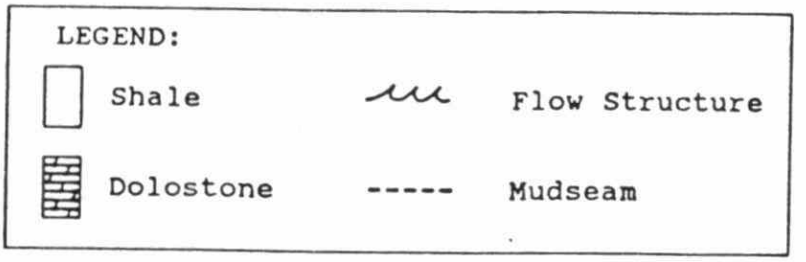

Figure A10: Lithology, fracture and aperture logs for UW10.

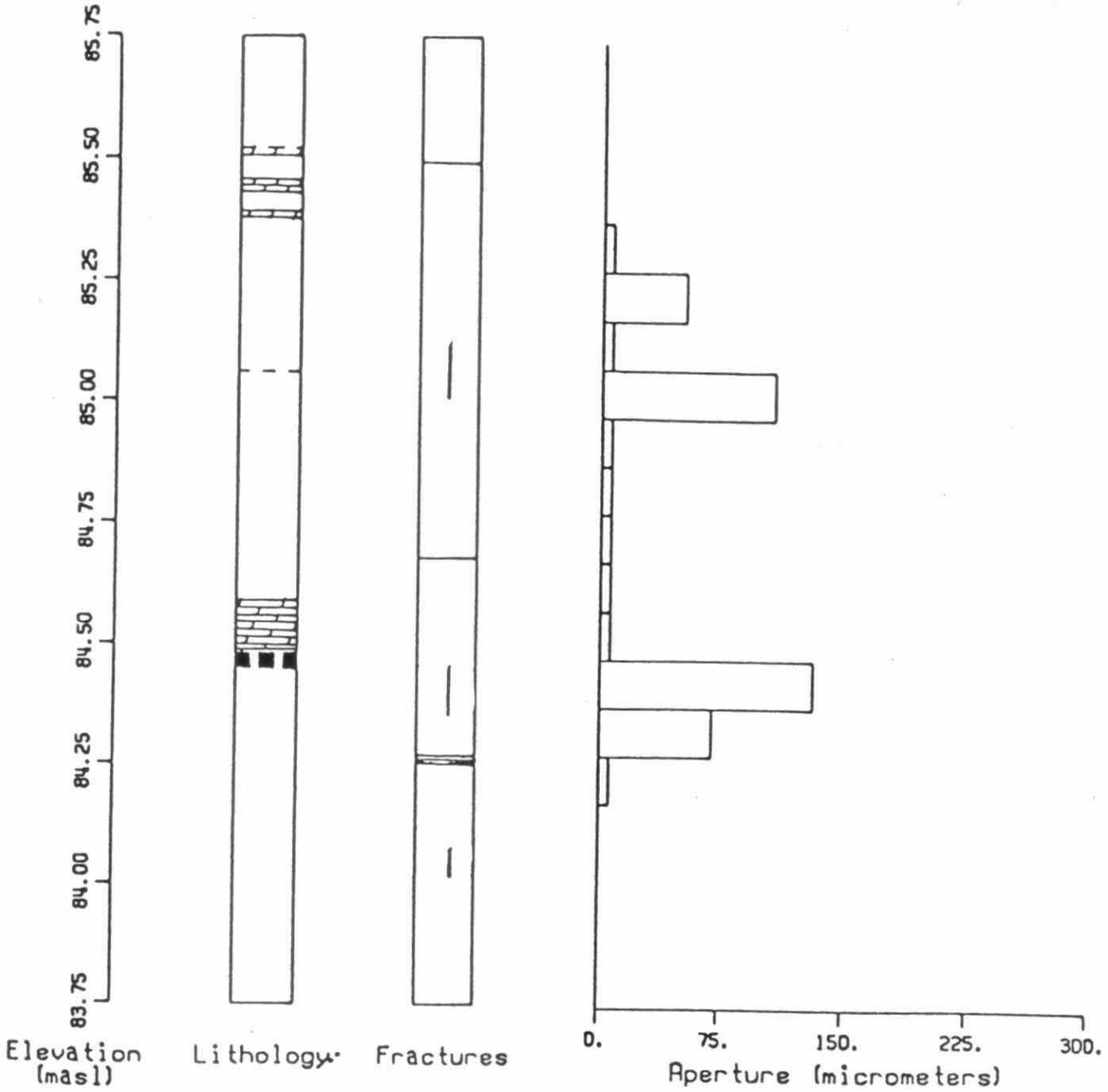

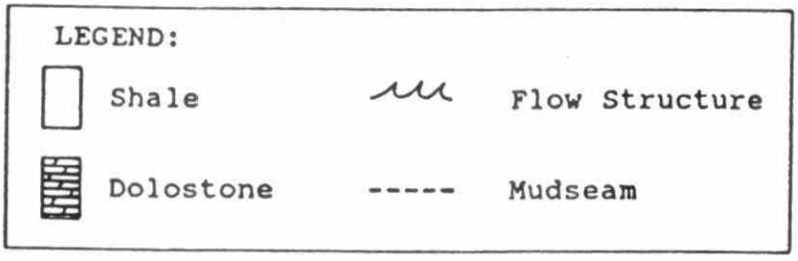

Figure A11: Lithology, fracture and aperture logs for UW11.

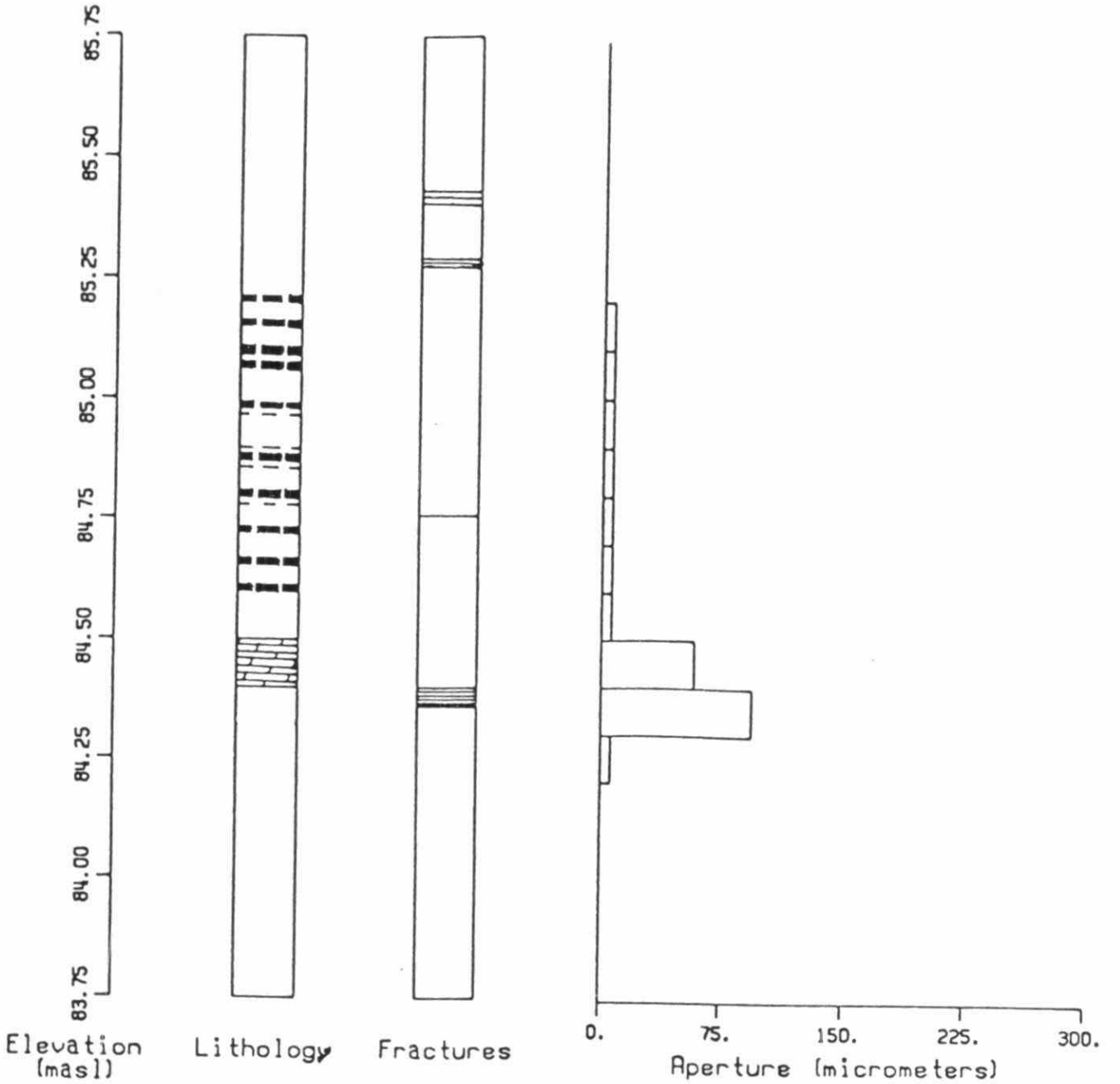

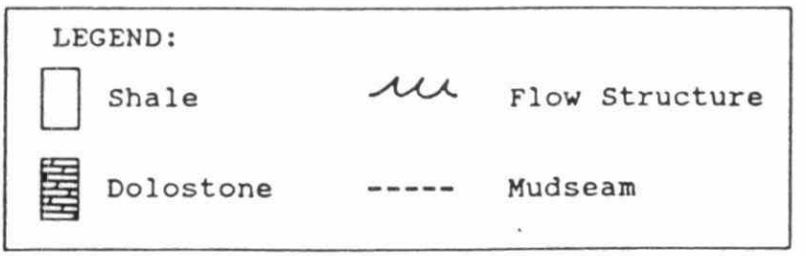

Figure A12: Lithology, fracture and aperture logs for UW12.

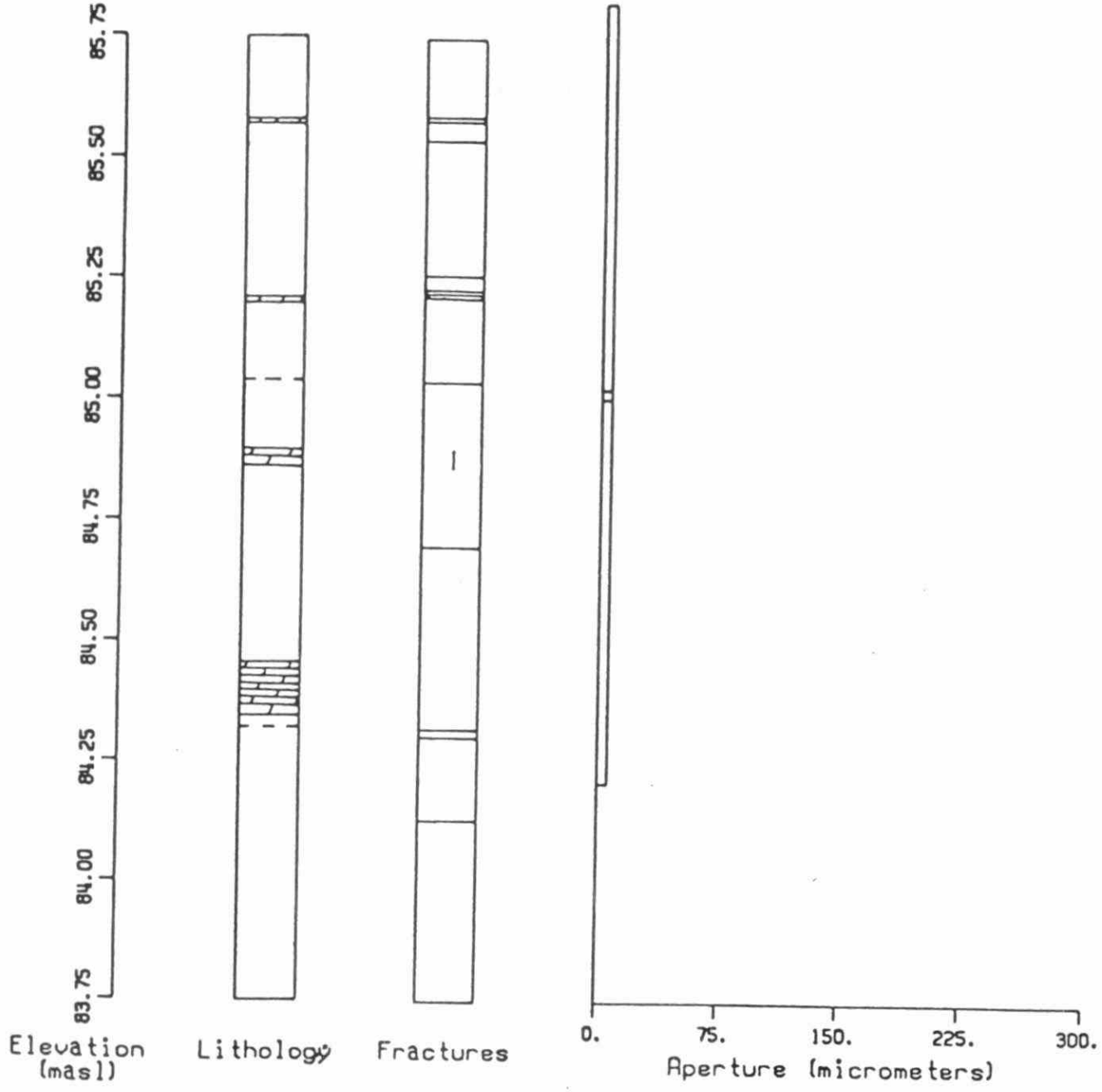

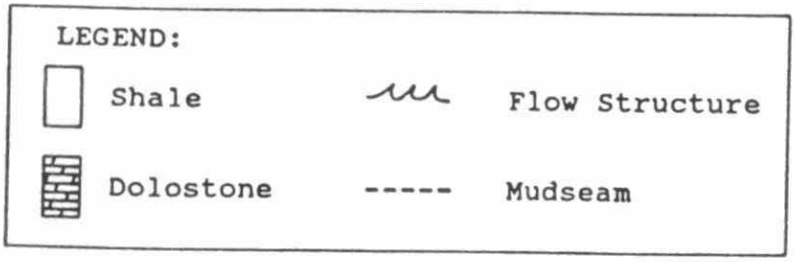

Figure A13: Lithology, fracture and aperture logs for UW13.

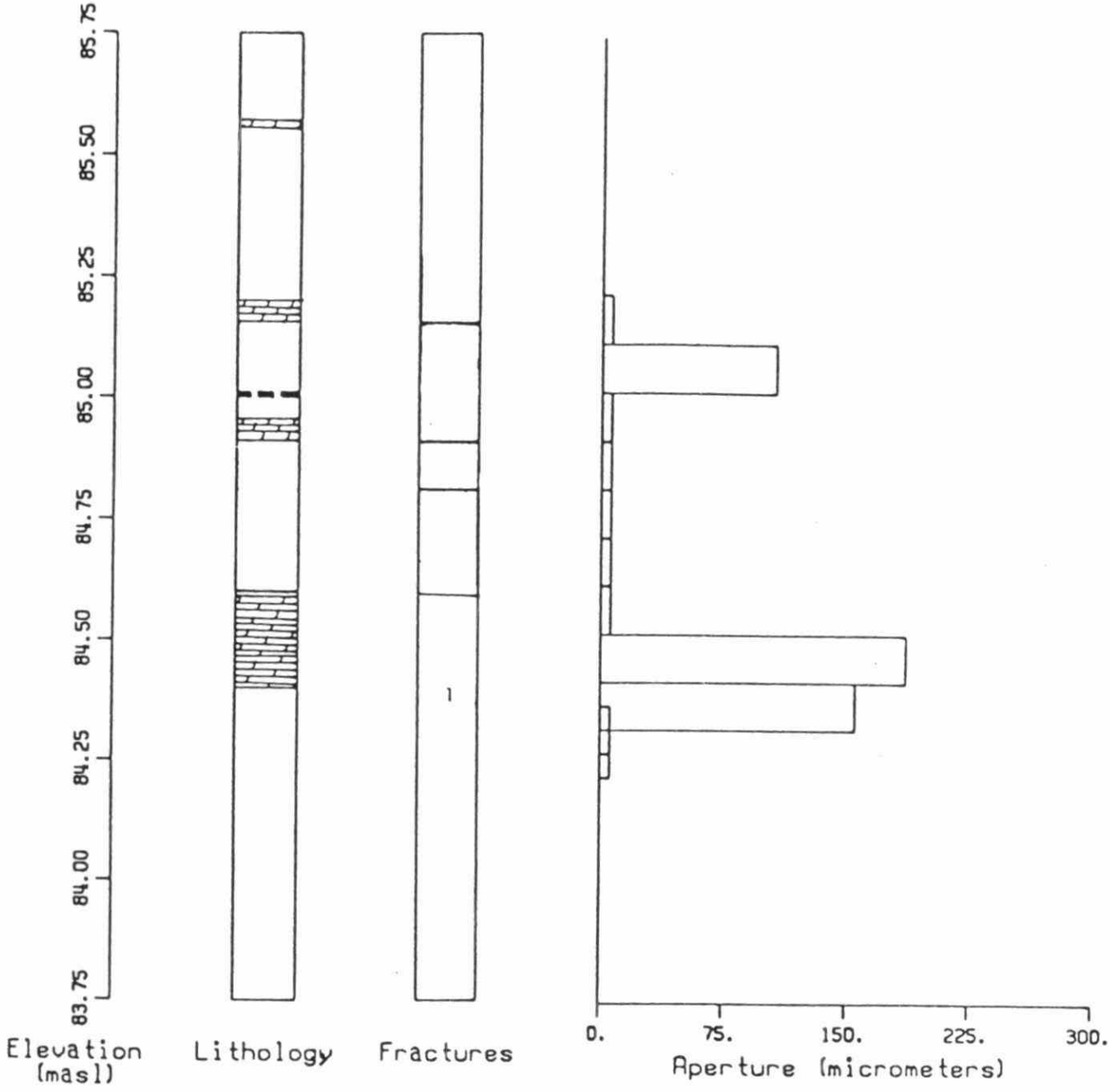

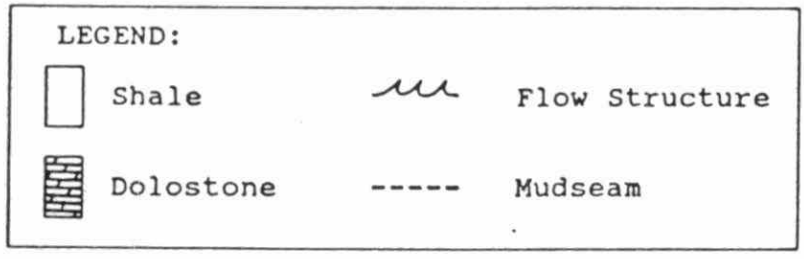

Figure A14: Lithology, fracture and aperture logs for UW14.

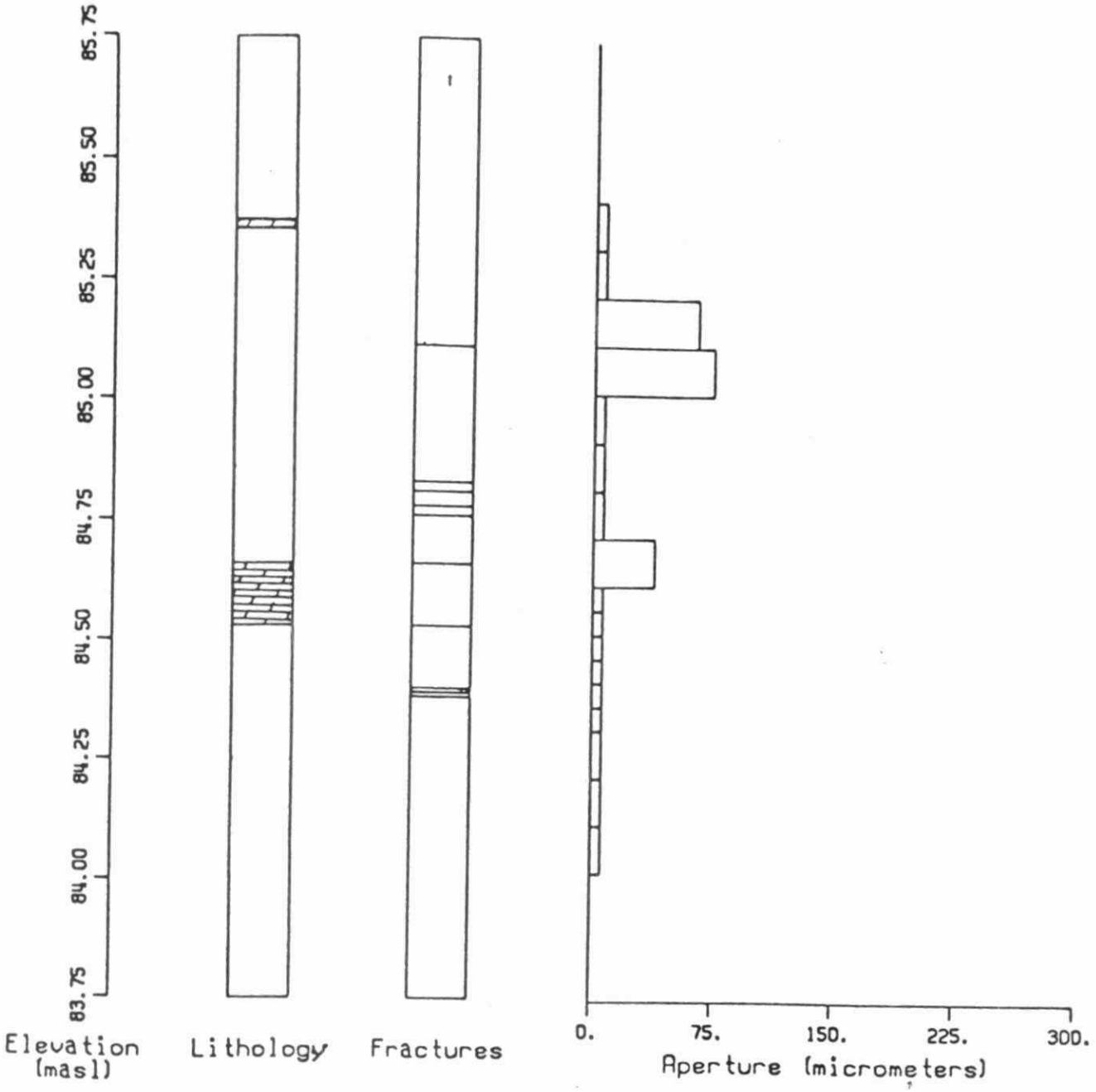

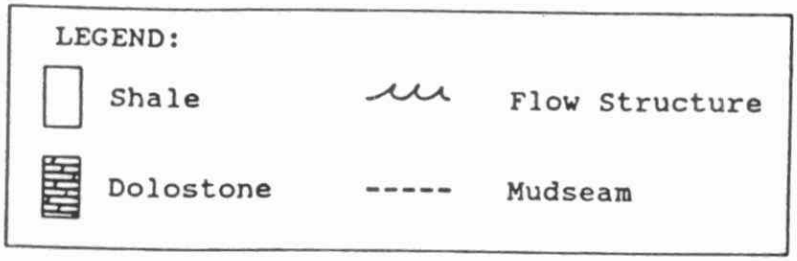

Figure A15: Lithology, fracture and aperture logs for UW15.

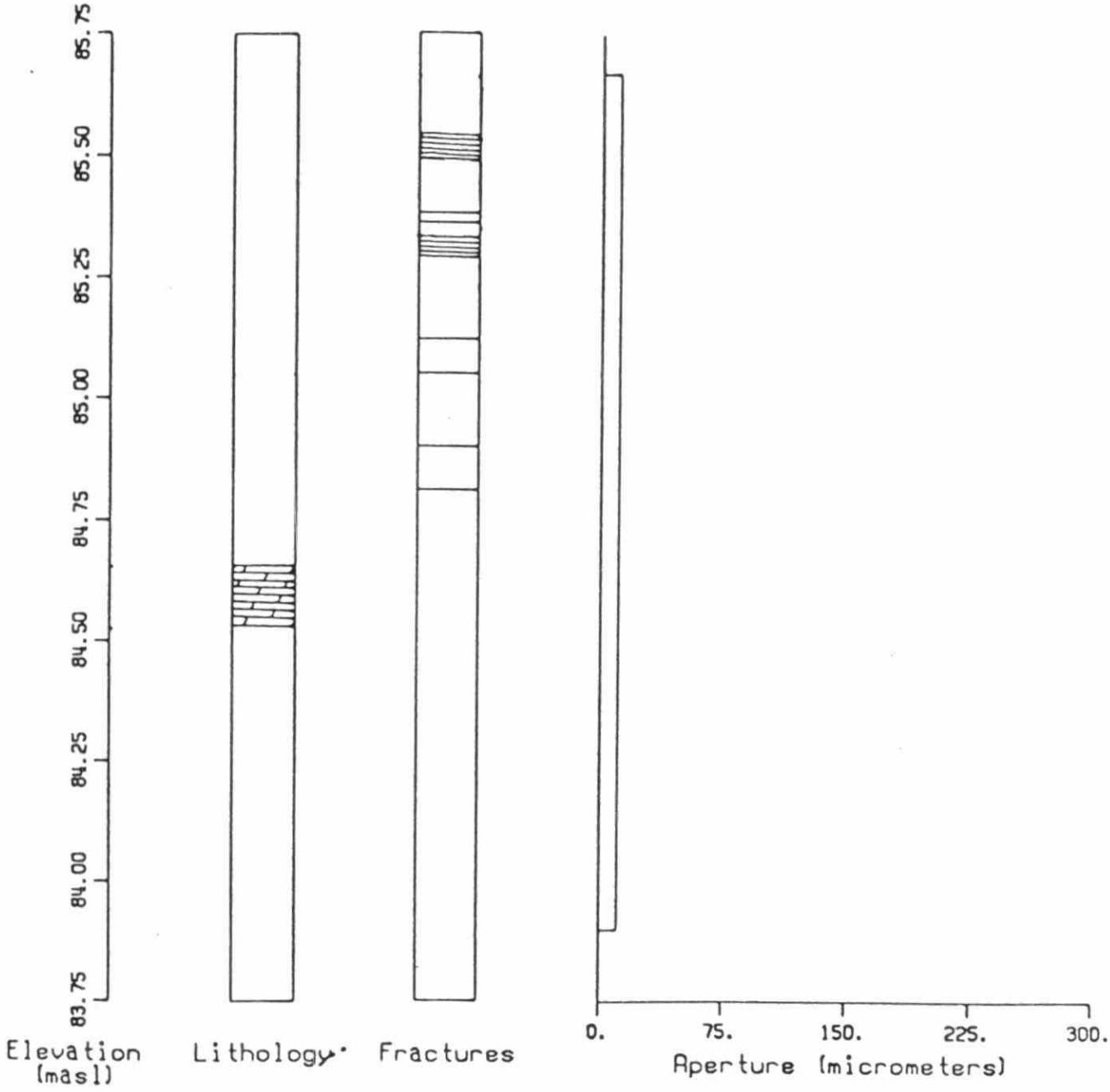

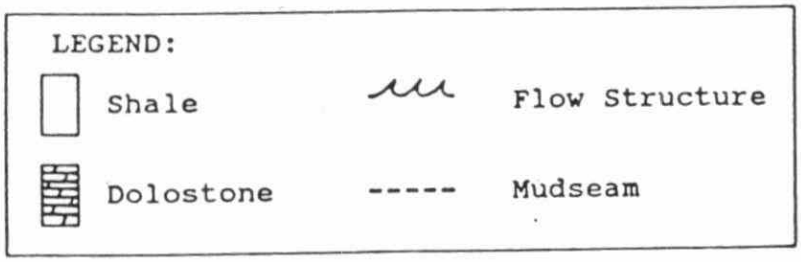

Figure A16: Lithology, fracture and aperture logs for UW16.

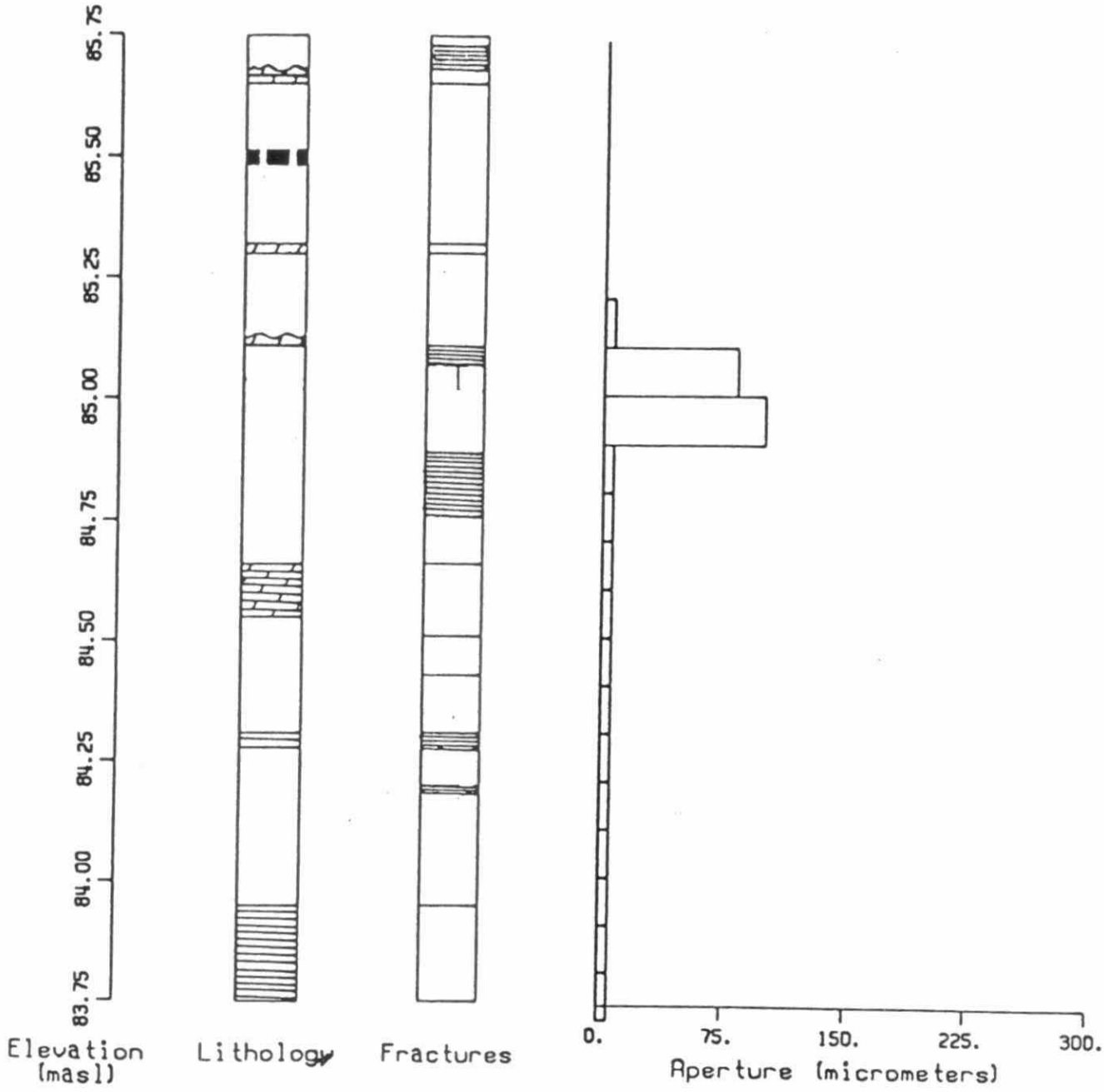

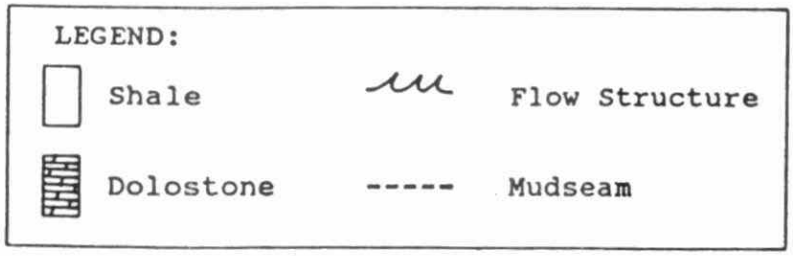

Figure A17: Lithology, fracture and aperture logs for UW17.

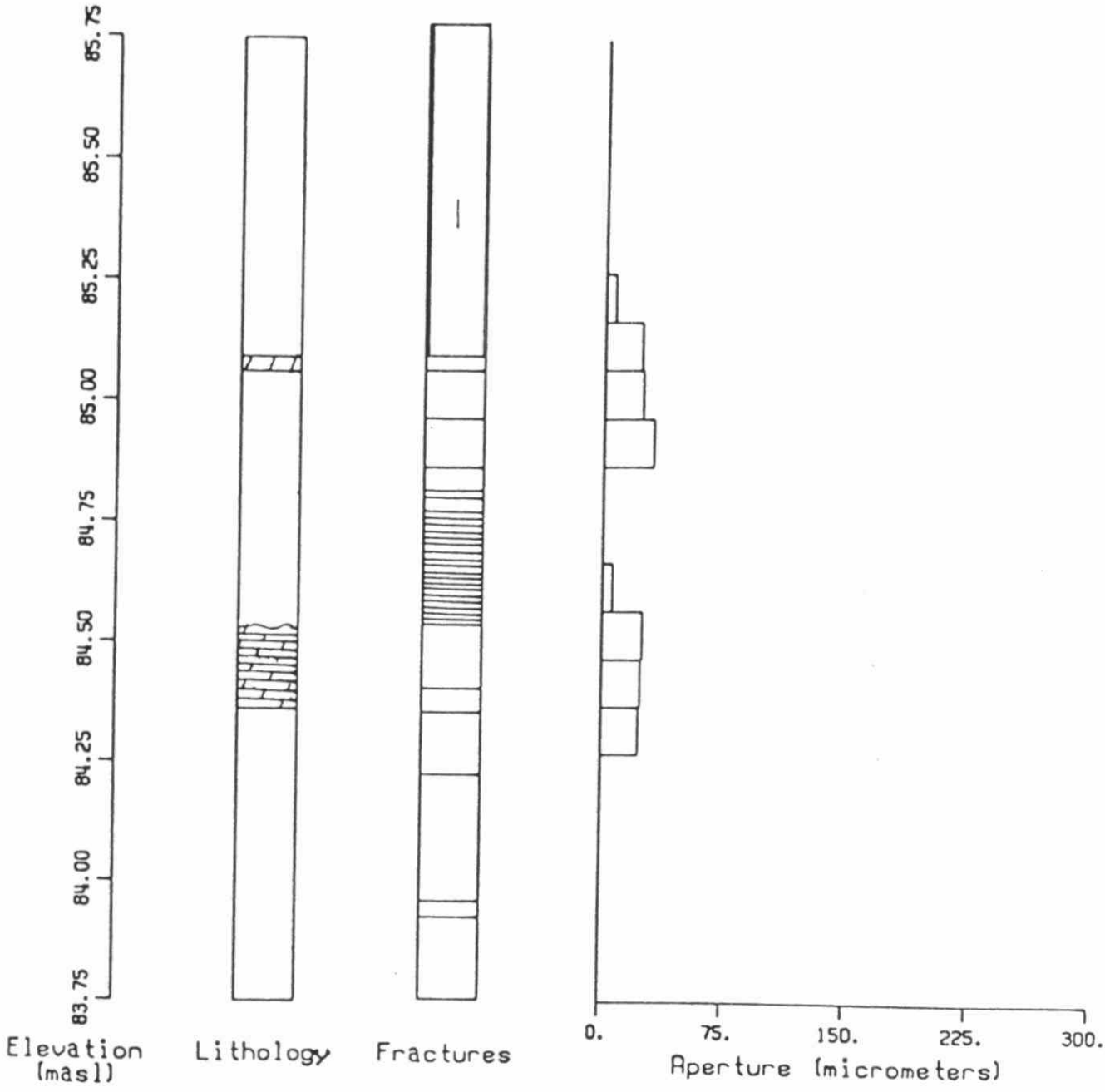

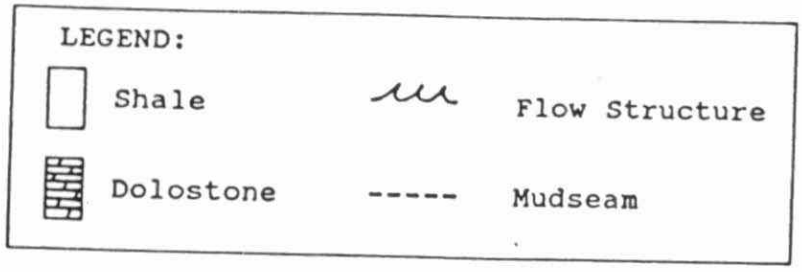

Figure A18: Lithology, fracture and aperture logs for UW18.

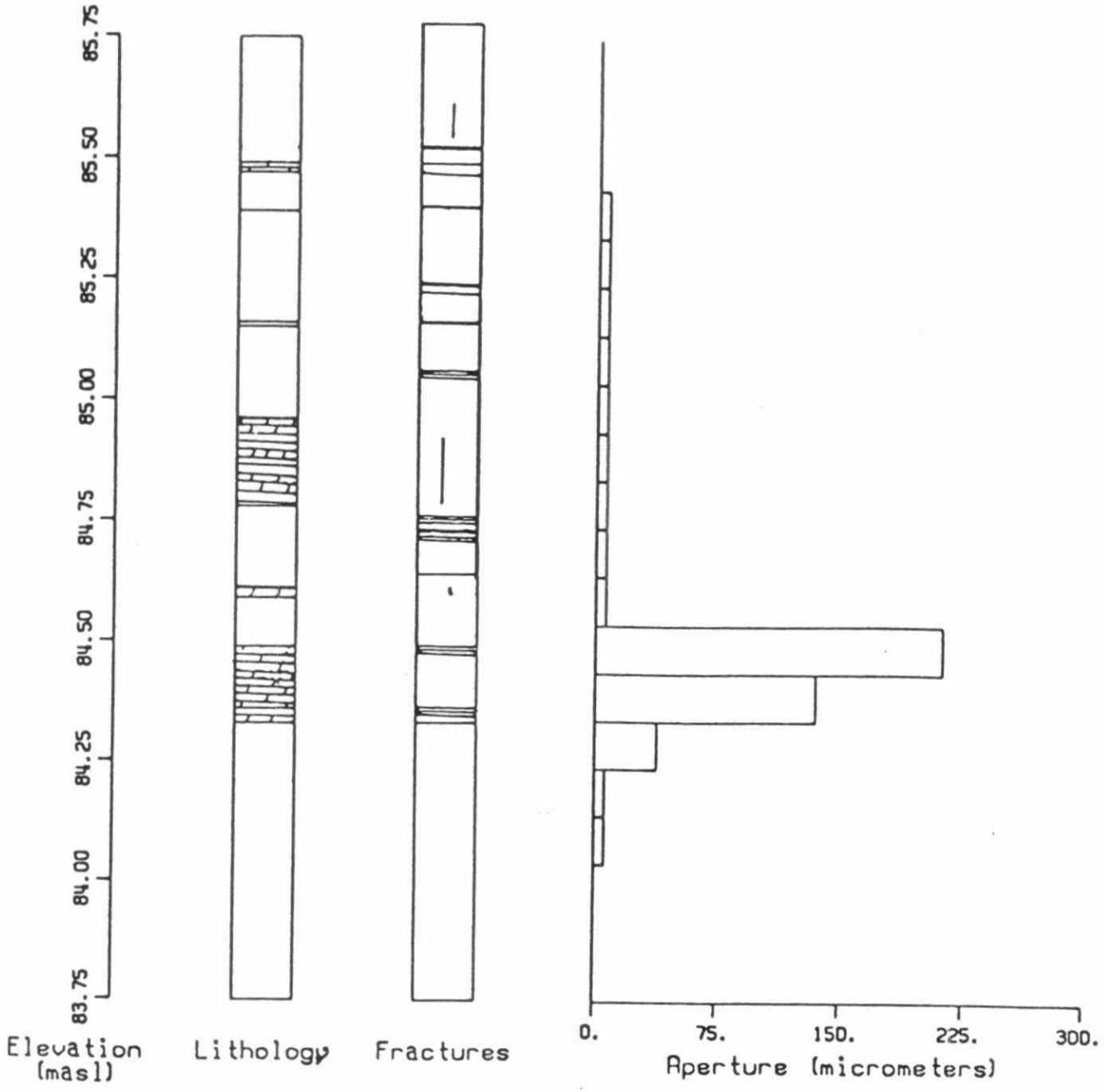

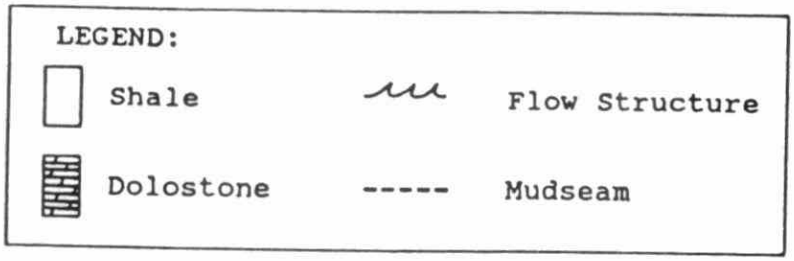

Figure A19: Lithology, fracture and aperture logs for UW19.

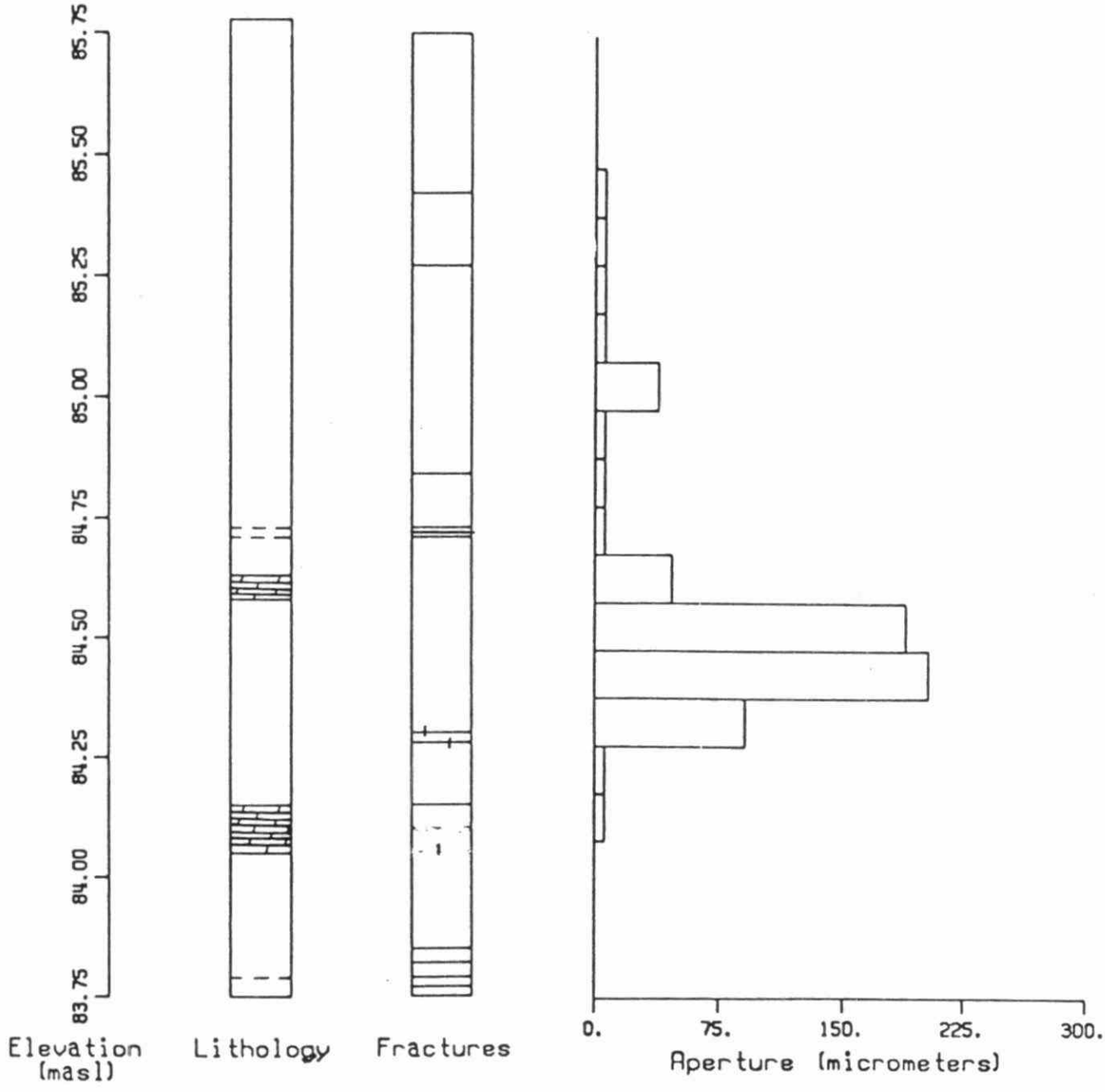

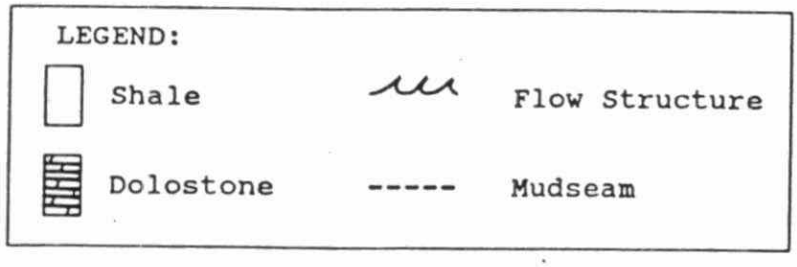

Figure A20: Lithology, fracture and aperture logs for UW20.

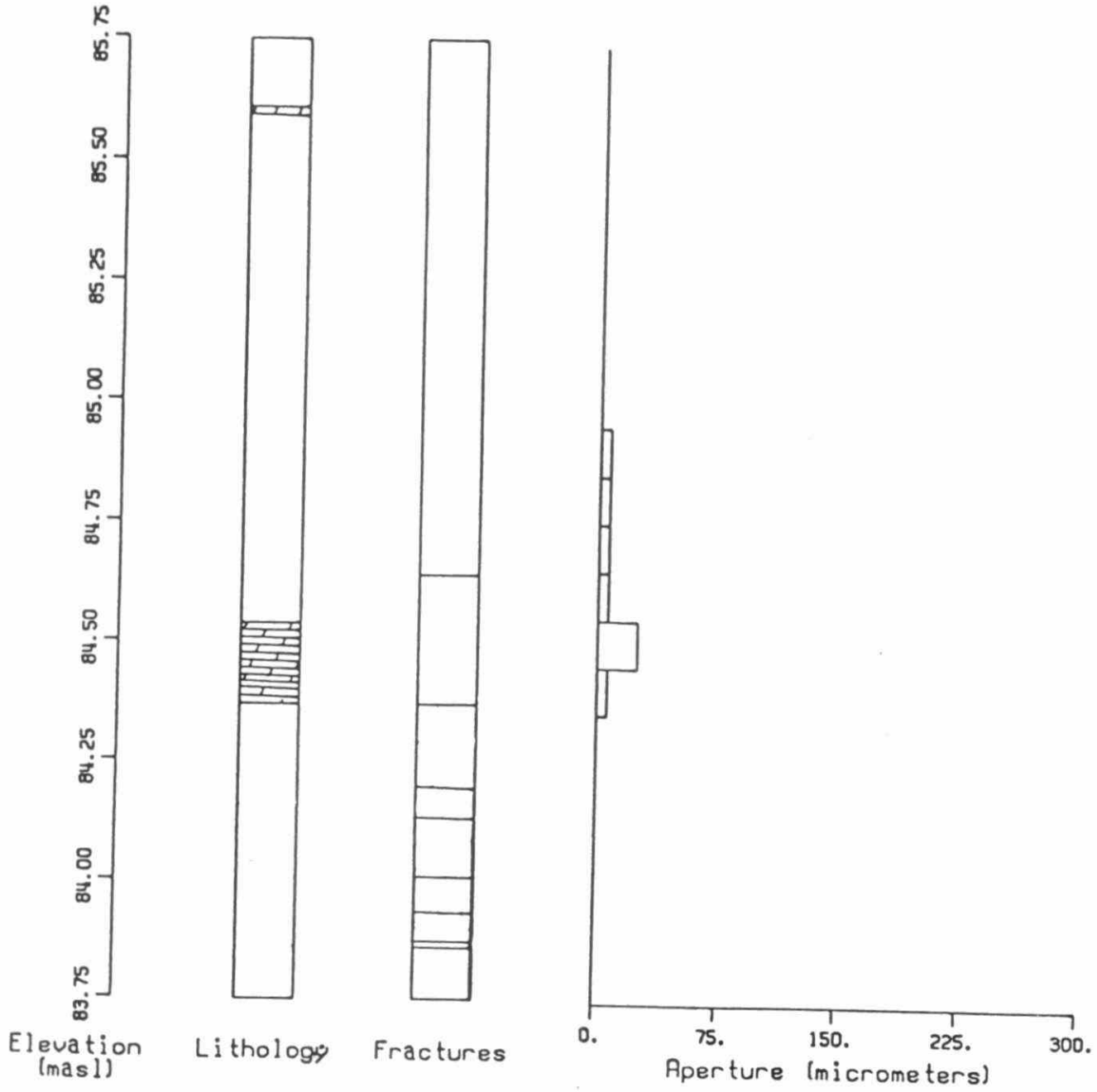

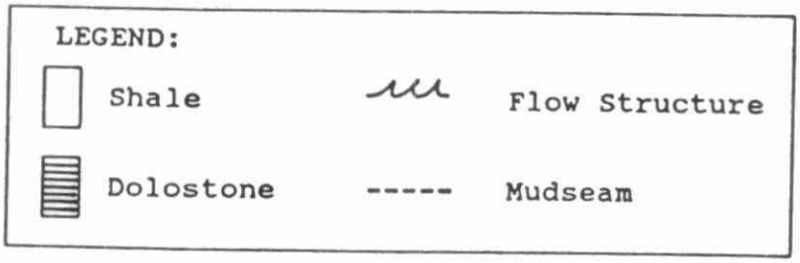

Figure A21: Lithology, fracture and aperture logs for UW21.

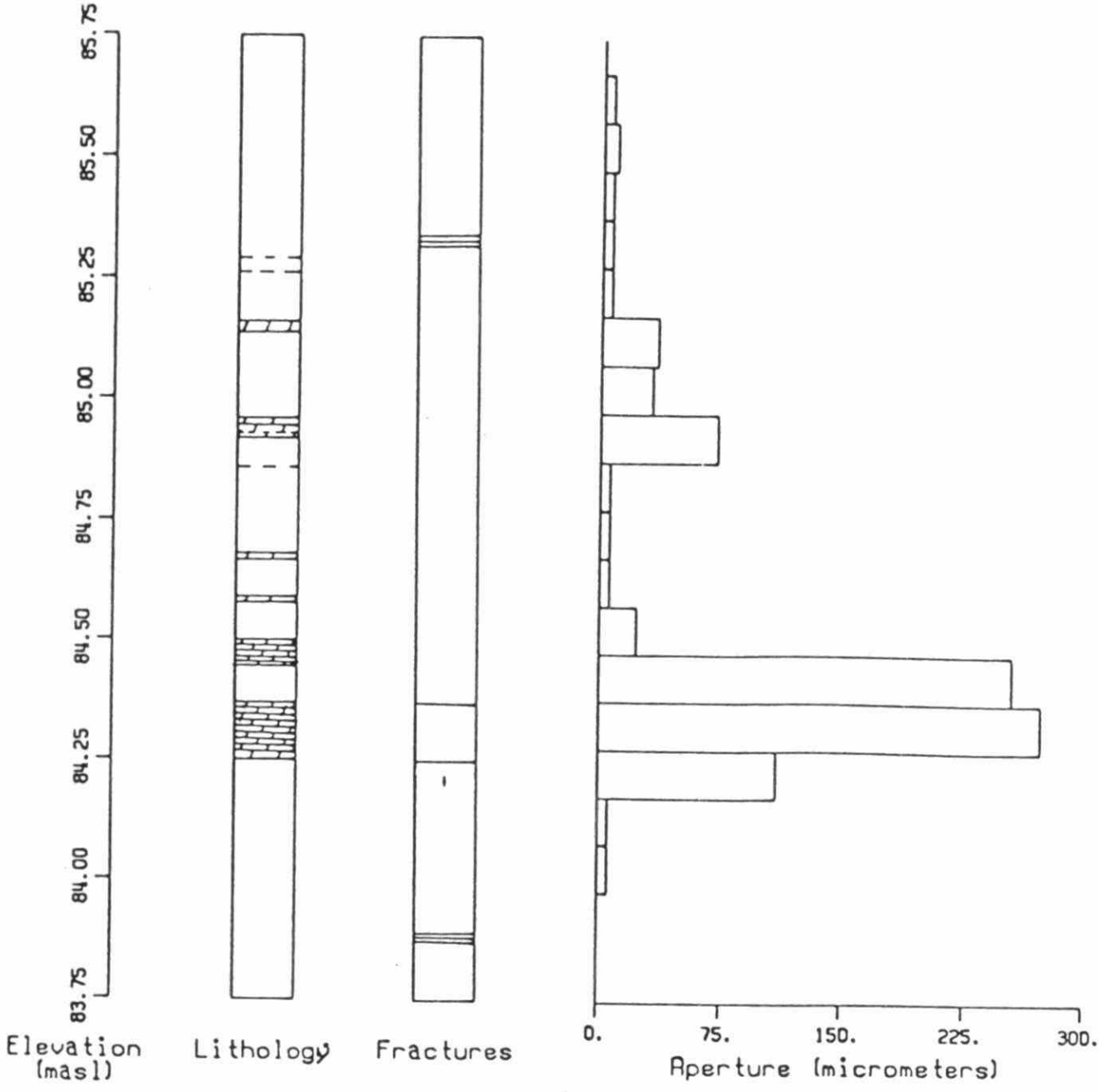

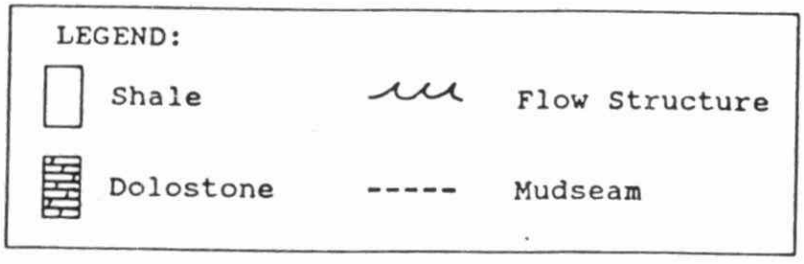

Figure A22: Lithology, fracture and aperture logs for UW22.

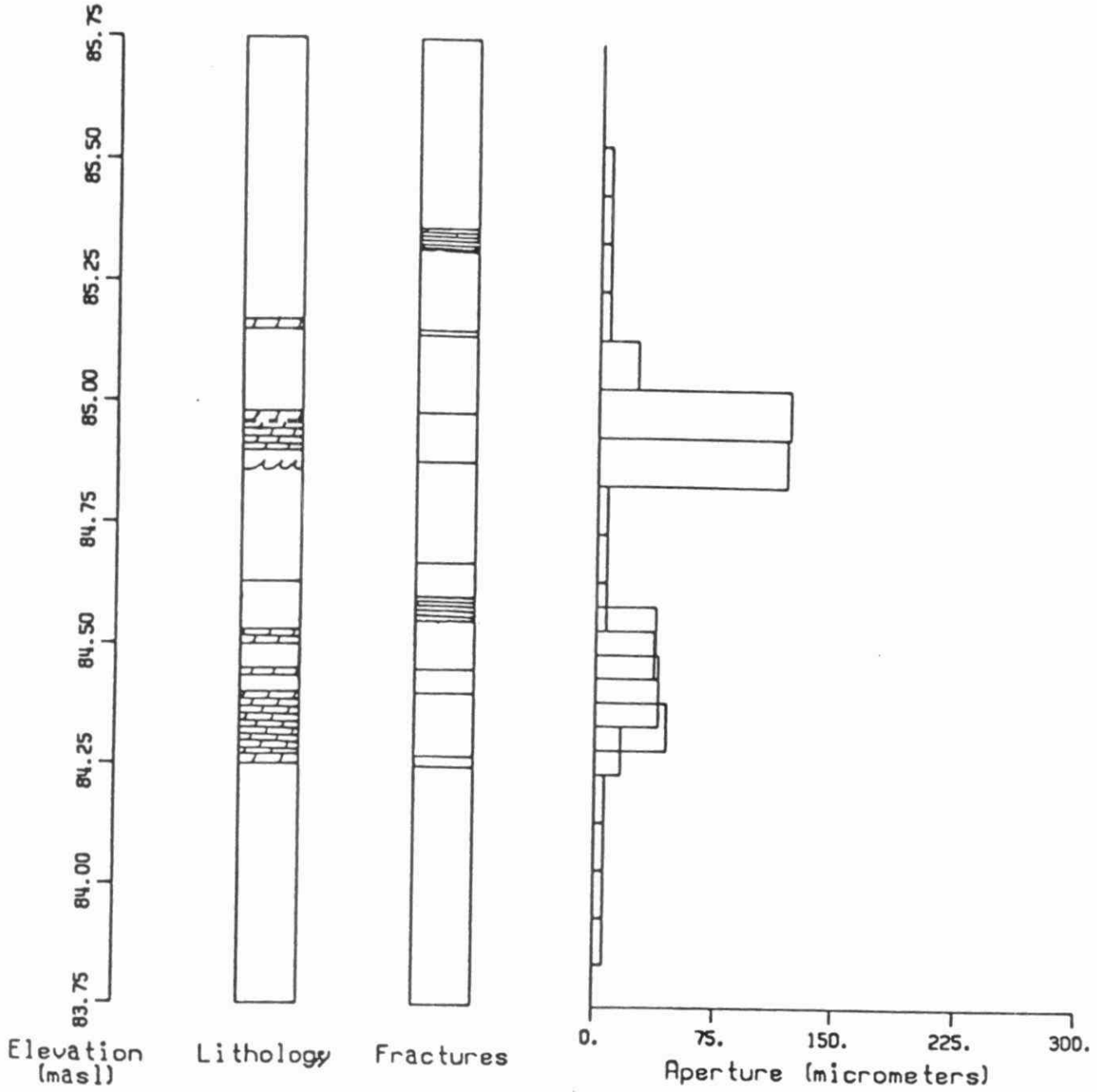

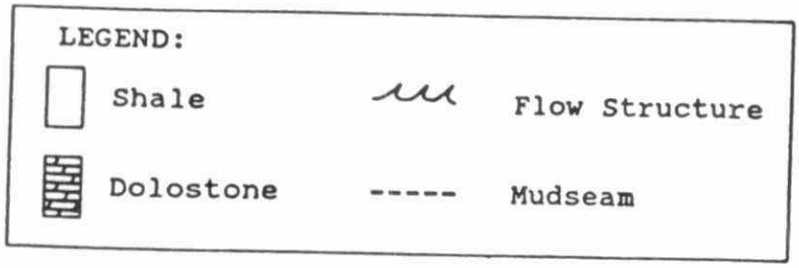

Figure A23: Lithology, fracture and aperture logs for UW23.

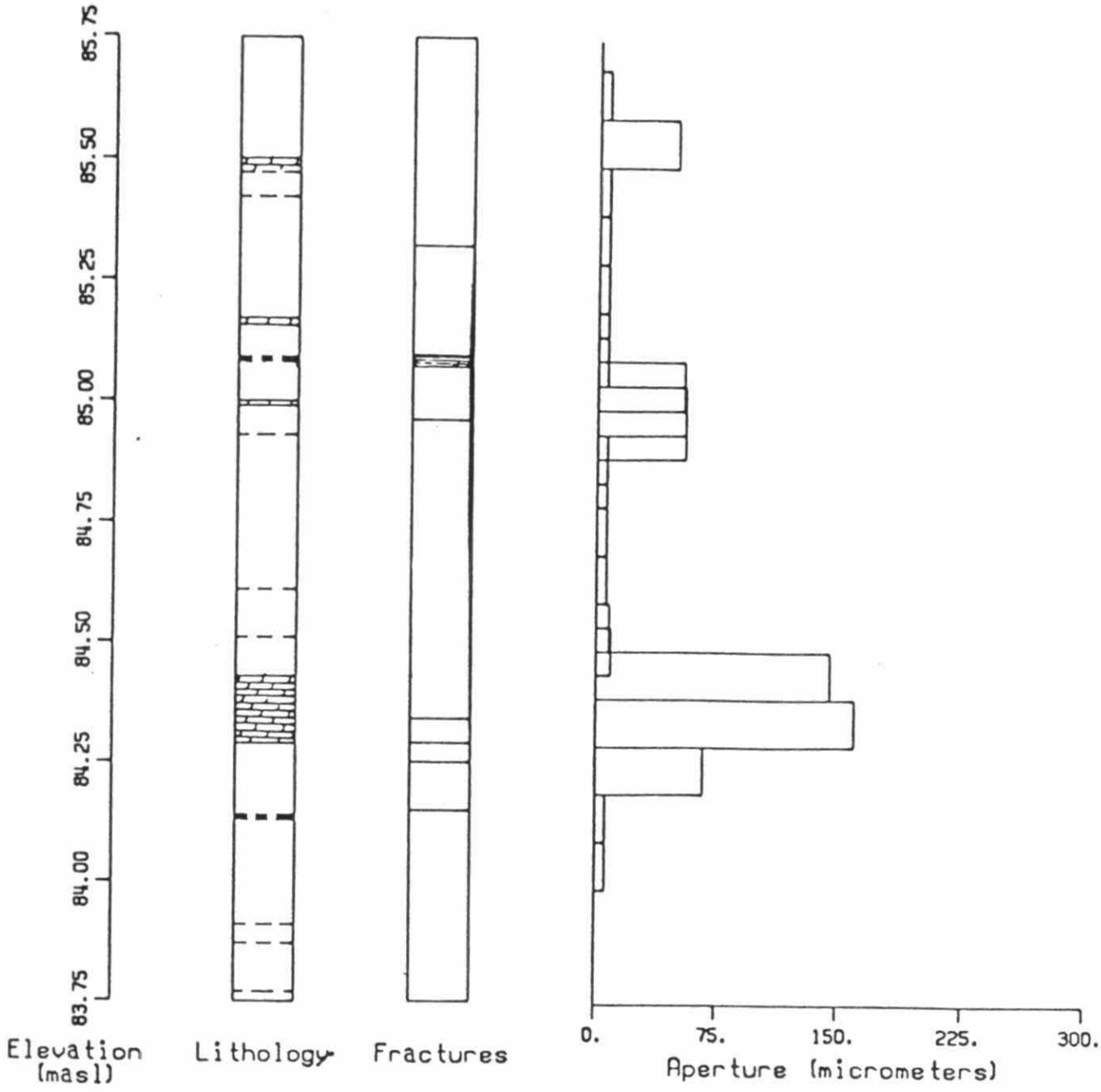

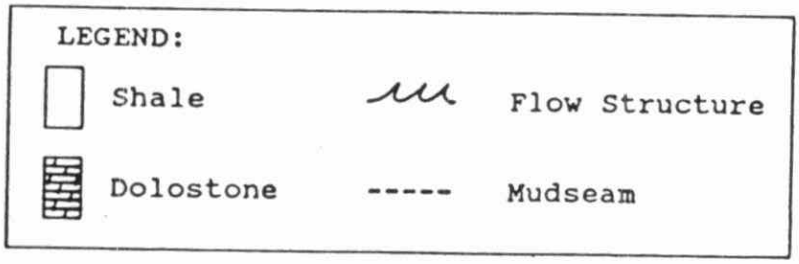

Figure A24: Lithology, fracture and aperture logs for UW24.

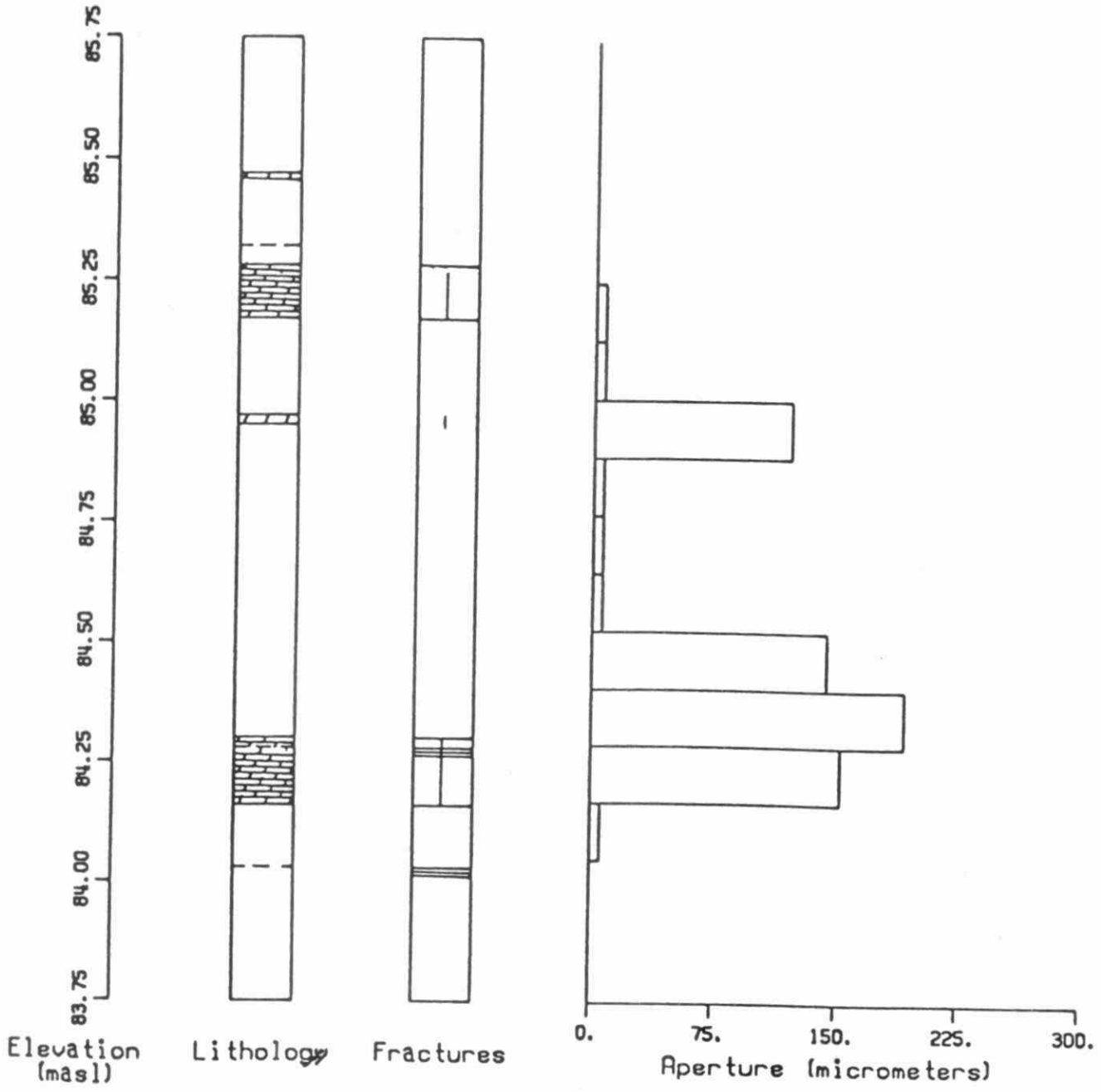

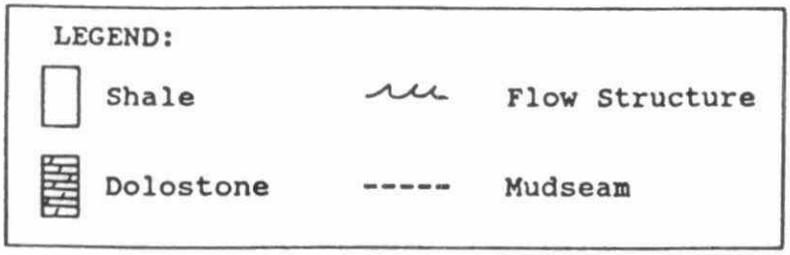

Figure A25: Lithology, fracture and aperture logs for UW25.

APPENDIX D

Hydraulic Head Measurements
1990-1991

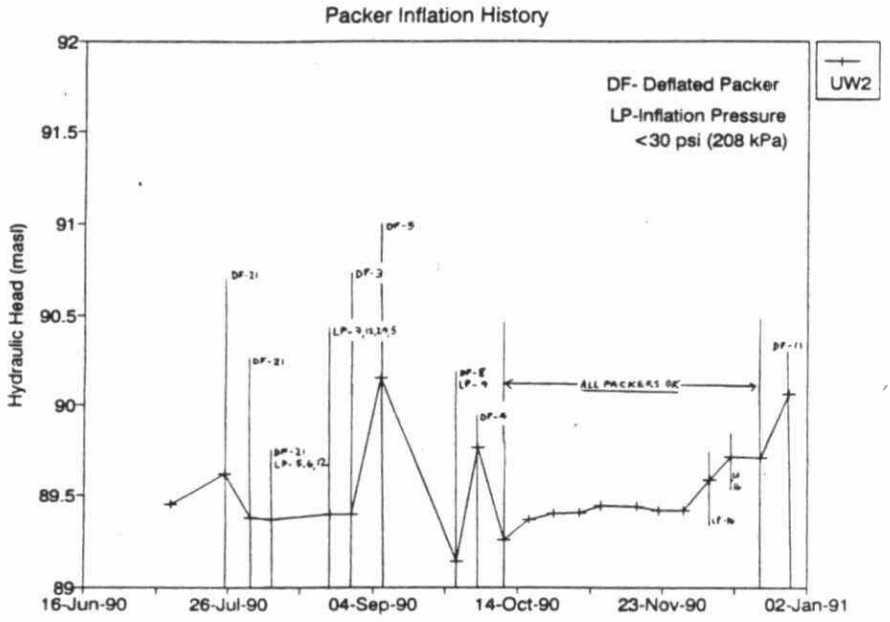

Figure D1: Status of borehole packers between June 1990 and December 1990, based on weekly measurements of packer inflation.

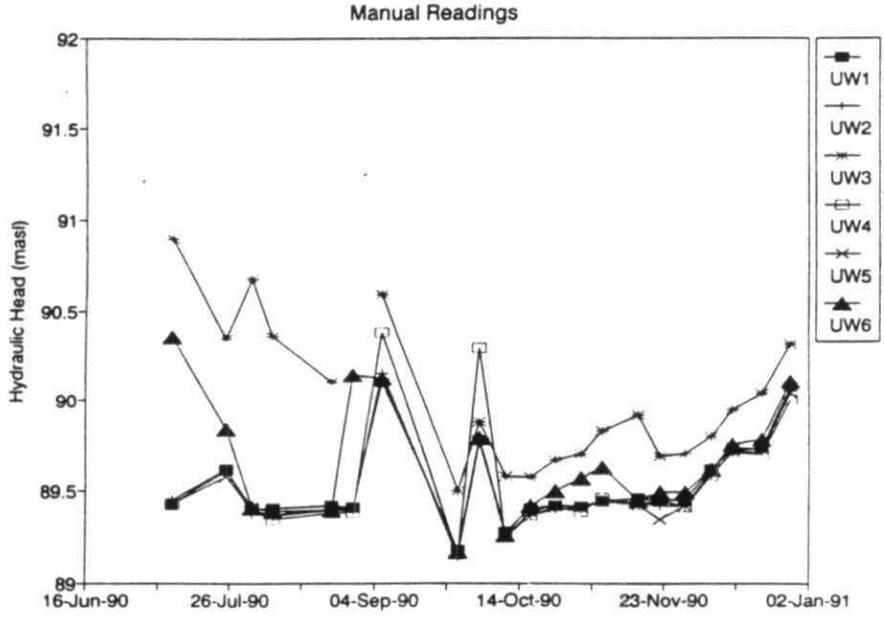

Figure D2: Hydraulic head in the lower fracture plane in UW1-UW6, based on weekly manual measurements (June -December 1990).

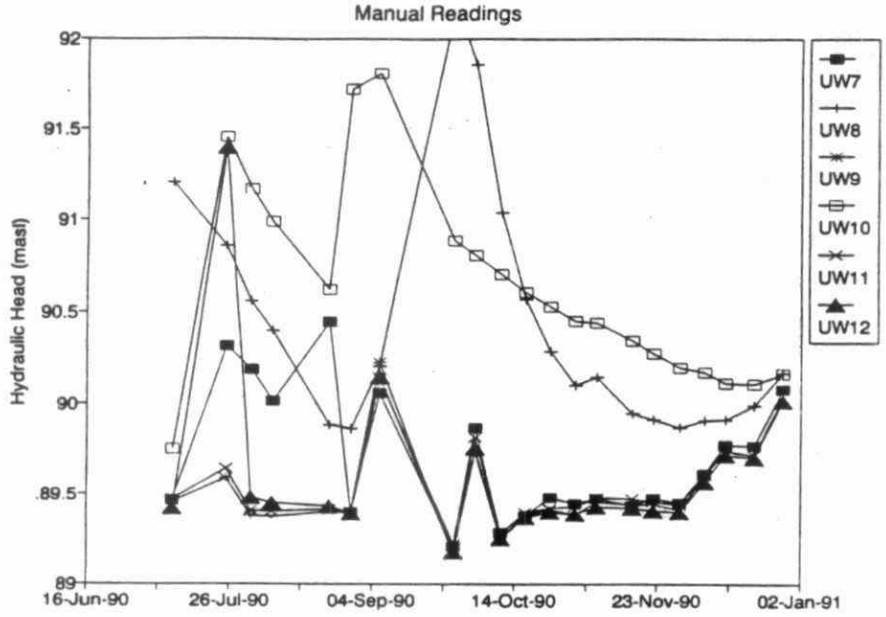

Figure D3: Hydraulic head in the lower fracture plane in UW7-UW12, based on weekly manual measurements (June -December 1990).

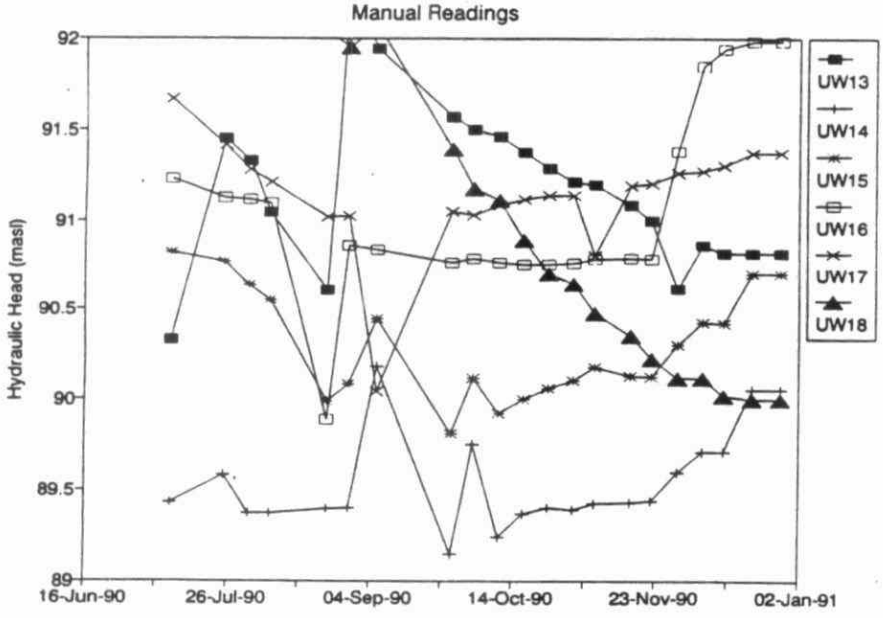

Figure D4: Hydraulic head in the lower fracture plane in UW13-UW18, based on weekly manual measurements (June -December 1990).

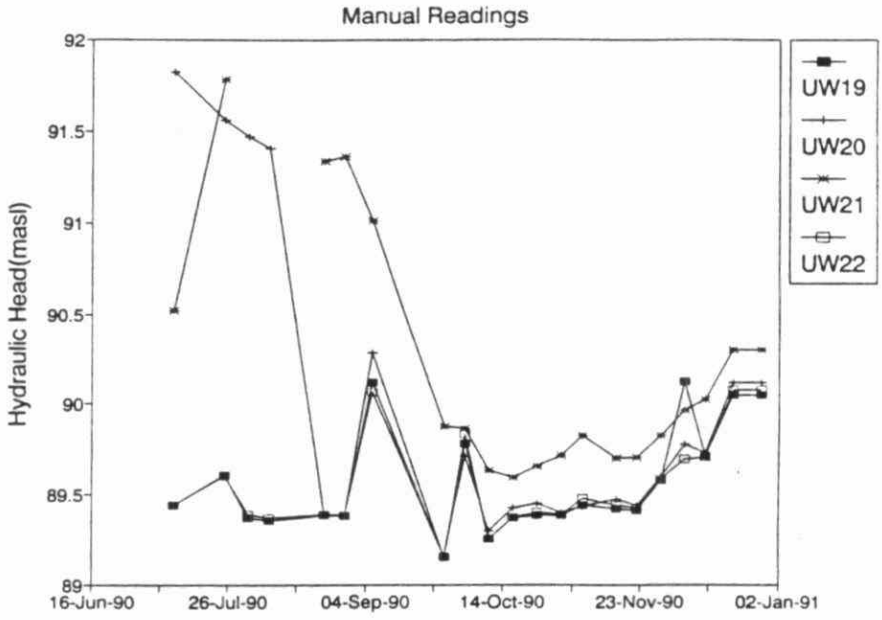

Figure D5: Hydraulic head in the lower fracture plane in UW19-UW22, based on weekly manual measurements (June -December 1990).

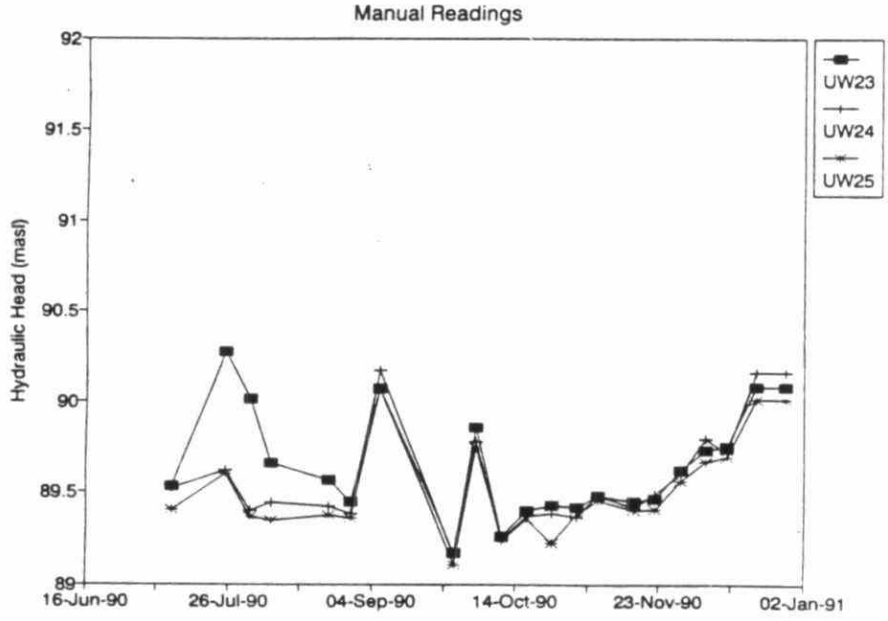

Figure D6: Hydraulic head in the lower fracture plane in UW23-UW25, based on weekly manual measurements (June -December 1990).

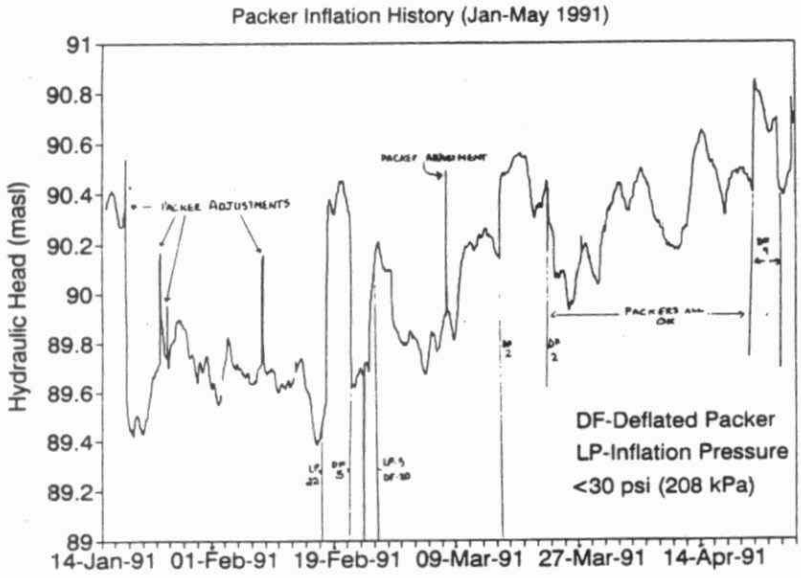

Figure D7: Status of borehole packers between Jan 1991 and May 1991, based on weekly measurements of packer inflation.

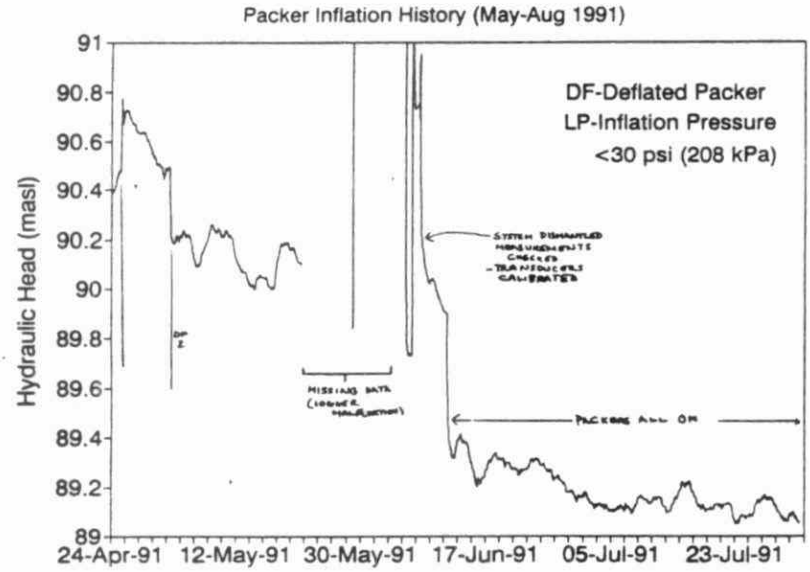

Figure D8: Status of borehole packers between May 1991 and August 1991, based on weekly measurements of packer inflation.

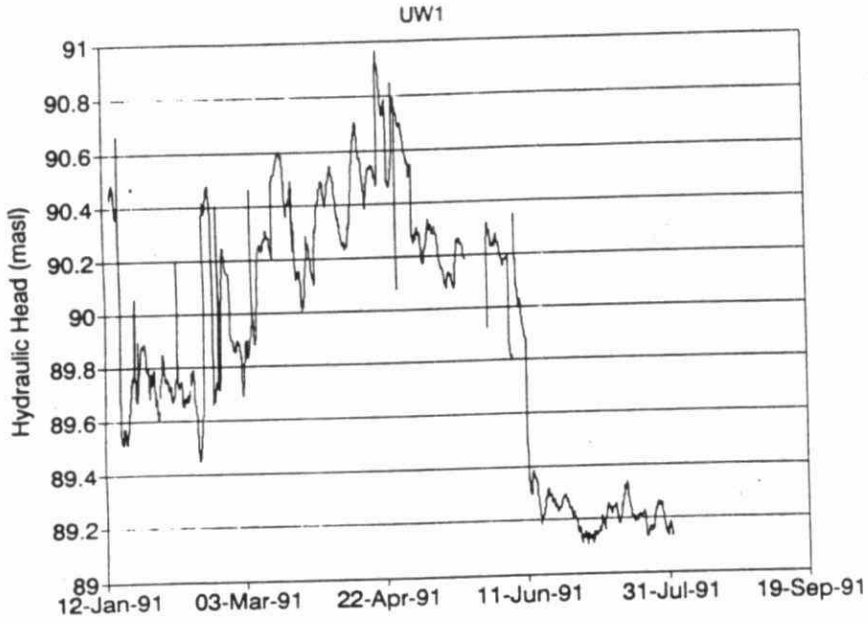

Figure D9: Hydraulic head in lower fracture plane in UW1, based on transducer measurements.

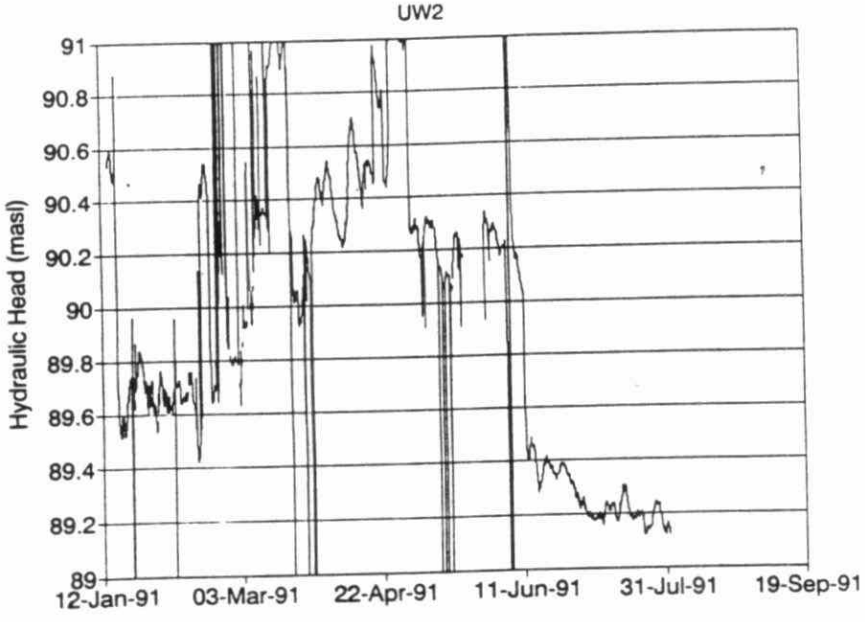

Figure D10: Hydraulic head in lower fracture plane in UW2, based on transducer measurements.

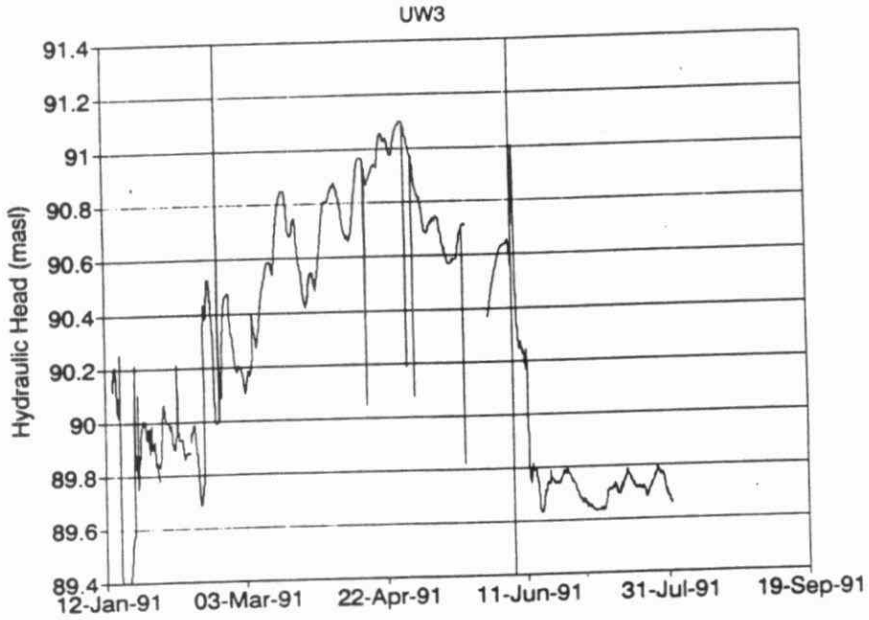

Figure D11: Hydraulic head in lower fracture plane in UW3, based on transducer measurements.

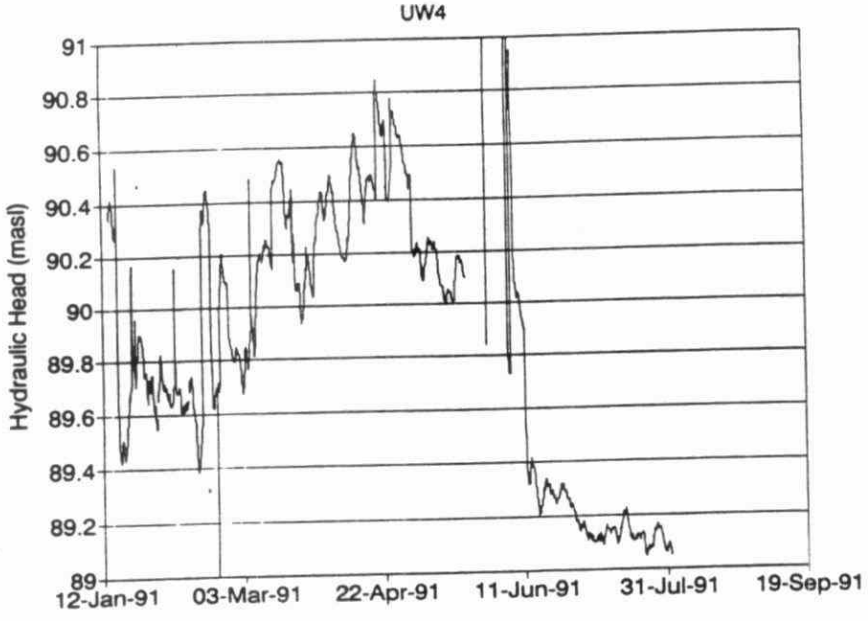

Figure D12: Hydraulic head in lower fracture plane in UW4, based on transducer measurements.

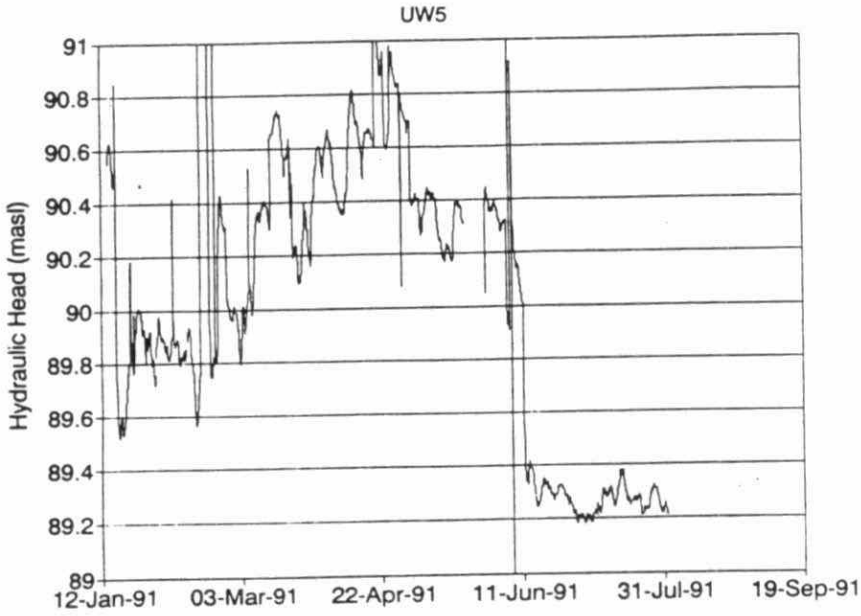

Figure D13: Hydraulic head in lower fracture plane in UW5, based on transducer measurements.

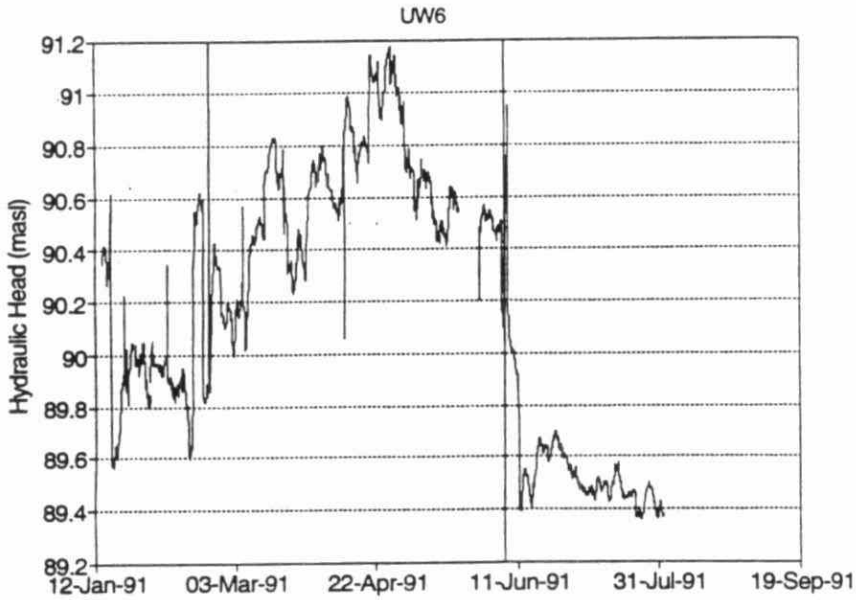

Figure D14: Hydraulic head in lower fracture plane in UW6, based on transducer measurements.

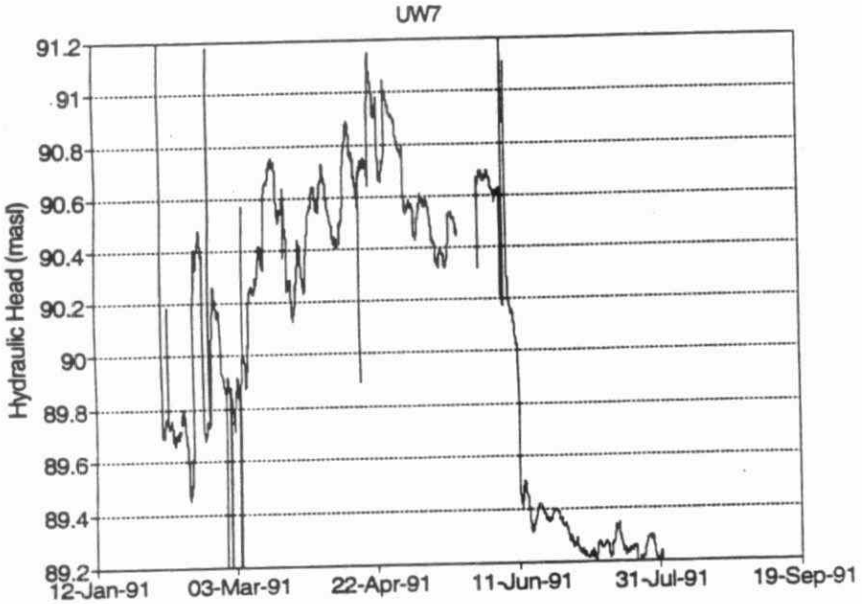

Figure D15: Hydraulic head in lower fracture plane in UW7, based on transducer measurements.

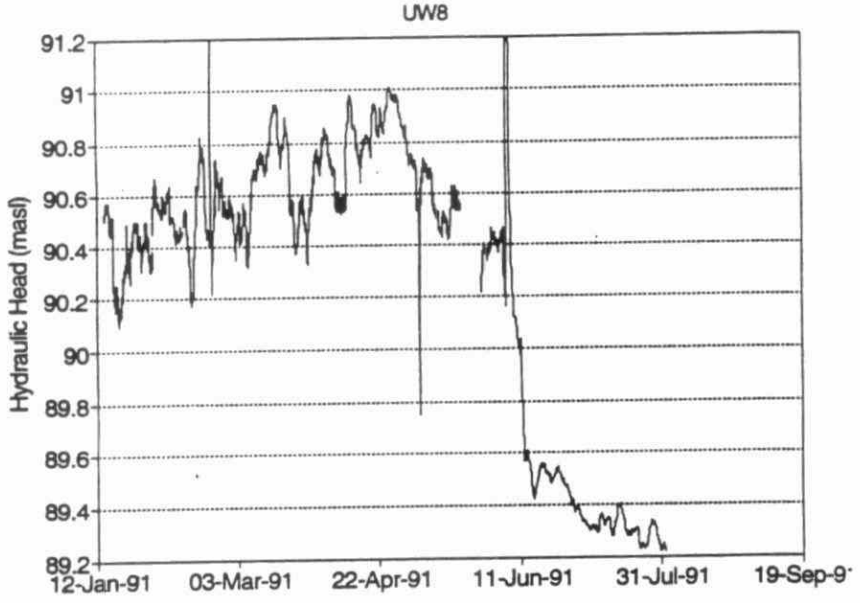

Figure D16: Hydraulic head in lower fracture plane in UW8, based on transducer measurements.

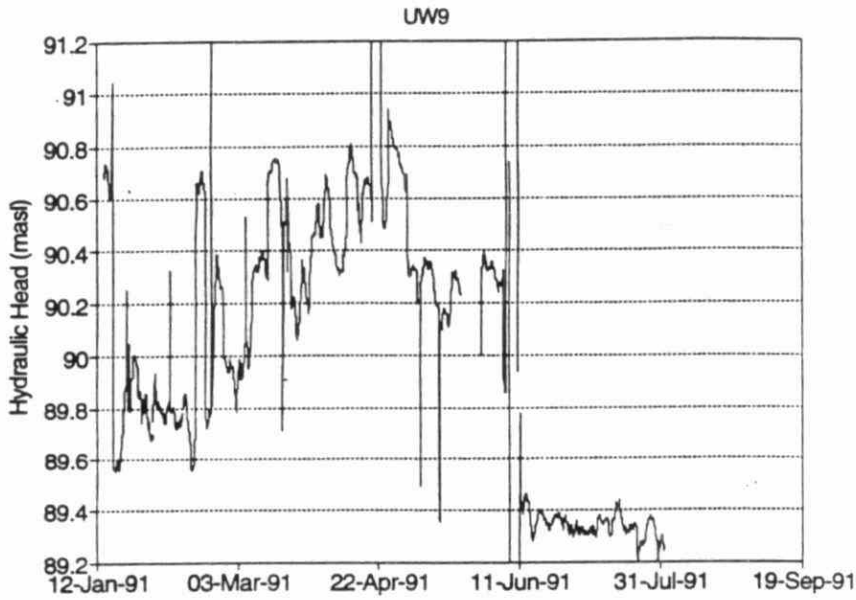

Figure D17: Hydraulic head in lower fracture plane in UW9, based on transducer measurements.

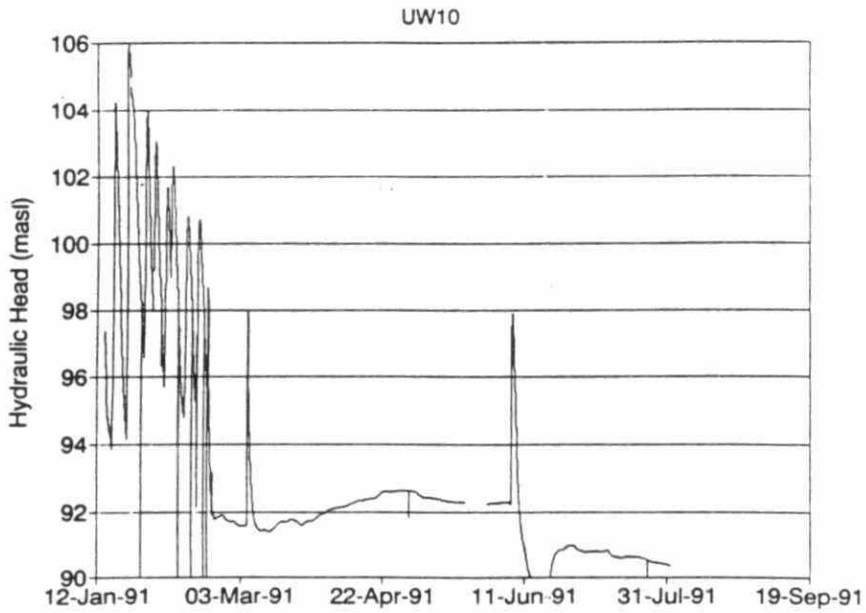

Figure D18: Hydraulic head in lower fracture plane in UW10, based on transducer measurements.

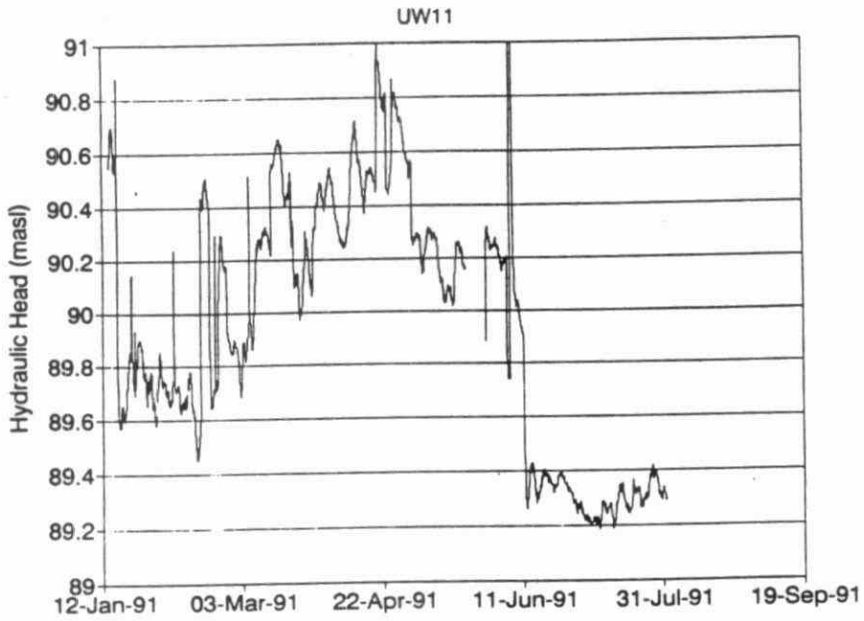

Figure D19: Hydraulic head in lower fracture plane in UW11, based on transducer measurements.

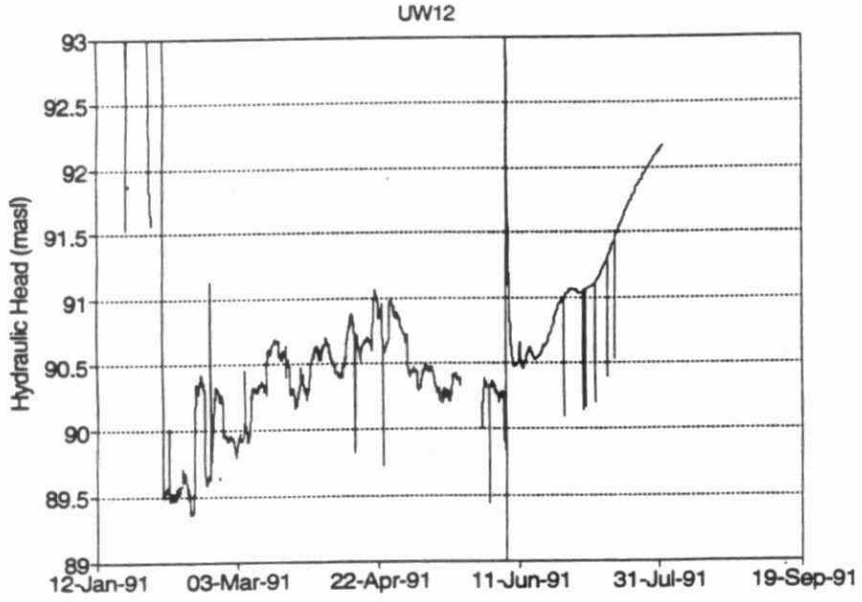

Figure D20: Hydraulic head in lower fracture plane in UW12, based on transducer measurements.

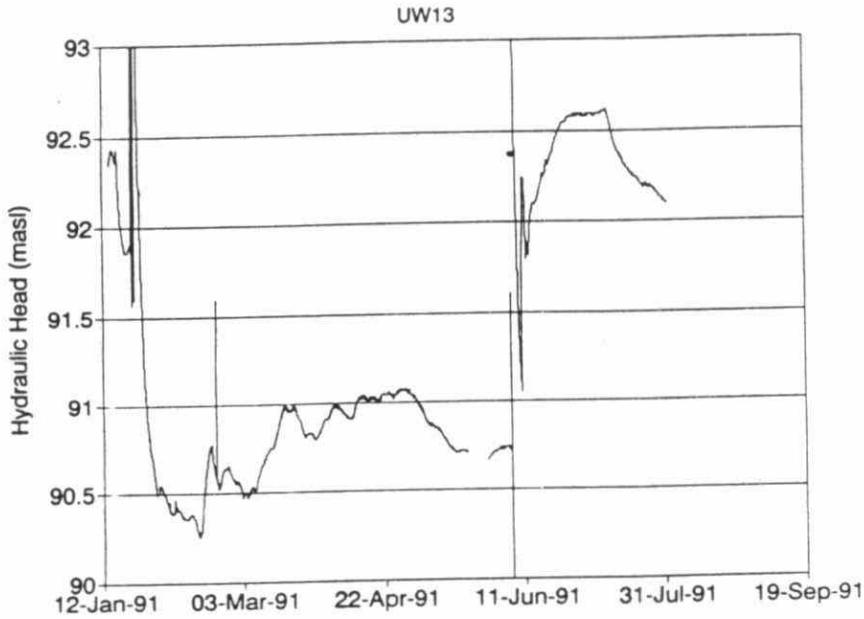

Figure D21: Hydraulic head in lower fracture plane in UW13, based on transducer measurements.

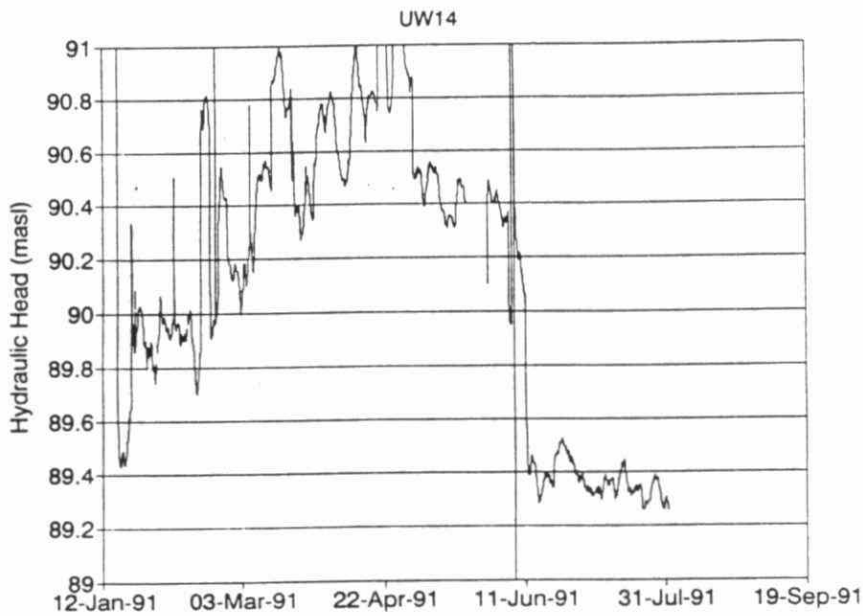

Figure D22: Hydraulic head in lower fracture plane in UW14, based on transducer measurements.

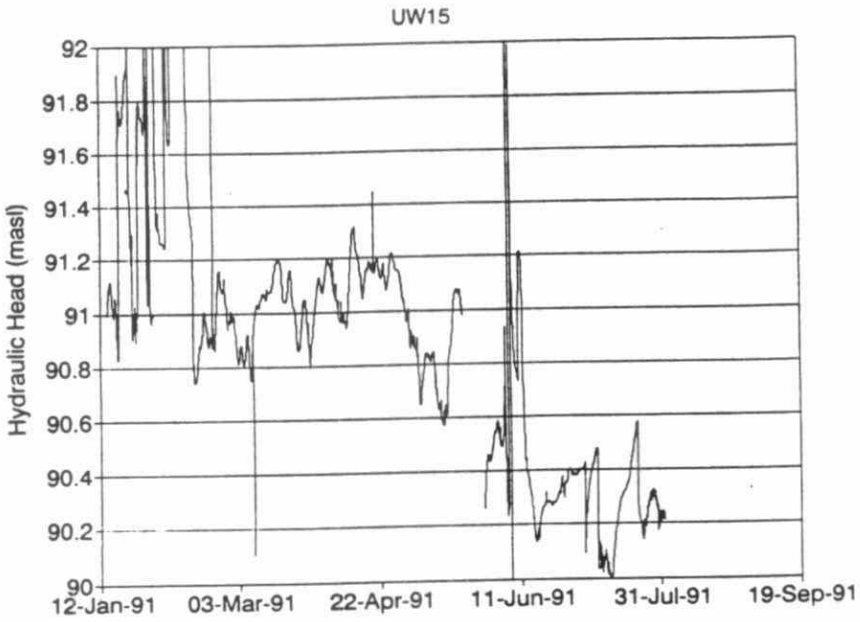

Figure D23: Hydraulic head in lower fracture plane in UW15, based on transducer measurements.

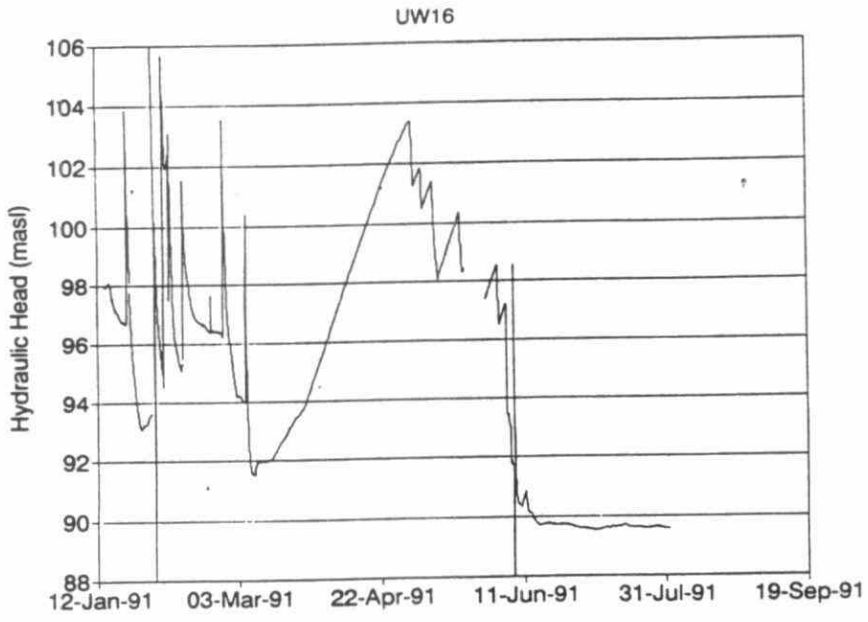

Figure D24: Hydraulic head in lower fracture plane in UW16, based on transducer measurements.

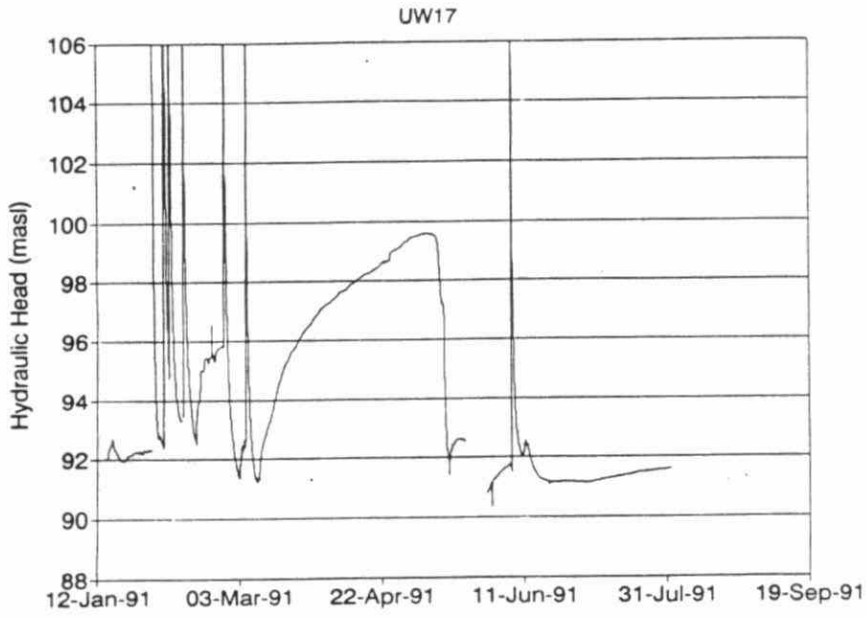

Figure D25: Hydraulic head in lower fracture plane in UW17, based on transducer measurements.

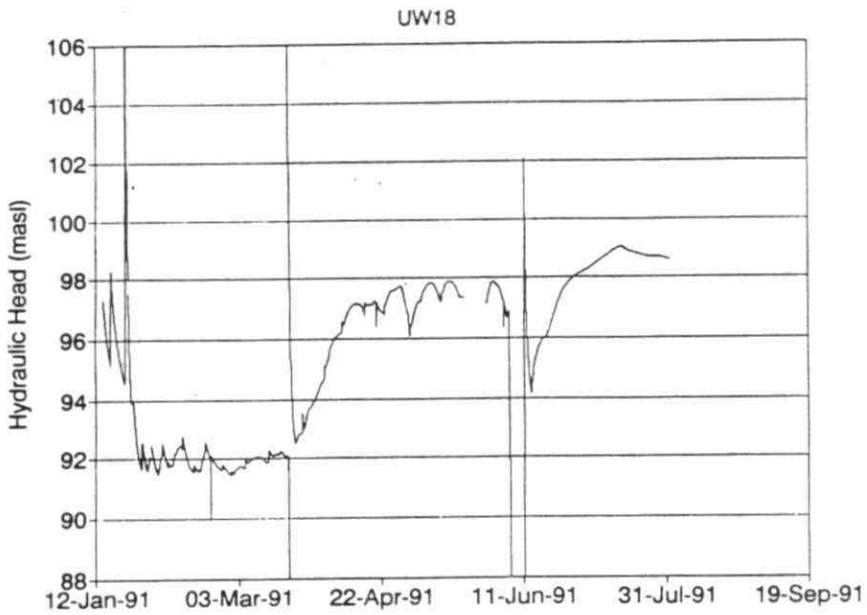

Figure D26: Hydraulic head in lower fracture plane in UW18, based on transducer measurements.

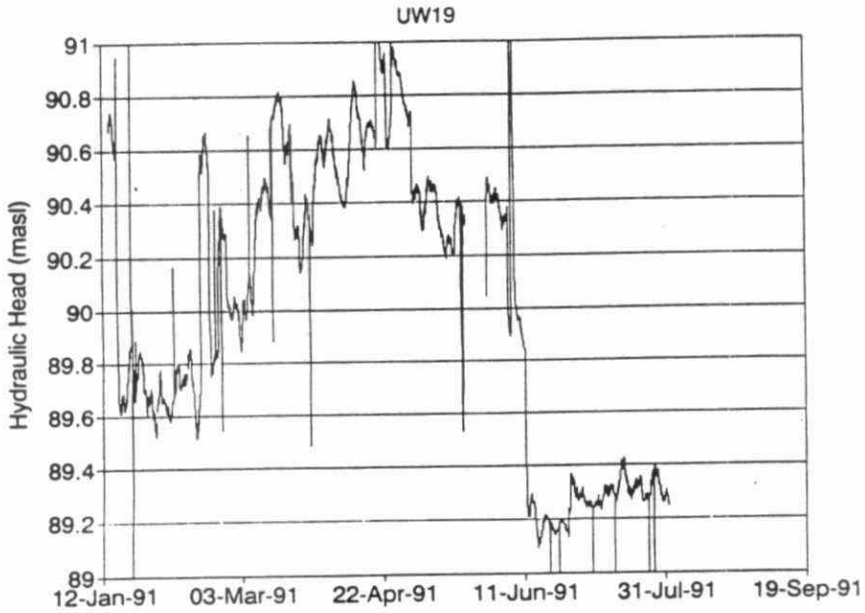

Figure D27: Hydraulic head in lower fracture plane in UW19, based on transducer measurements.

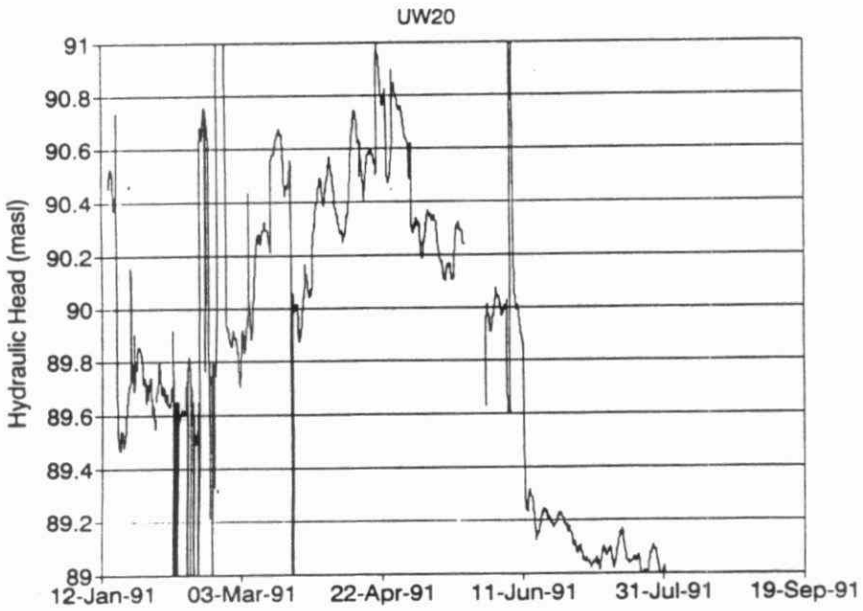

Figure D28: Hydraulic head in lower fracture plane in UW20, based on transducer measurements.

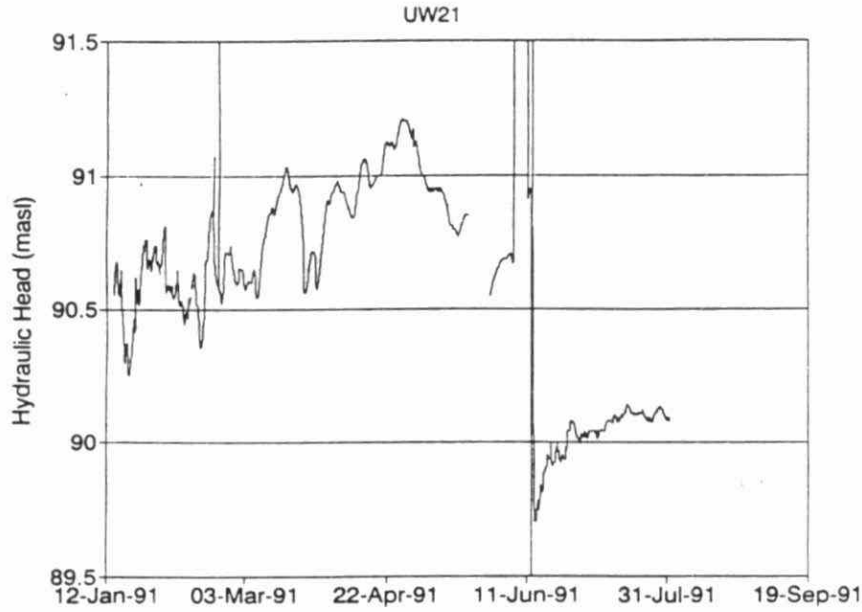

Figure D29: Hydraulic head in lower fracture plane in UW21, based on transducer measurements.

Figure D30: Hydraulic head in lower fracture plane in UW22, based on transducer measurements.

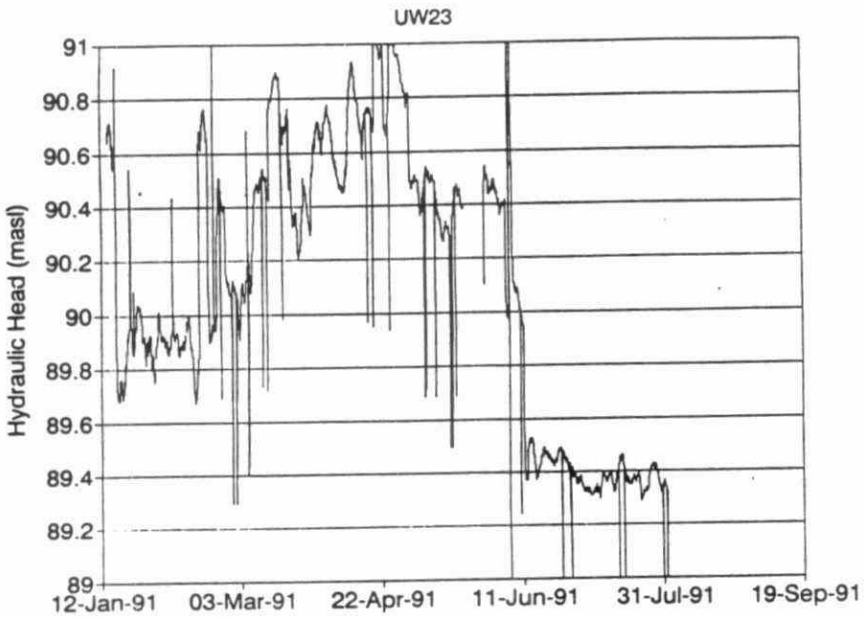

Figure D31: Hydraulic head in lower fracture plane in UW23, based on transducer measurements.

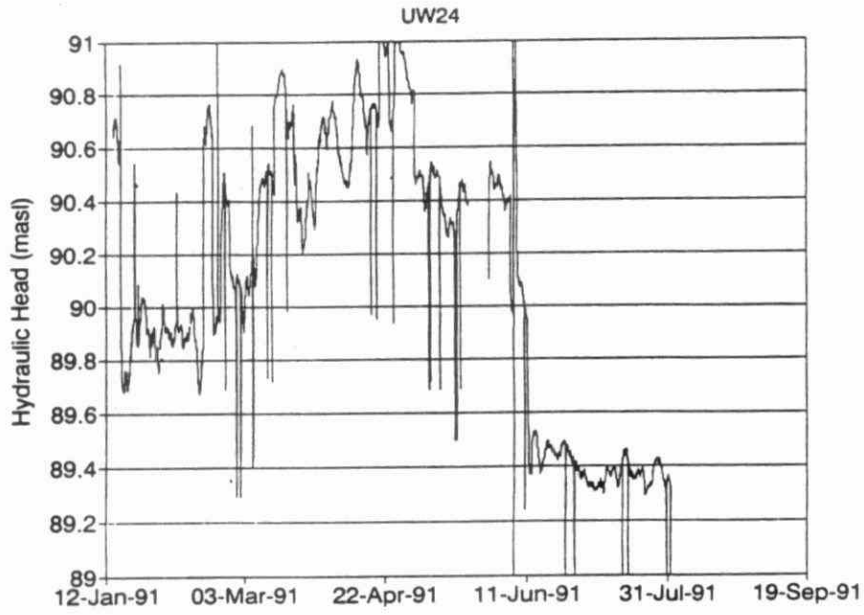

Figure D32: Hydraulic head in lower fracture plane in UW24, based on transducer measurements.

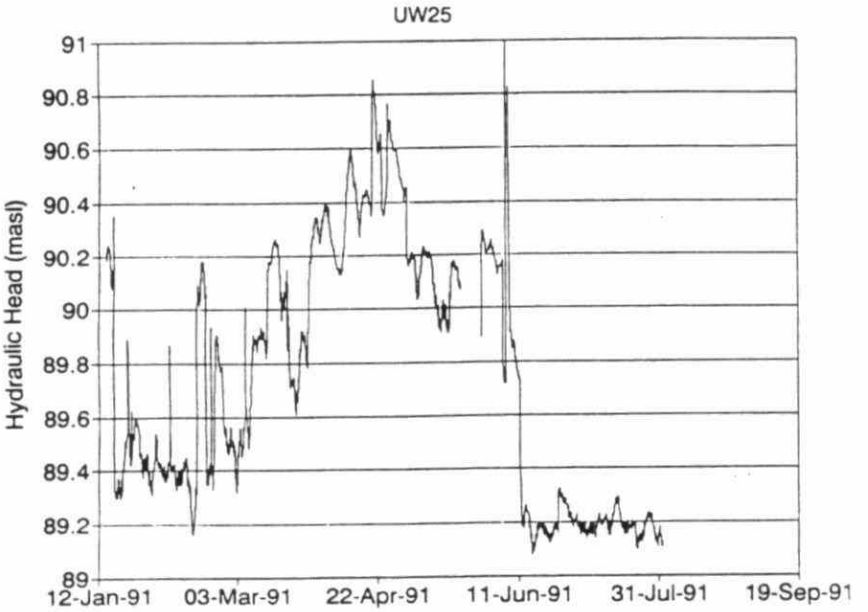

Figure D33: Hydraulic head in lower fracture plane in UW25, based on transducer measurements.

APPENDIX E

Report:

Determination of Fracture Aperture from the Response of Water Level in Wells to Natural Forces

by

G. Bickerton

UNIVERSITY OF WATERLOO
Faculty of Engineering

Determination of Fracture Aperture from the Response of Water Level in Wells to Natural Forces

Environment Canada
Canadian Centre for Inland Waters
National Water Research Institute
Rivers Research Branch
Burlington, Ontario

prepared by

Gregory Bickerton
ID 90357626
1A Civil Engineering
May 9, 1991

SUMMARY

This report is a preliminary investigation into the feasibility of determining the aperture of subsurface fractures utilizing the effects of natural forces (atmospheric and tidal) on well water levels.

Three models are presented each using different components of the natural forces to determine transmissivity and aperture, the SET approach utilizes tidal forces, the APV method atmospheric forces and CSA the combined effect of the two. Described are the theoretical background and mathematical techniques required to apply the models to field data, including descriptions of the limitations and data collection requirements. Preliminary results for an existing field site at Clarkson Ontario are shown with conclusions and recommendations made regarding areas for further research in natural forcings at this site.

It was concluded that the model could not be applied to the existing data set without modifications to the field set-up. Data collected prior to January 1991 can be used to calculate aperture, however the number of samples available is insufficient to produce a reliable estimate. If the monitoring system is not to be disturbed then an alternate approach must be found.

It is recommended that further research be done to derive an analytical solution to aperture involving barometric forcing in a closed well.

CONCLUSIONS

None of the models reviewed in both this paper and existing literature are directly applicable to the closed well system presently monitoring hydraulic head in an individual fracture at the Clarkson, Ontario field site.

The open well monitoring system that existed at Clarkson prior to January 1991, collected the required barometric and water level fluctuations necessary for the application of the APV model. However, the longest available monitoring period was significantly less than recommended and would be inadequate for a precise determination of transmissivity or aperture.

Preliminary results using the pre-January data indicate the fracture at Clarkson is insensitive to variation at tidal frequencies but responds to low frequency atmospheric variations.

A preliminary estimate of loading efficiency was calculated as 0.85

The apertures of the fracture at Clarkson lie in the identifiable window and should be able to be determined by the APV model.

RECOMMENDATIONS

The APV method is recommended for use at the Clarkson field site, the CSA approach will have no additional benefit due to the formation's insensitivity to tidal frequencies.

A future avenue of research to pursue is the derivation of an analytical solution to formation pressure response to atmospheric forces in a closed well. This would be more suited to Clarkson because the existing monitoring system would not have to be disrupted.

A data set consisting of 2048 hourly spaced samples obtained from a large aperture fracture should be analyzed to determine if the transmissivity lies in the detectable range of the model. This sample may be obtained from a new experiment or by reconstructing existing data through interpolation and adding it to the pre-January 1991 sample. If the largest aperture or transmissivity is undetectable the same will be true for smaller apertures making the model inapplicable to this particular site.

An investigation into the validity of assumptions and boundary conditions of the model should be considered, to determine whether the analysis is appropriate for Clarkson data.

INTRODUCTION

In the investigation of groundwater flow systems it may not always be desirable (or possible) to determine aquifer properties through hydraulic tests (ie. pumping or slug tests). For example, in an area where groundwater contamination has occurred, the removal of contaminated water is undesirable due to disposal cost. In such a situation it would be beneficial to have alternative approaches to parameter determination available. Motivations such as these have lead researchers into considering the use of natural forces in the determination of aquifer parameters. Hsieh *et al.* [1987], Rojstaczer [1988] and Ritzi [1989] have examined the response of water level in wells to natural forces and used this information to determine the transmissivity of an aquifer. Hsieh *et al.* [1987] considered the effects of lunar tides, Rojstaczer [1988] examined atmospheric forcing and Ritzi [1989] derived an analytic solution utilizing both atmospheric and tidal influences in the determination of transmissivity. The later of these approaches provides a significantly better estimate of transmissivity.

The Groundwater Section of the National Water Research Institute of Environment Canada is currently carrying out an on going study of flow and transport through subsurface fractures. As part of these studies, a multi-well monitoring system has been installed at a field site in Clarkson, Ontario. Here a single fracture intersected by 25 boreholes has been isolated and is being continuously monitored for variation in hydraulic head.

The purpose of this project was to research existing literature and investigate the feasibility of using natural forces to determine the transmissivity and aperture of an individual fracture; stating theoretical background, limitations and field data requirements. This report will serve as a preliminary investigation to be followed by more in depth research and experiments.

The nature of atmospheric changes and tidal effects will be examined in section 1.0 and 2.0 providing a general setting for the physical processes involved in a hydrogeologic context. In studies of natural forcing it is useful to examine the periodic and random components of the forces acting on the groundwater system; this is made possible through spectral analysis presented in section 3.0. Sections 4.0 and 5.0 introduce the theory and application of the model presented

by Ritzi [1989] and provide the modification required when considering an isolated fracture. Preliminary results from the Clarkson field site are presented in section 6.0. The findings provide insight into potential problems and suggest areas for further research.

1.0 TIDES

Tides are the response of the earth to forces provided by the sun and moon. These tidal forces not only produce noticeable effects in oceans, but also in the earth's crust. This information can be utilized for the purpose of estimating hydrologic parameters. The model considered in later sections will use tidal forcings and their effects, to calculate an estimate of transmissivity for both an aquifer and isolated fracture. This section provides a general introduction into the causes and effects of terrestrial tides.

Terrestrial tides are the result of interrelations between the earth, moon, sun and their respective orbits. The force of gravity between the celestial bodies provides the driving force necessary for tide generation. In order for the earth to maintain its shape, every particle in its make up must have the same centripetal acceleration [Thurman, 1988]. The gravitational attraction between objects supplies the acceleration. However, because the gravitational force is inversely proportional to distance, particles at greater distances from the disturbing body will receive a smaller components of force, while closer particles will receive a larger component of force. Accordingly, tides are the displacement of particles in a celestial body that result from a net force between the centripetal force required to maintain orbit and the gravitational attraction of neighbouring bodies [Godin, 1972].

Celestial orbits are periodic in nature and since tides are the result of orbital relations, they too display a periodic behaviour. As a result of astronomical observations these periods are known with great precision. The major tidal periods and associated disturbing body are presented in Table 1.1 Notice the sun and moon each produce diurnal and semi-diurnal effects.

Terrestrial tides are comprised of three components; solid earth tides, ocean (lake) tides and atmospheric tides. Solid earth tides and ocean (lake) tides are gravitationally driven, and exhibit the four major periods (M_1,S_2,O_1, and K_1). Atmospheric tides however, result from the daily solar warming and cooling of the atmosphere [Ritzi,1989]; consequently only solar influences are displayed.

Tidal forces are additive, and the total tidal force will vary depending on the relative orbital positions of the sun and moon. When the sun and moon are in conjunction, or opposition (Figure 1.1), the tide generating forces of the bodies act constructively, producing a maximum tidal range. During quadrature, the sun and moon are at right angles relative to the earth and minimum tidal variations result.

The elliptical nature of the earth's and moon's orbit continually alters the distances between the celestial bodies. The distance from the sun to earth ranges from the perihelion (January) to the aphelion (July). Similarly, the earth-moon radius ranges between the perigee to the apogee, with a lunar orbital period of 27.5 days. Greater tidal ranges are experienced during perigean and perihelion tides [Thurman, 1988]. For a more rigorous explanation of tidal periods and amplitudes consult Melchior [1978], or Thurman [1988] for a general discussion of tides.

Table 1.1 Tidal frequencies. Adapted from Melchior [1978] and Thurman [1988].

TIDE	FREQUENCY (cycles/hour)	DESCRIPTION
O_1	0.929535706	Main lunar (diurnal)
K_1	1.002737909	Declination variations of sun and moon throughout orbital cycle
M_2	1.932273614	Main lunar (semi-diurnal)
S_2	2.000000000	Main solar (semi-diurnal)

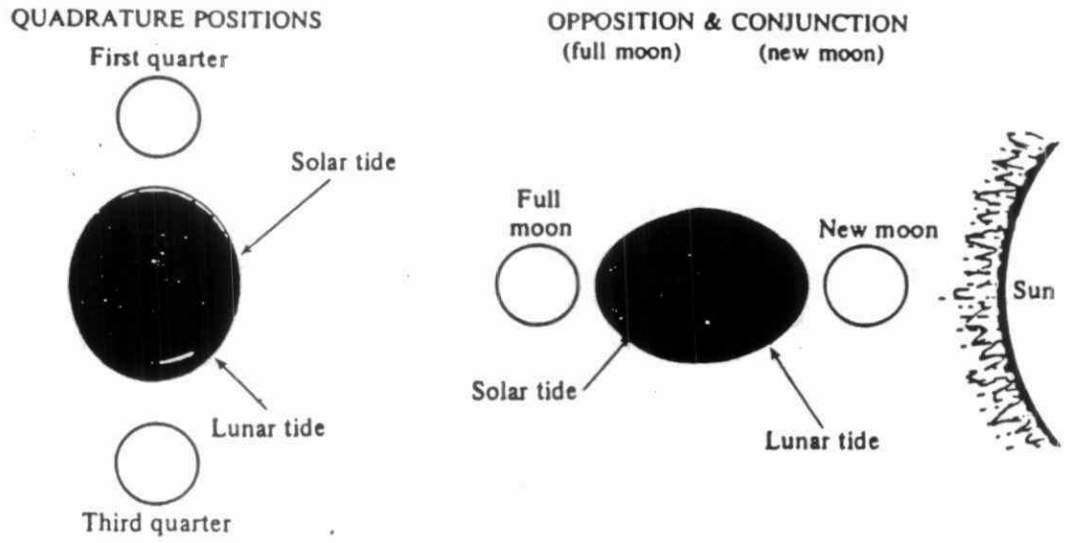

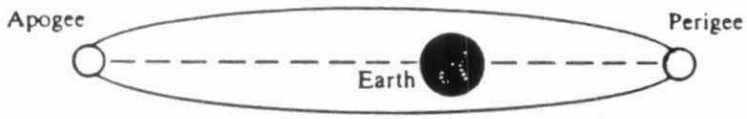

The moon moves from perigee of 375,200 km (233,000 mi) to apogee of 405,800 km (252,000 mi). Greater tidal ranges are experienced during perigean tides.

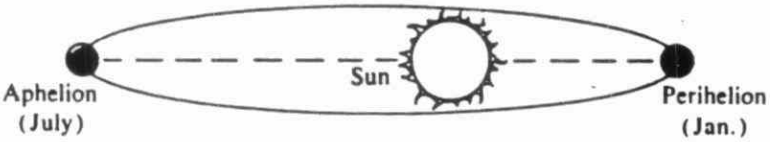

Perihelion brings the earth within 148,500,000 km (92,200,000 mi) of the sun. Aphelion distance is 152,200,000 km (94,500,000 mi). Greater tidal ranges are experienced during perihelion tides.

Figure 1.1 Lunar and solar orbital paths (from Thurman, 1988).

2.0 SOLID EARTH TIDES AND ATMOSPHERIC INFLUENCES IN GEOLOGICAL FORMATIONS AND WELLS

Components of terrestrial tides can be used in conjunction with atmospheric variations in the determination of transmissivity (T). Examination of water level fluctuations in the frequency domain allows the effects of individual tidal and atmospheric forcings to be determined. Individual forcings occur at certain frequencies which can be used to estimate transmissivity. This section describes the frequencies of interest in the estimation of transmissivity and also the physical processes responsible for groundwater response to different natural forcings. Although the formation mechanics are described in terms of a porous media it is analogous to the situation present in an individual fracture.

2.1 IMPORTANT FREQUENCIES

In order to use the natural forces it is important to know at what frequencies the disturbances occur. Generally only four tidal components (M_1,S_2,O_1, and K_1) are of practical importance in groundwater hydrology [Ritzi, 1989]. The amplitude spectra in Figure 2.1.1 shows the correspondence of dominant frequencies between well pressure and tidal potential. The tidal influence occurs primarily in the diurnal (O_1,K_1) and semi-diurnal (M_2,S_2) periods.

The atmospheric amplitude spectrum in Figure 2.1.1 shows the solar tidal periods, however, atmospheric pressure tides are thermally and not gravitationally driven, so there is an absence of lunar tide influence. General circulation and synoptic scale atmospheric variations contribute to the low frequency spectrum (Figure 2.1.2) [Ritzi, 1990]. The solid earth tide (SET) influence is purely periodic while the atmospheric pressure variation (APV) is comprised of both periodic and random constituents. The response of the well, reflected in the water level, will have a random component due to APV.

2.2 FORMATION MECHANICS

Both SET and APV cause perturbations of water levels in open wells. The individual disturbances however, differ in origin. Consider a saturated formation with incompressible grains, that experiences a step-wise change in formation stress ($\delta\sigma_T$). A fluctuation in formation stress will cause a proportional change in pore fluid pressure (δP_{pore}), related by [Ritzi, 1989]:

$$\delta P_{pore} = \xi \delta \sigma_T \ ,$$

$$\xi = \frac{1}{1 + \frac{\phi c_w}{c_e}} \ ,$$

where c_w is the fluid compressibility, c_e is the matrix compressibility, and ϕ is the formation porosity. The fraction ξ is referred to as the loading efficiency.

SET results from crustal distortions created by tide generating forces at various tidal periods. A SET dilation will cause a proportional change in the formation stress, which is borne in part by the pore fluid.

$$\delta P_{pore} = \xi \delta \sigma_{SET} \ ,$$

Fluid pressure in the well is unaffected.

$$\delta P_{well} = 0 \ ,$$

The disequilibrium created by the pore fluid change causes fluid to flow between the well and the formation until equilibrium is attained. For example, a positive change in formation stress, will produce flow towards the well increasing the water level accordingly [Ritzi, 1990].

If the step change in stress arises from a barometric load (δP_{atm}), The pore fluid pressure change (δP_{pore}), will be:

$$\delta P_{pore} = \xi \delta P_{atm} \ ,$$

and

$$\delta P_{well} = \delta P_{atm} \ .$$

A pressure disequilibrium will arise and fluid will flow in or out of the well until equilibrium is met. Since $|\delta P_{atm}| \geq |\xi \delta P_{atm}|$, a positive δP_{atm} will produce water flow away from the well thereby lowering the water level in the open well [Ritzi, 1989].

The magnitude of water level change in the well, will be the net resultant of the SET and APV components. However, formation geology and well depth may also effect the amplitude of the fluctuation [Melchior, 1978].

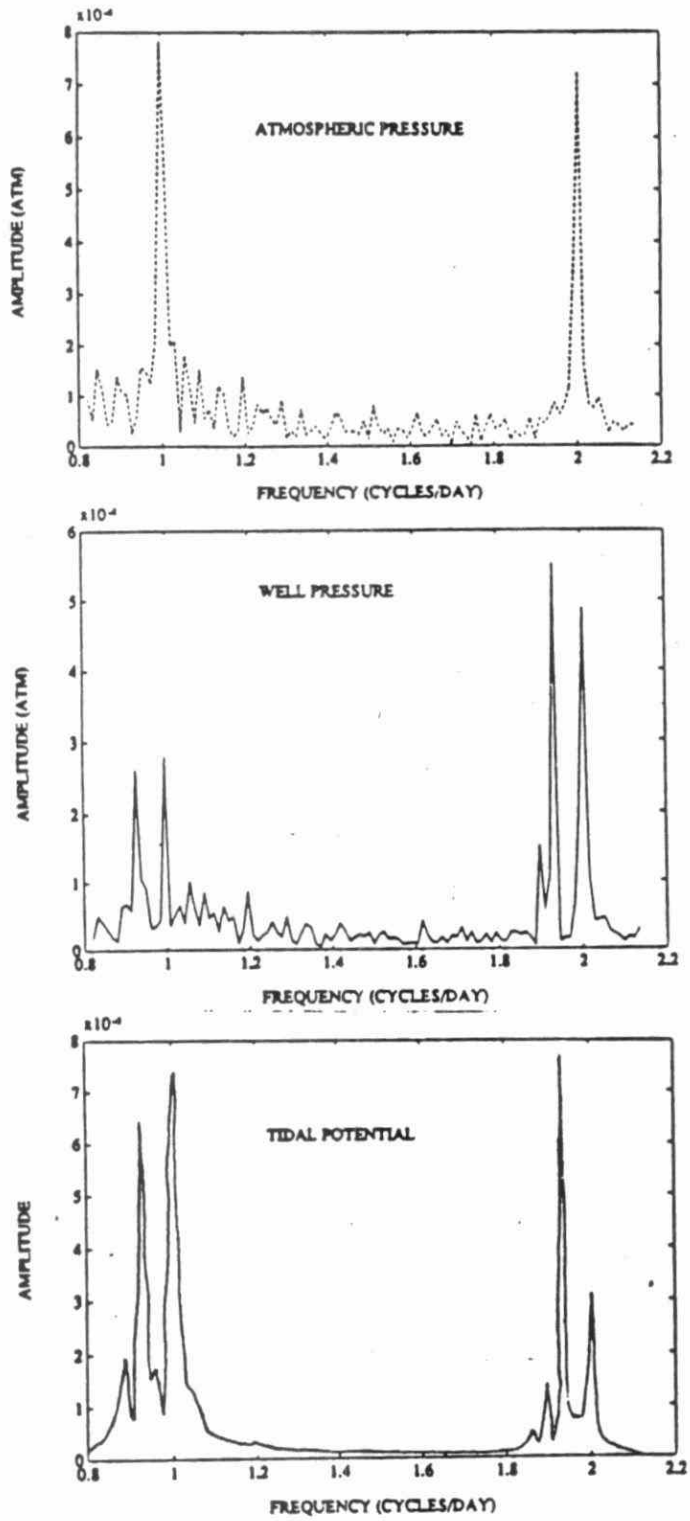

Figure 2.1.1 Amplitude spectra of atmospheric pressure, well pressure, and tidal potential (from Ritzi, 1989).

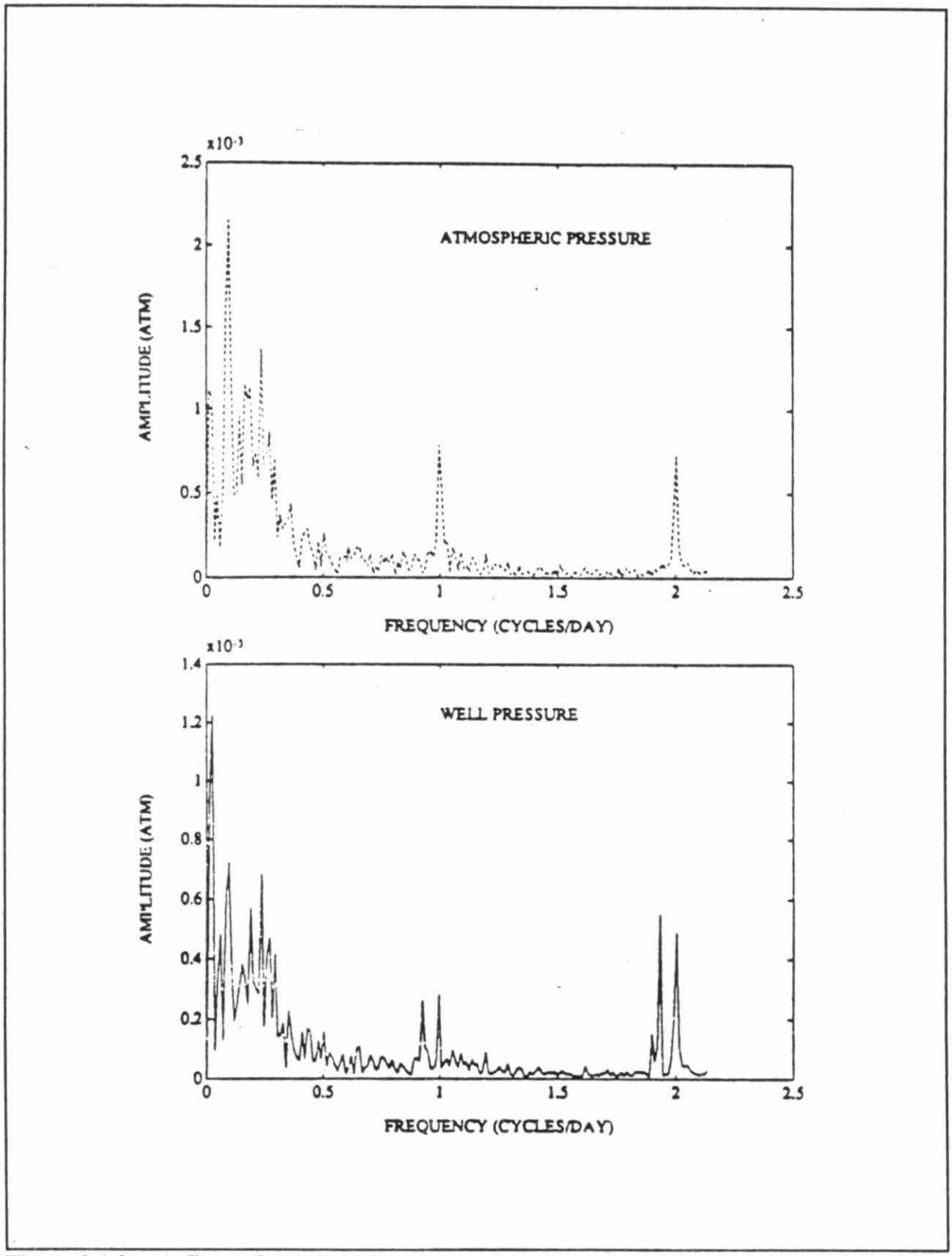

Figure 2.1.2 a) figure 2.1.1 but plotted over a wider range. Note the power in the low frequencies. b) Corresponding amplitude spectrum for well pressure (from Ritzi, 1989).

3.0 SPECTRAL ANALYSIS

Spectral analysis involves the description of variance of a time series according to the frequencies at which the variations take place [Ritzi, 1989]. A time series is merely a sequence of observations taken across time. Applying spectral analysis to water levels allows the detection of tidal and atmospheric periods in hydraulic head variations. The model presented in the following sections will show how this information may be utilized to determine the transmissivities of geological formations.

3.1 THE POWER SPECTRUM

In most practical applications data is collected at discrete intervals in time, therefore only digital spectral analysis will be considered. The time series h(t) is mapped into the frequency domain by use of the Discrete Fourier Transform:

$$\Gamma(f) = 2\sum_{t=0}^{N-1} h(t)\, e^{2\pi i f t}, \qquad f = \frac{0}{\Delta_t N}, \ldots, \frac{N/2}{\Delta_t N},$$

where f is frequency; t, the t^{th} element of the time series; Δ_t, the sampling interval, and N, the number of samples. The function $\Gamma(f)$ is referred to as the spectrum or power spectrum of h(t). The Fourier transform measures the amplitude of discrete frequencies, such that their combination will produce h(t). An analogous process is the decomposition of light through a prism.

The actual calculation of the Fourier transform is performed through the use of an algorithm known as the fast fourier transform, or FFT (see Press *et al.*, 1986). This algorithm has been coded in FORTRAN and details can be found in Appendix A.

3.2 THE CROSS SPECTRUM

The cross spectrum of two time series X and Y, is denoted as Γ_{XY}, and defined:

$$\Gamma_{XY}(f_n) = [\Gamma_Y(f_n)]\,[\Gamma_X(f_n)] \ ,$$

The cross spectrum measures the correlation between the power spectrums of X and Y. Its application gives a measure of what degree the output frequencies are due to the input frequencies. The model presented later in this report uses the angular frequency (ω) which is related to f by a constant:

$$\omega = 2\pi f \ .$$

3.3 ALIASING

An important phenomenon to consider when working with Fourier transforms is the effect of aliasing. For any sampling interval Δ_t, there is a critical frequency called the Nyquist frequency (f_c), given by:

$$f_c = \frac{1}{2\Delta_t} \ .$$

This represents the highest resolvable frequency. If the time series, h(t), has components with higher frequencies, their associated powers will be folded or aliased into the power spectrum of h(t). This results in an inaccurate power spectrum. To avoid aliasing, the sampling interval must be chosen such that the highest frequency component of the h(t) is less than f_c.

4.0 HYDRAULIC PARAMETER ESTIMATION IN THE FREQUENCY DOMAIN

Estimation of hydraulic parameters, such as T, in the frequency domain have been applied by other authors. Hsieh *et al.* [1987] considered only the use of SET, and Rojstaczer [1988] the tidal component of APV influences on open wells. A combined solid earth tide and atmospheric information (CSA) model developed by Ritzi [1989], will be considered in this paper. The CSA model was not simply a superposition of the two previous approaches (Hsieh *et al.* [1987] and Rojstaczer [1988]) as it also considered the cross spectrum between the well and forcing components. A more general treatment of the atmospheric variations was included to account for the probabilistic nature of the low frequency fluctuations. This was accomplished by deriving a stochastic model through the use of spectral methods. The additional frequencies considered in this model create a better estimate of transmissivity. This section presents the theory and properties of the model.

4.1 FREQUENCY RESPONSE FUNCTION (FRF)

The CSA model is based on a linear, time-invariant system. Fluctuations in groundwater levels will show the same periods as the SET and APV, but with some gain or attenuation. A finite time is required for water to flow between the well and formation, so a phase shift also exists. The phase shift and amplitude response for a given frequency are a function of the permeability of the rock and therefore can be used to estimate transmissivity (T), assuming storativity (S) is known.

The frequency response function (FRF), $H(\theta,\omega)$ is defined in the equation:

$$\Gamma_{YY}(\omega) = \Gamma_{XX}(\omega)\,|H(\theta,\omega)|^2 , \qquad (4.2.1)$$

where Γ_{YY} is the power spectrum of the systems response or output (ie. variations in hydraulic head), Γ_{XX} is the power spectrum of a given input or forcing (ie. barometric pressure), ω is the

angular frequency, and Θ is the hydraulic parameter being estimated (ie. T). The expression $|H(\Theta,\omega)|^2$ gives the amount of gain or attenuation in the variance between the input and output at a given frequency [Ritzi, 1989].

Because the atmospheric forcings are probabilistic in nature, both the forcing and response are random processes. Note however, that the underlying system relating them, $H(\Theta,\omega)$ is deterministic. Therefore, although equation (4.2.1) represents a stochastic model, the frequency response function, $H(\Theta,\omega)$, is independent of the input's nature (ie. periodic or stochastic) [Ritzi, 1989].

The frequency response function assumes a fully saturated, confined formation, penetrated by a well. The well is open to the full thickness of the formation, with well radius r_w. The system is considered to be semi-infinite radially from the well and bounded only by the well. Ritzi [1989] derived theoretical FRF for three different models:

(1.) FRF of a well to a formation SET forcing:

$$H(\theta,\omega) = \frac{\Gamma_{wf}}{\Gamma_{ff}} = [E(\theta,\omega) + iF(\theta,\omega)]^{-1} ,$$

with power spectrum response function (PSRF) given by:

$$\frac{\Gamma_{ww}}{\Gamma_{ff}} = [E^2(\theta,\omega) + F^2(\theta,\omega)]^{-1} ,$$

(2.) FRF for atmospheric pressure variations (APV):

$$H(\theta,\omega) = \frac{\Gamma_{wA}}{\Gamma_{AA}} = (\xi - 1)[E(\theta,\omega) + iF(\theta,\omega)]^{-1} ,$$

with PSRF given by:

$$\frac{\Gamma_{ww}}{\Gamma_{AA}} = (\xi - 1)^2 [E^2(\theta,\omega) + F^2(\theta,\omega)]^{-1} ,$$

(3.) the combined CSA response:

$$H(\theta,\omega) = \frac{\Gamma_{w(f-A)}}{\Gamma_{(f-A)(f-A)}} = [E(\theta,\omega)+iF(\theta,\omega)]^{-1} ,$$

with the PSRF given by:

$$\frac{\Gamma_{ww}}{\Gamma_{(f-A)(f-A)}} = [E^2(\theta,\omega)+F^2(\theta\omega)]^{-1} ,$$

The phase response for all models is the same:

$$\eta = -\tan^{-1}\left[\frac{F(\theta,\omega}{E(\theta,\omega)}\right] ,$$

The expressions **E** and **F** are functions of both frequency and Θ. They are defined by:

$$E = 1-\frac{\omega(r_c)^2}{2T}Kei(\alpha_w) ,$$

$$F = \frac{\omega(r_c)^2}{2T}Ker(\alpha_w) ,$$

with

$$\alpha_w = \left[\frac{(\omega S)^{\frac{1}{2}}}{T^{\frac{1}{2}}}\right]r_w ,$$

where S is storativity, and r_c is the casing radius. Solution to the Kelvin functions are found in Appendix B [Abramowitz *et al.*, 1964]. The solutions to the power spectrum and phase response function are plotted in Figure 4.1.1 and 4.1.2. Figure 4.1.3 shows the solutions plotted in the complex plane [Ritzi, 1989] where T_D is.

$$T_D = \frac{T}{fr_c} ,$$

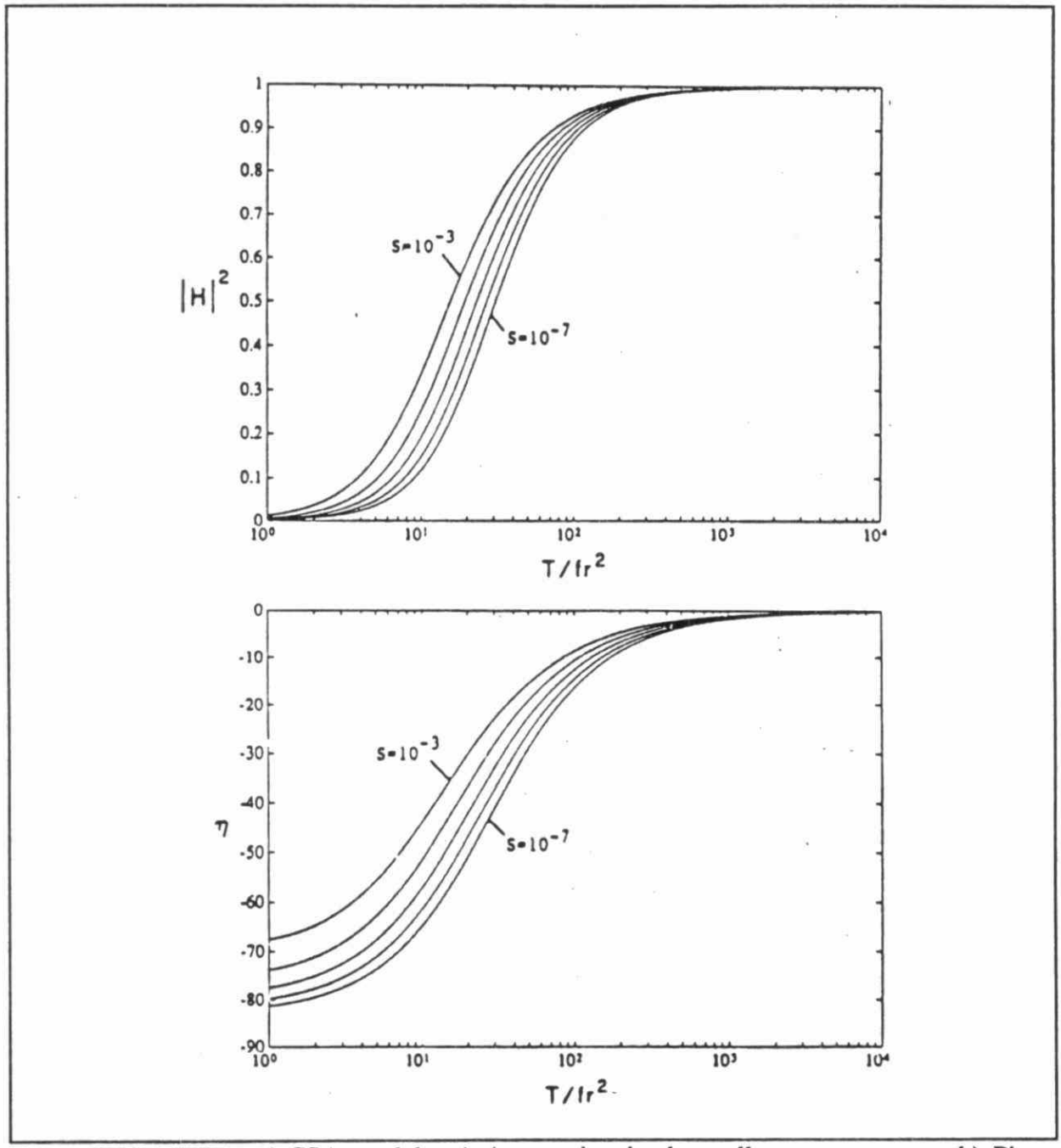

Figure 4.1.1 SET and CSA models. a) Attenuation in the well power spectrum b) Phase between forcing and well response (from Ritzi, 1989).

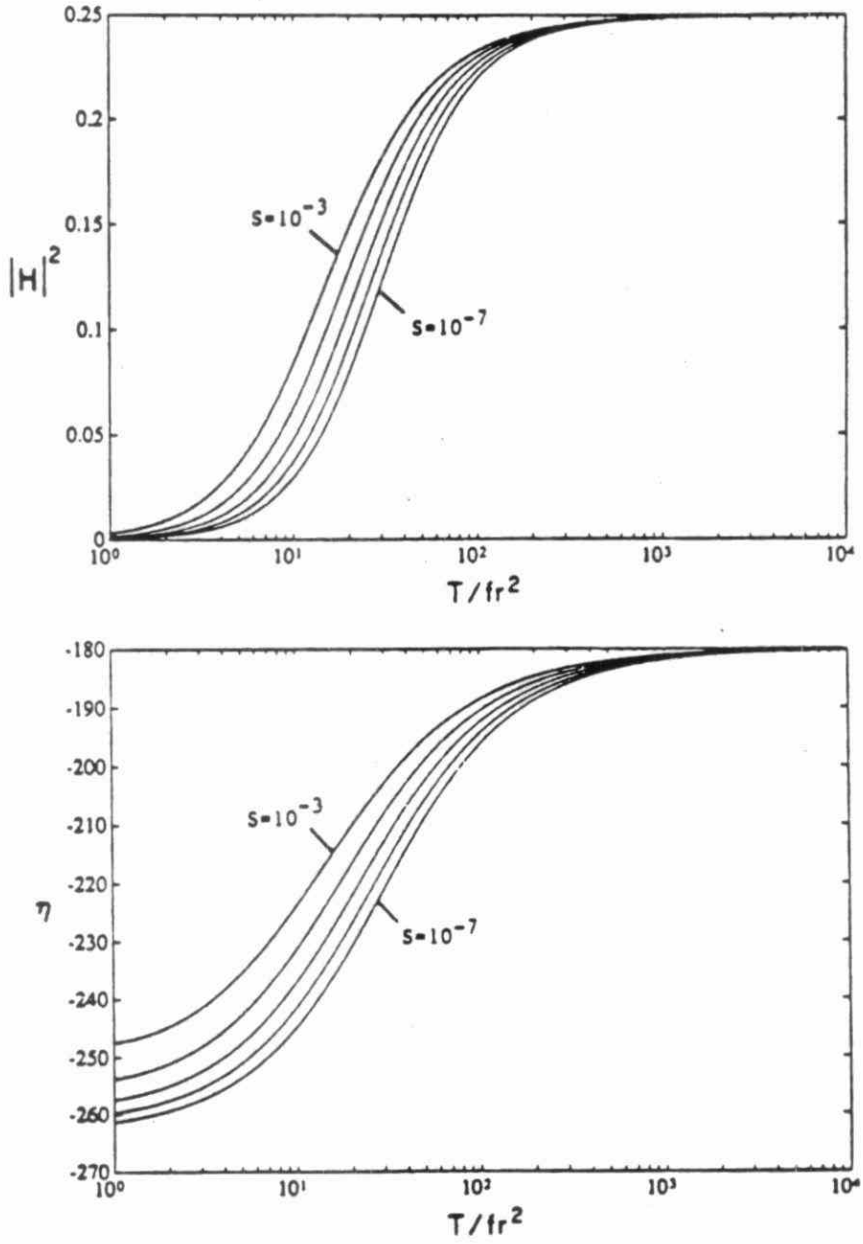

Figure 4.1.2 a) Barometric efficiency, giving attenuation in the well power spectrum. Loading efficiency is 0.5. b) Phase between forcing and well response (from Ritzi, 1989).

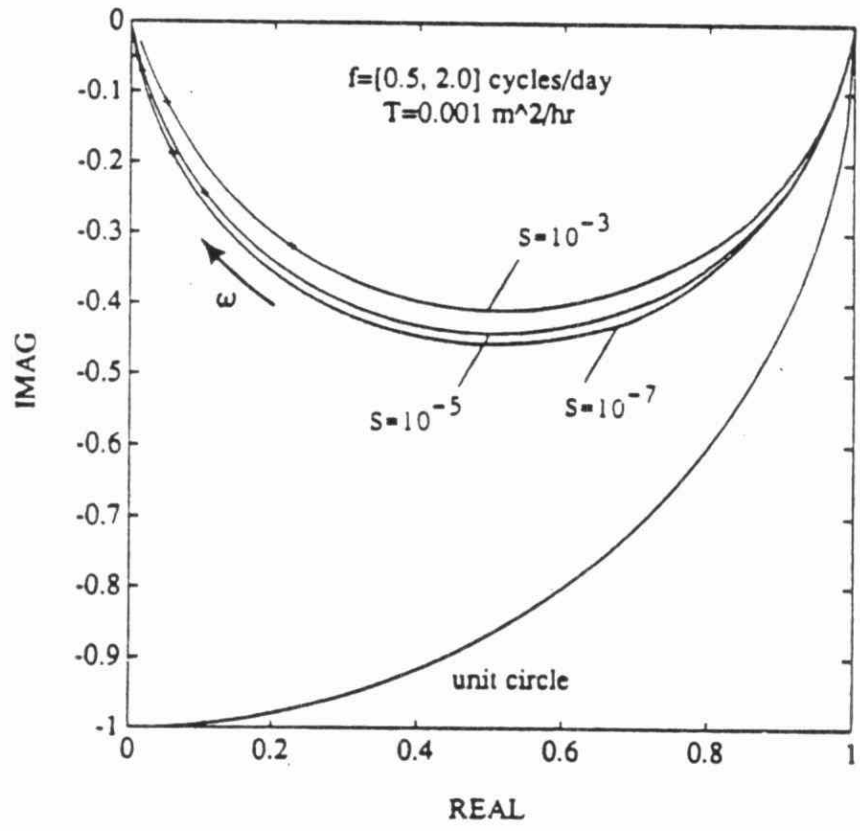

Figure 4.1SBT and CSA FRF curves in the complex plane (from Ritzi, 1989).

4.2 ESTIMATION OF THE LOADING EFFICIENCY (ξ)

When considering only APV forcings, the loading efficiency must be known. One method of estimating this parameter is the use of equation 2.2.1.:

$$\xi = \frac{1}{1+\frac{\phi C_w}{C_e}} \quad .$$

The formation porosity and matrix compressibility may be difficult to estimate, especially when dealing with fractured rock. An alternate method is to make use of the barometric efficiency. The barometric efficiency (BE) is defined as the ratio of change in well pressure to the change in atmospheric pressure [Ritzi, 1989]:

$$BE = \frac{\Delta P_w}{\Delta P_A} \quad .$$

The loading efficiency is usually assumed to equal the BE. A better estimate of ξ can be obtained by considering the frequency dependant power spectra barometric efficiency (PSBE) defined as:

$$PSBE(\omega) = \frac{\Gamma_{ww}(\omega)}{\Gamma_{AA}(\omega)} \quad .$$

Notice that this ratio is equal to the PSRF for APV forcing:

$$\frac{\Gamma_{ww}(\omega)}{\Gamma_{AA}(\omega)} = (\xi-1)^2 [E^2(\theta,\omega)+F^2(\theta,\omega)]^{-1} \quad .$$

This implies that the PSBE will have attenuation (and phase) dependent on frequency, in addition to T, S, and r_w. As T decreases there is a larger departure from a constant BE (figure 4.2.1). Therefore, the usual assumption that the barometric efficiency equals the loading efficiency becomes invalid. To estimate a value for ξ, notice that as $\omega \rightarrow 0$, PSBE(ω) approaches $(\xi-1)^2$. The large spikes are errors introduced by the tidal frequencies [Ritzi, 1989].

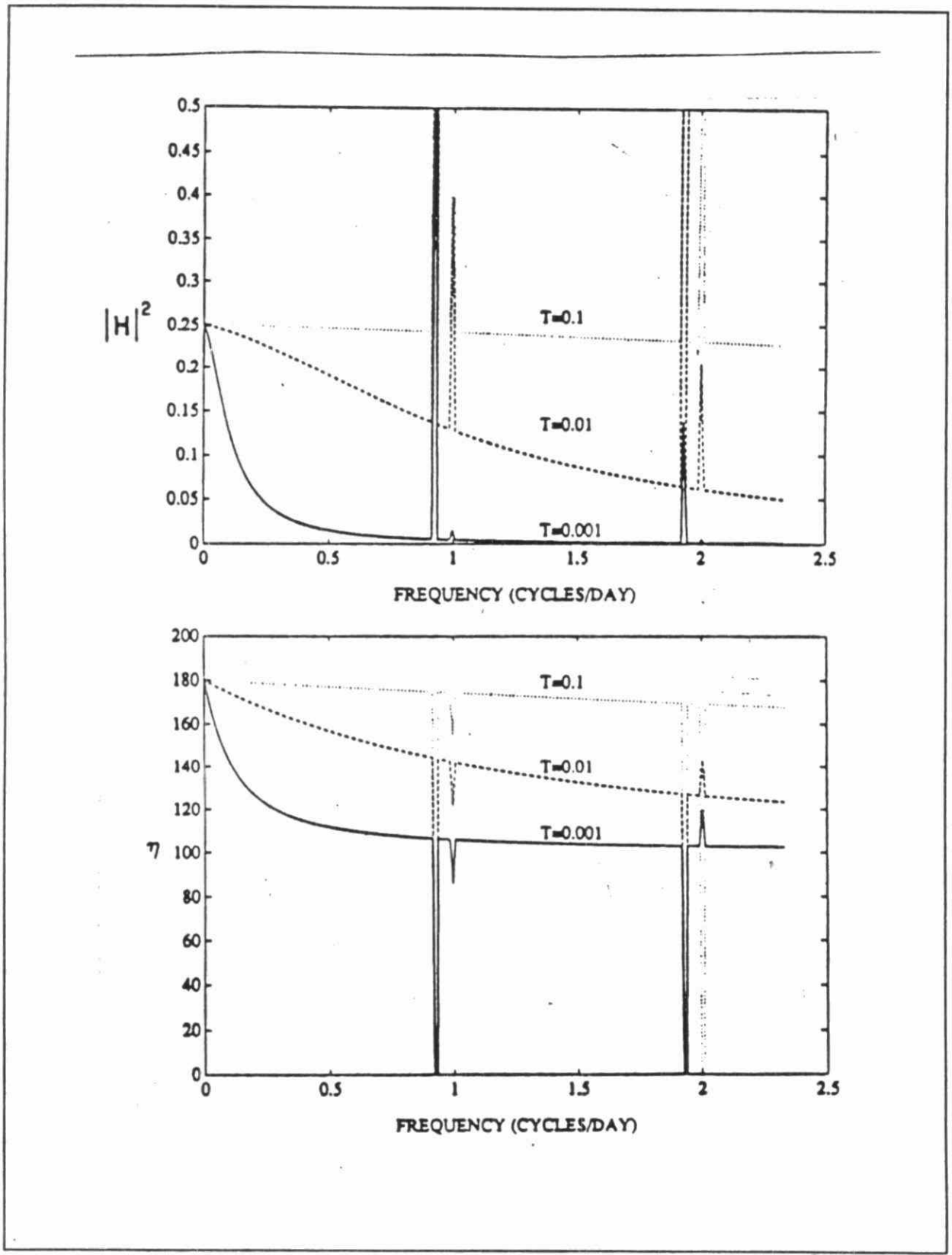

Figure 4.2.1 a) PSBE; T ranging over three orders of magnitude (values in m^2/hour). The loading efficiency is 0.5. b) Phase between atmosphere and well response (from Ritzi, 1989).

5.0 APPLICATION OF MODEL

5.1 GENERAL APPROACH

The general approach to parameter estimation in the frequency domain involves:

(1) collecting input and output data from the system to be modelled,

(2) calculating the sample frequency response function $H(\omega)$, from the data, and

(3) finding Θ such as to achieve the best possible fit between model , $H(\Theta,\omega)$, and observed, $H(\omega)$. The best fit is decided using an estimation criteria. The approach is outlined in Figure 5.1.1. [Ritzi, 1989].

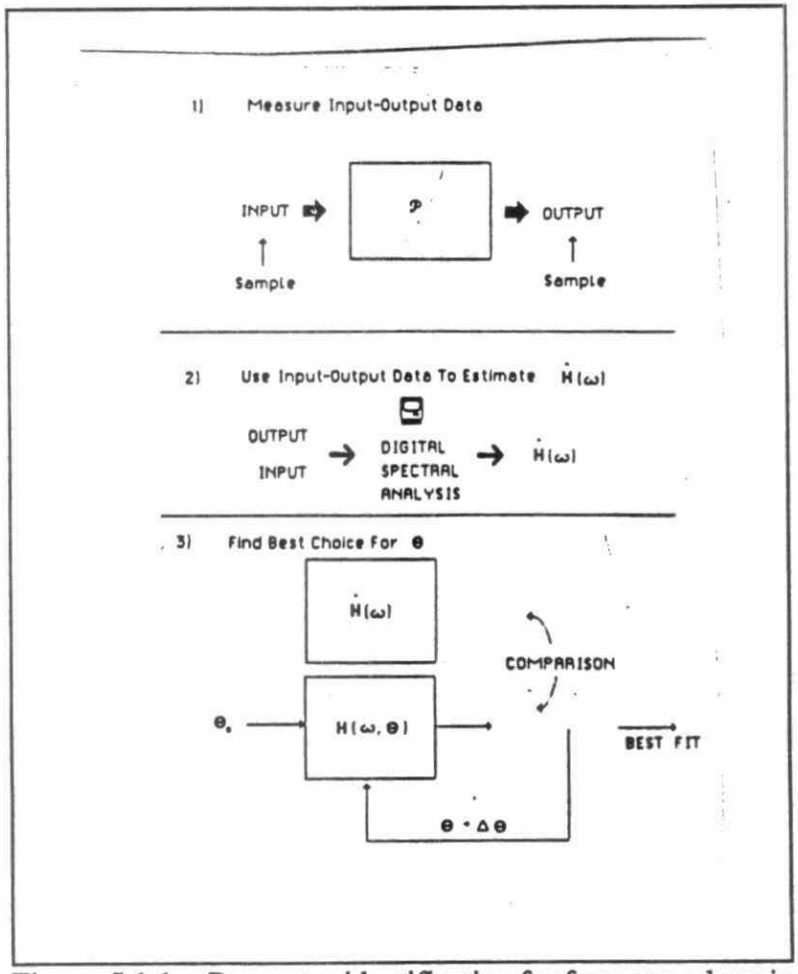

Figure 5.1.1 Parameter identification for frequency domain models (from Ritzi, 1989)

5.2 DATA REQUIREMENTS

To estimate transmissivity using one of the models described in section 4.0 requires different data, depending on which model is used: SET, APV, or combined CSA. The CSA approach will require time series records of the following (Figure 5.2.1):

(1) measurement reflecting hydraulic head of well open to the atmosphere (ie. water level or fluid pressure),

(2) formation pressure from a shut in well (ie. hydraulic head),

(3) atmospheric pressure.

Only the first two time series are required for the SET scheme, and only the first and third time series need be monitored for the APV approach.

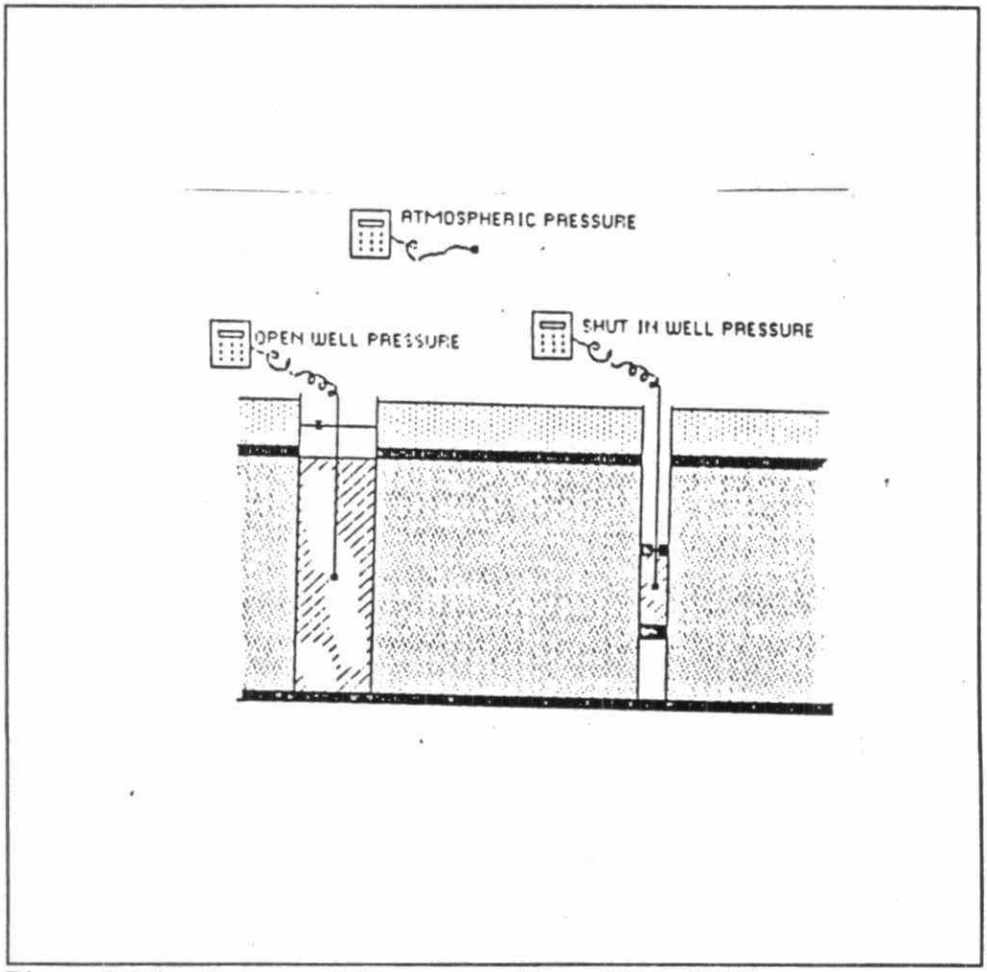

Figure 5.2.1 Data acquisition set up (from Ritzi, 1989).

5.3 DATA COLLECTION

There are two variables to consider in the collection of time series data, the sampling interval (Δ_t) and the length of the monitoring period (T). Δ_t must be small enough so that there are no frequency components greater than the Nyquist frequency (f_c):

$$f_c = \frac{1}{2\Delta_t} \quad ,$$

If Δ_t meets this condition aliasing of the spectrum will be avoided. The highest natural forcing frequency with significant power is the solar diurnal. Therefore, to prevent aliasing of the spectrum Δ_t must be no more than 6 hours. Common practice in tidal analysis is to sample at hourly intervals in order to allow a desirable margin of error between the diurnal frequencies and the Nyquist frequency.

Using Fourier transforms, the number of frequencies (N) obtained in the FRF is equal to N/2+1. The resolution between frequencies will be $1/N\Delta_t$. Increasing N will only improve resolution if Δ_t remains the same otherwise it will merely increase the number of high frequencies. These additions contain no new information for improving the transmissivity estimate; therefore the only way to improve results is by increasing the monitoring period.

5.4 IDENTIFIABLE WINDOW AND INFORMATION CONTENT

In order to determine T from this model, T_D must fall within an identifiable window approximately between values of 10^1 and 10^3 (Figures 4.1.1 and 4.1.2). Beyond this range the attenuation and phase shift are constant; therefore there is no unique solution for T outside the window. Hence, T will only be identifiable if $|\mathbf{H}(\omega)|^2$ takes on values different from zero and unity, and $\eta(\omega)$ is between zero and -80°. Therefore $\mathbf{H}(\omega)$ should be examined before continuing with parameter estimation [Ritzi, 1989].

When considering SET, only the two lunar tidal frequencies can be resolved in the sample FRF, because solar tidal frequencies are contaminated by barometric effects. Similarly, APV methods cannot use lunar tides because of SET influence. The advantage of the CSA method over individual SET and APV approaches is that it is more likely to produce a precise estimate of T. The larger number of frequencies it includes, increase the chance for more information to fall within the identifiable window, leading to better estimates.

5.5 ESTIMATION OF STORATIVITY (S)

Since the estimate of T requires storativity (S) to be known, it is important to know how the transmissivity estimates are influenced by S. In reexamining figures 4.1.1 to 4.1.3 it is apparent that the model response is relatively insensitive to changes in S. An estimate of T therefore, will be relatively independent from errors in the value of S [Ritzi, 1989].

APV data can be used to estimate storativity (S) using:

$$S = \gamma L(\phi C_w + C_e) \ ,$$

where γ is the specific weight of water; L the thickness of the aquifer; and C_e the compressibility of the aquifer. ϕC_w can be calculated from equation 2.2.1 using the value ξ obtained from:

$$\lim_{\omega \to 0} PSBE(\omega) = (\xi - 1)^2 \ ,$$

SET can also be used to calculate storativity, but only the two uncontaminated lunar tide frequencies may be used. In general, the APV estimate will have more degrees of freedom (more frequencies) associated and therefore provide a better estimate [Ritzi, 1989].

When considering an individual fracture, S may be calculated directly from the following:

$$S = \gamma(\alpha + 2bC_w) \ ,$$

where α is the compressibility of the fracture and b the aperture of the fracture [Doe *et al.*

1987].

It is important to remember that this extension to fractured rock assumes that the individual fracture can be represented by an equivalent porous medium.

5.6 ESTIMATION CRITERION

Discrepancies between $H(\omega)$ and $H(\Theta,\omega)$ may occur for several reasons. For example departure from a time invariant system, and measurement error introduced through the limitations of transducers and datalogging equipment can be major factors. Because the time series are usually discrete and not continuous, digital techniques used to calculate $H(\omega)$ will introduce numerical errors. Additional errors may be superimposed by deviations of the true system from assumptions made in the derivation of $H(\Theta,\omega)$. These include a fully penetrating well, horizontal radial symmetrical flow, and a confined homogeneous, isotropic formation [Ritzi, 1989].

At a given frequency ω_i, the error, ε_i, is defined as:

$$\varepsilon_i(\theta) = H(\omega_i) - H(\theta, \omega_i) \quad .$$

The estimation criterion ($EC(\Theta)$) will be some function of ε_i. The best linear unbiased estimator is the ordinary least squared approach [Ritzi, 1989]. To obtain the best fit this function must be minimized. Stated mathematically:

$$minimize\ EC(\theta) = \min \sum_i [H(\omega_i) - H(\theta, \omega_i)]\,[H(\omega_i) - H(\theta, \omega_i)]^* \quad .$$

where * indicates the complex conjugate.

Since the $EC(\Theta)$ involves complex valued expressions $H(\omega_i)$ and $H(\Theta,\omega_i)$, the estimation criterion is referred to as a complex vector estimation criterion. Ritzi [1989] showed that a complex vector criterion is superior to fitting modulus and phase estimators separately (as by Hsieh *et al.* [1987] and Rojstaczer [1988]). The complex vector had less bias and variance in

the estimates of T, and was more robust to errors outside the unit circle.

The difference $\mathbf{H}(\omega_i)$-$\mathbf{H}(\Theta,\omega_i)$ at a given ω_i represents a vector connecting these two points in the complex plane (Figure 5.6.1). At the minimum Θ, this vector will be orthogonal to the tangent of the model curve at $\mathbf{H}(\Theta,\omega)$. Expressing $\mathbf{H}(\omega_i)$ and $\mathbf{H}(\Theta,\omega)$ in complex form:

$$H(\theta,\omega_i) = a(\theta,\omega_i) + ib(\theta,\omega_i) \ ,$$

$$H(\omega_i) = c(\omega_i) + d(\omega_i) \ .$$

Substituting these relations into the EC(Θ) and simplifying gives:

$$EC(\theta) = \sum_{\omega} [(c-a)^2 + (d-b)^2] \ ,$$

or rewritten:

$$EC(\theta) = \sum_{\omega} [(e_R)^2 + (e_I)^2] \ ,$$

where ε_R and ε_I are the real and imaginary components of error respectively. Therefore the EC minimizes the sum of square distances in the length of the error vector [Ritzi, 1989].

The minimizing method is outlined by Ritzi [1989] as follows:

(1) Choose an initial guess of Θ_o.

(2) Determine a step direction vector Δ for the parameter at Θ_o and ensure that Δ is in the direction of the theoretical Θ. Δ is defined as:

$$\Delta = (HESS_o)^{-1}(G_o) \ ,$$

where $HESS_o$ is the hessian matrix at Θ_o and G_o the gradient at Θ_o given by:

$$HESS_o = (J_R)^T(J_R) + (J_I)^T(J_I) \ ,$$

where J_R and J_I are the real and imaginary Jacobian vectors (see Appendix C), the

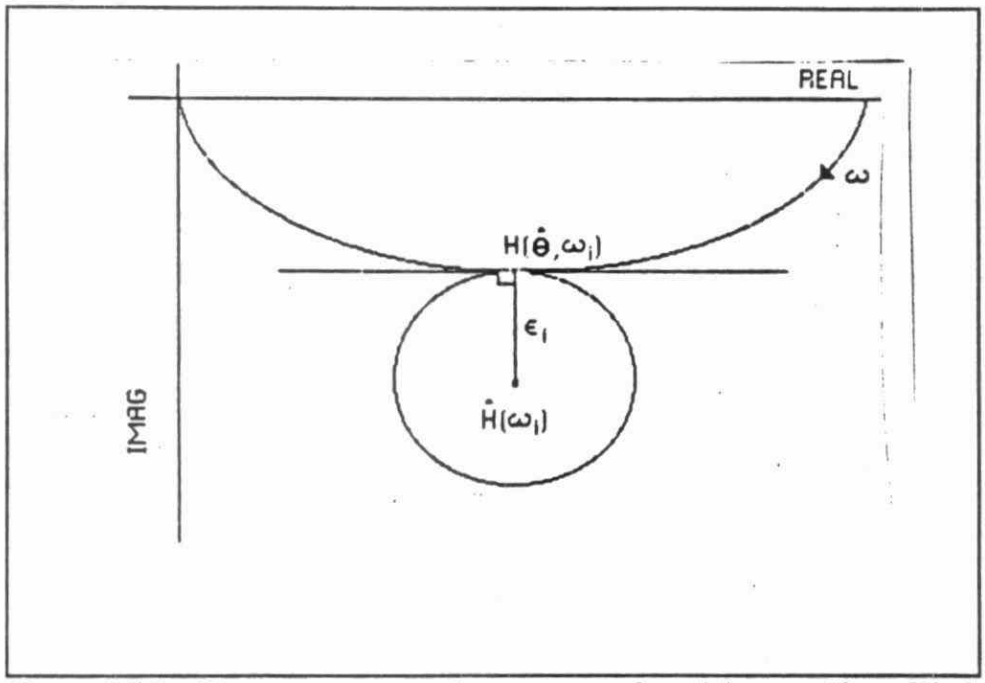

Figure 5.6.1 Error vector normal to tangent of model curve (from Ritzi, 1989).

superscript T indicates the transpose of the matrix, and ε_R and ε_I are the real and imaginary error vectors. In the specific case where only one parameter is being determined using n frequencies, such as in this study, J_R and J_I are [n x 1] column matrices and ε_R and ε_I are [1 x n] row matrices. Consequently both the HESS and gradient reduce to a [1 x 1] matrix; physically the HESS is the second derivative of the FRF with respect to transmissivity. The inverse of the HESS in this situation is simply the reciprocal, if this is positive then it is assured the step direction will be towards the minimum error, if not another guess of Θ_o must be made.

(3) A step size p is initially set to unity, and $\Theta_1=\Theta_o+p\Delta$ is tested. Θ_1 must reduce the magnitude of the EC, while also staying within physical bounds. If Θ_1 is not accepted, a smaller step size p/2 is taken and this step is repeated in a sub-iterative fashion.

(4) Check if the parameter has improved, and iterate back to step (2) until a termination criteria is satisfied. The termination criteria should be based on the amount of change in consecutive parameter estimates but a limit should also be set on the total number of iterations to be performed; Ritzi [1989] recommends a maximum of 15 iterations . The value returned after the termination criteria is met will be the accepted value of T.

5.7 PARAMETER PRECISION

Ritzi [1989] concluded, from analysis of synthetic data, that the reduction in variance gained from the windowing and averaging of spectral estimates is not significant. However, increasing the number of observations improves the parameter estimate, and since windowing and averaging effectively reduce the number of observations; the increase in precision of the spectral estimates may decrease the precision of the parameter estimate. Therefore it is recommended the raw spectral estimates be used in the estimation of transmissivity.

Considering the precision of the parameter estimate, Ritzi [1989] showed that both APV and CSA methods produce the best results. The SET method is not recommended because its low number of frequencies produces the poorest estimates. Although the CSA and APV estimates have similar precision, the CSA method is superior because it requires a significantly shorter monitoring period to obtain the result. Based on the synthetic data tests the CSA procedure requires only between 128 and 512 observations of hourly spaced data. Also there was no significant improvement of the estimate beyond 512 observations. The APV scheme, however required a minimum of 1048 samples, but it is recommended that at least 2048 be used. Therefore the CSA method is recommended based on its precision and short monitoring period.

The estimated $\mathbf{H}(\omega)$ at most frequencies is so greatly effected by error that they must be excluded if a precise value of T is to be determined. To determine what frequencies will be used involves examining the power at each frequency of the input and arranging them in decreasing power. The FRF is then arranged according to these frequencies (this arrangement is in order of increasing noise). Beginning with the first frequency the parameter estimation program is run, and rerun each time adding another frequency. With each run, confidence limits are calculated for the resultant T. The best estimate of T minimizes the width of the confidence interval [Ritzi, 1989], and will be the best estimate of transmissivity. The width of the 95% confidence interval is determined by examining +/- two standard deviations (σ)[Ritzi, 1989]:

$$\theta = \pm 2\sigma \quad ,$$

where

$$\sigma = \sqrt{(HESS_o)^{-1} \sum_{n=1}^{N\omega} \frac{(e_R)^n + (e_I)^n}{N\omega - N_p}} \quad ,$$

where Nω is the number of frequencies considered, and N_p is the number of parameters being estimated, for the application presented here N_p=1. To avoid negative values of T which may arise in this method, the determination of the confidence intervals is performed in log transformed parameter space; this involves multiplying the Jacobian vectors by Θln(10) and recalculating the Hessian.

5.8 CALCULATION OF FRACTURE APERTURE FROM TRANSMISSIVITY

Once the estimate for T has been arrived at the aperture (b) of a single fracture may be calculated from [Novakowski, 1988]:

$$T = \frac{\gamma (2b)^3}{12\mu} \quad , \qquad (5.8.1)$$

where u is the dynamic viscosity.

6.0 PRELIMINARY RESULTS

In this section methods presented in the study will be applied to real data collected from an existing study site in Clarkson Ontario. Presented here are preliminary findings, intended to provide suggestions where additional work is required.

The Clarkson field site was established to study the groundwater flow and mass transport through a single fracture; presently there are twenty-five boreholes that intersect the fracture. The fracture was isolated by employing packers with a pressure transducer attached to monitor variations in hydraulic head in each borehole. A barometric pressure transducer was included to provide simultaneous atmospheric readings with the water level measurements. The monitoring system after January 1991 used a closed well arrangement thereby removing direct atmospheric influence in the boreholes. The data collected from this configuration is comprised of only formation and atmospheric pressure changes. This data does contain the necessary information to apply any of the three described models. However, prior to January 1991, the wells at Clarkson were open to the atmosphere; this particular arrangement measured barometric pressure and open well water level. Recall from section 5.0 that this is the data requirement for application of the APV model. The longest data interval that could be extracted was 1024 hourly spaced samples, only half the length of the recommended minimum of 2048. This interval is used for illustration, however the results from Ritzi [1989] showed that a sample 1024 points only produced an estimate of transmissivity with 95% confidence intervals spanning three orders of magnitude.

Results of spectral analysis are shown in Figures 6.1 to 6.4. The barometric power spectrum (Figure 6.1) displays high power in the low frequency range due to weather patterns, but only the diurnal period is detected in the tidal frequencies. Examination of the output power spectrum (Figure 6.2) again reveal significant power in the low frequency range but no tidal frequencies were detected. The cross spectrum in Figure 6.3 indicate that only barometric variations below 0.5 cycles/day are reflected in the water level record; this implies that the formation at Clarkson may be insensitive to tidal forces. Therefore of the three models presented only the APV approach is applicable. The CSA scheme only provides an

improvement over the APV by using tidal frequencies, since the fracture at Clarkson appears to be insensitive to tidal effects the CSA reduces to the APV model.

In order to apply the APV model an estimation of loading efficiency is required, Figure 6.4 indicates that as ω approaches 0, the amplitude response approaches 0.022. This corresponds to ξ=0.85. Hydraulic tests performed at Clarkson indicate that the fracture aperture varies between 0-250 microns; using equation 5.8.1 the maximum transmissivity will be approximately 6.4 m^2/day. Considering only the atmospheric frequencies and a casing diameter of 5/8" (pre-January 1991) aperture values between 15 and 250 microns will have a T_D value lie within the identifiable window and so the APV model should contain sufficient information to produce an estimate of T. Increasing the casing diameter however, will decrease the detection at low aperture values and increase detection at higher values.

Finally, in order to continue with the estimation procedure the estimation criteria must be automated for practical reasons and a longer monitoring period must be obtained to effectively test the method on field data. It is important to remember that the model presented in this study was only tested on synthetic data [Ritzi, 1989] and its validity when applied to real situations will only be determined through application to different field sites.

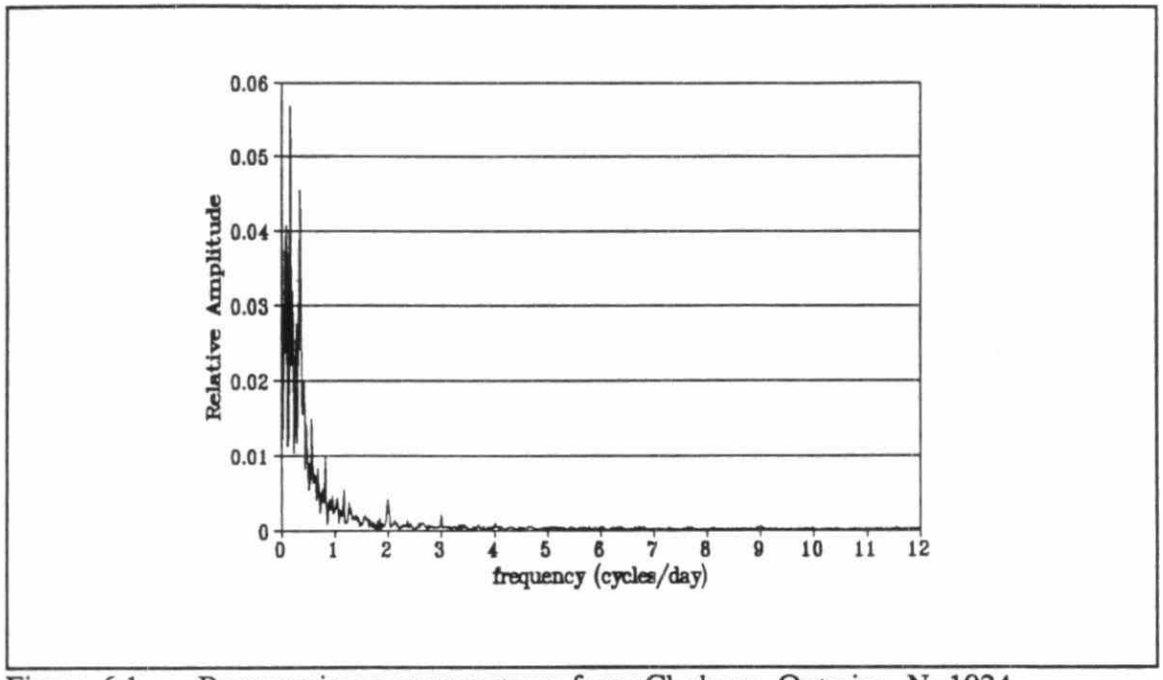

Figure 6.1 Barometric power spectrum from Clarkson, Ontario; N=1024.

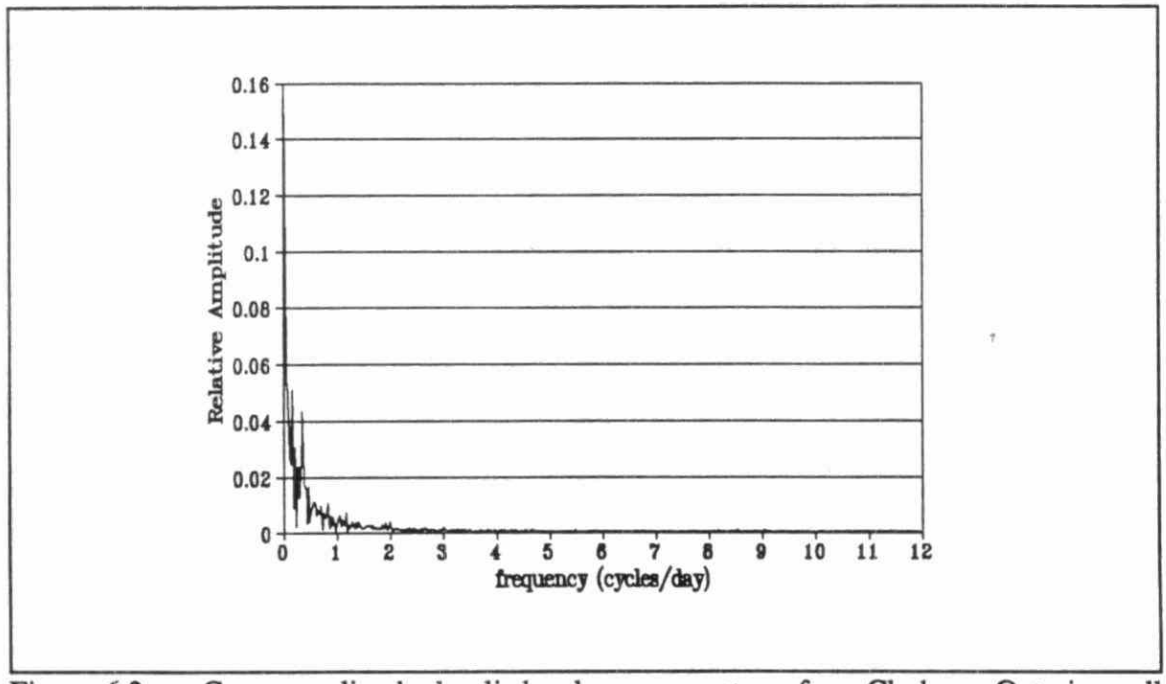

Figure 6.2 Corresponding hydraulic head power spectrum from Clarkson, Ontario; well number UW2; N=1024.

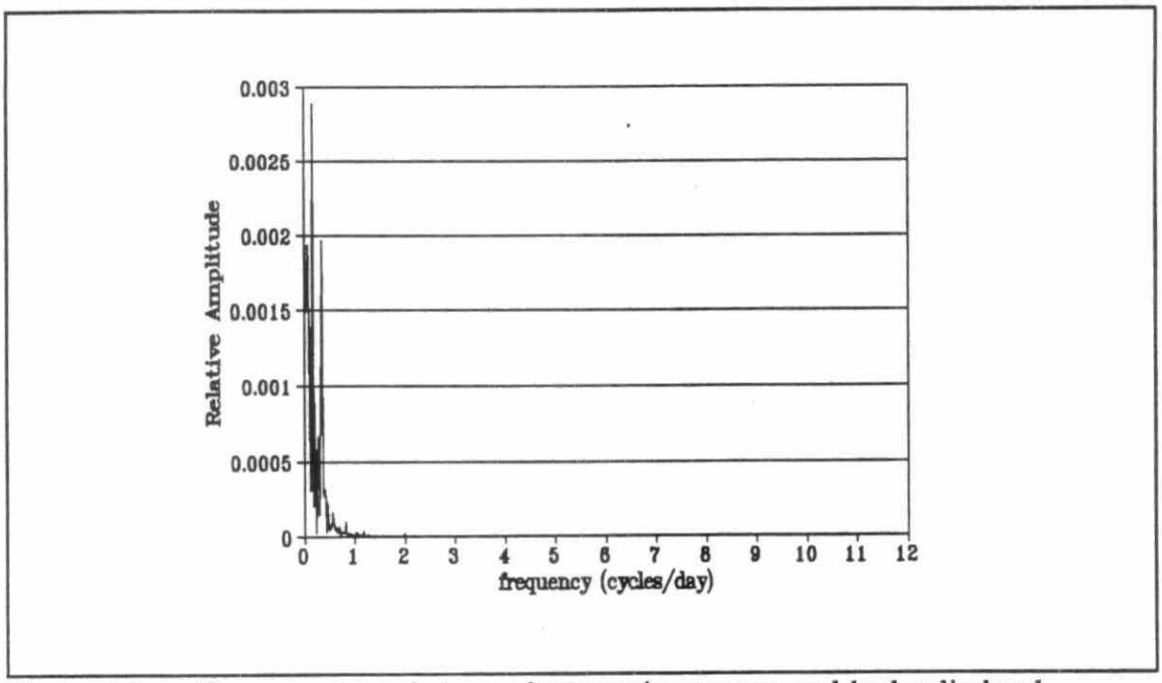

Figure 6.3 Cross spectrum between barometric pressure and hydraulic head.

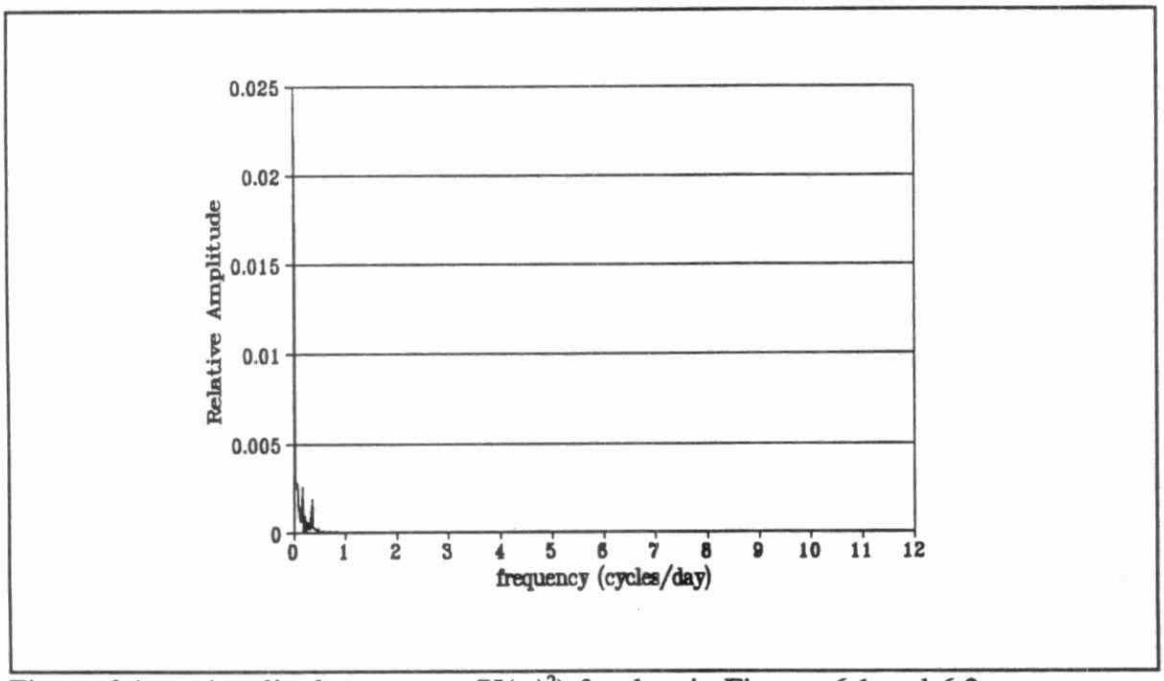

Figure 6.4 Amplitude response $(H(\omega)^2)$ for data in Figures 6.1 and 6.2.

REFERENCES

Abramowitz, M., I.A. Stegun (Eds.), *Handbook of Mathematical Functions, Applied Mathematical Series, 55;* National Bureau of Standards, Washington, D.C., 1964.

Bloomfield, P., *Fourier Analysis of Time Series: An Introduction*, John Wiley and Sons, 1976.

Doe, T., J. Osnes, M. Kenrick, Design of well testing for waste disposal in crystalline rock, In: 6th Congress of the International Society for Rock Mechanics, Montreal, Que., 1987.

Godin, G., *The Analysis of Tides,* University of Toronto Press, 1972.

Hsieh, P.A., J.D. Bredehoeft, J.M. Farr, Determination of aquifer transmissivity from earth tide analysis; *Water Resources Research*, 23(10), 1824-1832, 1987.

Jenkin, G.M., D.G. Watts, *Spectral Analysis and its Applications*, Holden-Day, 1968.

Melchior, P., *The Tides of the Planet Earth*, Pergamon Press, 1978.

Novakowski, K.S., Comparison of fracture aperture widths determined from hydraulic measurements and tracer experiments, In: Proc 4th. Canadian/American Conf. Hydrogeology., Banff, Alberta., 1988.

Press, W.H., B.P. Flannery, S.A. Teukolsky, W.T. Vetterling, *Numerical Recipes*, Cambridge University Press, 1986.

Ritzi, R.W., The use of well response to natural forces in the estimation of hydraulic parameters; Ph.D. Dissertation, Department of Hydrology and Water Resources, University of Arizona, 1989.

Ritzi, R.W., Inverse modelling in the frequency domain: the example of estimating transmissivity from observations of the combined solid earth tide and atmospheric pressure influences; Unpublished Manuscript, 1990.

Rojstaczer, S., Determination of fluid flow properties from the response of water levels to atmospheric loading; *Water Resources Research*, 24(11), 1927-1938, 1988.

Thurman, H.V., *Introductory Oceanography*, 5th Edition, Merrill Publishing, 1988.

LIST OF NOTATION AND SYMBOLS

α	fracture compressibility [LT^2/M]
APV	atmospheric pressure variation
b	fracture aperture [L]
BE	barometric efficiency
C_w,C_e	water compressibility, matrix compressibility [LT^2/M]
CSA	combined solid earth tides and atmospheric pressure variation
Δ	step direction
Δ_t	sample interval [T]
ε	error vector
EC	estimation criteria
η	phase shift
f	frequency [cycles/T]
f_c	Nyquist frequency [cycles/T]
FFT	fast fourier transform
FRF	frequency response function
G	gradient vector
γ	specific weight of water [$M/(TL)^2$]
Γ_{XX}	power spectrum of X
Γ_{XY}	cross spectrum of X and Y
$H(\omega)$	sample FRF
$H(\Theta,\omega)$	model FRF
HESS	hessian matrix
J_R,J_I	real and imaginary Jacobian vectors
μ	dynamic viscosity of water [L/LT]
Ker,Kei	modified Bessel functions, second kind, order zero
ω	angular frequency [radians/T]
P	pressure [M/LT^2]
p	step size

PSBE	power spectrum barometric efficiency
PSRF	power spectrum response function
ϕ	porosity [Dimensionless]
r_c, r_w	radius of casing, radius of well [L]
S	storativity [Dimensionless]
SET	solid earth tide
σ	in section 2.0: stress [M/LT^2]
	in section 5.8: standard deviation
T	transmissivity [L/T^2]
t	time [T]
T_D	dimensionless transmissivity
Θ	parameter being estimated
ξ	loading efficiency [Dimensionless]

APPENDIX A: FOURIER TRANSFORMS

The following program, coded in FORTRAN, calculates the Fourier transform of real data using the fast fourier transform (FFT) algorithm, it requires a column of real values for input. The program returns two columns; the first column of the array is the frequency in cycles per day and the second column is the power at the given frequency. The FFT algorithm requires an integer power of two (2^n; for integer n) samples, the program checks for this and uses the largest number of sample possible. The subroutine FFT is a modification of the subroutine FOUR described in Press *et al.* [1986].

```
      PROGRAM FFT (FAST FOURIER TRANSFORM)

      REAL DATA(2,20000),R
      INTEGER N,J,K
      CHARACTER*25 INPUT,OUTPUT

      WRITE(*,*) 'ENTER INPUT FILE [path][filename.prn]---->'
      READ(*,10) INPUT
10     FORMAT(A25)
      WRITE(*,*) 'ENTER OUTPUT FILE [path][filename.prn]---->'
      READ(*,10) OUTPUT
      WRITE(*,*) 'SELECT FORMAT OF OUTPUT'
      WRITE(*,*) '[1] +/- (CYCLES/DAY), A, B'
      WRITE(*,*) '[2] + (CYCLES/DAY), ((2A/N)^2+(2B/N)^2)^0.5
     + MODULUS (ABSOLUTE VALUE) NORMALIZED'
15     FORMAT(I2)
      READ(*,15) K
      WRITE(*,*) 'ENTER SAMPLING RATE IN HOURS (ie 1.0)---->'
      READ(*,16) R
16     FORMAT(F7.4)

      OPEN (UNIT=8,FILE=INPUT,STATUS='UNKNOWN')
      OPEN (UNIT=9,FILE=OUTPUT,STATUS='UNKNOWN')


      DO 20 I=1,20000
            READ(8,25,END=30,ERR=30) DATA(1,I)
20     CONTINUE
```

```
25     FORMAT(F15.7)
30     CLOSE(8)
       N=I-1

       J=1
       DO 35 I=1,20
             J=J*2
             IF (J.GE.N) GOTO 40
35     CONTINUE
40     IF (J.NE.N) N=J/2

       OPEN(UNIT=8,FILE=INPUT,STATUS='UNKNOWN')
       DO 45 I=1,N
             READ(8,50,END=55,ERR=55) DATA(1,I)
50           FORMAT(F15.7)
45     CONTINUE
55     WRITE(*,*) 'NUMBER OF OBSERVATIONS USED',N

       CALL FFT(DATA,N,1)

       IF (K.EQ.1) THEN
             DO 60 I=1,N/2+1
                WRITE(9,65) ((I-1)/(N*R))*24, DATA(1,I), DATA(2,I)
65              FORMAT(F9.4,E15.6,E15.6)
60           CONTINUE
             DO 70 I=N/2+2,N
               WRITE(9,65) -((N+1-I)/(N*R))*24,DATA(1,I),DATA(2,I)
70           CONTINUE
       ELSE
             WRITE(9,75)
     +       (((I-1)/(N*R))*24,((2*DATA(1,I)/N)**2
     +       +(2*DATA(2,I)/N)**2)**0.5, I=1,N/2+1)
75           FORMAT(F9.4,E15.6)
       ENDIF
100    END


       SUBROUTINE FFT(DATA,N,ISIGN)
       DIMENSION DATA(*)
       IP0=2
       IP3=IP0*N
       I3REV=1
       DO 50 I3=1,IP3,IP0
        IF (I3-I3REV) 10,20,20
```

```
10      TEMPR=DATA(I3)
        TEMPI=DATA(I3+1)
        DATA(I3)=DATA(I3REV)
        DATA(I3+1)=DATA(I3REV+1)
        DATA(I3REV)=TEMPR
        DATA(I3REV+1)=TEMPI
20      IP1=IP3/2
30      IF (I3REV-IP1) 50,50,40
40      I3REV=I3REV-IP1
        IP1=IP1/2
        IF (IP1-IP0) 50,30,30
50      I3REV=I3REV+IP1
        IP1=IP0
60        IF (IP1-IP3) 70,100,100
70      IP2=IP1*2
        THETA=6.283185307/FLOAT(ISIGN*IP2/IP0)
        SINTH=SIN(THETA/2.)
        WSTPR=-2.*SINTH*SINTH
        WSTPI=SIN(THETA)
        WR=1.
        WI=0.
        DO 90 I1=1,IP1,IP0
         DO 80 I3=I1,IP3,IP2
           I2A=I3
           I2B=I2A+IP1
           TEMPR=WR*DATA(I2B)-WI*DATA(I2B+1)
           TEMPI=WR*DATA(I2B+1)+WI*DATA(I2B)
           DATA(I2B)=DATA(I2A)-TEMPR
           DATA(I2B+1)=DATA(I2A+1)-TEMPI
           DATA(I2A)=DATA(I2A)+TEMPR
80        DATA(I2A+1)=DATA(I2A+1)+TEMPI
         TEMPR=WR
         WR=WR*WSTPR-WI*WSTPI+WR
90        WI=WI*WSTPR+TEMPR*WSTPI+WI
        IP1=IP2
        GOTO 60
100      RETURN
        END
```

APPENDIX B: POLYNOMIAL APPROXIMATIONS OF KELVIN FUNCTIONS

The Kelvin and Bessel functions required for the determination of the theoretical FRF are computed using polynomial approximations [Abramowitz *et al.*, 1972]. The required expansions are:

$$\ker(x) = -\ln(x/2)\,\mathrm{ber}(x)+(\pi/4)\,\mathrm{bei}(x)-0.57721566-59.05819744(x/8)^4+171.36272133(x/8)^8-60.60977451(x/8)^{12}+5.65539121(x/8)^{16}-0.19636347(x/8)^{20}+0.00309699(x/8)^{24}-0.00002458(x/8)^{28}$$

$$\mathrm{kei}(x) = -\ln(x/2)\,\mathrm{bei}(x)-(\pi/4)\,\mathrm{ber}(x)+6.76454936(x/8)^2-142.91827687(x/8)^6+124.23569650(x/8)^{10}-21.30060904(x/8)^{14}+1.17509064(x/8)^{18}-0.02695875(x/8)^{22}+0.00029532(x/8)^{26}$$

$$\mathrm{ber}(x) = 1-64(x/8)^4+113.77777774(x/8)^8-32.36345652(x/8)^{12}+2.64191397(x/8)^{16}-0.08349609(x/8)^{20}+0.00122552(x/8)^{24}-0.00000901(x/8)^{28}$$

$$\mathrm{bei}(x) = 16(x/8)^2-113.77777774(x/8)^6+72.81777742(x/8)^{10}-10.56765779(x/8)^{14}+0.52185615(x/8)^{18}-0.01103667(x/8)^{22}+0.00011346(x/8)^{26}$$

where ker and kei are the real and imaginary Kelvin functions, and ber and bei are the real and imaginary Bessel functions. The polynomial approximations hold for arguments (x) between 0 and 8.

APPENDIX C: MODEL JACOBIAN VECTORS

In order to perform the estimation scheme outlined in section 5.6 the model Jacobian vectors must be calculated for both the real and imaginary component of the FRF. Each element of the vector represents the derivative of the FRF with respect to transmissivity (T) at a particular frequency. Ritzi [1989] provides the following analytical solutions for the Jacobians for SET and CSA approaches:

$$J_R = \frac{dH_R}{dT} = -\frac{\beta Kei(\alpha_w) - \frac{\beta}{2}}{\gamma} + \frac{2E^2\beta Kei(\alpha_w)}{\gamma^2} - \frac{2EF\beta\left[Ker(\alpha_w) - \frac{1}{2}\right]}{\gamma^2}$$

$$J_I = \frac{dH_I}{dT} = -\frac{\beta\left[Kei(\alpha_w) - \frac{1}{2}\right]}{\gamma} - \frac{2EF\beta Kei(\alpha_w)}{\gamma^2} - \frac{2F^2\beta\left[Ker(\alpha_w) - \frac{1}{2}\right]}{\gamma^2}$$

where

$$\beta = -\frac{\omega (r_c)^2}{2T^2}$$

and

$$\gamma = E^2 + F^2 \ .$$

where J_R and J_I are the real and imaginary Jacobian vectors respectively. Definitions of E, F, and α_w can be found in section 4.1. For application of the APV methodology the Jacobians will be the same as above but multiplied by (ξ-1).

The Jacobian vectors must be returned as column vectors; if n frequencies are considered in the estimation of T, J_R and J_I will be [n x 1] matrices, that is to say n rows and one column.

APPENDIX F

Tracer Test Type Curve Matches
1991 and 1992 Compilation

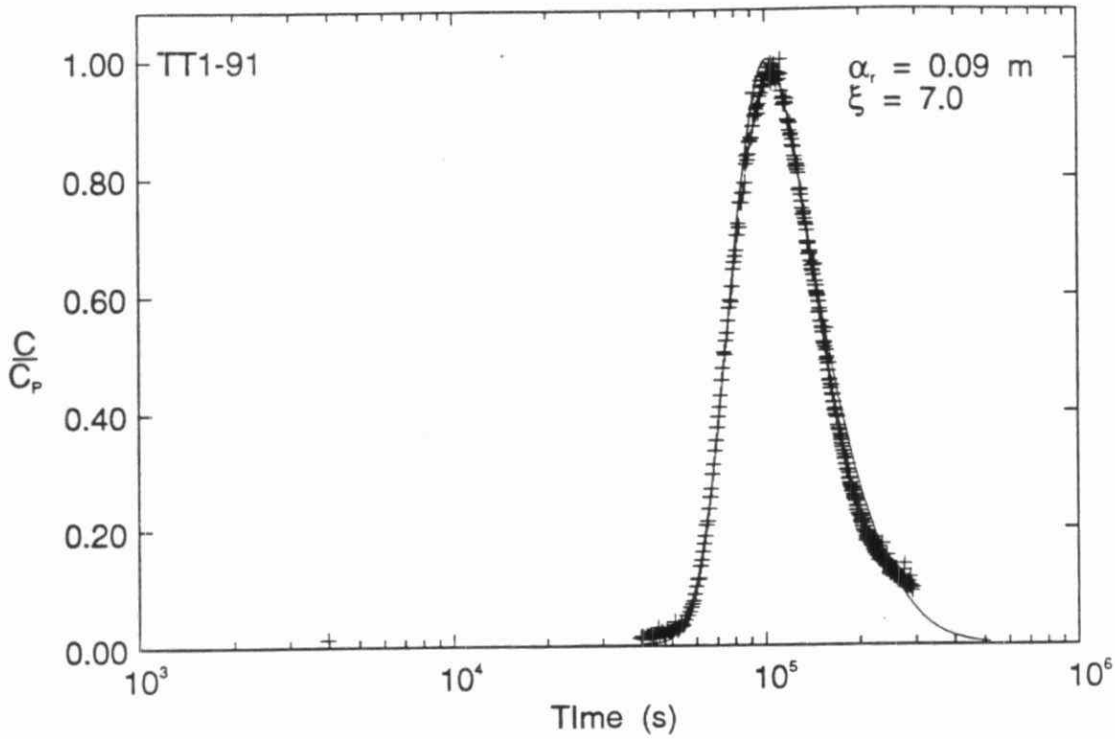

Figure F1: Type-curve match for radial convergent tracer test: TT1-91.

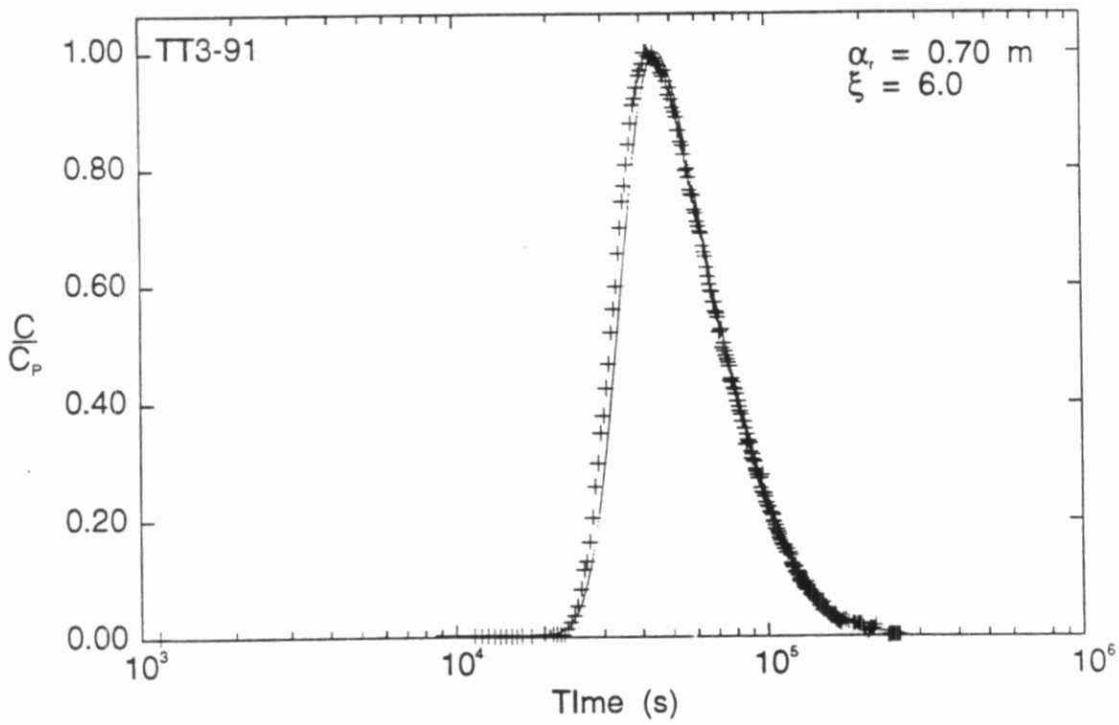

Figure F2: Type-curve match for radial convergent tracer test: TT3-91.

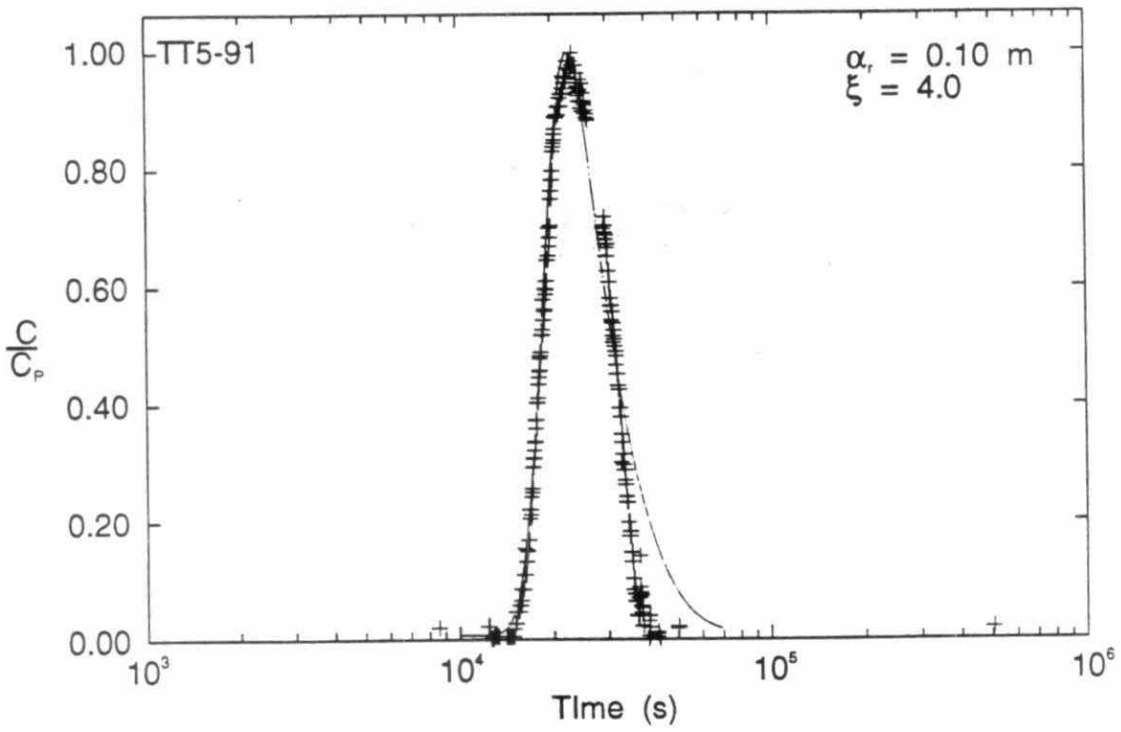

Figure F3: Type-curve match for radial convergent tracer test: TT5-91.

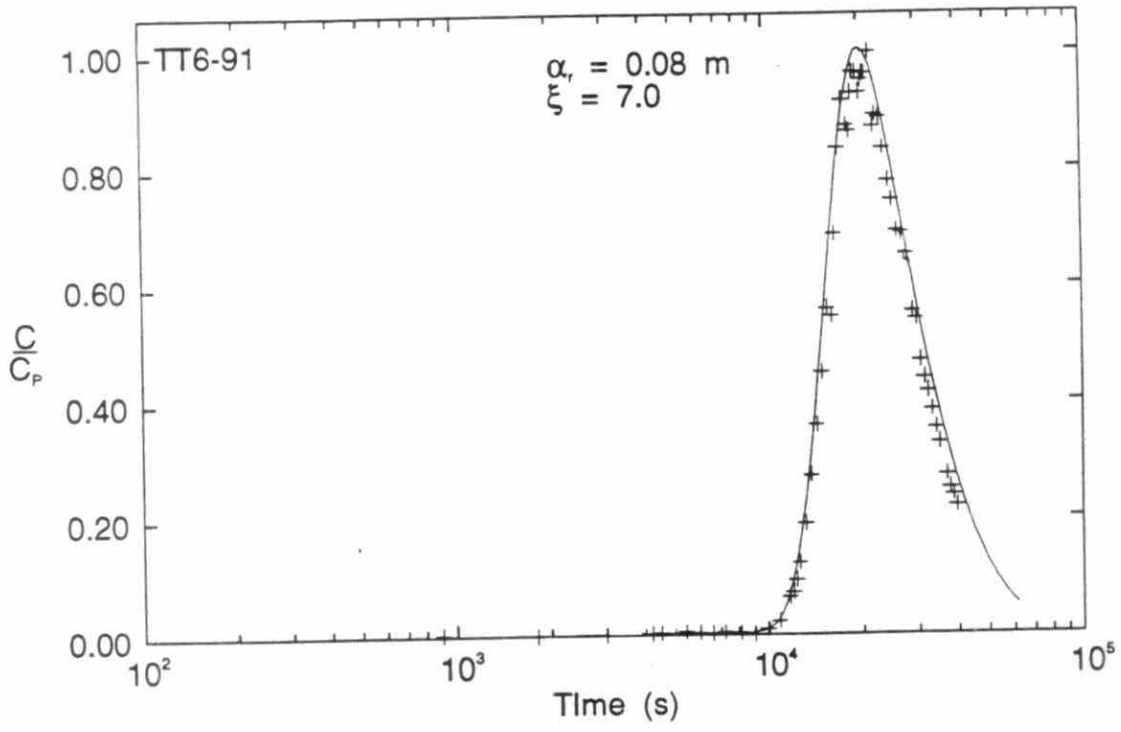

Figure F4: Type-curve match for radial convergent tracer test: TT6-91.

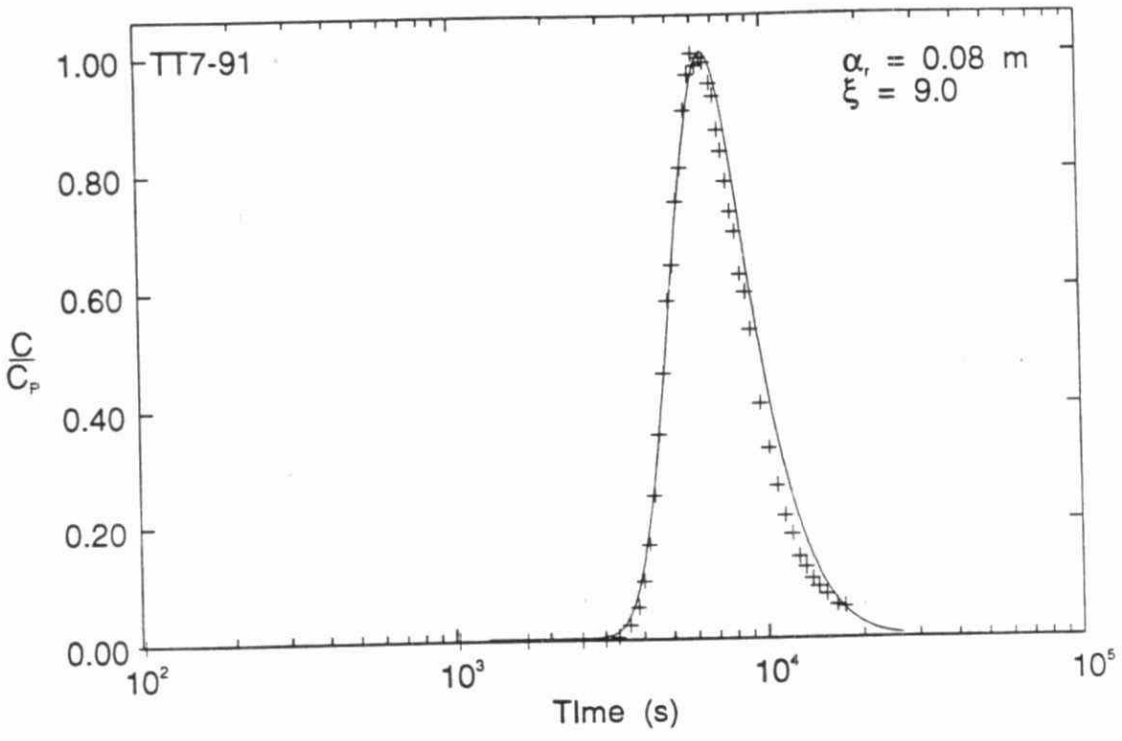

Figure F5: Type-curve match for radial convergent tracer test: TT7-91.

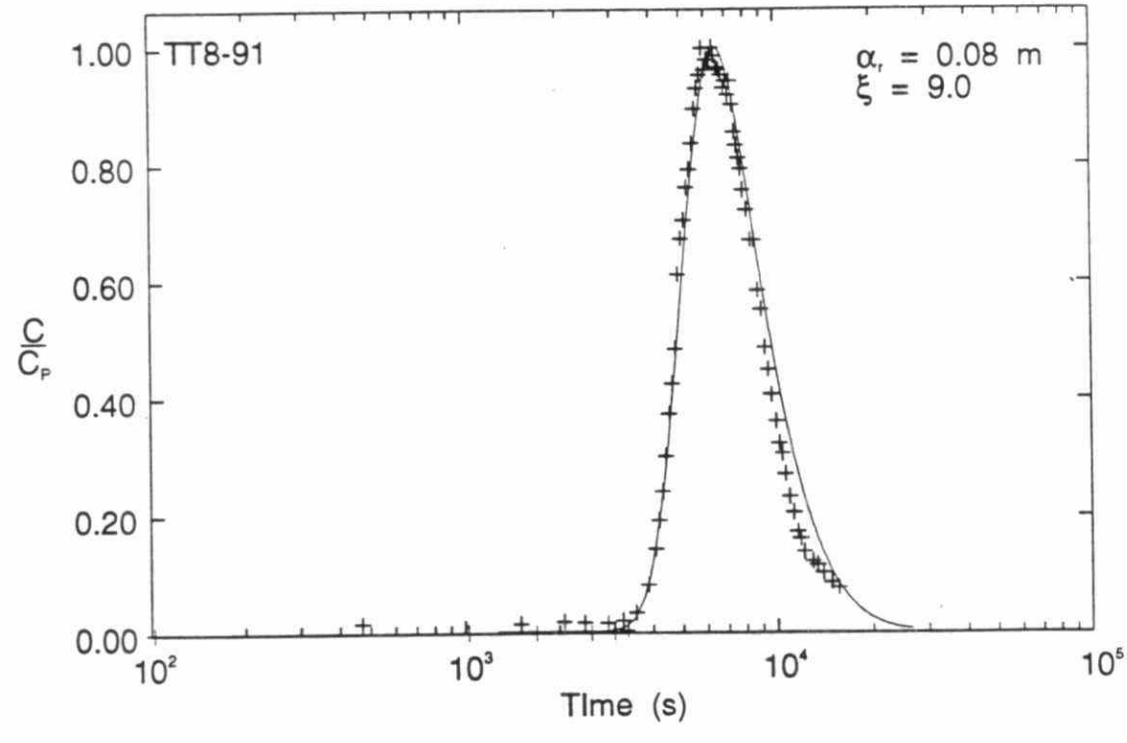

Figure F6: Type-curve match for radial convergent tracer test: TT8-91.

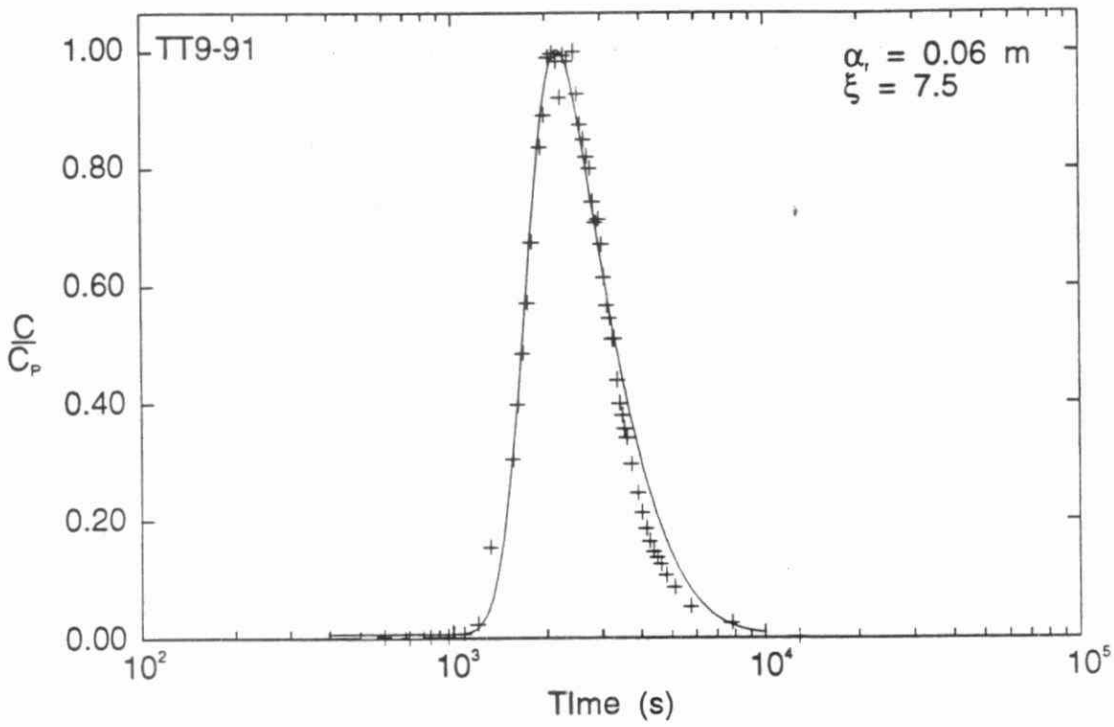

Figure F7: Type-curve match for radial convergent tracer test: TT9-91.

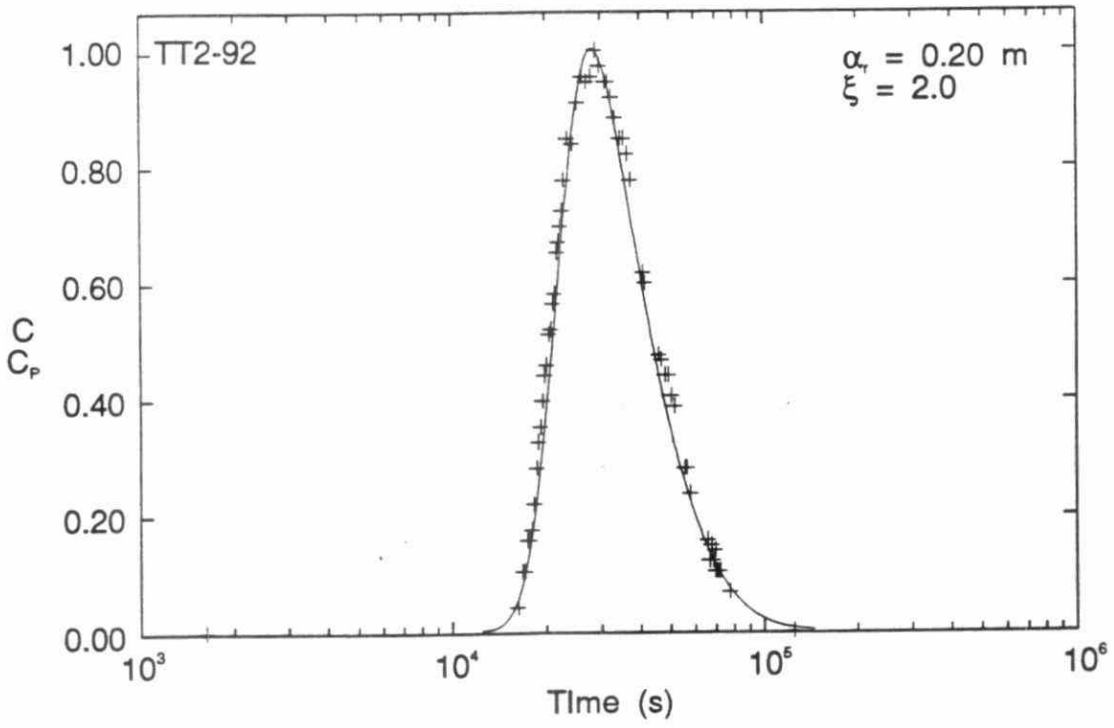

Figure F8: Type-curve match for radial convergent tracer test: TT2-92.

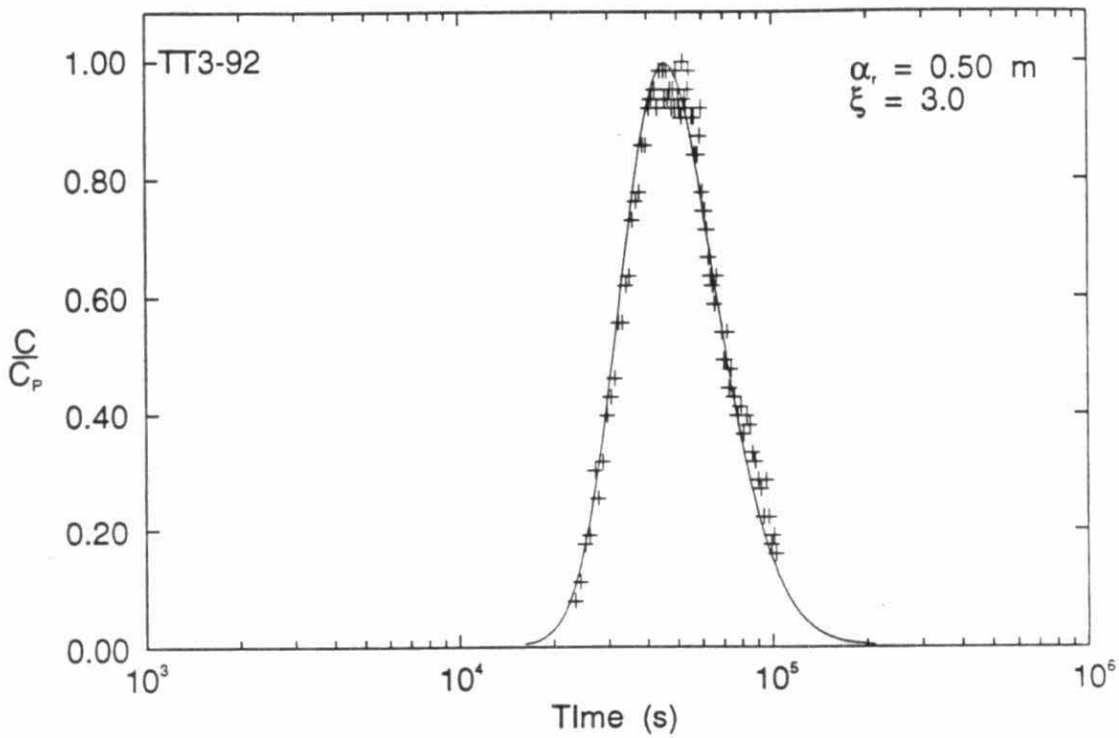

Figure F9: Type-curve match for radial convergent tracer test: TT3-92.

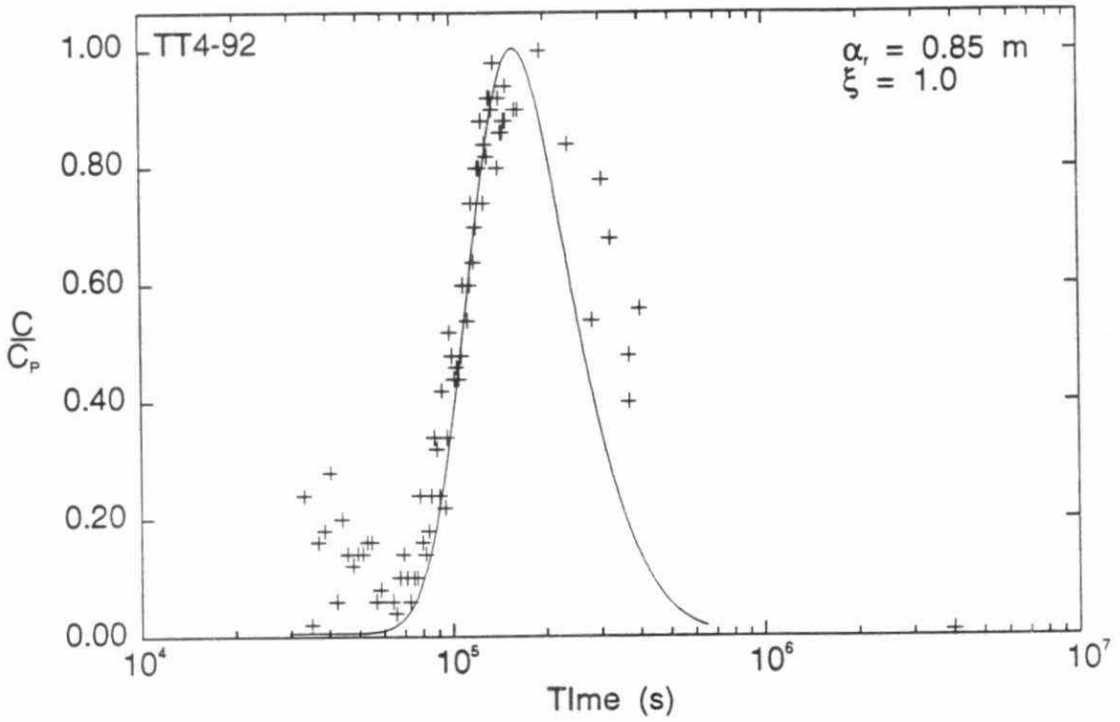

Figure F10: Type-curve match for radial convergent tracer test: TT4-92.

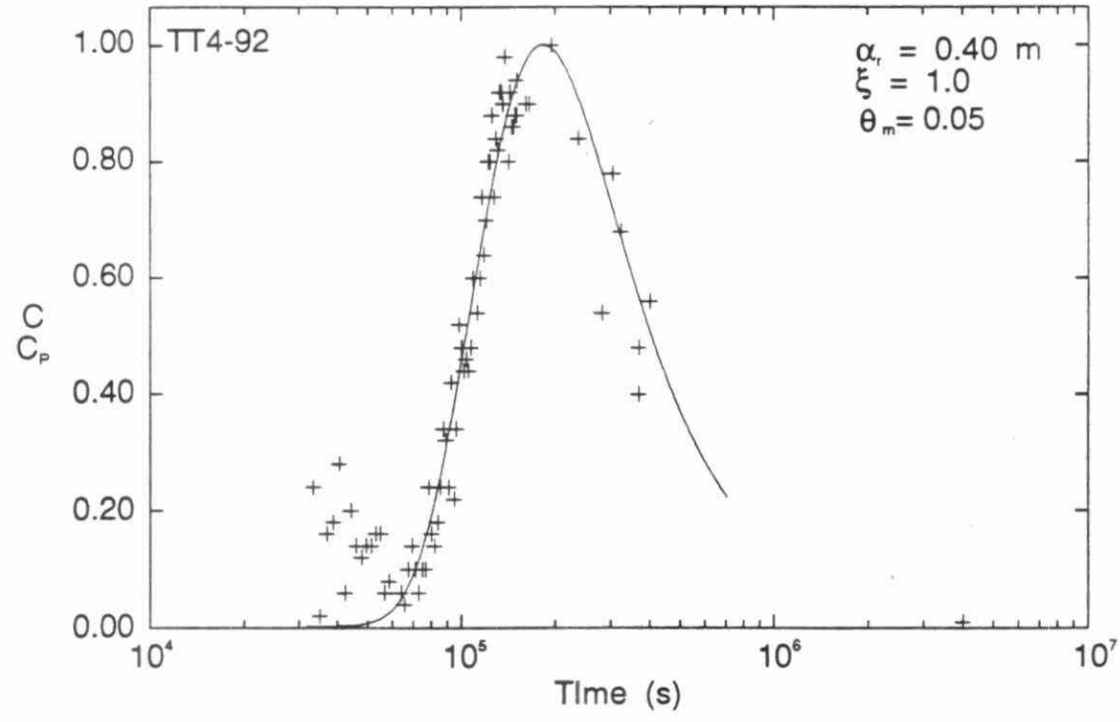

Figure F11: Type-curve match for radial convergent tracer test: TT4-92, $\theta_m > 0$.

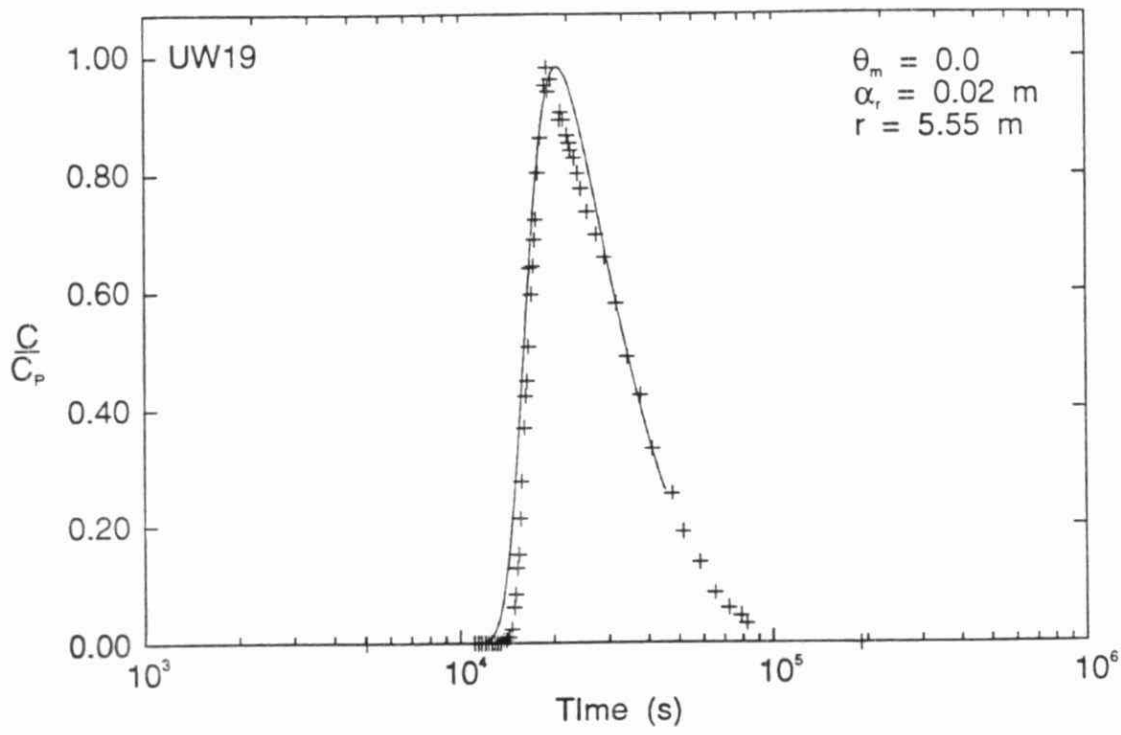

Figure F12: Type-curve match for radial divergent tracer test: RD1, UW19, Fit #1:C/Cp, θ_m=0 (ξ =7).

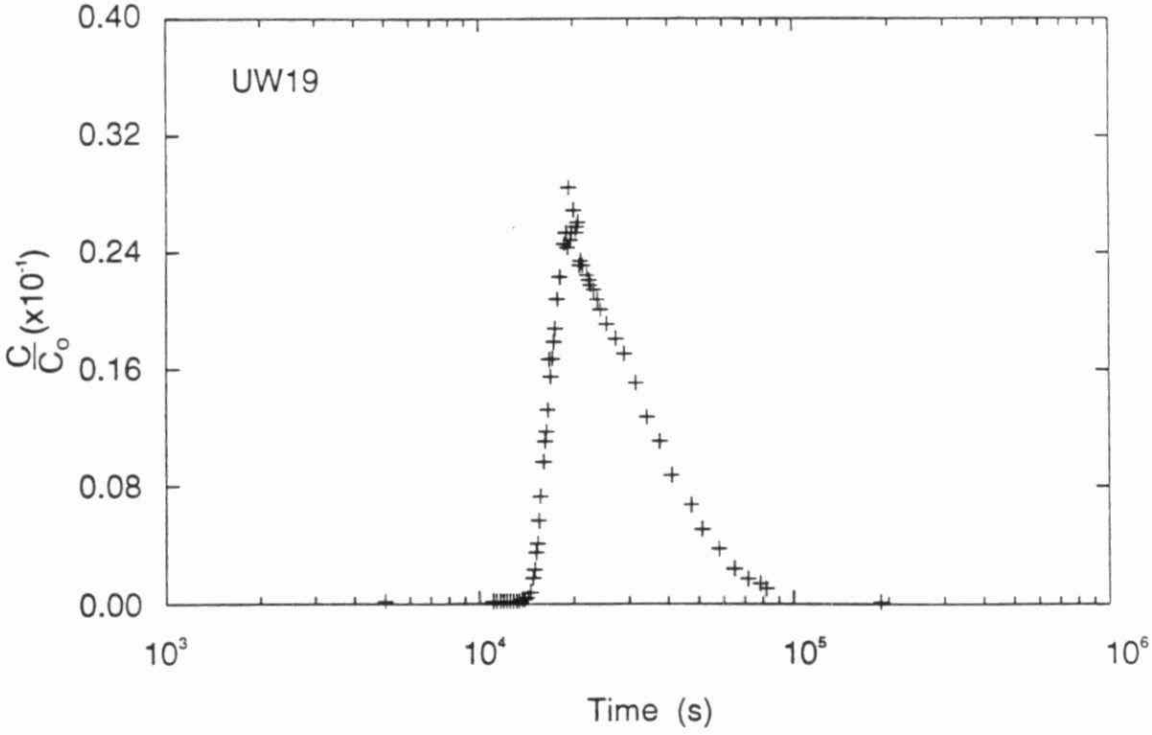

Figure F13: C/C_o data for radial divergent tracer test: RD1, UW19 (no fit obtained)

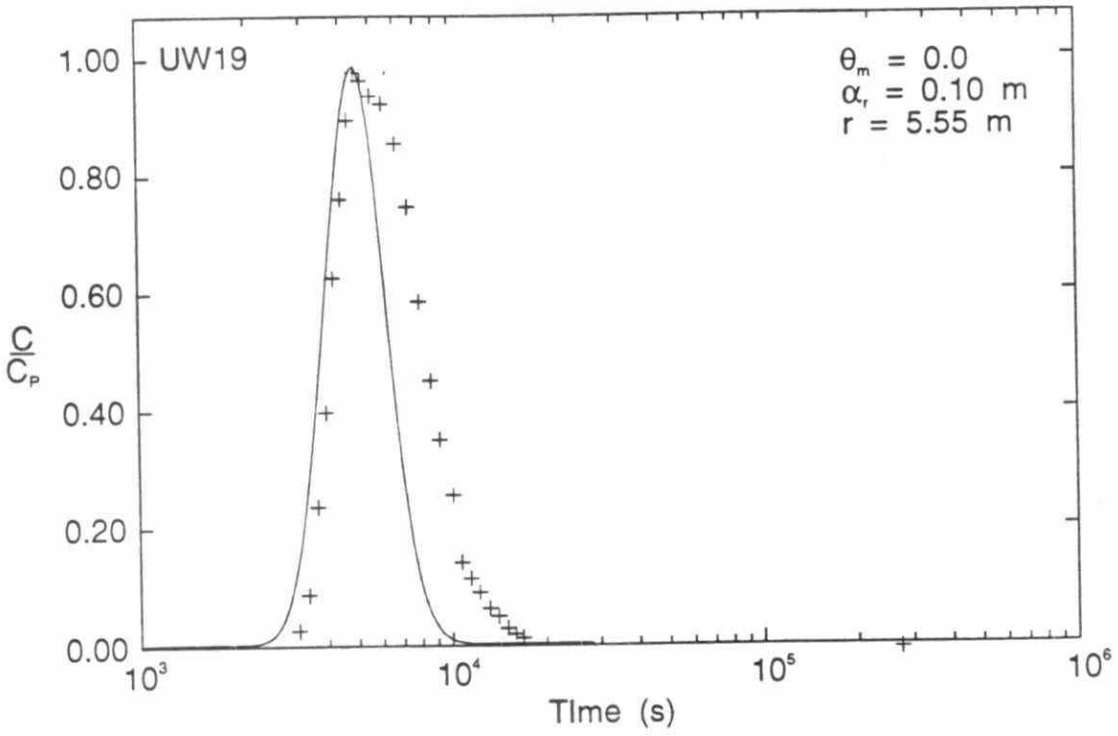

Figure F14: Type-curve match for radial divergent tracer test: RD2, UW19, Fit #1:C/Cp, θ_m=0.

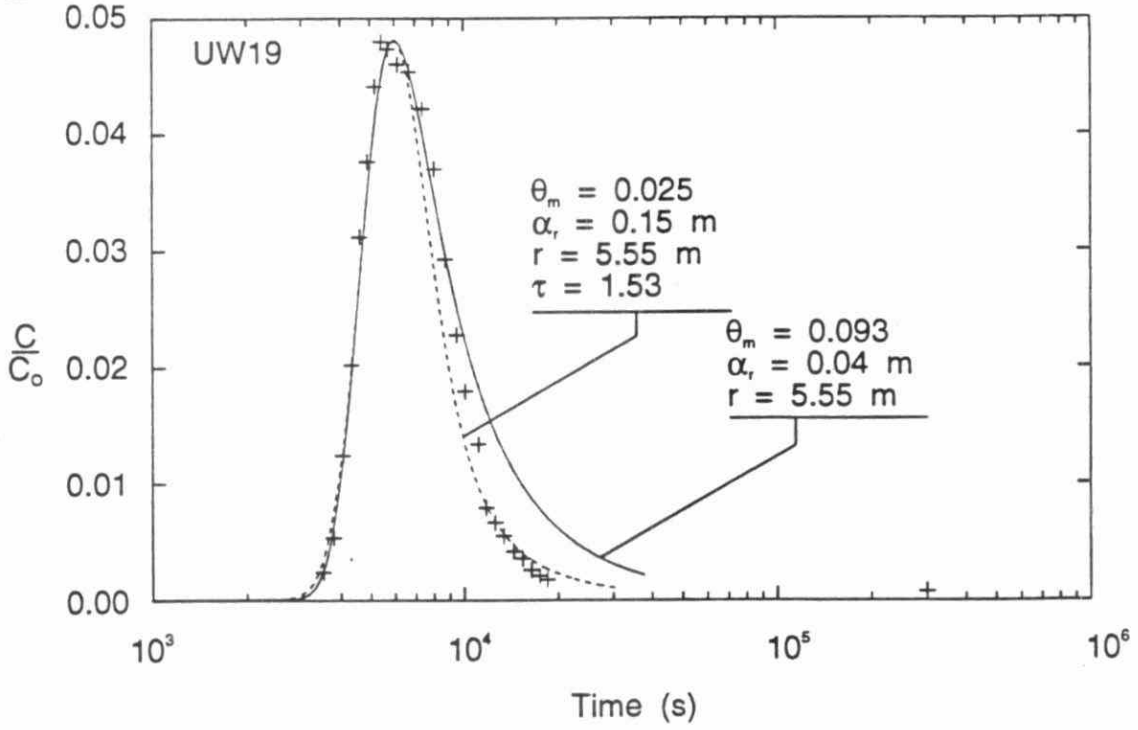

Figure F15: Type-curve match for radial divergent tracer test: RD2, UW19, Fit #2:C/C$_o$, $\theta_m > 0$ and Fit#3: C/C$_o$, $\theta_m > 0$, $\tau > 1$.

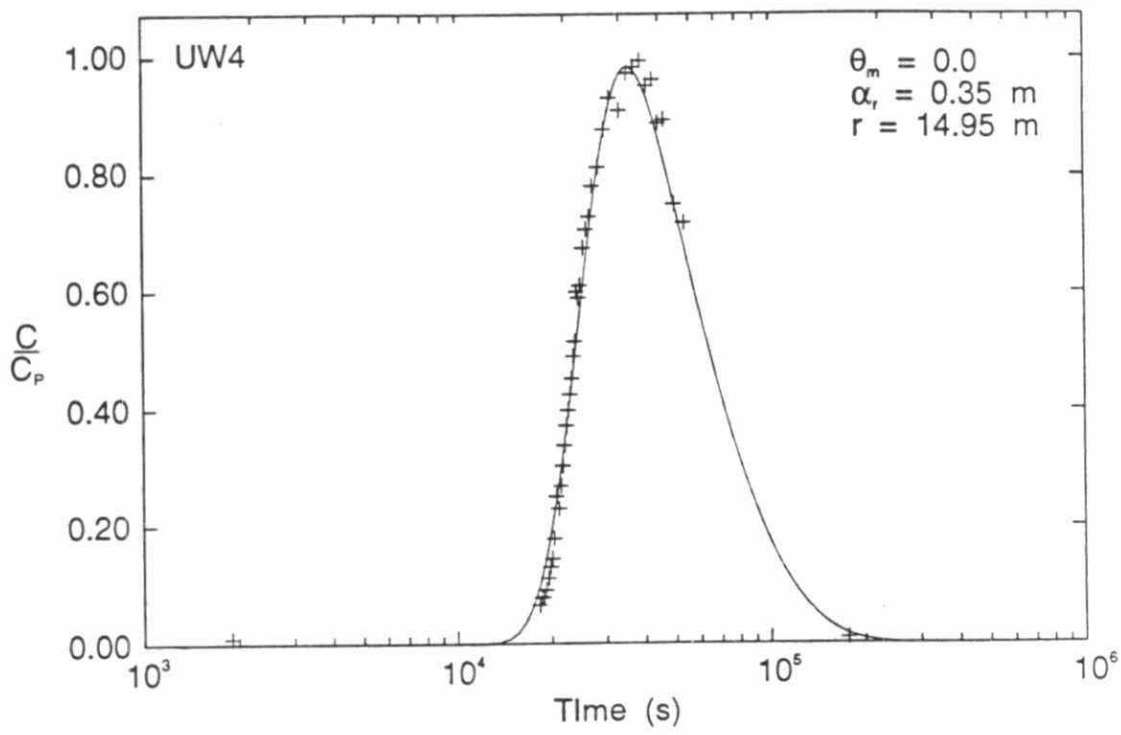

Figure F16: Type-curve match for radial divergent tracer test: RD2, UW4, Fit #1:C/Cp, $\theta_m=0$ (ξ =2.5).

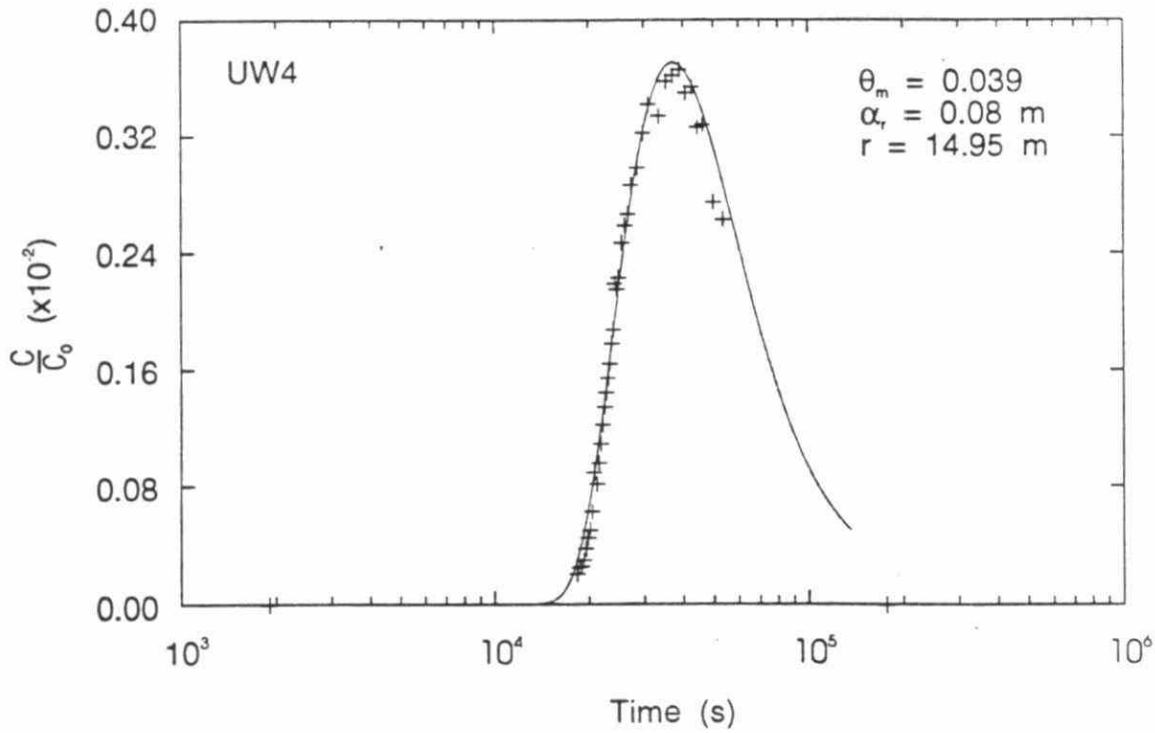

Figure F17: Type-curve match for radial divergent tracer test: RD2, UW4, Fit #2:C/C_o, $\theta_m>0$ and Fit#3: C/C_o, $\theta_m>0$, $\tau>1$ (ξ =4).

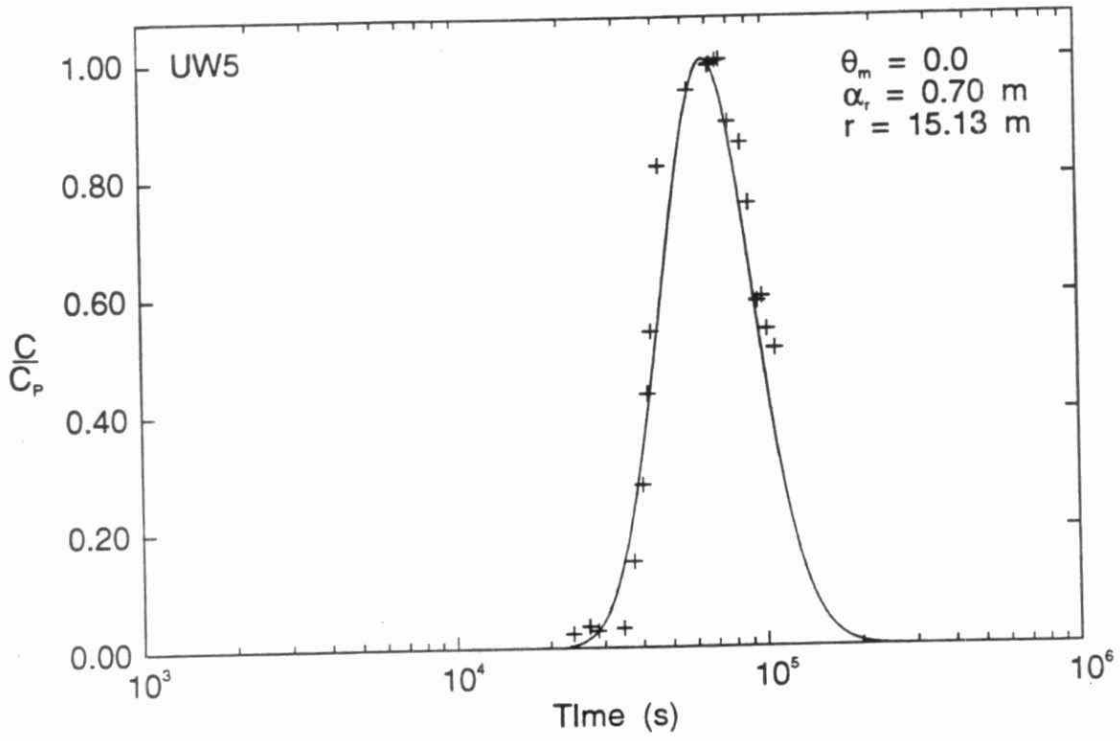

Figure F18: Type-curve match for radial divergent tracer test: RD3, UW5, Fit #1:C/Cp, θ_m=0.

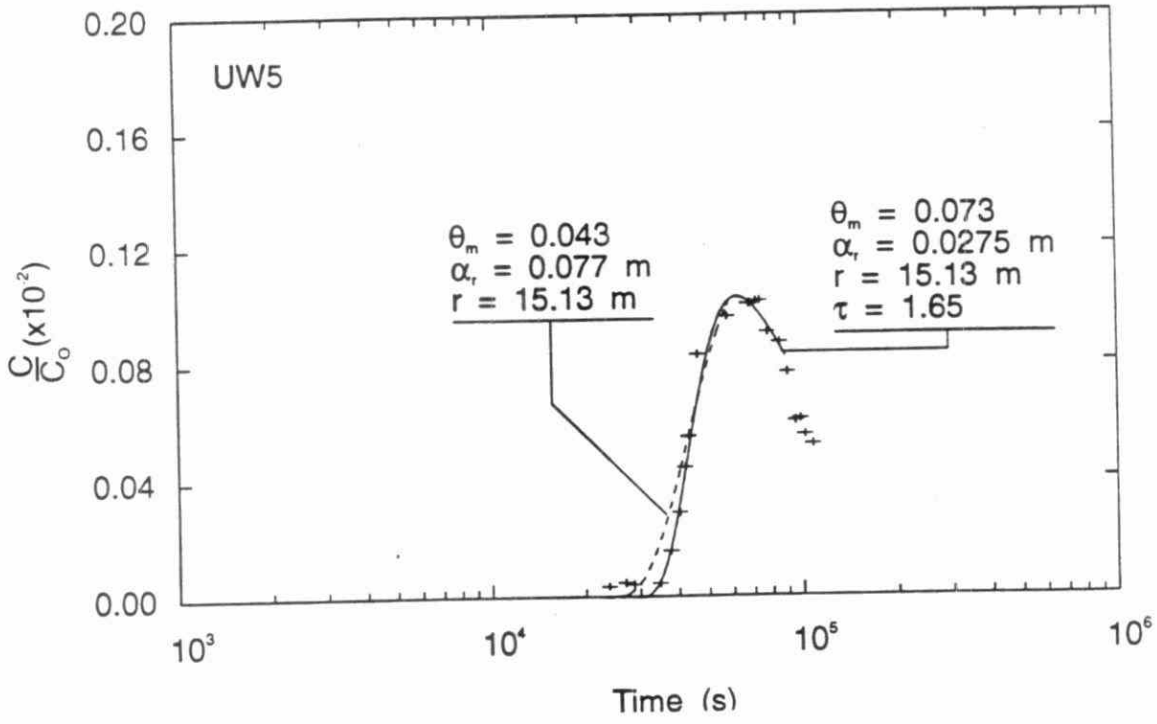

Figure F19: Type-curve match for radial divergent tracer test: RD3, UW5, Fit #2:C/C$_o$, $\theta_m > 0$ and Fit#3: C/C$_o$, $\theta_m > 0$, $\tau > 1$.

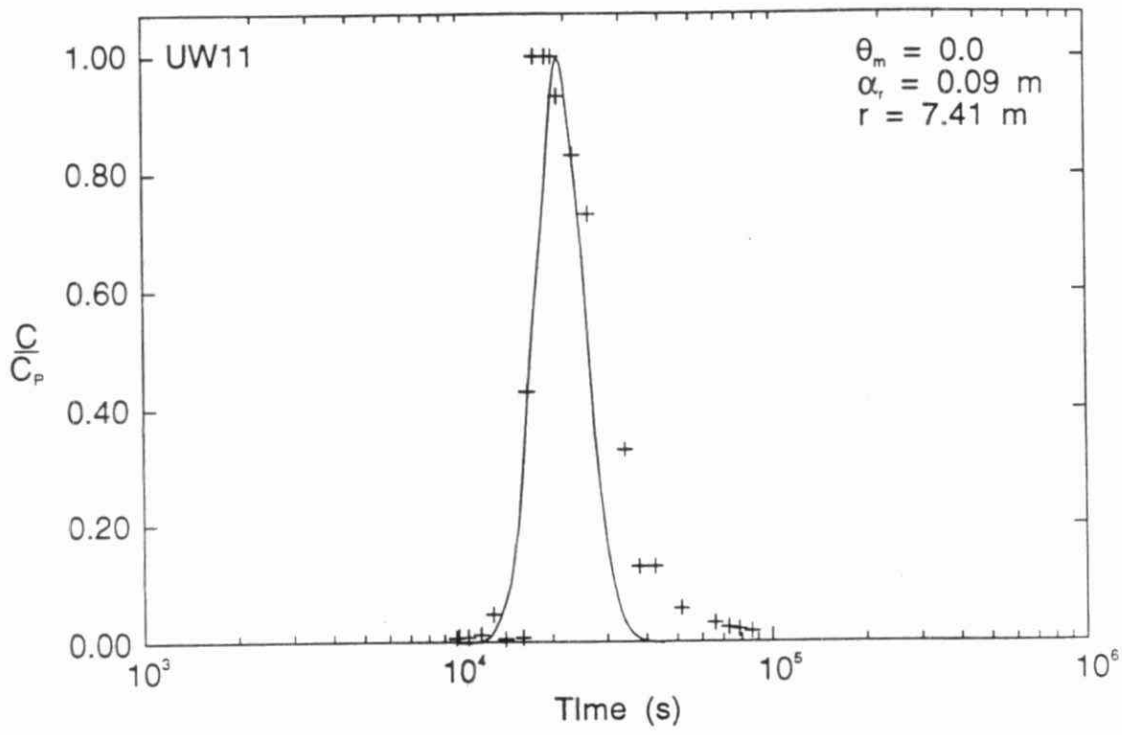

Figure F20: Type-curve match for radial divergent tracer test: RD3, UW11, Fit#1:C/C_p, $\theta_m = 0$.

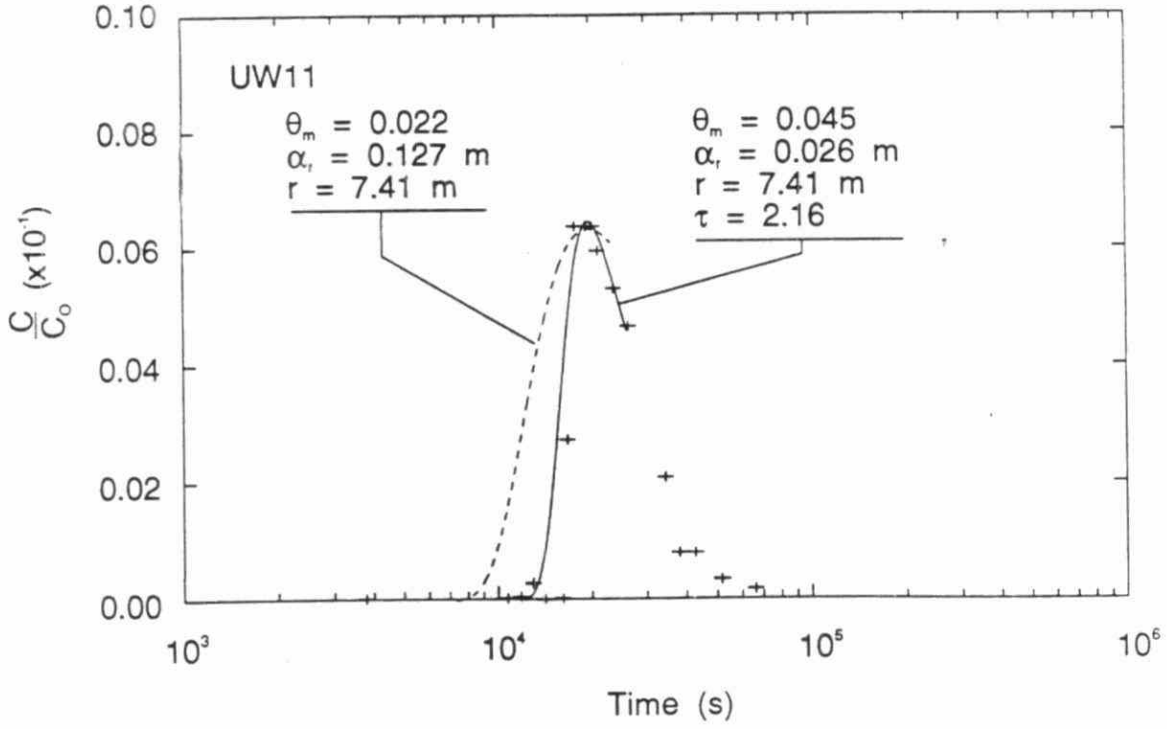

Figure F21: Type-curve match for radial divergent tracer test: RD3, UW11, Fit#2:C/C_o, $\theta_m > 0$ and Fit#3: C/C_o, $\theta_m > 0$, $\tau > 1$.

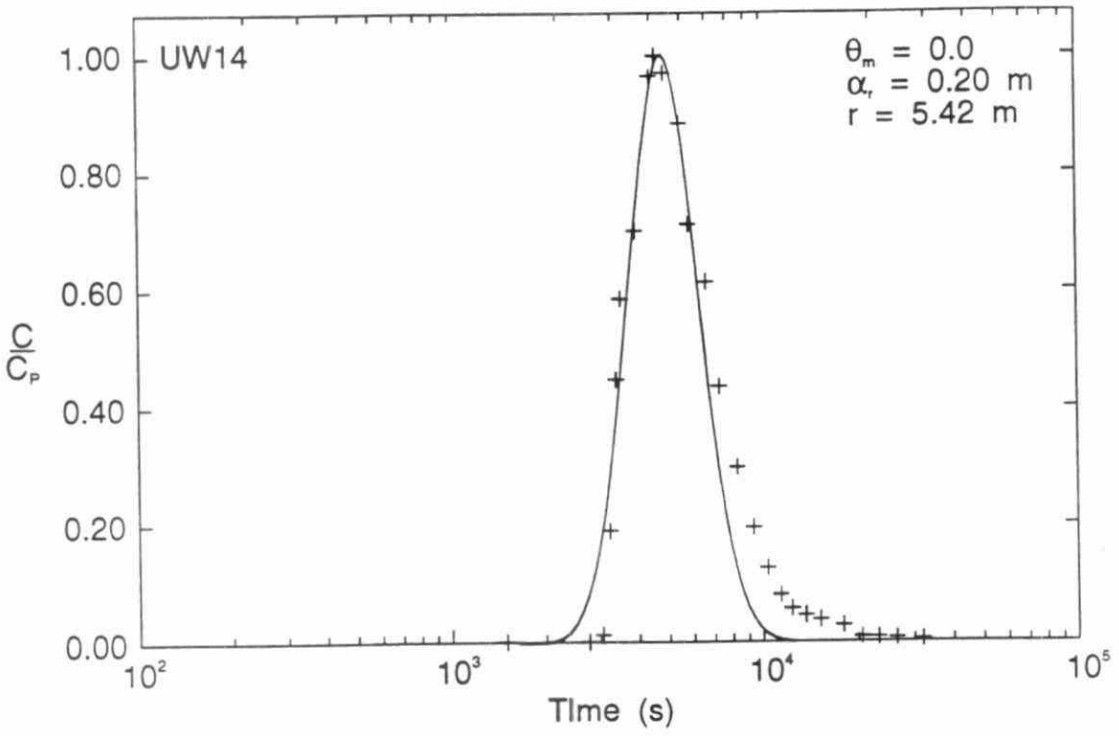

Figure F22: Type-curve match for radial divergent tracer test: RD3, UW14, Fit#1:C/Cp, $\theta_m=0$.

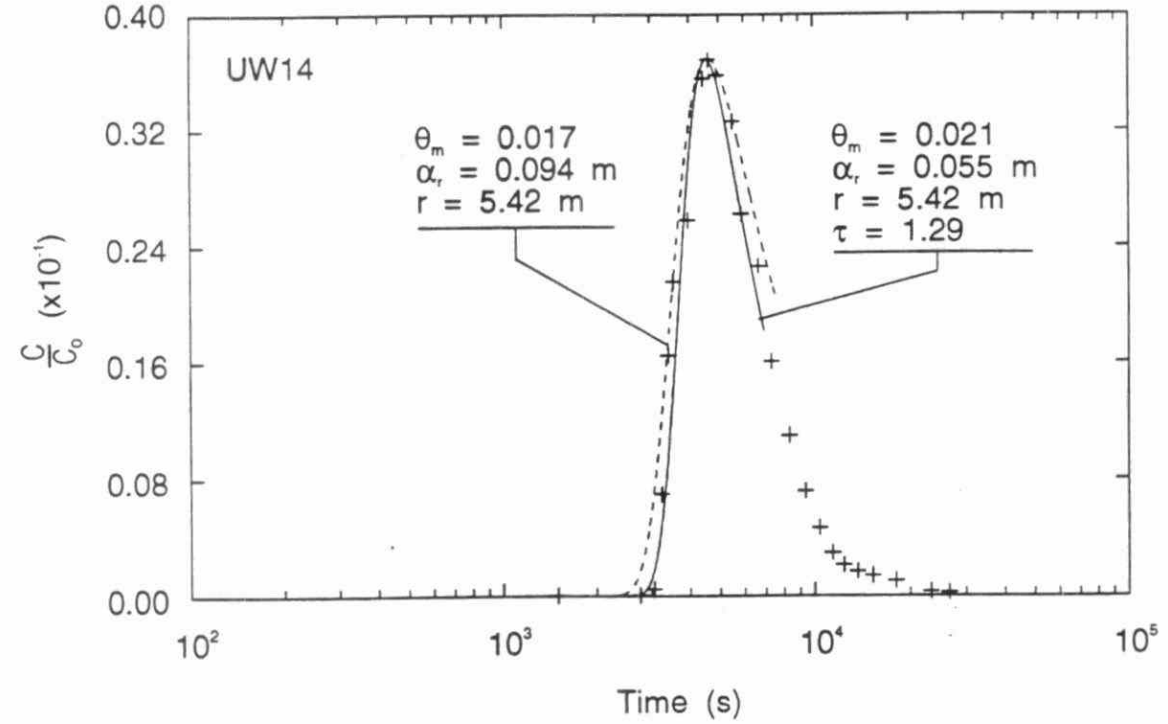

Figure F23: Type-curve match for radial divergent tracer test: RD3, UW14, Fit#2:C/C_o, $\theta_m>0$ and Fit#3: C/C_o, $\theta_m>0$, $\tau>1$.

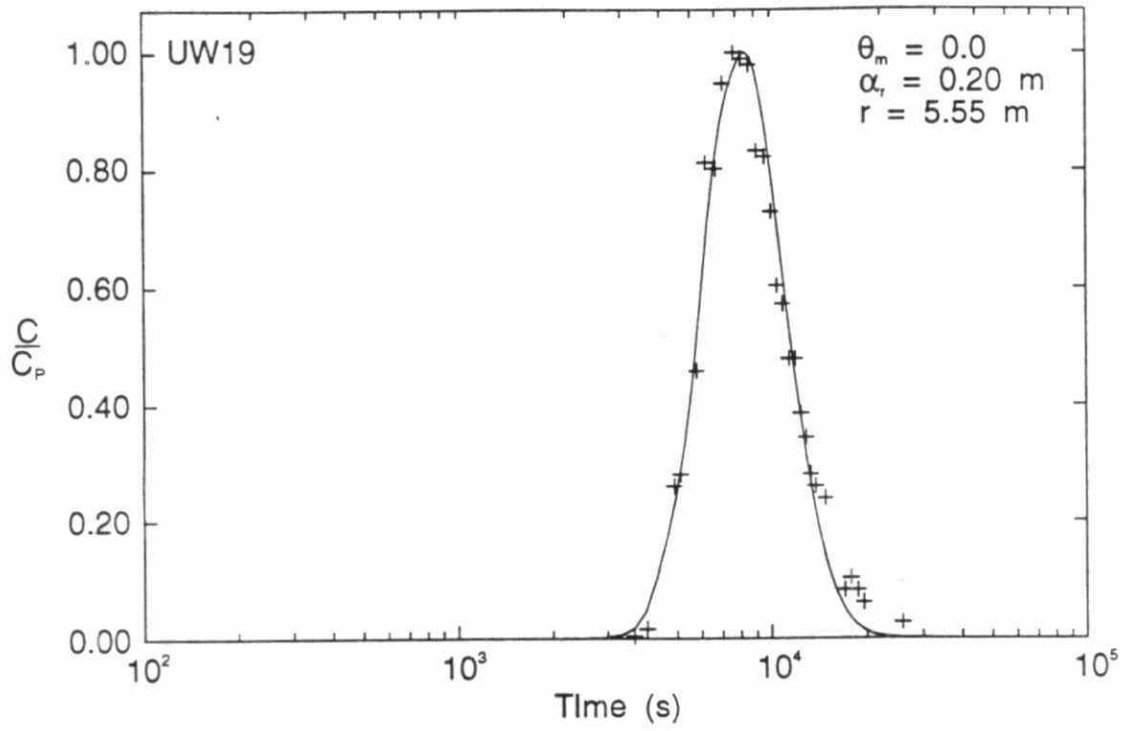

Figure F24: Type-curve match for radial divergent tracer test: RD3, UW19, Fit#1:C/Cp, θ_m=0.

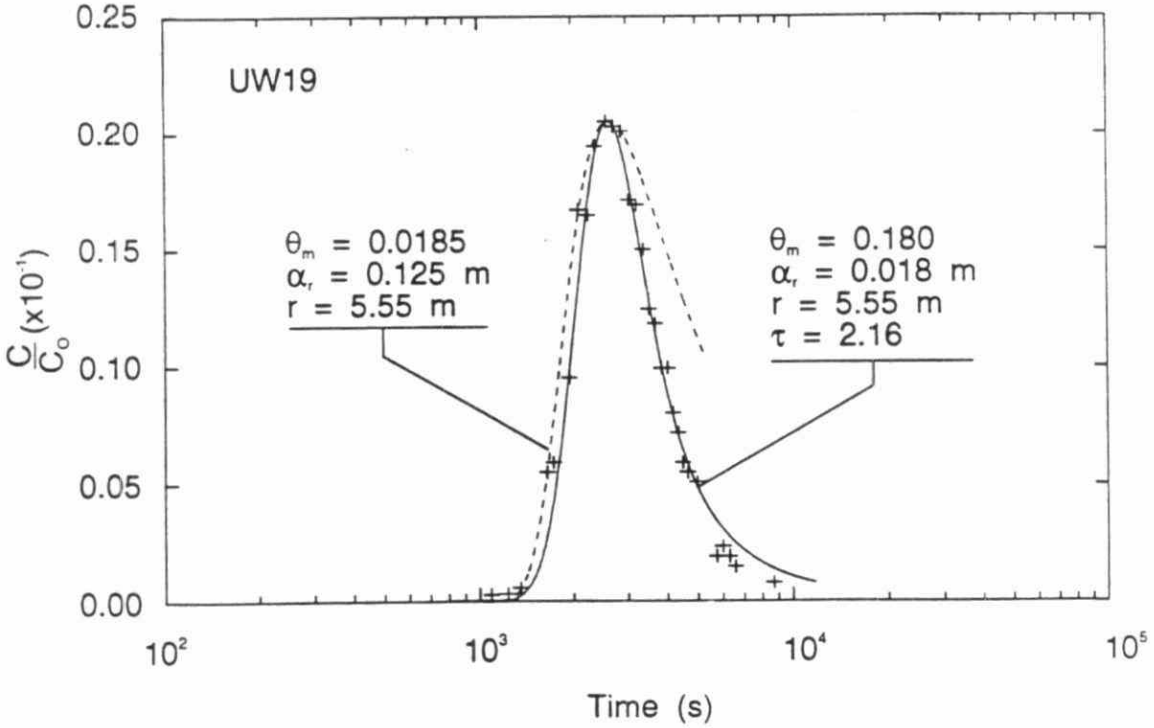

Figure F25: Type-curve match for radial divergent tracer test: RD3, UW19, Fit#2:C/C_o, $\theta_m > 0$ and Fit#3: C/C_o, $\theta_m > 0$, $\tau > 1$.

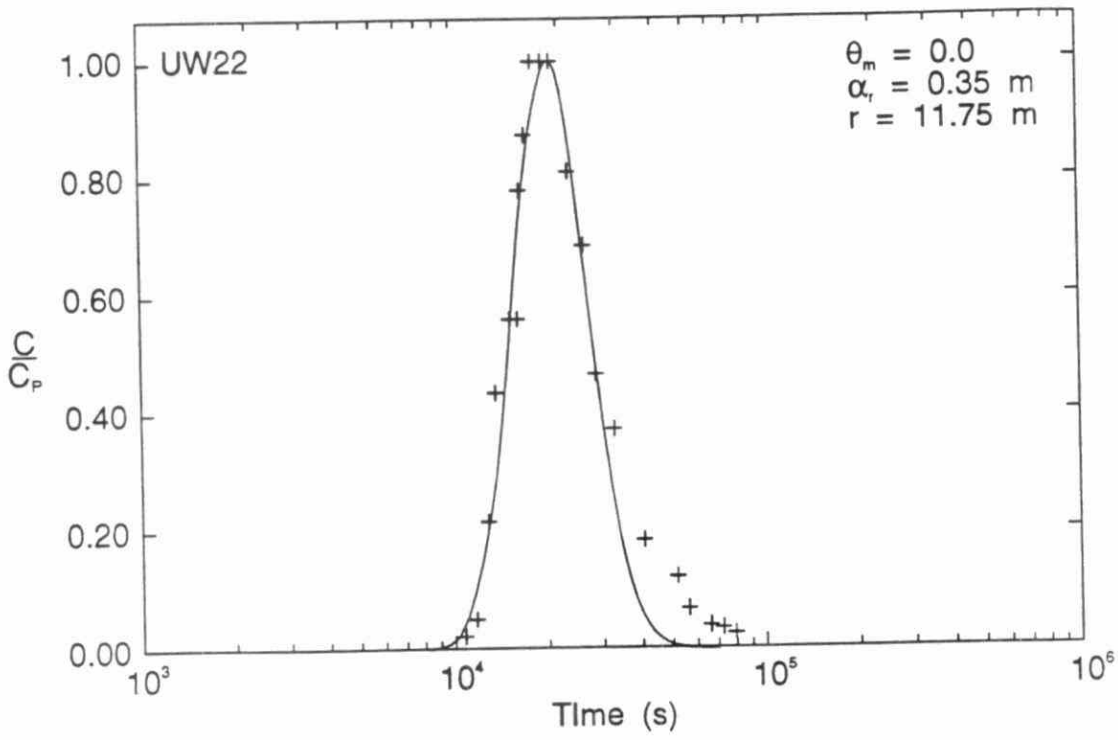

Figure F26: Type-curve match for radial divergent tracer test: RD3, UW22, Fit#1:C/Cp, θ_m=0.

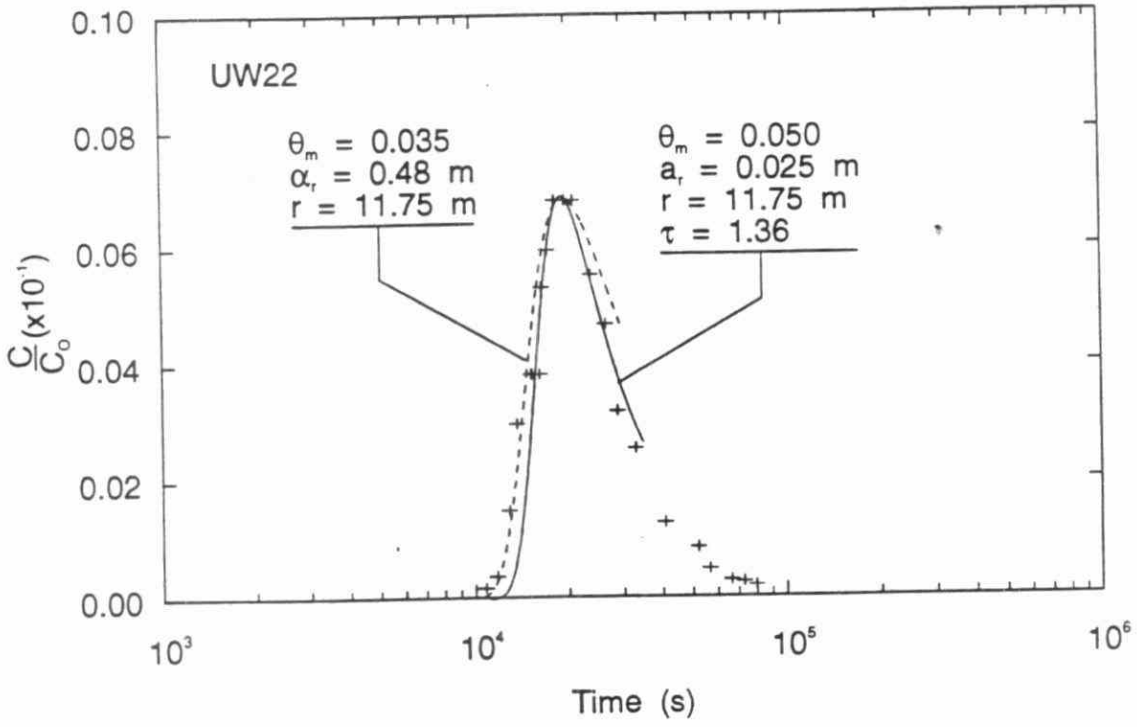

Figure F27: Type-curve match for radial divergent tracer test: RD3, UW22, Fit#2:C/C_o, $\theta_m > 0$ and Fit#3: C/C_o, $\theta_m > 0$, $\tau > 1$.

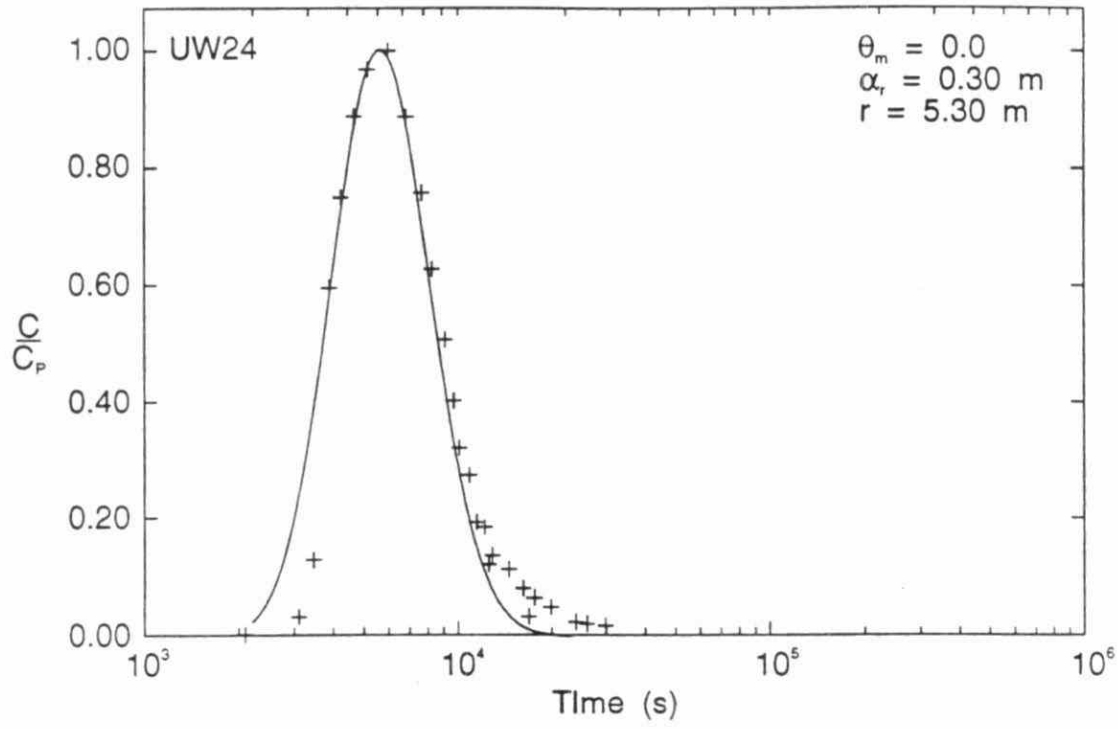

Figure F28: Type-curve match for radial divergent tracer test: RD3, UW24, Fit#1:C/Cp, θ_m=0.

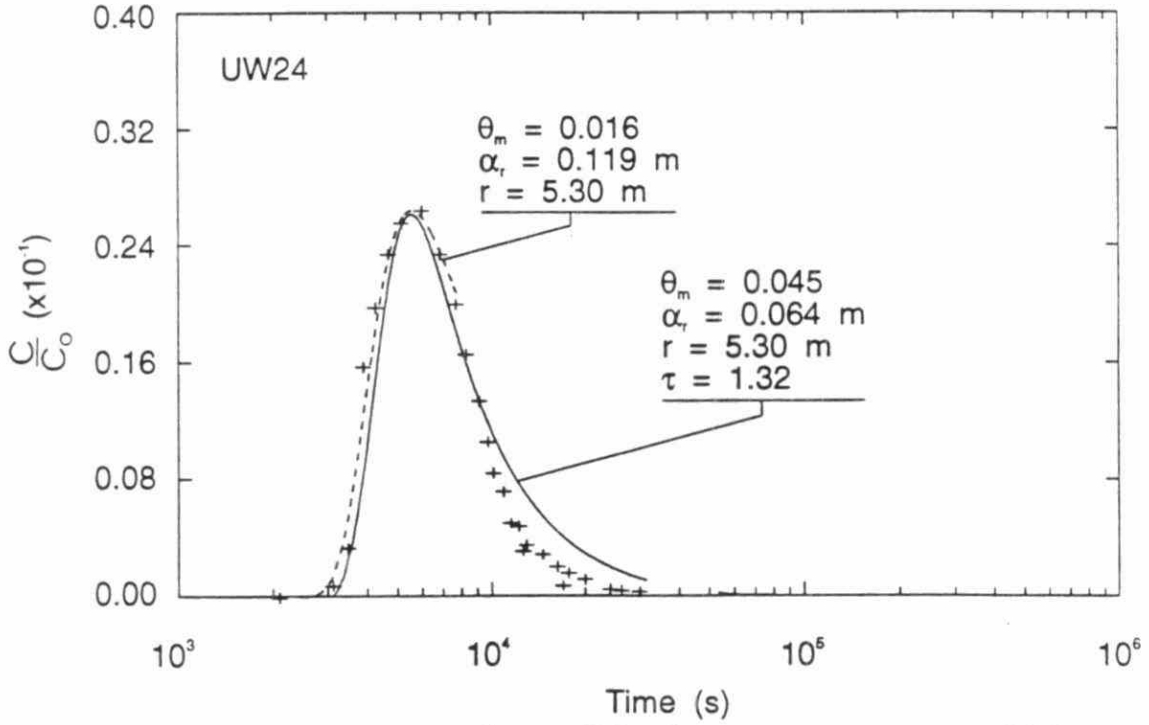

Figure F29: Type-curve match for radial divergent tracer test: RD3, UW24, Fit#2:C/C_o, $\theta_m > 0$ and Fit#3: C/C_o, $\theta_m > 0$, $\tau > 1$.

APPENDIX G

The Analysis of Tracer Experiments
Conducted in Divergent Flow Fields
by
Kent S. Novakowski

For submission to
Water Resources Research

February 1992

THE ANALYSIS OF TRACER EXPERIMENTS CONDUCTED IN DIVERGENT RADIAL FLOW FIELDS

BY
KENT S. NOVAKOWSKI

NATIONAL WATER RESEARCH INSTITUTE
867 LAKESHORE RD.
BURLINGTON, ONT.
CANADA
L7R 4A6
416-336-4610

For submission to
Water Resources Research

February 1992

ABSTRACT

Analytical models are developed to interpret tracer experiments conducted in divergent flow fields. The models account for the mixing of tracer in both the source and observation wells. A solution for the particular case of an observation well of infinitesimally small volume is also presented. Solutions are derived for both resident and flux concentrations and for macroscopically discontinuous conditions at both the inlet and outlet boundaries. The solutions for resident and flux concentration are identical when the mixing volume in the observation well is of finite volume. A similar solution for convergent flow cannot be derived, although, it was found that the solutions for divergent flow can be used to interpret convergent tracer experiments provided that the coefficients which descibe the mixing process in the wells are properly defined. Two tracer experiments were conducted in a horizontally fractured shale to demonstrate the application of the new analytical models. Experiments were conducted with observation wells of finite and infinitesimal volume. The results show that the analytical models developed in this paper yield an improved estimate of the transport properties of the fracture zone relative to models which do not account for mixing in the source and observation wells.

INTRODUCTION

Prediction of the rate of solute migration in groundwater environments is traditionally undertaken using models based constant coefficients to describe the advective and dispersive components of the transport process. Although it is widely recognized that this approach inherently leads to error and uncertainty due to scaling effects in the coefficients which are the result of natural heterogeneity in most geological media (Mercado, 1966; Pickens and Grisak, 1981; Gelhar and Axness, 1983; Molz et al., 1983; Sudicky, 1986; Killey and Moltyaner, 1988), these methods continue to be employed for simulating solute transport. A large component of the uncertainty and error associated with model prediction is dependent on the estimates of the advective and dispersive coefficients which are often not obtained at scales similar to the scale employed for the model prediction. Therefore, to improve the reliability of the modeling study, it is best to determine the coefficients from a tracer experiment conducted in induced or natural flow conditions at the field scale. Because tracer experiments conducted under natural flow conditions can be very time consuming and expensive, the former approach is most widely employed (Gelhar et al., 1985).

Tracer experiments can be conducted in three ways: 1) injection followed by withdrawal from a single borehole, 2) steady injection into one borehole with withdrawal at the same flow rate from another, and 3) either divergent or convergent radial flow. The former of these methods is not often employed due to transient effects associated with starting and stopping flow (Kreft and

Zuber, 1978) and other operational difficulties associated with switching from injection to withdrawal in the same well. In addition, uncertainty in the geometry of the flow field for some injection-withdrawal experiments (eg. Novakowski, 1988) suggests that, of the three methods, experiments conducted in radially convergent or divergent flow fields may provide the most accurate estimates of field-scale dispersivity.

Experiments conducted in convergent flow fields are sometimes most attractive because the tracer concentration is removed from the flow field, leaving little or no tracer residue behind. However, unless multiple tracers are employed, only one source and withdrawal well pair can be used during a given experiment. In the case of divergent flow, many observation wells can be employed using a single tracer. In addition, in cases where it is desirable to determine the concentration directly from the formation (see following definition of resident concentration), measurements in convergent flow fields are difficult if not impossible to obtain while such measurements are easily obtained during experiments conducted in radially divergent flow fields.

Although only a few examples of tracer experiments conducted in divergent flow fields have appeared in the literature (Mercado, 1966; Hoopes and Harleman, 1967; Novakowski et al., 1985; Ward et al., 1990), numerous analytical and numerical models have been developed for interpretation of these tests (Ogata, 1958; Raimondi et al., 1959; Hoopes and Harleman, 1967; Tang and Babu, 1979; Sauty, 1980; Chen, 1985; Chen, 1986; Hsieh, 1986; Valocchi, 1986;

Chen, 1987; Moench, 1989a). Most of the recently developed models were derived using analytical or semi-analytical methods and incorporate, for example, matrix diffusion (Chen, 1985), chemical retardation (Valocchi, 1986) and a variety of inlet and sampling boundary conditions (Moench, 1989a).

Despite the fact that convergent tracer experiments are often easier to conduct, there are few field examples of these experiments in the literature (Mercado, 1966; Landstrom et al., 1978; Novakowski, 1988; Raven et al., 1988). Again, there are numerous models for the interpretation of convergent solute transport (Ogata, 1970; Al-Niami and Rushton, 1978; Sauty, 1980; Hodgkinson and Lever, 1983; Guvanasen and Guvanasen, 1987; Chen and Woodside, 1988; Moench, 1989b). Two of these models (Hodgkinson and Lever, 1983; Moench, 1989b) provide particularily detailed descriptions of the physics of convergent transport including a complete description of the mixing and injection processes in the source and withdrawal wells.

Recently, it has been suggested that solute concentrations obtained from large-scale measuring devices such as sampling wells or pan lysimeters represent flux-averaged rather than volume-averaged (or resident) values (Kreft and Zuber, 1978; van Genuchten and Parker, 1984). Kreft and Zuber (1978) define the resident concentration as the mass of solute per elementary volume of the porous medium at a given time and flux concentration as the mass of solute crossing a unit area per element of time. Thus, the flux transformation (Kreft and Zuber, 1978; van Genuchten and Parker,

1984) is often incorporated into analytical models so that field-scale measurements can be interpreted.

In addition, the use of third-type boundary conditions has been proposed (Chen, 1987) to more properly describe the macroscopic discontinuity in tracer concentration between the boundary (i.e. the well) and the formation. Novakowski (1991a; 1991b) reviewed these issues for conditions of uniform flow and concluded that the use of first-type boundaries to describe continuity of concentration across the well-formation interface is physically unjustifiable. Doubt was also cast on the use of the flux transformation to modify analytical models where the boundary conditions are time-dependent. Both the Hodgkinson and Lever (1983) and Moench (1989b) models apply first-type conditions at the well-formation interface; and Moench (1989b) employs a flux transformation.

The objective of this paper is to present the derivation of a semi-analytical model which describes the divergent transport of a conservative solute in a steady radial flow field. The model is developed following the procedure employed in Novakowski (1991a) for macroscopically discontinuous concentrations in a uniform flow field. Conditions of time-dependent mixing in the source and observation wells are incorporated and solutions are found for both resident and flux-averaged concentrations. The resulting solution is compared to the solution for convergent transport of Moench (1989b) under a variety of flow conditions. In addition, the effect of matrix diffusion on the results of tracer experiments conducted

in radially-divergent flow is investigated. Finally, field examples of tracer experiments conducted in fractured rock are presented to demonstrate the use of the analytical model.

MATHEMATICAL DEVELOPMENT

In the following development, the process of matrix diffusion is integrated into the governing equation for radial solute transport. This makes the analytical model applicable to most field conditions. It is recognized, however, that matrix diffusion is rarely important for interpreting the results of short-term advective experiments (Maloszewski and Zuber, 1985).

The mathematical development is undertaken by deriving the general solution for solute transport in a divergent flow field. The similarity between the solutions for divergent and convergent transport is shown and further derivation is conducted using the specific boundary conditions for the source and observation wells. The schematic diagrams given in Figure 1 depict the physical problem for both porous and fractured media.

The governing equation for solute transport in a divergent flow field where solute concentration in the formation is influenced by diffusion of solute into adjacent strata is given by:

$$b\left[\frac{\partial C}{\partial t}-\frac{1}{r}\frac{\partial}{\partial r}\left(rD_r\frac{\partial C}{\partial r}\right)+v\frac{\partial C}{\partial r}\right]+q=0 \qquad r_w \le r \le \infty \qquad [1]$$

where r is radial distance, groundwater velocity, v, is a function of r, C is resident concentration, b is formation thickness, q is the sink term for matrix diffusion and the hydrodynamic dispersion

coefficient, D_r, is given by:

$$D_r = \alpha_r |v| \qquad [2]$$

The coefficient α_r is defined as radial dispersivity. Equation [1] is given assuming that advection predominates over diffusion in the radial direction and that the flow field is radially symmetric. Transverse dispersion is ignored as justified by Sauty, (1980); Hodgkinson and Lever, (1983); and Guvanasen and Guvanasen, (1987).

Velocity can be defined in a number of ways depending on the manner in which the tracer experiment is conducted and on the type of media in which the experiment is carried out. For porous media, the traditional definition of velocity is (Hsieh, 1986):

$$v = A/r \qquad [3]$$

where

$$A = Q/2\pi b\theta \qquad [4]$$

The flowrate, Q, is defined as the volumetric rate of injection into the source borehole and θ is the porosity of the formation. Alternatively, A can be defined by substitution of the Theim equation into [4] and thus the interpretation is conducted on the basis of hydraulic gradient rather than flowrate:

$$A = \frac{\Delta H T}{\ln(r/r_w) b\theta} \qquad [5]$$

where r is radial distance between the source and observation point, ΔH is the difference in hydraulic head between the source and observation point, T is transmissivity and r_w is the radius of

the source well.

In the case where a tracer experiment is conducted in fractured media, expressions equivalent to equations [4] and [5] can be derived. Assuming an equivalent single fracture and plug flow displacement, A, is defined as:

$$A = Q/2\pi(2b) \qquad [6]$$

where 2b is the equivalent aperture of the fracture. For an interpretation based on hydraulic head, A is defined as:

$$A = \frac{\Delta H \rho g (2b)^2}{12 \mu \ln(r/r_w)} \qquad [7]$$

where μ is the dynamic viscosity, and ρg is specific weight of the fluid.

To account for solute lost to matrix diffusion, the sink term in [1] is given by Fick's first law:

$$q = -\theta D_d \left. \frac{\partial C_m}{\partial z} \right|_{z=0} \qquad [8]$$

where z is the vertical direction in the matrix or adjacent aquitard, D_d is the effective diffusion coefficient of the matrix, and C_m is the concentration of tracer in the matrix. The coefficient D_d is equal to the molecular diffusion coefficient for the tracer, D_m, times a tortuosity factor for the matrix (usually about 0.72 for porous media).

By assuming symmetry (i.e., b/2), equation [1] may be re-written as:

$$\frac{\partial C}{\partial t} - \frac{1}{r}\frac{\partial}{\partial r}\left(rD_r\frac{\partial C}{\partial r}\right) + v\frac{\partial C}{\partial r} - \frac{2D_m}{b}\frac{\partial C_m}{\partial z}\bigg|_{z=0} = 0 \qquad [9]$$

and the governing equation for the matrix is given by:

$$\frac{\partial C_m}{\partial t} - D_d\frac{\partial^2 C_m}{\partial z^2} = 0 \qquad [10]$$

where the initial condition is:

$$C_m(z,0) = 0 \qquad [11]$$

and the inner and outer boundary conditions are:

$$C_m(0,t) = C(r,t) \qquad [12]$$

and

$$C_m(\infty,t) = 0 \qquad [13]$$

The diffusion process described in this problem is an approximation because it is assumed that the solute lost through diffusion is transported instantaneously across the entire formation thickness. For formations of substantial thickness, this is clearly not a realistic assumption.

Using the following dimensionless variables (adapted from Hsieh, 1986), equations [9] and [10] can be rendered dimensionless to facilitate the solution method:

$$C_D=C/C_0 \quad C_{mD}=C_m/C_0 \quad t_D=At/\alpha_r^2$$
$$r_D=r/\alpha_r \quad r_{De}=r_w/\alpha_r \quad r_{Di}=r_i/\alpha_r \quad z_D=z/\alpha_r \qquad [14]$$

where r_i is the radial distance between the source and observation well and C_0 is the initial concentration in the source well.

The general solution to equations [9] and [10], in dimensionless form, is obtained by applying the Laplace transform method with respect to time. This solution method is given in Chen (1985). In the nomenclature of the present paper, the general solution is given by:

$$\bar{C}_D(r_D,p)=C_1\exp\{\frac{y}{2}\}Ai(\phi^{1/3}y)+C_2\exp\{\frac{y}{2}\}Bi(\phi^{1/3}y) \qquad [15]$$

where the overbar indicates the Laplace transformed variable, Ai and Bi are independent Airy functions of first and second order, respectively (Abramowitz and Stegun, 1964), and:

$$y=r_D+\frac{1}{4\phi}$$
$$\phi=\{p+\omega\left(\frac{p}{\psi}\right)^{1/2}\} \qquad [16]$$

where p is the Laplace variable and:

$$\omega=\frac{2D_m\alpha_r}{Ab}$$
$$\psi=\frac{D_d}{A} \qquad [17]$$

For convergent flow with boundary conditions identical to those given above, the same general solution applies except that the

terms inside the exponentials become negative.

Particular Solution for Divergent Flow

Development of the particular solution for divergent flow is undertaken following the solution method of Novakowski (1991a). The boundary value problem is formulated to include mixing in the source and observation wells with macroscopically discontinuous concentration at the well-formation boundary at each well. To find the particular solution for the observation well, a solution must first be obtained for concentration in the formation.

The inlet boundary condition, which is used to describe the instantaneous introduction of a spike of tracer into a continuously mixed section of the source well, consists of two components. The first component is a description of the mass balance in the wellbore mixing volume:

$$V_i \frac{dC_i(t)}{dt} = -\gamma_i |v| C_f(t) \qquad [18]$$

where V_i is the volume of the well in which the mixing takes place, γ_i is the cross-sectional area through which flow leaves the well, and C_i is the concentration in the well. To complete the boundary condition, a mass balance is required on the formation side of the boundary:

$$|v| C_f(t) = v C(r_w, t) - D_r \frac{\partial C(r_w, t)}{\partial r} \qquad [19]$$

The initial condition for [18] is given by:

$$C_i(0)=C_0 \qquad [20]$$

Using the following dimensionless variables;

$$C_{Di}=\frac{C_i}{C_0} \qquad \beta_{Di}=\frac{V_i r_w}{\alpha_r^2 \gamma_i} \qquad [21]$$

equations [18] and [19] are re-written in dimensionless form and using the forward Laplace transform, [18] and [19] are reduced to:

$$\frac{\beta_{Di}}{(\beta_{Di}p+1)}=\bar{C}_D(r_{De},p)-\frac{\partial \bar{C}_D(R_{De},p)}{\partial r_D} \qquad [22]$$

In this derivation, only one of the two independent solutions in equation [15] is required. Thus, by limiting the concentration at the outer boundary to zero for equation [1], C_2 is forced to zero and the general solution is reduced to:

$$\bar{C}_D(r_{De},p)=C_1\exp\{\frac{y}{2}\}Ai(\phi^{1/3}y) \qquad [23]$$

By substitution of equation [23] into the boundary condition, equation [22], the particular solution for concentration in the formation is obtained:

$$\bar{C}_D(r_{De},p)=\frac{\beta_{Di}}{(\beta_{Di}p+1)}\exp\{\frac{r_D-r_{De}}{2}\}\cdot\frac{Ai(\phi^{1/3}y)}{[1/2Ai(\phi^{1/3}y_e)-\phi^{1/3}Ai'(\phi^{1/3}y_e)]} \qquad [24]$$

where

$$y_e = r_{De} + \frac{1}{4\phi} \qquad [25]$$

and Ai' is the derivative of the Airy function. This solution can be used to interpret field experiments where resident concentration is measured at an observation well of infinitesimally small volume.

To obtain the particular solution for concentration in an observation well where the volume of the mixing zone in the well is non-zero, a mass balance is formulated in a manner similar to that for the source well. It is assumed that the volume in the observation well is continuously mixed and the mass balance can be described by:

$$V_e \frac{dC_e(t)}{dt} = M_L(t) - \gamma_e |v| C_e(t) \qquad [26]$$

where V_e is the volume of the mixing zone in the observation well, M_L is the mass leaving the formation and entering the well, γ_e is the cross-sectional area through which flow enters the well, and C_e is the concentration in the observation well. The mass entering the well is given by:

$$M_L(t) = \gamma_e [v C(r_p, t) - D_r \frac{\partial C(r_p, t)}{\partial r}] \qquad [27]$$

and the initial condition for equation [26] is:

$$C_e(0)=0 \qquad [28]$$

Using the dimensionless variables:

$$C_{De}=\frac{C_e}{C_0} \quad \beta_{De}=\frac{V_e r_i}{\alpha_r^2 \gamma_e} \qquad [29]$$

equations [26]-[28] are re-written in dimensionless form and the particular solution is found by application of the Laplace transform. In the Laplace domain, the boundary equation for the observation well is:

$$\bar{C}_{De}(p)\cdot(\beta_{De}p+1)=\bar{C}_D(r_{Di}p)-\frac{\partial \bar{C}_D(r_{Di}p)}{\partial r_D} \qquad [30]$$

To find the particular solution for concentration in the observation well, equation [24] is substituted into [30]. This gives:

$$\bar{C}_{De}(p)=\frac{\beta_{Di}}{(\beta_{Di}p+1)(\beta_{De}p+1)}\exp\{\frac{r_{Di}-r_{De}}{2}\}\cdot\frac{[1/2Ai(\phi^{1/3}y_r)-\phi^{1/3}Ai'(\phi^{1/3}y_r)]}{[1/2Ai(\phi^{1/3}y_e)-\phi^{1/3}Ai'(\phi^{1/3}y_e)]} \qquad [31]$$

where

$$y_r=r_{Di}+\frac{1}{4\phi} \qquad [32]$$

Note that this solution is a function of the properties of the source and observation wells only; and conveys no information regarding concentration in the formation.

The coefficients γ_i and γ_e are dependent on the type of

formation in which the tracer experiment is conducted. For experiments conducted in porous media, γ_i is defined by:

$$\gamma_i = 2\pi r_w b\theta \qquad [33]$$

In the case of horizontally fractured media, $b\theta$ is replaced by the equivalent single fracture width, 2b.

The definition of γ_e is less concise and is derived from point dilution theory (Grisak et al., 1977). For porous media, γ_e is given by:

$$\gamma_e = \pi r_{wo} b\theta\xi \qquad [34]$$

where r_{wo} is the radius of the observation well, and ξ is a dimensionless correction factor accounting for additional flow captured by the open well (see Drost et al. [1968] for several pictorial examples). Values of ξ can vary substantially (from 0.5 to 4.0) although there are reliable methods for making accurate estimations provided that information regarding the well completion is known (Drost et al., 1968). Again, for fractured media, $b\theta$ is replaced by 2b. In this case, the correction factor may be large (see Ketcheson [1985] for examples), as a result of heterogeneity in the aperture distribution of the fracture adjacent to the borehole.

Particular Solution for Convergent Flow

To find a particular solution for convergent flow equivalent to equation [31], the boundary conditions stated above must be slightly re-written to account for the inward direction of flow.

Thus, equation [19] is rewritten for the source well as:

$$|v|C_i(t) = -[vC(r_p,t) - D_r\frac{\partial C(r_p,t)}{\partial r}] \qquad [35]$$

and equation [27] is rewritten for the withdrawal well as:

$$M_L(t) = -\gamma_e[vC(r_w,t) - D_r\frac{\partial C(r_w,t)}{\partial r}] \qquad [36]$$

where the definitions for γ_i and γ_e as given above, are exchanged. The velocity is also redefined as v=-A/r.

Unfortunately, a particular solution to this problem using the solution method employed above can not be obtained. This is because the second independent solution in equation [15] must be considered. When deriving the solution, it is found that there are two equations (one for each of the inlet and outlet boundaries), and three unknowns, C_1, C_2 and C_{De} rendering the problem indeterminate. Consequently, an additional equation is required to solve this problem. Previous authors (Hodgkinson and Lever, 1983; Moench, 1989a and 1989b) have employed a continuity condition which eliminates C_{De} and reduces the number of unknowns to two. However, considering the arguments put forth in Novakowski (1991b) with regard to the use of continuity conditions, the fact that a solution accounting for discontinuous boundaries can not be found for convergent flow must be considered a drawback for the general use of this type of tracer experiment in highly-dispersive media.

For comparative purposes, the solution of Moench (1989b) for convergent transport is presented. In the nomenclature of the

present paper, the equation for resident concentration at the withdrawal well is given by (Moench ,1989b):

$$\bar{C}_D(r_{De},p)=\frac{\beta_{Di}\chi_4}{\lambda}\exp\{-y_e\}Ai(\phi^{1/3}y_e)-\frac{\beta_{Di}\chi_3}{\lambda}\exp\{-y_e\}Bi(\phi^{1/3}y_e) \quad [37]$$

where

$$\lambda=\chi_1\chi_4\exp\{-\frac{(y_r+y_e)}{2}\}-\chi_2\chi_3\exp\{-\frac{(y_r+y_e)}{2}\} \quad [38]$$

and

$$\begin{aligned}\chi_1&=[Ai(\phi^{1/3}y_r)\cdot(\beta_{Di}p+1/2)+\phi^{1/3}Ai'(\phi^{1/3}y_r)]\\ \chi_2&=[Bi(\phi^{1/3}y_r)\cdot(\beta_{Di}p+1/2)+\phi^{1/3}Bi'(\phi^{1/3}y_r)]\\ \chi_3&=[Ai(\phi^{1/3}y_e)\cdot(\beta_{De}p+1/2)-\phi^{1/3}Ai'(\phi^{1/3}y_e)]\\ \chi_4&=[Bi(\phi^{1/3}y_e)\cdot(\beta_{De}p+1/2)-\phi^{1/3}Bi'(\phi^{1/3}y_e)]\end{aligned} \quad [39]$$

where y_r and y_e are as defined previously for divergent flow.

Flux-Averaged Transformation

The flux-averaged transformation for divergent radial flow is given by (Valocchi, 1986):

$$C_{DF}=C_D-\frac{\partial C_D}{\partial r_D} \quad [40]$$

where C_{DF} is flux concentration. For uniform flow conditions, there are two methods of obtaining solutions for flux concentrations: 1) by substitution of the particular solutions directly into [40] or 2) by substitution of [40] into the original boundary value problem (Novakowski, 1991a). However, as noted by Chen (1987), if the latter method is used in the case of radial transport, solution of the transformed problem will not result in the same expression as

in the isolated zone is employed to measure hydraulic head. All flow rate and hydraulic head data are recorded on a computer-based data aquisition system programmed to sample each signal once per minute.

A similar system is employed in the observation borehole with the exception that no net injection or withdrawal is undertaken. The fracture zone is isolated using packers separated by helically shaped static mixers approximately 0.12 m in length. A selenoid recirculation pump is installed below the bottom packer and a recirculation pump is located at ground surface. Both pumps are operated continuously throughout the experiment. Although it is important to minimize the volume of the mixing zone in the observation borehole, it is also important to maintain convergent flow towards the isolated section (Novakowski and Cherry, 1989). Thus, only static mixers are employed to reduce the volume in the test section. The entire volume of water contained in the test section and both arrangements of recirculation tubing is approximately 0.43 L.

Tracer arrival at the observation borehole is monitored by means of both an in-line tracer detector installed in the recirculation tubing and the analysis of small-volume samples obtained in the same fashion as for the source borehole. The signals obtained from the in-line detector and from a pressure transducer installed in the isolated section, are recorded at the same rate as those from the source borehole.

To obtain the concentration in the formation for

interpretation using equation [24], samples must be obtained directly from the fracture plane. This can only be accomplished by eliminating all of the standing water volume in the observation borehole. Thus, a sampling packer was devised based on a concept originally developed by Teutsch and Ptak (1989). Here a packer gland is used to fill the wellbore volume and groundwater samples are obtained through the wall of the packer. Figure 7 shows a schematic diagram of the sampling packer designed for this study. The packer body is approximately 0.60 m in length with a grooved plate attached to one side. The plate is approximately 15 mm in width and 200 mm in length. A small diameter hole is drilled through the center of the plate and through the wall of the packer to provide a conduit for sample abstraction. Inside the packer, the sample tube is divided to provide for the measurement of hydraulic head. Small diameter nylon tubing is used for the remainder of the sample line to ground surface. A pressure transducer is installed immediately above the sample packer.

In using the sampling packer, the fracture or fracture zone need only be intersected by a small portion of the grooved plate. To insure that the sample tubing is purged during each sampling event, larger volume samples (on the order of 0.030-0.04 L) are required than that obtained when using the mixing system. This is presummed to have minimal influence on the direction and geometry of the radial flow field.

A fluorescent dye tracer is used in both experiments. The dye is of the green type known commercially as Lissamine or Lissamine

FF and has been determined to be stable and resistent to sorptive losses for most applications (Smart and Laidlaw, 1977). In addition, several convergent tracer experiments were conducted between an observation well located within 5.0 m of the source well to compare the behavior of the Lissamine tracer to that of another conservative tracer, bromide. No retardation of the Lissamine was observed and mass recovery for each of the tracers were identical. Concentration of Lissamine is determined using standard fluorometric techniques in both flow-through and grab-sample modes.

Experimental Method

To conduct a tracer experiment, a steady-flow field is established by injecting the stored water into the source borehole over a period of 4-24 hrs prior to tracer injection. Injection flowrates were 440 and 270 mL/min for experiments 1 and 2, respectively. Because the storativity of the fracture set is very small, steady conditions (defined as a change in hydraulic gradient between the source and observation well of less than 1% in one hour) are achieved in only a few hours. During this period, several backgound samples of the groundwater are obtained from both the source and observation wells. The tracer is injected using a concentrated source (45-90 mL of 1 g/L Lissamine) which is quickly pumped into the recirculation tubing by means of a peristaltic pump.

Immediately following tracer injection, small-volume samples are obtained from the source borehole at frequencies ranging from one per minute at early times to one per ten minutes at late times.

The duration of a decay of three orders of magnitude in concentration occurs over approximately one hour depending on the injection flowrate. Initial concentrations, C_0, of Lissamine for experiments 1 and 2 are 37 and 26 mg/L, respectively.

During the course of each experiment, samples are obtained from the observation borehole at a frequency of one per 5-10 minutes. After the first arrival of tracer at the observation borehole, the frequency of sampling is based on the number of points required to define the breakthrough curve. In both experiments, at least 20-30 samples were obtained to define the curve, with the greatest concentration of sampling points located in the area of peak tracer concentration.

Table 1 shows a summary of the test conditions for each of the two tracer experiments. Experiment 1 was conducted using the 0.43 L mixing system installed in observation borehole 4. Experiment 2 was conducted with the sampling packer system installed in observation borehole 5.

Results and Interpretation

To insure that the tracer is correctly mixed in the source borehole, the concentrations obtained from the source well are plotted semi-logarithmically against linear time. Regression analysis was conducted on these data for the two experiments and corellation coefficients of 0.991 and 0.997 were determined. Thus, uniform and complete mixing in the source well was achieved during both experiments.

The concentrations observed at the observation boreholes are

converted to dimensionless values and normalized relative to the peak concentration. This is done to avoid plotting the very small values of dimensionless concentration observed during these experiments. Based on previous experience in using this method (Novakowski et al., 1985) and by conducting a sensitivity analysis, it is assumed that the model fits obtained using peak-normalized data are completely unique. In addition, the normalized concentration data is plotted against the logarithm of real time to facilitate type curve matching (see Novakowski, 1991b for an example).

Type curve fits are obtained by adjusting the values of the dimensionless coefficients. It was found that the solutions are sensitive to the Pe number, which determines the relative peakedness of the curve. The overall size of the breakthrough curve is sensitive to the value of the inlet and outlet mixing coefficients. These, however, are not manipulated in obtaining a type curve fit.

The type curves are defined solely on the basis of α_r for the case where the observation well volume is negligible and on two parameters, α_r, and ξ, where it is not. The correction factor, ξ, influences only the outlet mixing coefficient and was found to be independent of the other matching parameter. The aperture, 2b, is determined from the type curve match using the dimensionless variable for time as shown in Novakowski (1991b).

Type curve analysis was conducted manually. Previous experience (Novakowski, 1991b) with this method suggests that

numerical optimization methods are not likely to provide better results.

Determining mass recovery for experiments conducted in a divergent flow field is difficult due to potential uncertainties with regard to flow field geometry. The only accurate estimate of recovery is derived from the fit to the theoretical model. For the experiments presented herein, it was found that the model results overestimated the field concentrations by as much as a factor of ten. This indicates that mass recovery is as low as 10%. The reason for poor mass recovery is unknown, but is not believed to influence the interpretation of 2b and α_r. In addition, experiments conducted in convergent flow fields (unpublished data) between the the same boreholes showed mass recoveries in the range of 80-100%. A discussion of the difference between the results of experiments conducted in divergent and convergent flow fields is beyond the scope of the present paper and will be addressed in future study.

Figure 8 shows the results of experiment 1 and the match obtained using equation [31]. The quality of the match is excellent over most of the field curve. The fit was obtained using a $\xi = 1.1$ and Pe = 75. Also shown is the fit obtained using the derivative of the line source solution of Chen (1987), which is easily obtained from [43] using the differential properties of the Laplace transform. The fit obtained with this solution, using the same value of Pe, is very poor. In fact, a good match cannot be obtained with this solution for any value of Pe. Therefore, it is inappropriate to use this solution to interpret tracer experiments

conducted in fractured media.

Figure 9 compares the results of experiment 2 to the match obtained using equation [24]. Again the quality of the match is very good over the majority of the range of data points. In this case, it is estimated that Pe = 25. Because the value of the inlet mixing coefficient is small and that for the outlet mixing coefficient is zero, the derivative of the line source solution of Chen (1987) can be used in this case and will yield results identical to those obtained using equation [24].

The Pe obtained from experiment 2 differs by a factor of three from that obtained from experiment 1. This despite the fact that the experiments are conducted at identical distances. It is possible that the difference is due to directional properties of α_L although additional experimentation would be required to confirm this.

In addition, the values of Pe determined from both experiments are considerably greater than those obtained from previous experiments conducted using convergent flow between the same boreholes (Novakowski, 1988, Novakowski, unpublished data). Mixing in the source and withdrawal wells was not accounted for in the interpretation of the previous experiments. A value of Pe = 33 was determined for an experiment conducted between the source borehole and observation borehole 4, and a value of 16 was obtained from an experiment conducted between the source borehole and observation borehole 5. Assuming that the parameter obtained from convergent and divergent experiments conducted between the same boreholes can

be expected to be identical (i.e., source/withdrawal borehole the same in each case), this illustrates the importance of either accounting for (experiment 1) or eliminating (experiment 2) the mixing zone in the source and/or observation boreholes for experiments conducted in fractured rock. Furthermore, the results of previously published experiments conducted under similar conditions (Novakowski et al., 1985; Raven et al., 1988; Shapiro and Nicholas, 1989) are probably influenced in a similar manner.

The results of the experiments presented herein can also be interpreted to determine fracture aperture. This can be done using either an expression based on flowrate (equation [6]) or on hydraulic head (equation [7]). Table 2 provides a summary of the calculated apertures as compared to apertures determined from transient pumping tests (Novakowski, 1988; Novakowski, unpublished data). It is interesting to note that the results of experiment 1 are in good agreement with the hydraulic aperture while those for experiment 2 are not. The results of experiment 2 are in agreement with previously published comparisons between apertures determined from tracer experiments and apertures determined from hydraulic tests (Novakowski et al., 1985; Novakowski, 1988; Raven et al., 1988; Silliman, 1989; Tsang, 1992) with explanations for the discrepancies given therein. Therefore, the result of experiment 1 must be considered anomolous and will be the focus of future study.

CONCLUSIONS

An analytical model was developed to interpret tracer

experiments conducted in radially divergent flow fields. A solution was obtained for both resident and flux concentrations in the formation and in an observation borehole. Diffusion of solute into adjacent strata is represented by coupling the solute concentration in the formation to the concentration in the aquitard. The volume of both the source and observation boreholes is assumed to be non-zero and mixed on a continual basis. A solution is also obtained for an observation well of infinitesimally small volume. Macroscopically discontinuous conditions are applied at both the inlet and outlet boundaries of the formation. The solutions for flux and resident concentrations are identical when discontinuous boundary conditions are employed for the case of source and observation boreholes of finite volume. An equivalent solution for the case of convergent flow was found to be not tractable without applying a continuity condition at both of the boundaries.

Although it has been shown that solutions for solute transport for uniform flow are equivalent to those for radial flow under conditions of small dispersion, this was not found to be the case for the solutions developed in this paper. However, it was found that the solutions for divergent flow can be employed to interpret tracer experiments conducted in convergent flow fields provided that the mixing coefficients are properly defined. The solutions developed in this paper can also be employed to determine the diffusive properties of an aquitard provided that dispersivity is small and the radial distance between source and observation well is large. The influence of the volume of the outlet reservoir was

found to be negligible with respect to the determination of the properties of the aquitard.

Two tracer experiments were conducted between three boreholes intersecting a horizontal fracture zone to demonstrate the application of the new solutions. The tracer experiments were conducted using a divergent radial flow field with an injection zone of finite volume. In one experiment, the observation borehole was instrumented with a packer system also having a finite volume. In the other experiment, the observation borehole was instrumented with a single packer system from which groundwater samples were obtained through the packer wall, thus negating the well bore volume. Results show that the new solutions can be uniquely fit to the breakthrough concentrations obtained from the observation boreholes. The data was also interpreted using a radial transport model which does not account for the mixing effects in the source and observation boreholes. It was found that a unique fit could not be obtained and that interpretation based on this model would lead to a significant overestimate of dispersivity. It was also determined that interpretation of fracture aperture from the results of these experiments may be similarly affected. Therefore, for tracer experiments conducted in fractured rock, use of the solutions developed in this paper will provide considerably more accurate estimates of the transport properties of the fractures.

NOTATION

A	flow coefficient, L^2/T
b	formation thickness, L
C	resident concentration, M/L^3
C_D	dimensionless resident concentration, C/C_0
C_m	resident concentration in the matrix, M/L^3
C_{mD}	dimensionless concentration in the matrix, C_m/C_0
C_{De}	dimensionless concentration in the observation well, C_e/C_0
C_{DF}	dimensionless flux concentration, C_F/C_0
C_{Di}	dimensionless concentration in the source well, C_i/C_0
C_e	concentration in the observation well, M/L^3
C_i	concentration in the source well, M/L^3
C_F	flux concentration, M/L^3
C_0	initial concentration, M/L^3
C_1	constant to be determined from boundary conditions
C_2	constant to be determined from boundary conditions
D_r	coefficient of hydrodynamic dispersion, L^2/T
D_d	effective diffusion coefficient, L^2/T
D_m	coefficient of molecular diffusion, L^2/T
M_L	mass leaving medium per unit time, M/T
p	Laplace variable
Pe	Peclet number, r/α_r
q	sink term for matrix diffusion
Q	volumetric flow rate, L^3/T
r	radial distance, L
r_D	dimensionless radial distance, r/α_r

r_{De} dimensionless radius of source well, r_w/α_r

r_{Di} dimensionless distance between source and observation well, r_i/α_r

r_i distance between source and observation wells, L

r_w radius of source well, L

r_{wo} radius of ~~source~~ well, L

t time, T

t_D dimensionless time, At/α_r^2

T transmissivity, L^2/T

v groundwater velocity, L/T

V_e volume of the isolated zone in the observation well, L^3

V_i volume of the isolated zone in the source well, L^3

y $r_D+1/(4\phi)$

y_e $r_{De}+1/(4\phi)$

y_r $r_{Di}+1/(4\phi)$

z vertical distance in the adjacent strata, L

z_D dimensionless vertical distance, z/α_r

α_r dispersivity, L

β_{Di} dimensionless mixing coefficient for the source well, $(V_i r_w)/(\alpha_r^2 \gamma_i)$

β_{De} dimensionless mixing coefficient for the observation well, $(V_e r_i)/(\alpha_r^2 \gamma_e)$

γ_e cross-sectional area available for flow at observation well, $\pi r_{wo} b\theta\xi$, L^2

γ_i cross-sectional area available for flow at source well, $2\pi r_w b\theta$, L^2

ΔH difference in hydraulic head between source and observation well, L

ξ correction factor, dim.

θ porosity, L^3/L^3

ϕ $p+\omega(p/\psi)^{1/2}$

ψ D_d/A

ω $(2D_m\alpha_r)/(Ab)$

2b fracture aperture, L

Ai, Ai' and Bi, Bi' are Airy functions and derivatives of first and second order, respectively.

ACKNOWLEDGEMENTS

The author is grateful to P. Lapcevic, G. Bobba, I. Noor and especially J. Voralek and G. Bickerton for assistance with the field experiments. Discussions with A. Moench and S. Silliman regarding the use of the Amos subroutines and the solution for convergent flow are gratefully acknowledged. The draft manuscript was kindly reviewed by A. Piggott.

REFERENCES

Abramowitz, M. and I. A. Stegun (Eds.), Handbook of Mathematical Functions, Appl. Math. Ser. 55, National Bureau Of Standards, Washington, D. C., 1964.

Al-Niami, A.N.S. and K.R. Rushton, Radial dispersion to an abstraction well, J. Hydrol., 39, 287-300, 1978.

Amos, D.E., Algorithm 644, a portable package for Bessel functions of a complex argument and nonnegative order, ACM Trans. Math. Software, 12(3), 265-273, 1986.

Chen, C.-S., Analytical and approximate solutions to radial dispersion from an injection well to a geological unit with simultaneous diffusion into adjacent strata, Water Resour. Res., 21(8), 1069-1076, 1985.

Chen, C.-S., Solutions for radianuclide transport from an injection

well into a single fracture in a porous formation, Water Resour. Res., 22(4), 508-518, 1986.

Chen, C.-S., Analytical solutions for radial dispersion with Cauchy boundary at injection well, Water Resour. Res., 23(7), 1217-1224, 1987.

Chen, C.-S. and G.D. Woodside, Analytical solution for aquifer decontamination by pumping, Water Resour. Res., 24(8), 1329-1338, 1988.

De Hoog, F.R., J.H. Knight and A.N. Stokes, An improved method for numerical inversion of Laplace transforms, SIAM J. Sci. Statist. Comput., 3(3), 357-366, 1982.

Drost, W., D. Klotz, A. Koch, H. Moser, F. Neumaier and W. Rauert, Point dilution methods of investigating groundwater flow by means of radioisotopes, Water Resour. Res., 4(1), 125-146, 1968.

Gelhar, L.W. and C.L. Axness, Three-dimensional stochastic analysis of macrodispersion in aquifers, Water Resour. Res., 19(1), 161-180, 1983.

Gelhar, L.W., A. Mantoglou, C. Welty and D.R. Rehfeldt, A review of field scale physical solute transport processes in saturated and unsaturated porous media, Report EA-4190, Electric Power Res.

Inst., Palo Alto, Calif., 1985.

Grisak, G.E., W.F. Merritt and D.W. Williams, A flouride borehole dilution apparatus, Can. Geotech. J., 14(4), 554-561, 1977.

Guvanasen, V, and V.M. Guvanasen, An approximate semi-analytical solution for tracer injection tests in a confined aquifer with a radially converging flow field and finite volume of tracer and chase fluid, Water Resour. Res., 23(8), 1607-1619, 1987.

Hodgkinson, D.P. and D.A. Lever, Interpretation of a field experiment on the transport of sorbed and non-sorbed tracers through a fracture in crystalline rock, Rad. Waste Mang. Nucl. Fuel Cycle, 4(2), 129-158, 1983.

Hoopes, J.A. and D.R.F. Harleman, Dispersion in radial flow from a recharge well, J. Geophys. Res., 72(14), 3595-3607, 1967.

Hsieh, P.A., A new formula for the analytical solution of the radial dispersion problem. Water Resour. Res., 22(11), 1597-1605, 1986.

Ketcheson, D.R., Velocity correction for borehole dilution analysis, M.A.Sc Thesis, University of Waterloo, Waterloo, Ont., 1985.

Killey, R.W.D. and G.L. Moltyaner, Twin lakes tracer tests: Setting, methodology, and hydraulic conductivity distribution, Water Resour. Res., 24(10), 1585-1612, 1988.

Kreft, A. and A. Zuber, On the physical meaning of the dispersion equation and its solutions for different initial and boundary conditions, Chem. Eng. Sci., 1471-1480, 1978.

Landstrom, O., C.E. Klockars, K.-E. Holmberg and S. Westerberg, In situ experiments on nuclide migration in fractured crystalline rocks, Tech. Rep. 110, KBS Nucl. Fuel Saft. Proj., Stockholm, 1978.

Maloszewski, P. and A. Zuber, On the theory of tracer experiments in fissured rocks with a porous matrix, J. Hydrol., 79(1985), 333-358, 1985.

Mercado, A., Recharge and mixing tests at Yavne 20 well field, Underground Water Storage Study Tech. Rep. No. 12, Tahal Water Planning for Israel Ltd., Tel Aviv, 1966.

Moench, A.F., Radial dispersion from a finite-diameter well due to tracer input at a constant rate, unpublished manuscript, 1989a.

Moench, A.F., Convergent radial dispersion: A Laplace transform solution for aquifer tracer testing, Water Resour. Res., 25(3), 439-447, 1989b.

Moench, A.F., Convergent radial dispersion: a note on evaluation of the Laplace transform solution, Water Resour. Res., 27(12), 3261-3264, 1991.

Molz, F.J., O. Guven and J.G. Melville, An examination of scale-dependent dispersion coefficients, Ground Water, 21(6), 715-725, 1983.

Novakowski, K.S., G.V. Evans, D.A. Lever and K.G. Raven, A field example of measuring hydrodynamic dispersion in a single fracture, Water Resour. Res., 21(8), 1165-1174, 1985.

Novakowski, K.S., Comparison of fracture aperture widths determined from hydraulic measurements and tracer experiments, In Proc: 4th Canadian/American Conference on Hydrogeology, Ed: B. Hitchon and S, Bachu, Nat. Water Well Assoc., Dublin, Ohio, pp. 68-80, 1988.

Novakowski, K.S. and J.A. Cherry, The effect of wellbore dilution on the results of tracer experiments conducted in fractured rock, In Proc: Tech. Trans. Conf., Ministry of Envir. Ont., Toronto, Ont., Vol. II, pp. 68-77, 1989.

Novakowski, K.S., An evaluation of boundary conditions for one-dimensional solute transport, 1, mathematical development, Water Resour. Res., in submittal, 1991.

Novakowski, K.S., An evaluation of boundary conditions for one-dimensional solute transport, 2, column experiments, Water Resour. Res., in submittal, 1991.

Ogata, A., Dispersion in porous media, Ph.D. Thesis, Northwestern Univ., Evanston, Ill., 1958.

Ogata, A., Theory of dispersion in a granular medium, U.S. Geol. Surv. Prof. Pap. 411-I, 1970.

Pickens, J.F. and G.E. Grisak, Scale-dependent dispersion in a stratified granular aquifer, Water Resour. Res., 17(4), 1191-1211, 1981.

Raimondi, P., G.H.F. Gardner and C.B. Petrick, Effect of pore structure and molecular diffusion on the mixing of miscible fluids flowing in porous media, In Proc: Symposium on Oil Recovery Methods, Soc. Petrol. Tech., San Francisco, Ca., 1959.

Raven, K.G., K.S. Novakowski, and P.A. Lapcevic, Interpretation of field tracer tests of a single fracture using a transient solute storage model, Water Resour. Res., 24(12), 2019-2032, 1988.

Sauty, J.-P., An analysis of hydrodispersive transfer in aquifers, Water Resour. Res., 16(1), 145-158, 1980.

Shapiro, A.M. and J.R. Nicholas, Assessing the validity of the channel model of a fracture aperture under field conditions, Water Resour. Res., 25(5), 817-828, 1989.

Silliman, S.E., Interpretation of the difference between aperture estimates derived from hydraulic and tracer tests in a single fracture, Water Resour. Res., 25(10), 2275-2283, 1989.

Smart, P.L. and I.M.S. Laidlaw, An evaluation of some fluorescent dyes for water tracing, Water Resour. Res., 13(1), 15-33, 1977.

Sudicky, E.A., A natural-gradient experiment on solute transport in a sand aquifer: Spatial variability of hydraulic conductivity and its role in the dispersion process, Water Resour. Res., 22(13), 2069-2082, 1986.

Talbot, A., The accurate numerical inversion of Laplace transforms, J. Inst. Maths Applics., 23, 97-120, 1979.

Tang, D.H. and D.K. Babu, Analytical solution of a velocity dependent dispersion problem, Water Resour. Res., 15(6), 1471-1478, 1979.

Tsang, Y.W., Usage of "equivalent" apertures for rock fractures as derived from hydrological and tracer tests, Water Resour. Res., in submittal, 1992.

Teutsch, G. and T. Ptak, The in-line packer system: a modular multilevel sampler for collecting undisturbed groundwater samples, In Proc: Int. Symp. Cont. Trans. in Groundwater, Stuttgart, 1989.

Valocchi, A.J., Effect of radial flow on deviations from local equilibrium during sorbing solute transport through homogenous soils, Water Resour. Res., 22(12), 1693-1701, 1986.

van Genuchten, M. Th. and J.C. Parker, Boundary conditions for displacement experiments through short laboratory columns, Soil Sci. Soc. Am. J., 48(4), 703-708, 1984.

Ward, R.S., M.A. Sen, G.M. Williams, and P.D. Jackson, Automatic monitoring of radial injection tracer tests using a novel multi-electrode resistivity system, In Proc: Int. Conf. Trans. and Mass Exch. Process. in Sand and Gravel Aquif.: Field and Modelling Studies, Vol. 1, pp. 285-303, 1990.

Table 1. Summary of experimental conditions.

Test Number	Obs. Borehole No.	V_e (L)	r (m)	Mean Q (mL/min)	Mean ΔH (m)	C_0 (mg/L)
1	4	0.43	15.0	441.2	0.81	37
2	5	Nil	15.0	268.8	0.75	26

Table 2. Values of fracture aperture determined from type curve analysis.

Test Number	2b based on Q (μm)	2b based on ΔH (μm)	2b from pumping test (μm)
1	254	240	228
2	745	140	213

FIGURES

Figure 1. Illustration of the physical problem for divergent and convergent flow.

Figure 2. Comparison of the solutions for divergent and convergent solute transport at small Peclet numbers.

Figure 3. Comparison of the solutions for divergent and convergent solute transport for small and large Peclet numbers and a large observation well mixing coefficient.

Figure 4. The effect of matrix porosity on the results of a divergent tracer experiment with Pe = 5-80.

Figure 5. The influence of the magnitude of the mixing coefficient in the observation well on the effect of matrix diffusion. The comparison is conducted for large Peclet numbers.

Figure 6. Schematic diagram of the apparatus employed in the field experiments.

Figure 7. Schematic diagram of the sampling packer used in experiment 2.

Figure 8. Results of experiment 1 as compared to the solution developed in the present paper (equation [31]) and the modified form of the Chen (1987) solution.

Figure 9. Results of experiment 2 compared to the solution developed for the present paper (equation [24]).

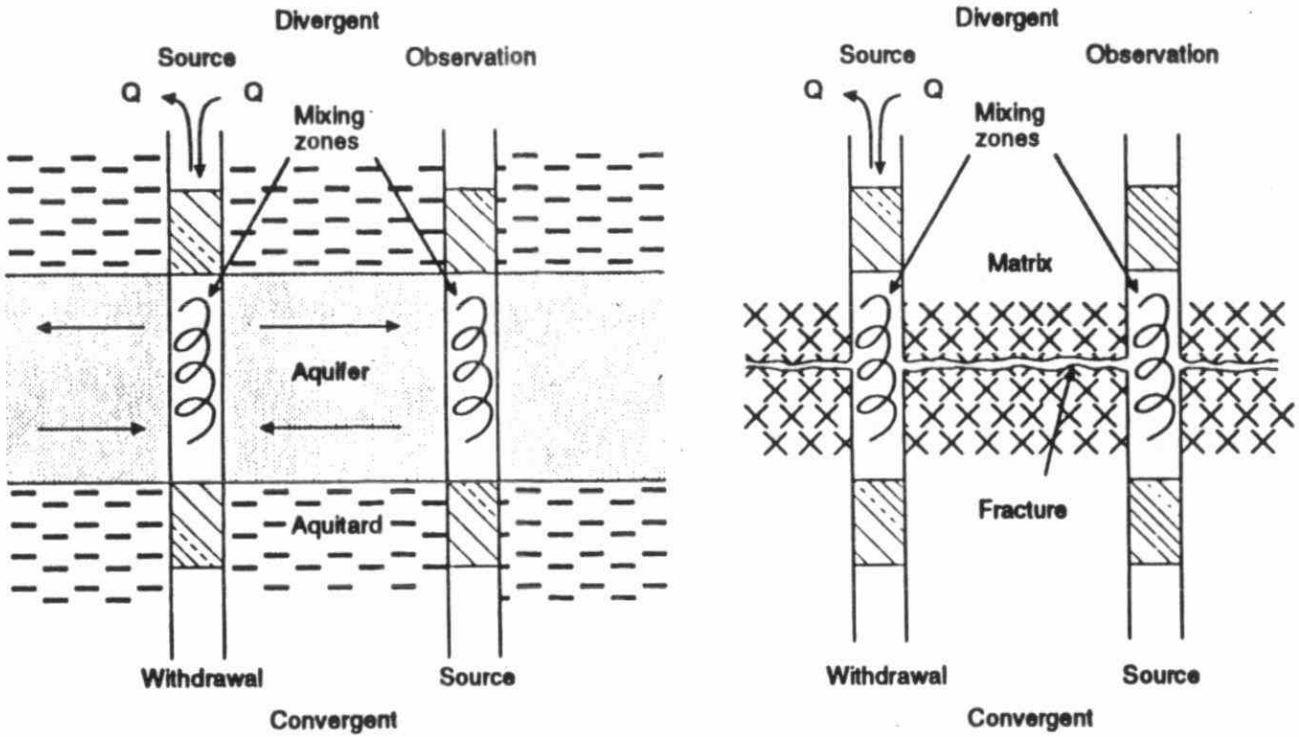

Figure 1. Illustration of the physical problem for divergent and convergent flow.

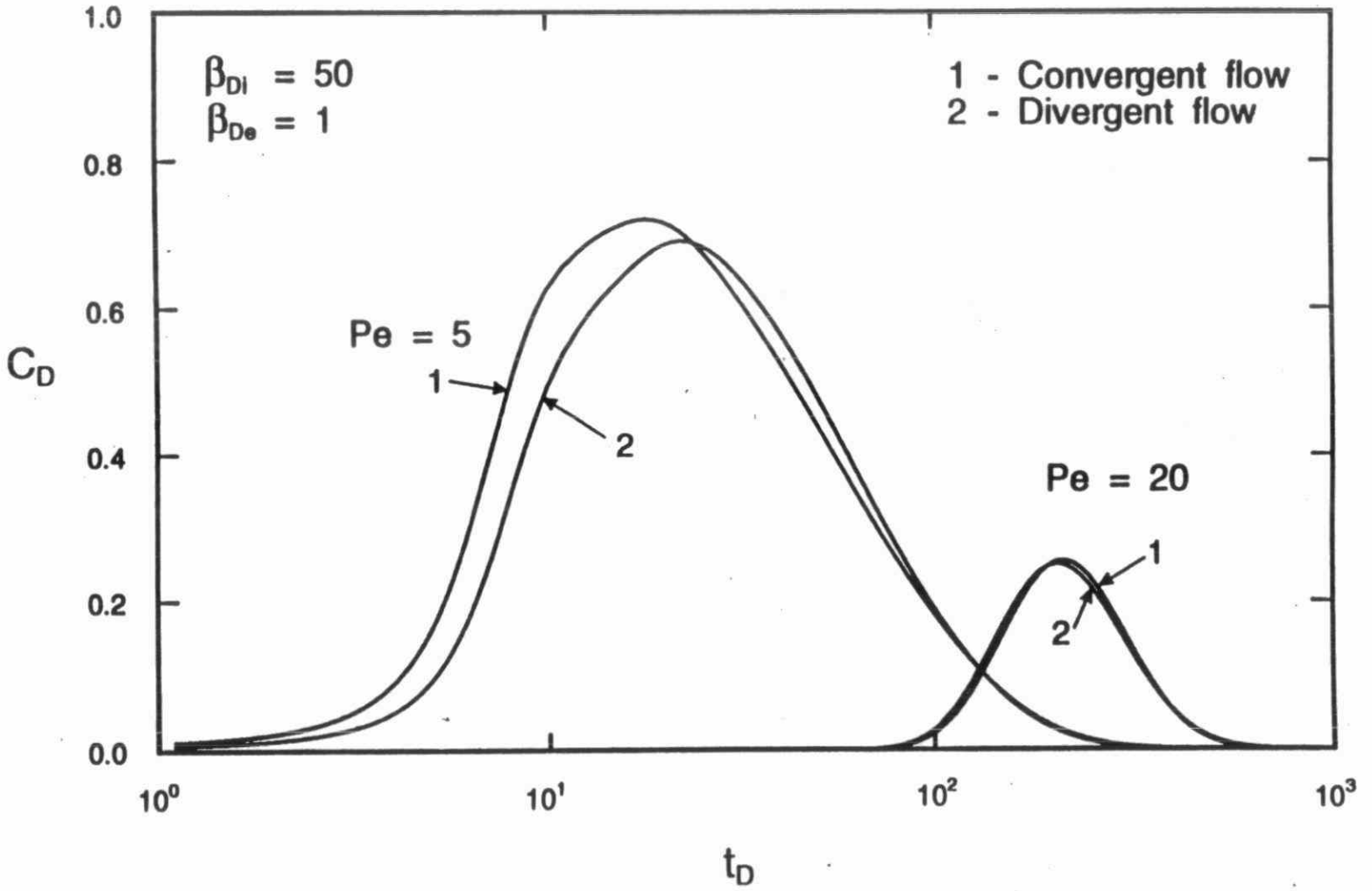

Figure 2. Comparison of the solutions for divergent and convergent solute transport at small Peclet numbers.

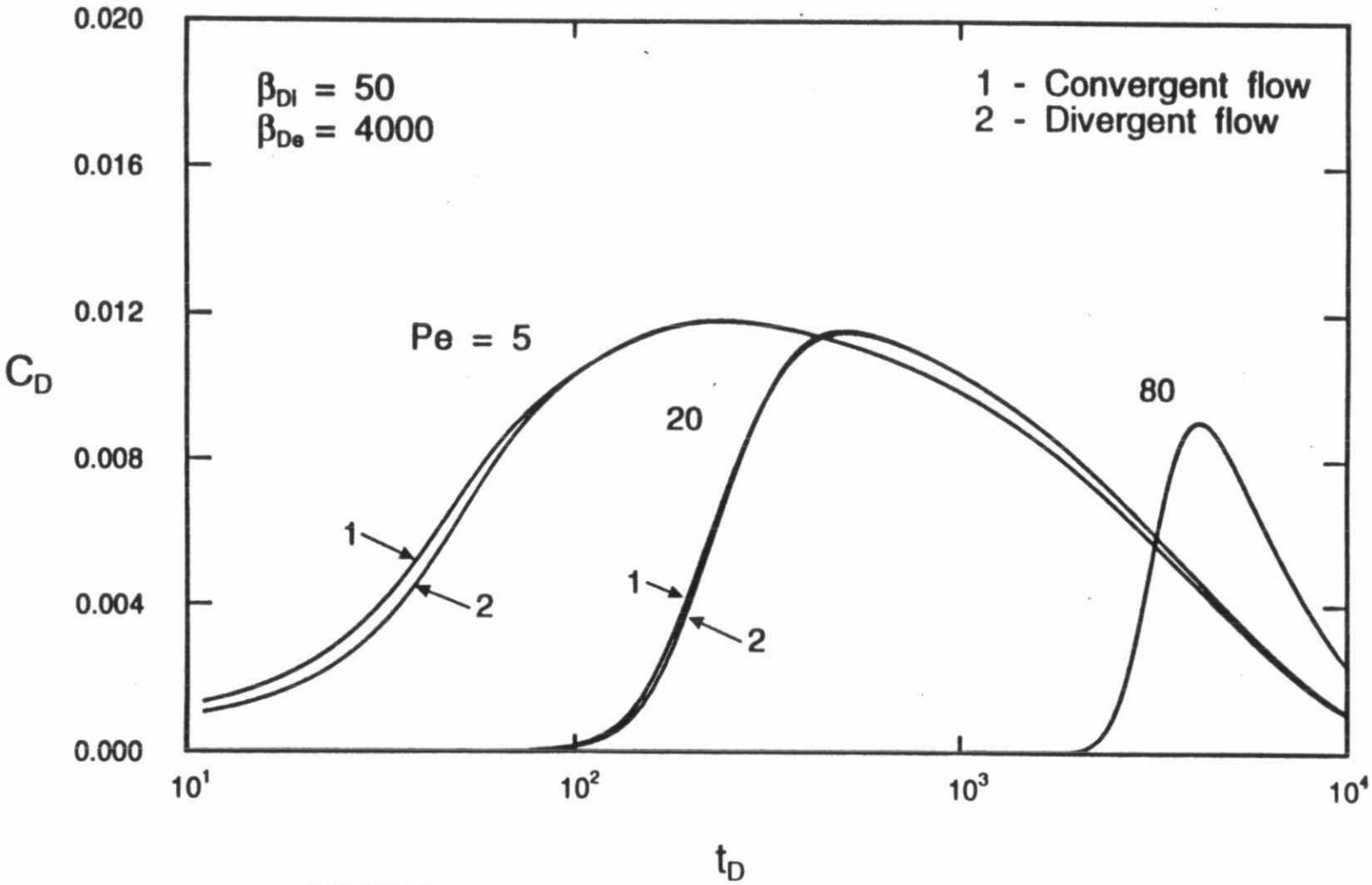

Figure 3. Comparison of the solutions for divergent and convergent solute transport for small and large Peclet numbers and a large observation well mixing coefficient.

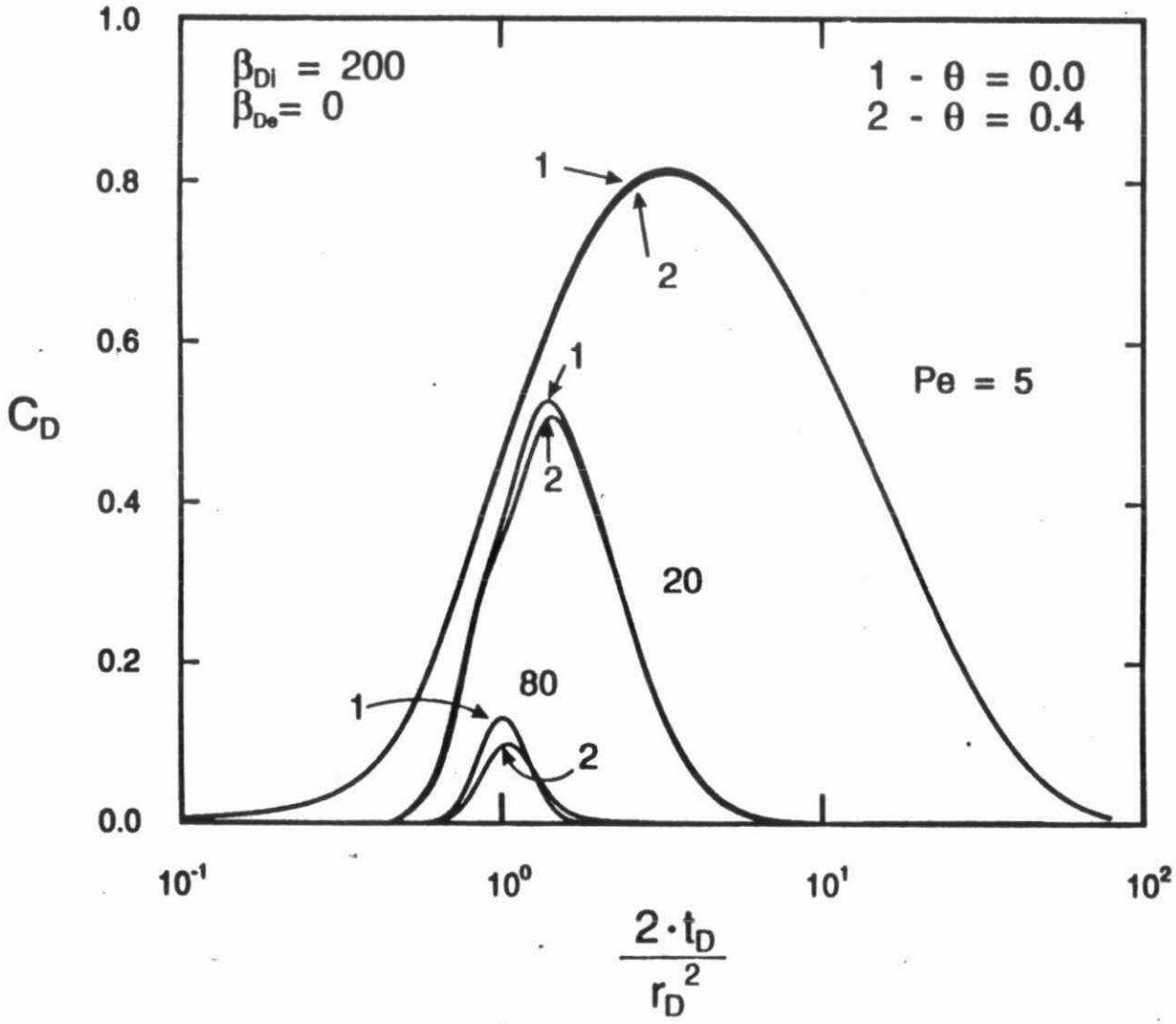

Figure 4. The effect of matrix porosity on the results of a divergent tracer experiment with Pe = 5-80.

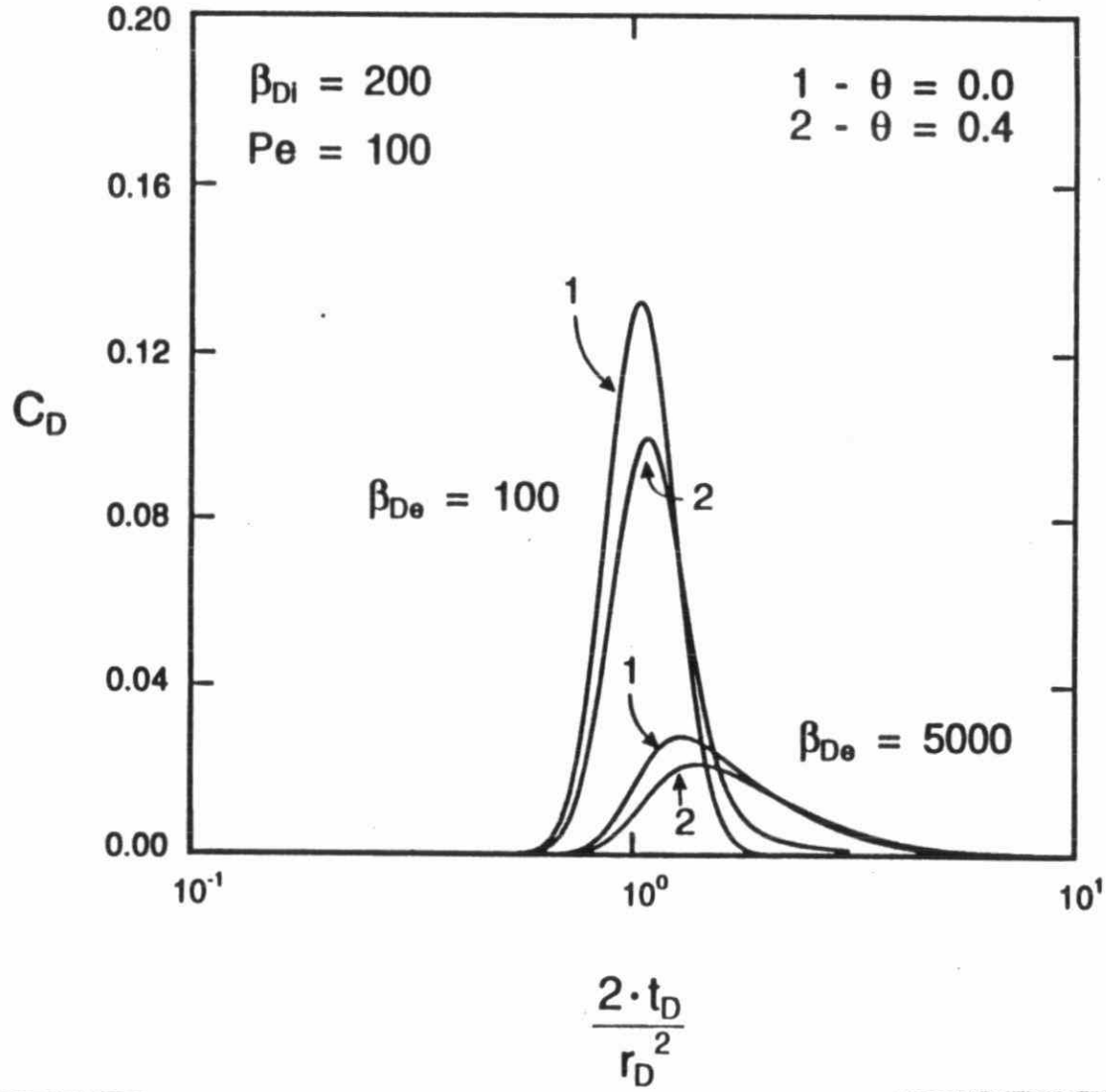

Figure 5. The influence of the magnitude of the mixing coefficient in the observation well on the effect of matrix diffusion. The comparison is conducted for large Peclet numbers.

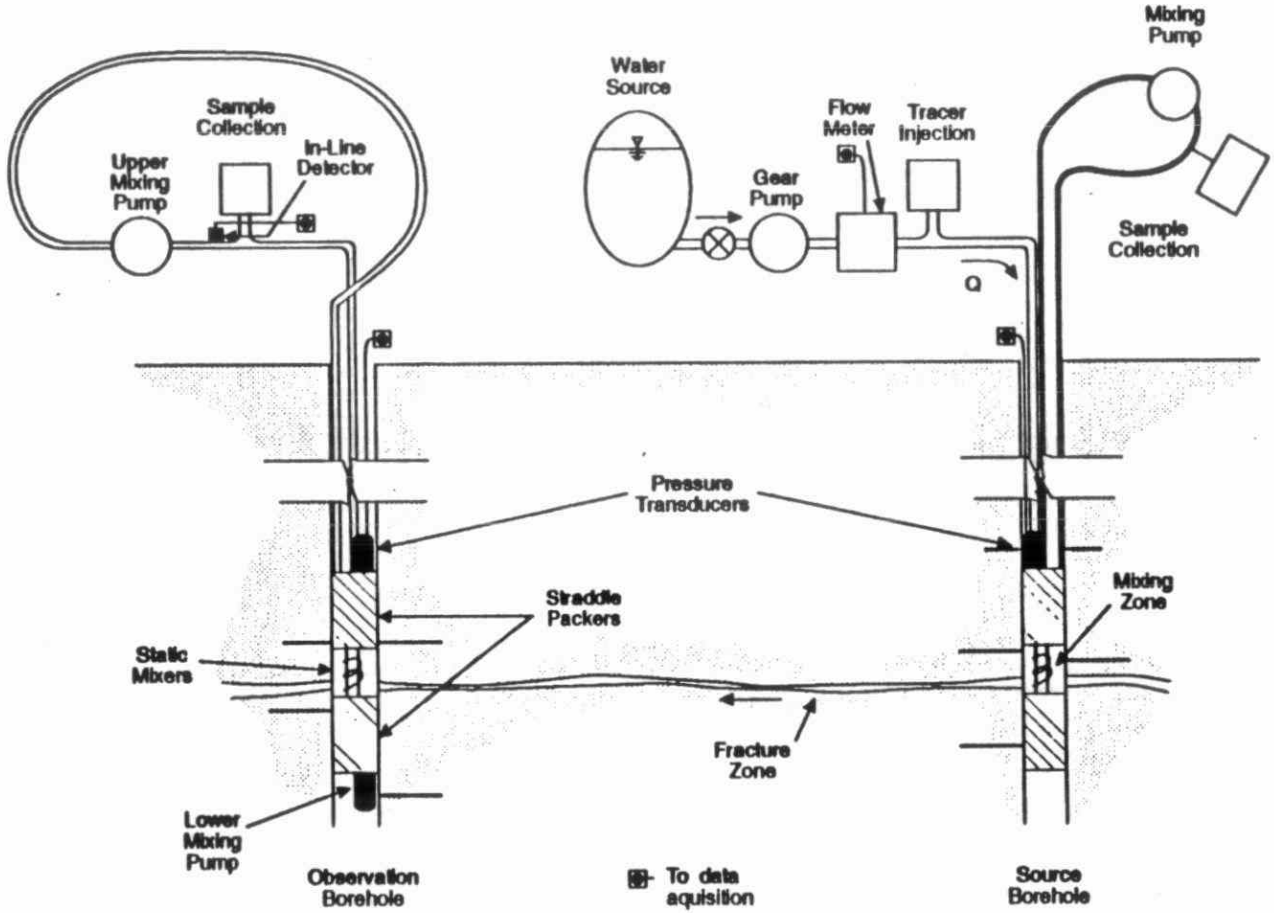

Figure 6. Schematic diagram of the apparatus employed in the field experiments.

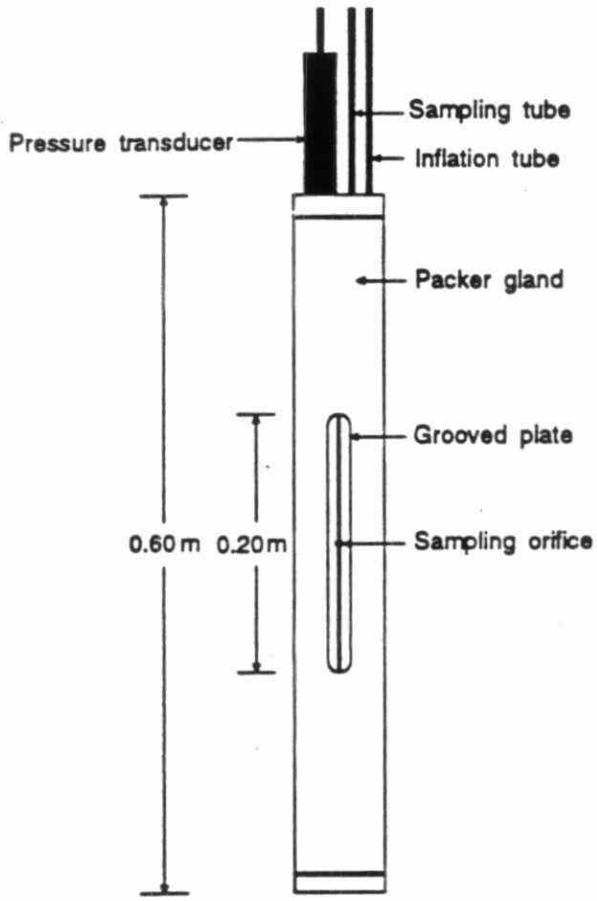

Figure 7. Schematic diagram of the sampling packer used in experiment 2.

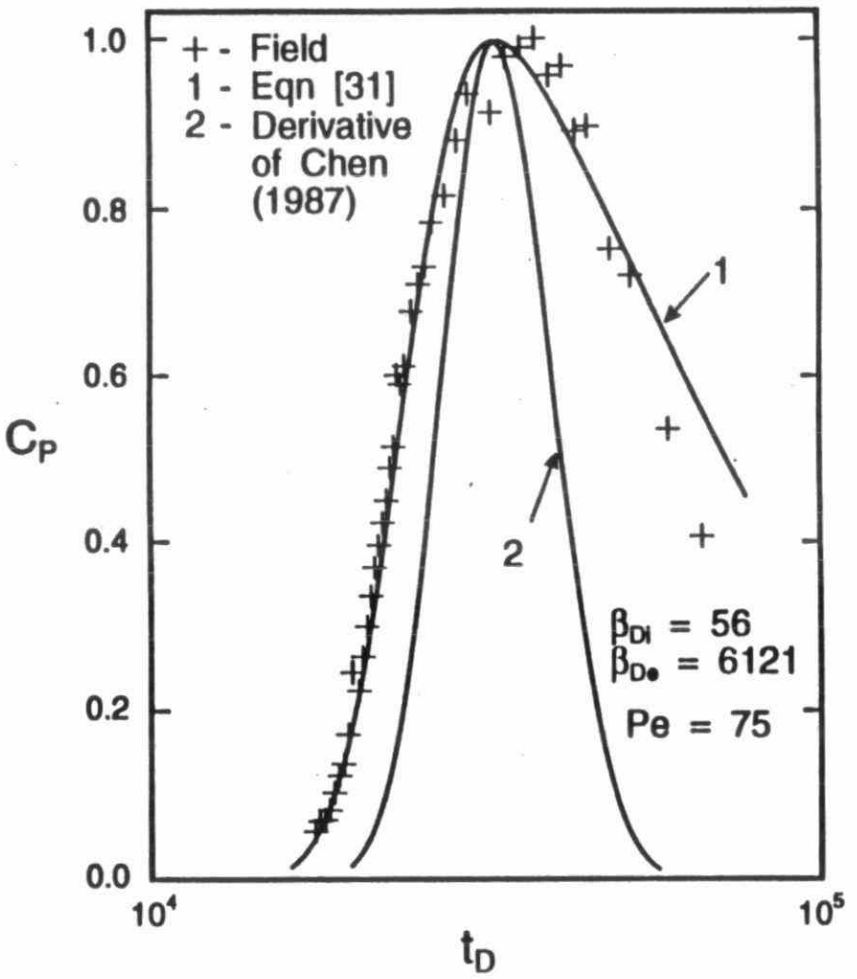

Figure 8. Results of experiment 1 as compared to the solution developed in the present paper (equation [31]) and the modified form of the Chen (1987) solution.

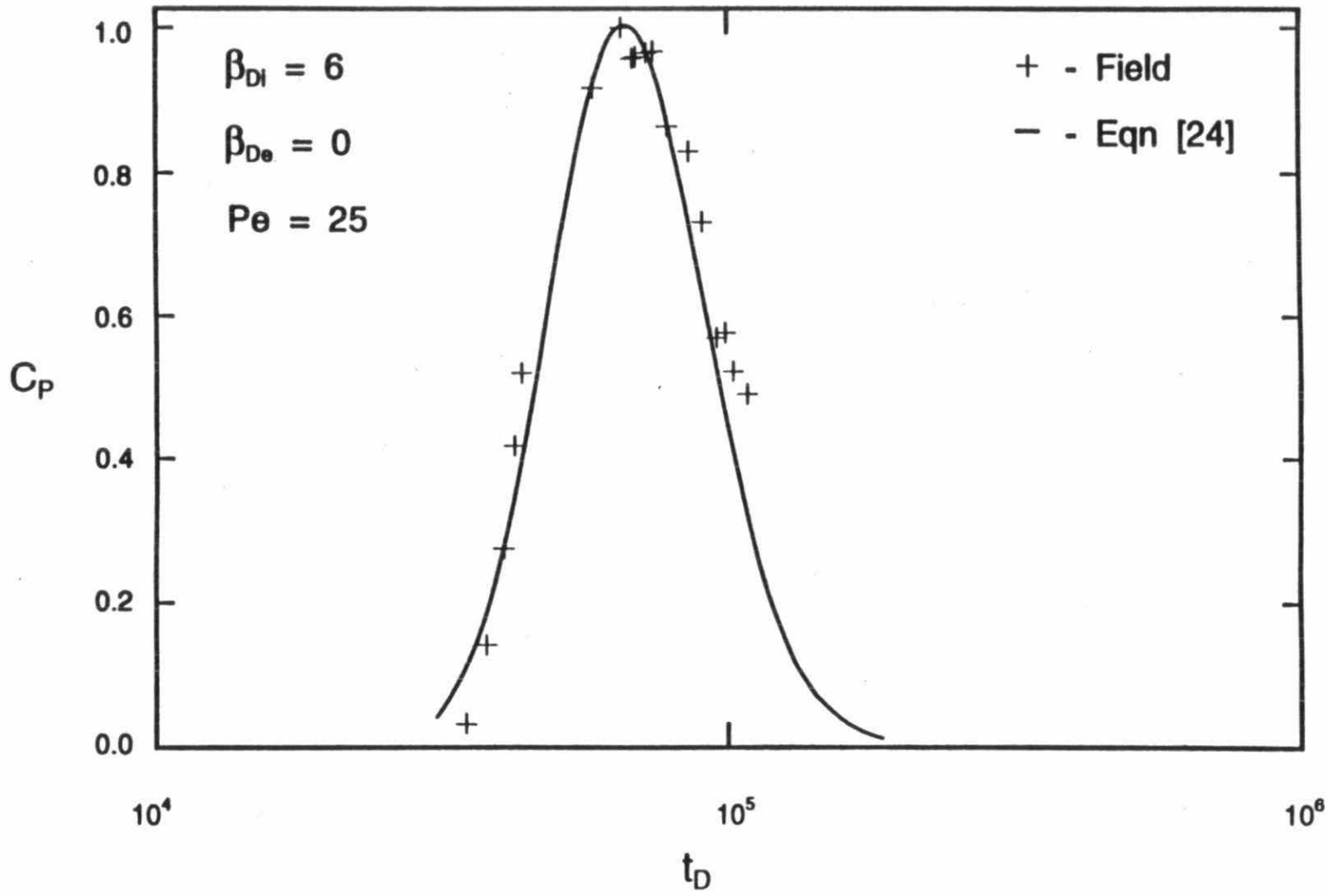

Figure 9. Results of experiment 2 compared to the solution developed for the present paper (equation [24]).

TC
171
.C44
M43
1993

Measuring groundwater velocity and hydrodynamic dispersion in a single fracture in fractured shale / Lapcevic, P. A.

77018

NATIONAL WATER RESEARCH INSTITUTE
P.O. BOX 5050, BURLINGTON, ONTARIO L7R 4A6

Environment Canada Environnement Canada

Canada

INSTITUT NATIONAL DE RECHERCHE SUR LES EAUX
C.P. 5050, BURLINGTON (ONTARIO) L7R 4A6

Think Recycling!

Pensez à recycler !